THERMAL AND RESISTIVE INSTABILITIES IN THE SOLAR ATMOSPHERE

E. A. Smith

A Thesis Submitted for the Degree of PhD
at the
University of St Andrews

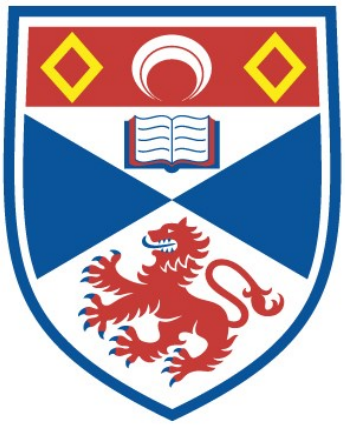

1977

THERMAL AND RESISTIVE INSTABILITIES IN THE SOLAR ATMOSPHERE.

E.A. SMITH

Thesis submitted for the Degree of Doctor of Philosophy of the University of St. Andrews.

ProQuest LLC.
789 East Eisenhower Parkway
P.O. Box 1346
Ann Arbor, MI 48106 – 1346

THERMAL AND RESISTIVE INSTABILITIES IN THE SOLAR ATMOSPHERE

ABSTRACT

The magnetic field greatly influences the plasma in the solar atmosphere and in this thesis we consider the effect of the field on the stability of the plasma.

The many observations that have been made suggest that two types of field structure play a major role. Firstly a current sheet - this has field lines which change direction in a thin, current forming region, but are fairly uniform outside. We consider the case where the field strength is zero along the neutral line so that a gas pressure gradient is required across the sheet to balance the magnetic pressure gradient. Secondly a force-free field - here the magnetic force is zero, which requires the magnetic pressure to be much larger than the gas pressure. In the neutral current sheet we examine the thermal instability and the tearing-mode instability. While in the force-free magnetic arch system we look for a thermal instability which can occur when the foot points of the arch are sheared.

When we investigated the thermal stability of the current sheet we found that as its length increases it passes through a series of stable equilibria until a value, L_{max}, is reached when the sheet cools down to a new stable equilibrium. For coronal conditions, values for L_{max} and cooling time are in fair agreement with the observed values for quiescent prominences.

We calculate the growth rate of the tearing-mode instability in a neutral current sheet with no energy sources or sinks and find that the maximum growth rate can be significantly larger in the current sheet than in the sheared field of constant magnitude considered by others. Also the growth rate decreases when the ratio of gas to magnetic pressure is reduced. We find that the growth rate is significantly inhibited if the current sheet has a transverse magnetic field which is large enough.

Lastly we examine the thermal balance in a sheared, force-free magnetic field and show that thermal instability can occur if the field is sheared enough. We assume thermal equilibrium between radiative loss and thermal conduction and we take gravity balanced by a pressure gradient. If, for example, the density at the base of the field is ten times larger than the normal coronal value, as it may be in coronal condensations, then there is instability if the shear angle is greater than 63°. The presence of a large enough mechanical heating is found to prevent the instability occurring.

ACKNOWLEDGEMENTS

I would like to thank Dr. Eric Priest for his encouragement and supervision during the past three years.

I would also like to thank Mrs. Hamilton for typing this Thesis.

I am grateful to the Science Research Council for financial support.

DECLARATION

I declare that the following Thesis is a record of research work carried out by me, that the Thesis is my own composition, and that it has not been previously presented in application for a higher degree.

(Edward Alexander Smith).

POSTGRADUATE CAREER

I was admitted into the University of St. Andrews as a research student under Ordinance General No. 12 in October 1973 to work on aspects of thermal and tearing mode instabilities in the solar atmosphere under the supervision of Dr. E.R. Priest. I was admitted under the above resolution as a candidate for the degree of Ph.D. in October 1974.

CERTIFICATE

I certify that Edward A. Smith has satisfied the conditions of the Ordinance and Regulations and is thus qualified to submit the accompanying application for the degree of Doctor of Philosophy.

C O N T E N T S

CHAPTER 1.: INTRODUCTION.

The object of this thesis is to study two instabilities that may be of importance in a wide variety of phenomena in the solar atmosphere, but are of particular relevance for the formation of solar prominences. We begin this rather extensive introduction by describing the basic equations we shall employ and the assumptions involved in their derivation. In particular, the possible terms that may appear in the energy balance equation are described at some length.

Next (Section 1.2) a comprehensive summary of previous work on the type of thermal instability in which we are interested is presented. This acts as background for the work of Chapters 2 and 4, in which the possible occurrence of the instability in current sheets or sheared magnetic structures is investigated with relevance to prominence formation.

In(Section 1.3)a summary of resistive instabilities in sheared fields, especially the tearing mode, is given including an outline of the numerical technique of Cross and Van Hoven for finding the growth rate. Their technique is extended in Chapter 3 to current sheets both with and without a transverse field component.

Then (Section 1.4) a description of solar prominences is presented. This is followed by an account of the suggestion that prominences may form in current sheets, which acts as a basis for Chapter 2.

Finally, (Section 1.5) the main objects of the research of this thesis.

1.1: THE BASIC EQUATIONS

The study of the motion of individual particles in an ionized gas or plasma has advanced greatly over the past few decades. However, to make the problems tractable it is necessary to approximate by using the macroscopic equations of motion. For rigorous results in situation with small scale lengths, the study of each particle cannot be avoided but we shall find that in the plasma of the solar atmosphere the macroscopic equations are for many purposes adequate.

The macroscopic quantities, electric current density, $\underline{J}$, and mean velocity, $\underline{V}$, are related by the macroscopic equations of motion. It is possible to derive these equations from the Boltzmann equation (see for example Spitzer (1962) which is a source for much of this Section). The equation, in electromagnetic units, for ions of mass m_i and charge Z e/c (e denotes the electron charge in electrostatic units) is

$$n_i m_i \left(\frac{\partial \underline{v}_i}{\partial t} + (\underline{v}_i . \underline{\nabla}) \underline{v}_i \right) = \frac{n_i Z e}{c} (\underline{E} + \underline{v}_i \wedge \underline{B}) - \underline{\nabla} . \underline{\chi}_i - n_i m_i \underline{\nabla} \phi + \underline{P}_{ie} \quad , \qquad (1.1)$$

where n_i is the particle density, ϕ is the gravitational potential and $\underline{V}_i$, the mean velocity of the particles in an element of volume ΔV, is

$$\underline{V}_i = \frac{1}{n_i \Delta V} \sum \underline{W}_i$$

and $\underline{W}_i$ the velocity of each ion. The quantity $\underline{\chi}_i$ is the stress tensor defined by

$$\underline{\chi}_i = \frac{m_i}{\Delta V} \sum (\underline{W}_i - \underline{V}_i)(\underline{W}_i - \underline{V}_i) \quad ,$$

the summation extending over the volume element.

1.1: THE BASIC EQUATIONS (Contd.)

$\underline{P}_{ie}$ is the total momentum transferred to the ions per unit volume and time by collisions with the electrons where we assume that only electrons and one type of ion are present. The electrons have a similar equation of motion with e and i interchanged and $Z = -1$.
Although equation (1.1) is exact, it is not very useful unless the stress tensor is simple. If the distribution of random velocities $(\underline{W}_i - \underline{V}_i)$ is isotropic then we have the simple case

$$\underline{\nabla} \cdot \underline{\chi} = \underline{\nabla} p \quad , \qquad (1.2)$$

where p is the scalar gas pressure. The velocity distribution becomes isotropic if these collisions are frequent enough, so this is valid when the mean-free path for collisions between particles is short compared to the distance over which the macroscopic quantities vary. In $\underline{\chi}$, only the main diagonal terms of the stress tensor have been retained, the off-diagonal terms giving rise to the viscous stress which we shall neglect.
From equation (1.1) and the corresponding equation for the electrons we get an equation relating the macroscopic variables, $\underline{V}$ and $\underline{J}$, which are defined as

$$\underline{V} = \frac{1}{\rho} \left(n_i m_i \underline{V}_i + n_e m_e \underline{V}_e \right) ,$$

$$\underline{J} = \frac{e}{c} \left(n_i Z \underline{V}_i - n_e \underline{V}_e \right) ,$$

where the mass density ρ is

$$\rho = n_i m_i + n_e m_e \quad .$$

1.1: THE BASIC EQUATIONS (Contd.)

From the equations of motion (1.1) we get with (1.2)

$$\rho\left(\frac{\partial \underline{v}}{\partial t} + (\underline{v}.\underline{\nabla})\underline{v}\right) = \rho_c \underline{E} + \underline{J} \wedge \underline{B} - \underline{\nabla} p - \rho \underline{\nabla}\phi \,, \qquad (1.3)$$

where the charge density is

$$\rho_c = n_i \frac{Z e}{c} - n_e \frac{e}{c} \,.$$

The interaction terms P_{ei} and P_{ie} have cancelled out by Newton's third law of motion.

Also from equation (1.1) and the corresponding one for the electrons we deduce

$$\frac{m_i m_e c^2}{Z \rho e^2} \frac{\partial \underline{J}}{\partial t} = \underline{E} + \underline{v} \wedge \underline{B} - \eta \underline{J}$$

$$+ \frac{c}{e Z \rho}\left(m_i \underline{\nabla} p_e - Z m_e \underline{\nabla} p_i - (m_i - Z m_e)\underline{J} \wedge \underline{B}\right) ,$$

where we have neglected terms of order $\underline{J}^2$. Also we have assumed electrical neutrality ($\rho_c = 0$), and let, following Spitzer,

$$\underline{P}_{ei} = \frac{\eta e n_e}{c} \underline{J} \,.$$

When $\partial \underline{J}/\partial t$, $\underline{B}$, $\underline{\nabla} p_e$ and $\underline{\nabla} p_i$ all vanish, the equation reduces to Ohm's Law, with η equal to the electrical resistivity which Spitzer gives as

$$\eta = 6{\cdot}53 \times 10^{12} \frac{\ln \Lambda}{T^{3/2}} \text{ e.m.u.} , \qquad (1.4)$$

where the Coulomb logarithm $\ln \Lambda$ is tabulated by him.

1.1.: THE BASIC EQUATIONS (Contd.

These equations are supplemented by the equation of continuity of matter,

$$\frac{\partial \rho}{\partial t} + \nabla . (\rho \underline{V}) = 0 \quad , \qquad (1.5)$$

and Maxwell's equations, namely,

$$\nabla . \underline{D} = 4\pi \rho_c \quad , \qquad (1.6)$$

$$\nabla . \underline{B} = 0 \quad , \qquad (1.7)$$

$$\nabla \wedge \underline{E} = - \frac{\partial \underline{B}}{\partial t} \quad , \qquad (1.8)$$

$$\nabla \wedge \underline{H} = 4\pi \underline{J} + \frac{\partial \underline{D}}{\partial t} \quad , \qquad (1.9)$$

Another useful equation which describes charge conservation is, from (1.6) and (1.9)

$$\nabla . \underline{J} + \frac{\partial \rho_c}{\partial t} = 0 \quad .$$

The constitutive equations are, for a linear, plasma medium

$$\underline{D} = \frac{1}{c^2} \underline{E} + 4\pi \underline{P} \quad ,$$

$$\underline{B} = \underline{H} - 4\pi \underline{M} \quad ,$$

Where the velocity of light $C = 3 \times 10^{10} cm\ s^{-1}$, $\underline{P}$ is the polarization and $\underline{M}$ the magnetization vector.

The boundary conditions at medium interfaces are

$$\underline{E}_1 \wedge \underline{n} = \underline{E}_2 \wedge \underline{n} \quad ,$$

$$\underline{D}_1 . \underline{n} = \underline{D}_2 . \underline{n} + 4\pi \rho_s \quad ,$$

$$\underline{B}_1 . \underline{n} = \underline{B}_2 . \underline{n} \quad ,$$

$$\underline{H}_1 \wedge \underline{n} = \underline{H}_2 \wedge \underline{n} + 4\pi \underline{\phi} \quad .$$

1.1: THE BASIC EQUATIONS (Contd.)

The unit normal vector $\underline{n}$ points from medium 2 into medium 1. $\underline{\mathcal{J}}$ is the current sheet density at the interface and ρ_s is the charge layer density there. We have been discussing the equations so far from a laboratory frame of reference relative to which the plasma is moving with a velocity $\underline{V}$. However, they may be re-written in the rest frame of the fluid by using the Lorentz transformations. For non-relativistic velocities $(|\underline{V}|^2 \ll c^2)$ the transformations are

$$\underline{E}' = \underline{E} + \underline{V} \wedge \underline{B} \ ,$$

$$\underline{D}' = \underline{D} + \frac{\underline{V} \wedge \underline{H}}{c^2} \ ,$$

$$\underline{B}' = \underline{B} - \frac{\underline{V} \wedge \underline{E}}{c^2} \ ,$$

$$\underline{H}' = \underline{H} - \underline{V} \wedge \underline{D} \ ,$$

$$\underline{J}' = \underline{J} - \rho_c \underline{V} \ ,$$

$$\rho_c' = \rho_c - \frac{\underline{V} . \underline{J}}{c^2} \ .$$

These are exact for transformation between unaccelerated frames of reference and are good approximations if the acceleration is not too large. Primed and unprimed quantities refer to the rest frame and laboratory frame respectively.

THE M.H.D. APPROXIMATION

In addition to the non-relativistic approximation certain additional simplifications can be made for flow which is steady or has low frequency time variations and in which the imposed electric field is of the same order of magnitude as the induced field $\underline{V} \wedge \underline{B}$.

1.1: THE BASIC EQUATIONS (Contd.)

This type of flow is usually referred to as magneto hydro dynamic (MHD) flow.

The following assumptions are made in the M.H.D. approximation

1. $|\underline{V}|^2 \ll C^2$ (The non-relativistic approximation)

2. The electric fields are of order $\underline{V} \wedge \underline{B}$. This implies that the magnetic field is the same in all frames of reference:

$$\underline{B} = \underline{B}'$$

since the Doppler shift $\underline{V} \wedge \underline{E}/c^2 = O(|\underline{V}|^2 B/c^2) \ll B$ by 1. However, the full Lorentz transformed electric field must be retained since all the terms are of the same magnitude. Certain results can be deduced from 1 and 2.:

a) Phenomena involving high frequencies are not considered in the M.H.D. approximation, so that the displacement current $\partial \underline{D}/\partial t$ is neglected compared to $\underline{J}$, the conduction current, and equation (1.9) becomes

$$\nabla \wedge \underline{H} = 4\pi \underline{J}$$

This follows because $\underline{J} \simeq \frac{B}{\rho}$ and $\frac{\partial \underline{D}}{\partial t} \simeq \frac{E}{c^2 t} \simeq \frac{VB}{c^2 t}$

$$\Rightarrow \frac{\partial \underline{D}/\partial t}{\underline{J}} \simeq V^2/c^2 ,$$

so that the displacement current is much less than the conduction current by 1.

1.1: THE BASIC EQUATIONS (Contd.)

b) The electric energy is negligible compared to the magnetic energy. Comparing $\frac{E^2}{C^2}$ to H^2, to order $V^2/C^2 \ll 1$ with $\underline{E} = O(\underline{V} \wedge \underline{B})$, we get

$$\frac{E^2}{c^2} = O\left(\frac{|\underline{V} \wedge \underline{H}|^2}{c^2}\right) = O\left(\frac{V^2}{c^2} H^2\right) ,$$

which is negligible compared to H^2. Since the displacement current and the electric field energy are neglected, the main interaction is between the magnetic field and the fluid.

c) The force density is represented by

$$\underline{f} = \rho_c \underline{E} + \underline{J} \wedge \underline{B} ,$$

however by 1 we are able to neglect $\rho_c \underline{E}$.
The ratio of $\frac{\rho_c \underline{E}}{\underline{J} \wedge \underline{B}} \simeq \frac{\rho_c E}{JB} \simeq \frac{E^2}{c^2 \rho JB} \simeq \frac{V^2 B^2}{c^2 B^2} \frac{\rho}{\rho} \simeq \frac{V^2}{c^2}$ is very much less than one and so the $\rho_c \underline{E}$ term can be ignored compared with $\underline{J} \wedge \underline{B}$.

Under the MHD approximations Maxwell's equations become

$$\underline{\nabla} \wedge \underline{E} = - \frac{\partial \underline{B}}{\partial t} , \qquad (1.10)$$

$$\underline{\nabla} \wedge \underline{H} = 4\pi \underline{J} , \qquad (1.11)$$

$$\underline{\nabla} \cdot \underline{B} = 0 , \qquad (1.12)$$

$$\underline{\nabla} \cdot \underline{J} = - \frac{\partial \rho_c}{\partial t} , \qquad (1.13)$$

1.1.: THE BASIC EQUATIONS (Contd.)

A useful equation is the induction equation, which is a result of Ohm's law and Maxwell's equations. From the curl of Ohm's law, we have

$$\underline{\nabla} \wedge (\eta \underline{J}) = \underline{\nabla} \wedge (\underline{E} + \underline{v} \wedge \underline{B}) \quad . \qquad (1.14)$$

Then from equations (1.10), (1.11) and (1.14) we get

$$\frac{\partial \underline{B}}{\partial t} = \underline{\nabla} \wedge (\underline{v} \wedge \underline{B}) - \underline{\nabla} \wedge \left(\frac{\eta}{4\pi} \underline{\nabla} \wedge \underline{B} \right) \qquad (1.15)$$

If the first term on the right hand side dominates then the magnetic flux through any loop moving with the local fluid velocity is constant in time. We say that the lines of force are frozen into the fluid and are carried along with it. If the second term dominates then the magnetic field will decay in the diffusion time,

$$\tau_R = \frac{4\pi \ell^2}{\eta} \quad ,$$

where ℓ is the length scale of the magnetic field variations.

In summary, the basic equations we shall use are (1.15) together with the equation of motion from (1.3) and (1.11)

$$\rho \left(\frac{\partial \underline{v}}{\partial t} + (\underline{v} . \underline{\nabla}) \underline{v} \right) = - \underline{\nabla} p + \frac{1}{4\pi} (\underline{\nabla} \wedge \underline{B}) \wedge \underline{B} \qquad (1.16)$$

1.1 : THE BASIC EQUATIONS (Contd.)

The equation of continuity,

$$\frac{\partial \rho}{\partial t} + \underline{\nabla} . (\rho \underline{v}) = 0 \qquad (1.5)$$

and the equation of state for a perfect gas,

$$p = R \rho T \qquad (1.17)$$

where R is the universal constant.

Equations (1.15), (1.16), (1.5) and (1.17) determine $\underline{v}$, $\underline{B}$, ρ and p and are supplemented by an energy equation for T, which we derive below.

The Energy Equation.

This is a statement of the first law of thermodynamics in a volume of the plasma. The increase of heat per unit time of a unit volume as it moves in space, $\rho T \frac{dS}{dt}$, is equated to the heat influx, $-\mathcal{L}$, due to various sources and sinks in the plasma:

$$\rho T \frac{dS}{dt} = - \mathcal{L}(\rho, T) \qquad (1.18)$$

where S, the entropy per unit mass of the plasma, is given by

$$T \frac{dS}{dt} = \frac{de}{dt} + p \frac{d}{dt}\left(\frac{1}{\rho}\right) \qquad (1.19)$$

in terms of the temperature T, the internal energy, e, per unit mass and the density ρ. The internal energy of an ideal gas is dependent only on the temperature T.

1.1.: THE BASIC EQUATIONS (Contd.)

When, as is usually the case, the energy is assumed to be proportional to T, the gas is called polytropic and we have

$$e = C_v T \ , \qquad (1.20)$$

where C_v is the specific heat at constant volume. Using equations (1.18), (1.19), (1.20) and the perfect gas law (1.17) we have

$$\frac{dp}{dt} - \frac{\gamma p}{\rho}\frac{d\rho}{dt} = -(\gamma-1)\mathcal{L}(\rho,T) \ ,$$

or alternatively, at constant pressure,

$$C_p \frac{dT}{dt} = -\frac{\mathcal{L}}{\rho} \ ,$$

where C_p is the specific heat at constant pressure. Normally the energy supplied by conduction is taken out of the $\mathcal{L}$ term which is then written as

$$\mathcal{L}(\rho,T) = L - \underline{\nabla}.(\underline{\underline{K}}.\underline{\nabla}T) \qquad (1.21)$$

where $\underline{\underline{K}}$ is the tensor coefficient of thermal condictivity. For heat conducted parallel to the magnetic field, the relevant coefficient of thermal conductivity is, from Spitzer (1962),

$$K_{11} = \delta_T \, 2\times10^{-5} \frac{T^{5/2}}{\ln.\Lambda} \ \text{ergs sec}^{-1}\,\text{deg}^{-1}\,\text{cm}^{-1} \qquad (1.22)$$

1.1.: THE BASIC EQUATIONS (Contd.)

where $\delta_T = 0.225$ for a hydrogen plasma. While, for heat conducted perpendicular to the magnetic field, the coefficient of thermal conduction is, also from Spitzer (1962),

$$K_\perp = 1{\cdot}5 \times 10^{-25} \frac{n_i^2 \ln.\Lambda}{T^{1/2} B^2} \text{ ergs sec}^{-1} \text{ deg}^{-1} \text{ cm}^{-1} \quad (1{\cdot}23)$$

which is valid only for

$$\omega \tau \equiv 1{\cdot}1 \times 10^5 \frac{B T^{3/2}}{\ln.\Lambda \, n_i} >> 1 \, ,$$

where ω is the ion cyclotron frequency and τ is the ion collision time. Spitzer (1962) has tabulated values of the Coulomb logarithm which we reproduce here,

Values of $\ln.\Lambda$

n_e cm^{-3} / T °K	10^6	10^9	10^{12}
10^4	16·3	12·8	9·4
10^5	19·7	16·3	12·8
10^6	22·8	19·3	15·9
10^7	25·1	21·6	18·1

For most of the thesis we use $\ln.\Lambda = 20$. Also for many applications $K_\parallel >> K_\perp$, which has important effects that we shall consider later.

The energy equation then becomes

$$\rho C_p \frac{dT}{dt} = -L + \underline{\nabla} . (\underline{\underline{K}} . \underline{\nabla} T) \, , \quad (1.24)$$

where the operator $d/dt = \left(\partial/\partial t + (\underline{v} . \underline{\nabla}) \right)$.

1.1. : THE BASIC EQUATIONS (Contd.)

This is the form used throughout the thesis.

Various alternative forms of the energy equation can be derived by combining the energy equation with the equation of motion. Now the total energy per unit volume is

$$U = \frac{1}{2} \rho V^2 + \rho e \quad ,$$

ignoring gravity and magnetic field effects. Then, after differentiating this equation with respect to time and using equations (1.5), (1.16), (1.18), (1.19) and (1.21), we find

$$\frac{\partial U}{\partial t} + \underline{\nabla} . \left(\rho \underline{V} \left(\frac{1}{2} \underline{V}^2 + i \right) - K \underline{\nabla} T \right) = - L \quad , \qquad (1.25)$$

where $i = e + \frac{p}{\rho}$ is the enthalpy per unit mass.

Using equations (1.17) and (1.20) the enthalpy can also be written as

$$i = \frac{5}{2} \frac{k}{m} T \quad , \qquad (1.26)$$

where m is the average mass of the particles and k is Boltzmann's constant.

1.1.: THE BASIC EQUATIONS (Contd.)

The Energy sources and sinks in the Corona and Chromosphere.

In the last section we stated the energy equation (1.24) in terms of a general energy loss function L, which we will now discuss in more detail.

The amount of energy radiated out of a plasma has been calculated for an optically thin medium, as a function of temperature, by many authors (e.g. Cox and Tucker, 1969). A simplified version of this function has been used by Nakagawa (1970) and Hildner (1971), who represent the temperature variation by a piecewise linear function, so that the radiative loss per unit volume and time takes the form

$$L_{RAD} = \chi \rho^2 T^{\alpha},$$

in each of three temperature regions. The value of the constants, χ and α, taken from Hildner (1971) are

χ (ergs $sec^{-1} cm^3 g^{-2} T^{-\alpha}$)	α	
1.28×10^{36}	-1.8	$T > 2.5 \times 10^5$ °K
3.6×10^{26}	0	$5 \times 10^4 < T < 2.5 \times 10^5$ °K
9.2×10^{5}	4.37	$T < 5 \times 10^4$ °K

This simplified radiative loss function is plotted in Figure (1) page 14, along with those radiative loss functions calculated by several authors from which Hildner derived this approximate version.

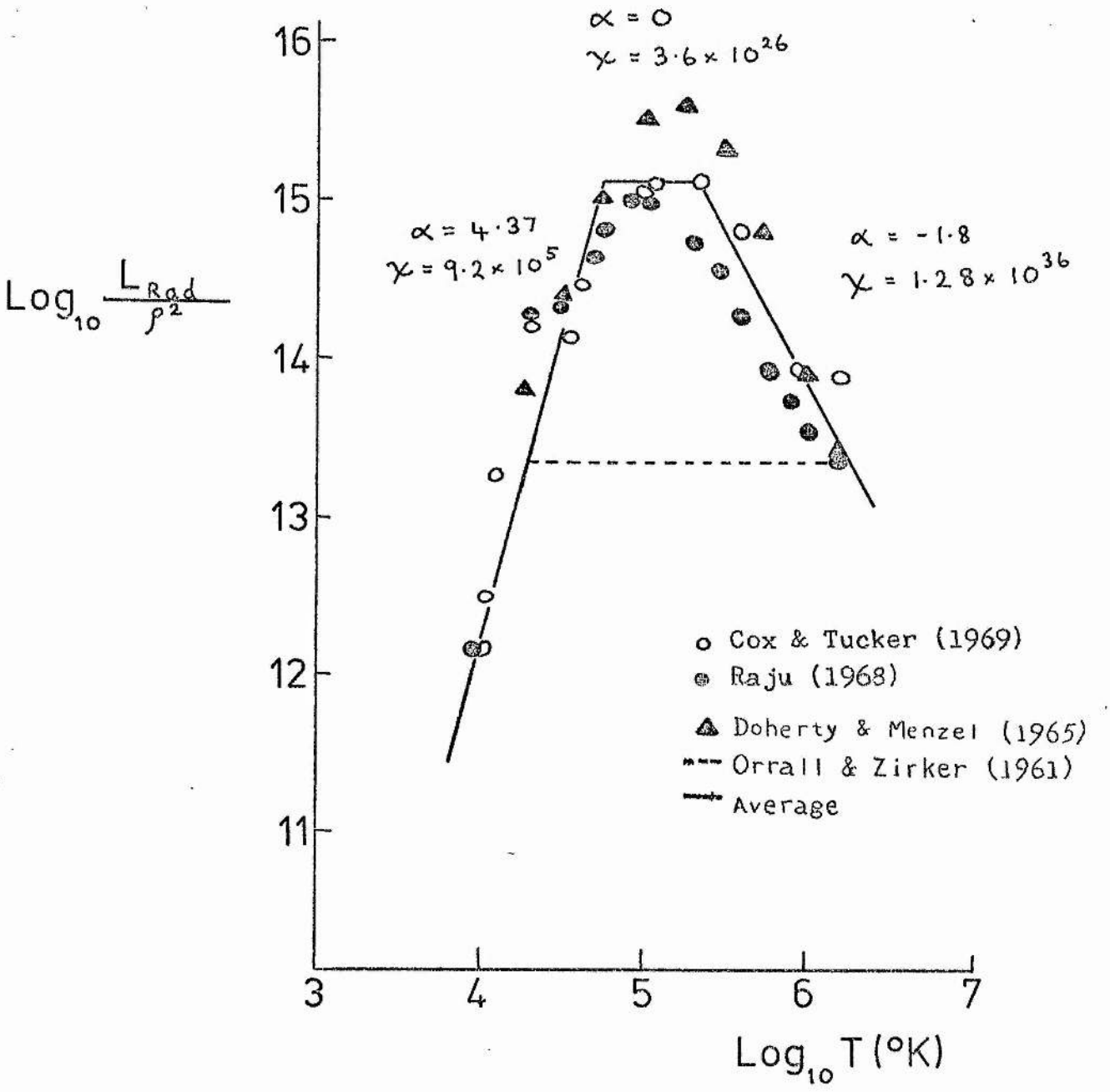

Figure (1). The radiative loss function per unit volume and time, $L_{RAD} \equiv \chi \rho^2 T^{\alpha}$ ergs sec^{-1} cm^{-3}, used in this thesis. It is the one devised by Hildner (1971), and is an approximation to the radiative loss , in an optically thin plasma calculated by several authors as a function of the temperature T. The various symbols represent the functions derived by each of the people shown.

1.1.: THE BASIC EQUATIONS (Contd.)

Hildner (1974) has also used a radiative loss function similar to this one but divided into five temperature regions. In this case χ and α are given by

χ (ergs $sec^{-1} cm^3 g^{-2} T^{-\alpha}$)	α	
4.96×10^{24}	-1.0	$T \geq 8 \times 10^5$ °K
3.55×10^{33}	-2.5	$3 \times 10^5 \leq T < 8 \times 10^5$
7.20×10^{19}	0	$8 \times 10^4 \leq T < 3 \times 10^5$
1.08×10^{11}	1.8	$1.5 \times 10^4 \leq T < 8 \times 10^4$
4.43×10^{-13}	7.4	$T < 1.5 \times 10^4$ °K

(1.27)

We have, however, decided to use his original function drawn in Figure (1) page 14. The function is unreliable for temperatures much below 10^5 °K, where radiative transfer effects become important.

The problem of how the corona is heated is not fully resolved, but the generally accepted mechanism (see, for example, Raju 1968) is that waves propagate up from the convective zone into the corona and steepen into shock waves which then dissipate and release their energy. The energy in a wave is transferred locally into kinetic energy of the particles that are subjected to the ordered forces of the wave. When a wave is dissipated the wave energy is thermalised by collisions into the kinetic energy of random motion.

1.1. : THE BASIC EQUATIONS (Contd.)

Thus dissipation is faster the more particles there are present. So the heat input by wave dissipation is generally assumed to be proportioned to density, as suggested by Weymann (1960). Thus an approximation to the heat input is

$$b\rho \ ,$$

where b is a constant that will in some of our models be determined by the equilibrium conditions in the corona and ρ represents the density.

It is assumed that b has the same value throughout the magnetic configurations we consider, but it could be that the heating mechanism is affected by a magnetic field. However, this effect, and also any temperature variation will, since they are not sufficiently well understood, be ignored.

In a recent paper by Pneuman & Kopp (1977), it has been suggested that material that has been carried up into the corona by spicules returns to the surface of the sun after being heated to coronal temperatures, and deposits this extra energy in the transition region.

1.1.: THE BASIC EQUATIONS (Contd.)

There have been several observations of a steady downflow of material at a few kilometers per second in the transition region overlying the chromosphere network. Pneuman & Kopp calculate that about 4×10^{15} particles cm^{-2} sec^{-1} are falling and note that this is about the same as the upward particle flux in spicules (Beckers, 1972) so they suggest that the downflow is simply matter returning after being carried into the corona by spicules.

The importance of the downflow is shown by comparing the energy that it releases with other energy sources and sinks in the transition region. The energy equation is, from equations (1.25) and (1.26)

$$\underline{\nabla} \cdot \left[N \underline{V} \left(\tfrac{1}{2} m V^2 + \tfrac{5}{2} kT \right) - K \underline{\nabla} T \right] = - L(\rho, T)$$

or, for one-dimensional (h) variations

$$\frac{1}{A} \frac{d}{dh} \left[q \left(\tfrac{5}{2} kT + \tfrac{1}{2} m V^2 \right) + A K_o T^{5/2} \frac{dT}{dh} \right] = L ,$$

where the effects of gravity and the magnetic fields are neglected. The only energy sources are the enthalpy per unit mass, $\iota = \frac{5}{2} \frac{k}{m} T$, and thermal conduction and the only energy sink that Pneuman & Kopp consider is radiation.

1.1.: THE BASIC EQUATIONS (Contd.)

The downward particle flux, taken as positive, is

$$q = N V A$$

where N is the number density, V the velocity, and A the fractional area of the solar surface occupied by the emission network. They comment that, since the flow is subsonic, the dominant energy source associated with the flow is the enthalpy flux.

The ratio R of the enthalpy flux to the conductive flux is

$$R = \frac{\frac{5}{2} k q T}{A K_0 T^{\frac{5}{2}} \frac{dT}{dh}} .$$

Pneuman & Kopp calculate R for the transition region by noting that the observed emission measure E =

$$A N_e^2 T (dT/dh)^{-1} \simeq 1.3 \times 10^{26} \text{ cm}^{-5} \text{ (Gabriel, 1976)}$$

Then with $V = -10$ km sec^{-1} , $T = 10^5$ °K

and $q = 10^{15}$ to 10^{16} cm^{-2} sec^{-1}

they get $R = 10$ to 100 .

Thus the enthalpy flux is larger than the conductive flux and so should certainly be included in any study of the transition region energetics. We have, however, not included it in the calculations of this thesis because the importance of this energy source has only recently been noted.

As far as the corona is concerned, the much cooler spicule matter extracts heat and so acts as a sink, but its importance relative to the other energy terms in the corona is not clear.

1.1.: THE BASIC EQUATIONS (Contd.)

We can, however, see that spicules can inject matter into the corona. We estimate the maximum height that particles will reach if they are projected vertically with the spicular velocity, u , under the influence of gravity, g :

$$h = u^2/2g$$

If u is the observed spicular velocity, 30 km sec^{-1} (Zirin, 1966), then $h = 1{\cdot}6 \times 10^8$ cm, which in our model atmosphere Figure (2) page 20 is at the base of the transition region, but if u is only slightly larger, 50 km sec^{-1}, then $h = 4{\cdot}6 \times 10^8$ cm which takes us into the corona.

Another possible energy source for prominences is gravitational energy released by vertical motions. Quiescent prominences are observed to have material flowing down at about 10 km sec^{-1} (Rompolt, 1967), which is very much less than the free fall velocity of 100 km sec^{-1}, so some of the potential energy is presumably converted into heat rather than kinetic energy of downward motion. Order of magnitude estimates by Raadu & Kuperus (1973) indicate that the release of this gravitational energy is as important as the radiative loss term for quiescent prominences. They point out that the gravitational energy would be released at the rate

$$\rho g V \simeq 2{\cdot}29 \times 10^{-14} \text{ ergs particles}^{-1} \text{ sec}^{-1}$$

for a vertical velocity V of 10^6 cm sec^{-1}.

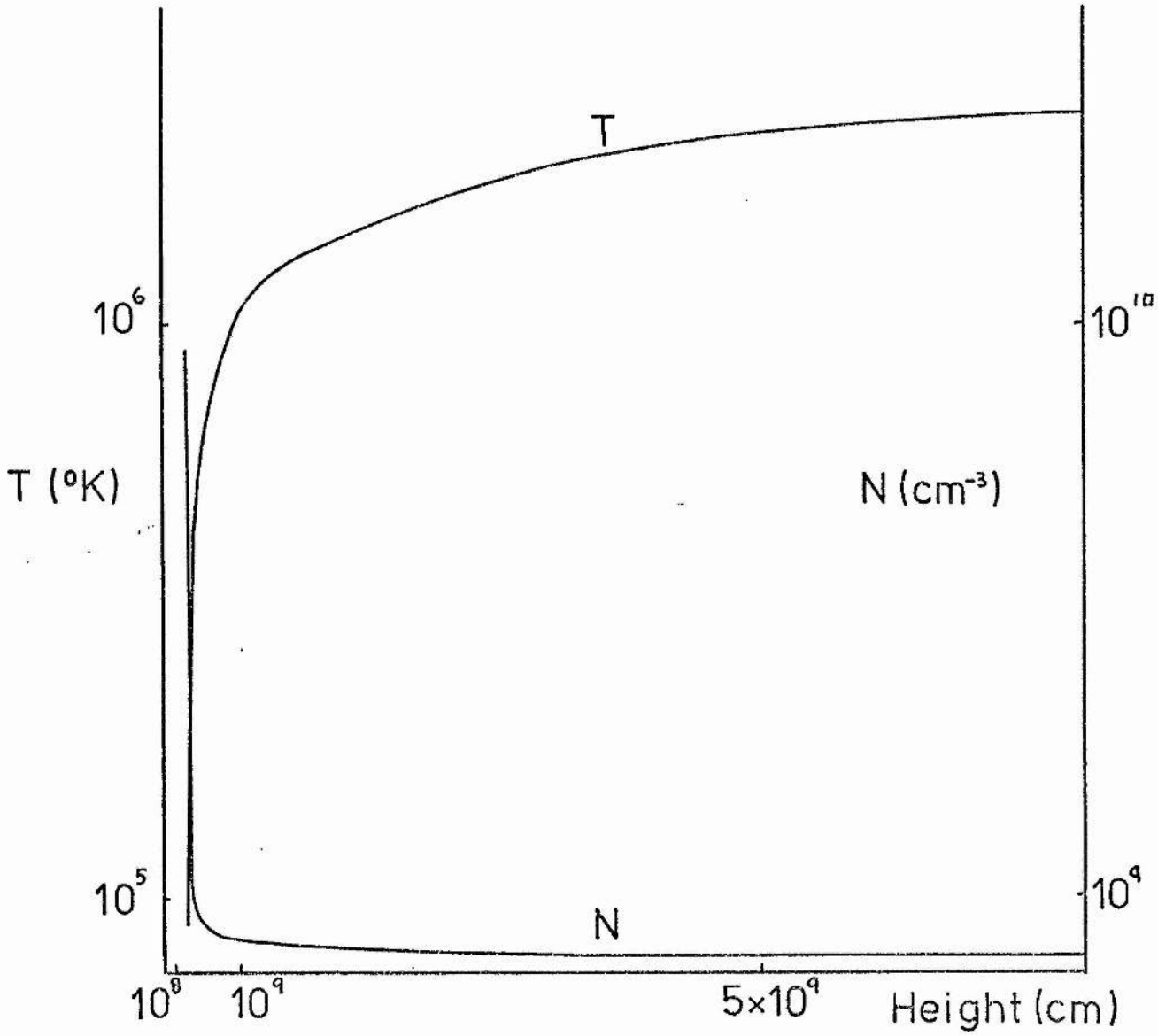

Figure (2). The Billings & Alvarez (1975) model for a quiet region of the chromosphere and corona. The temperature, T, and number density, N, are plotted as a function of height above the photosphere using values given in Table I.

1.1.: THE BASIC EQUATIONS (Contd.)

This is comparable to the radiative loss in prominence material

$$L_{RAD} \simeq 3 \times 10^{-14} \text{ ergs particle}^{-1} \text{ sec}^{-1} ,$$

where we have taken $n = 10^{11} \text{ cm}^{-3}$ and $T = 8 \times 10^{3} \, ^{\circ}K$

and also comparable to the radiative loss in the uncondensed coronal material (Cox & Tucker , 1969)

$$L_{RAD} \simeq 6 \times 10^{-14} \text{ ergs particle}^{-1} \text{ sec}^{-1}$$

$$\text{with} \quad n = 10^{9} \text{ cm}^{-3} \quad \text{and} \quad T = 1{\cdot}5 \times 10^{6} \, ^{\circ}K .$$

Thus this energy source should be important in neutral sheets in the corona and in prominences. However, it will, for simplicity, not be included in the energy equation.

The heating of the plasma by the current density is ηJ^2 ergs cm^{-3} sec^{-1}

where the electrical resistivity, η , is given by (1.4) as

$$\eta = 6{\cdot}53 \times 10^{12} \frac{\rho_n \Lambda}{T^{3/2}} \quad \text{e.m.u.}$$

This heating term will be neglected for prominences but we shall leave the justification until Chapter 2.

Finally, in summary, the energy equation that we shall use in the rest of the thesis is

$$\rho C_p \frac{dT}{dt} = b\rho - \chi \rho^2 T^{\alpha} + \underline{\nabla} . (\underline{\underline{K}} . \underline{\nabla} T) \qquad (1{\cdot}28)$$

where χ and α are given by Figure 1 page 14, $\underline{\underline{K}}$ is given by (1.22) and (1.23) and C_p is the specific heat at constant pressure.

1.2.: THERMAL INSTABILITY

ORDER OF MAGNITUDE DESCRIPTION

It was Parker (1953) who first pointed out that, if thermal conduction were ineffective, thermal instabilities would occur in the corona and upper chromosphere, because of the form of the radiative loss term in the energy equation. To illustrate this effect, suppose that the plasma is initially in equilibrium under a balance between a constant mechanical heating, h , and an energy loss by radiation. The energy lost by radiation per unit mass and time may for simplicity, be assumed to be proportional to density with a constant of proportionality $a = 6{\cdot}3 \times 10^{24}$ ergs cm^3 g^{-2} sec^{-1} (Orrall & Zirker, 1961), so that the equilibrium equation is

$$0 = h - a\rho_0 .$$

In his analysis, Parker assumed a temperature perturbation at constant density. However, as pointed out by Field (1965), such a perturbation is inconsistent with the equations of motion and continuity, since a temperature decrease leads to a pressure decrease, which produces an inflow of matter and so a density increase. So Field suggested that a constant pressure perturbation would be the relevant one. The perturbed density and temperature then satisfy the energy equation

$$c_p \frac{\partial T}{\partial t} = h - a\rho , \qquad (1.29)$$

1.2.: THERMAL INSTABILITY (Contd.)

where, from the equilibrium equation,

$$h = a \rho_0$$

and the perfect gas law at constant pressure p_0 gives

$$p_0 = R \rho T .$$

A reduction in temperature from equilibrium therefore causes an increase in density, which in turn makes $\partial T/\partial t$ negative according to (1.29) and so drives the instability. Similarly, an increase in temperature causes the plasma to heat up. The time scale for this thermal instability, driven by radiative loss, is found by equating the orders of magnitude on both sides of (1.29) to be

$$t_R = \frac{C_p T}{a \rho} .$$

However, in general the coronal plasma is not unstable. The conduction of heat prevents the thermal instability from developing, since the heat is, in many situations, transported more rapidly by conduction than by radiation. In a flux tube or a current sheet of length L, the time scale for heat to be conducted along the distance L is

$$t_c = \frac{L^2 \rho C_p T}{K_{\parallel} \Delta T} ,$$

where $K_{\parallel}$, the coefficient of thermal conductivity along the field lines is, from (1.22), for coronal conditions ($T = 10^6 {}^\circ K$, $n = 10^8 \text{ cm}^{-3}$, $B = 1$ Gauss)

$K_{\parallel} = 2 \times 10^{-6} T^{5/2}$ ergs deg^{-1} sec^{-1} cm^{-1},

and ΔT is the temperature difference between the interior of the flux tube or sheet and its ends.

1.2.: THERMAL INSTABILITY (Contd.)

This time scale, t_c , may be compared with the radiative time scale t_R . The plasma is stabilized by thermal conduction $t_c < t_R$.

However, if the length of the flux tube or sheet is so large that $t_c > t_R$, then the destabilizing effect of the radiative loss term dominates and the plasma is cooled or heated. The critical length above which the flux tube or sheet becomes unstable is given by equating t_c and t_R as

$$L_c = \sqrt{\left(\frac{K_{\parallel}\Delta T}{a\rho^2}\right)}$$

If $T = 10^6\,^{\circ}K$ and $\rho = 2\times10^{-16}\ g\ cm^{-3}$, characteristic of the lower corona, then with $\Delta T = T/10$ we find

$$L_c \simeq 3\times10^{10}\ cm .$$

It may be noted that this value of L_c is the same in order of magnitude as the height of a large quiescent prominence or the length of a large X-ray loop.

The value of L_c is important because it gives an order of magnitude estimate of the length at which a current sheet or flux loop becomes thermally unstable. A better estimate, which we call L_{crit} , for such a critical length can be found by using the less crude approximation for the radiative loss term, namely

$$L_{RAD} = \chi\,\rho\,T^{\alpha}\ ergs\ sec^{-1}\ g^{-1},$$

where χ and α are given on Figure (1) page 14.

If $\Delta T \simeq T$, the corresponding critical length is found to be given by

$$L^2_{crit} = \frac{T^{7/2-\alpha}}{\chi\,\rho}\,3\times10^{-6} \qquad (1.30)$$

1.2.: THERMAL INSTABILITY (Contd.)

it is plotted in Figure (3) page 26 as a function of height for the model chromosphere and corona drawn in Figure (2) page 20. The model atmosphere on which this is based, Billings & Alvarez (1975), measures height from the centre of the transition region ($T = 10^5 °K$) and so, in order to give the variation of L_{crit} with height above the photosphere, it has been assumed that this point in the transition region is $2{\cdot}4 \times 10^8$ cm above the photosphere (Vernazza, Avrett and Loeser, 1973). There are two main sources of error in using L_{crit} to estimate the length at which a current sheet or flux loop becomes thermally unstable. It approximates ΔT by the temperature T outside the tube or sheet and the value of the density inside by its value outside. A more accurate value of the length at which instability first occurs for a current sheet is given in Chapter 2.

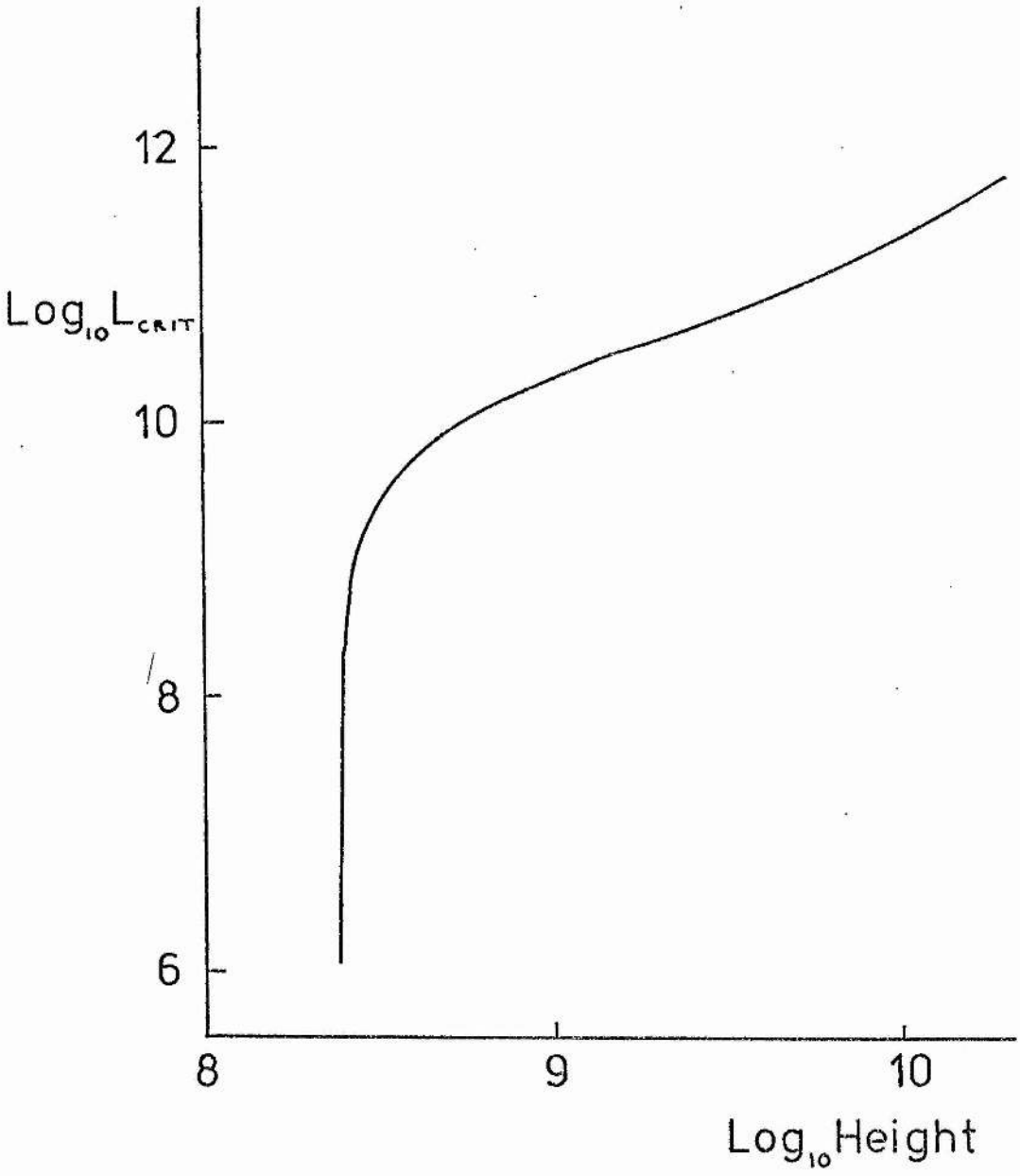

Figure (3). The critical value L crit (cm) from equation (1.30) as a function of height (cm) for the atmosphere model given in Figure (2), page 20. L crit is the order of magnitude estimate for the length of a current sheet or magnetic flux tube above which a thermal instability occurs.

1.2.:PREVIOUS WORK ON THERMAL INSTABILITY

Parker (1953) suggested that, if the thermal equilibrium of the medium is a balance between temperature-independent energy gains and temperature-dependent radiative losses, instability results if, near equilibrium the losses increase with decreasing temperature. Then the cooler-than-average region cools more effectively that its surroundings, and its temperature rapidly drops below the initial equilibrium value.

Other authors, notably Zanstra (1955 a,b) pointed out that the strong tendency towards pressure equilibrium in the medium would naturally result in compression of the cool regions and expansion of the hot ones and in this way one could understand the formation of cool condensations in a medium of high temperature.

Field (1965) in a thorough analysis of this problem points out however that Weymann (1960) was the first to give the correct instability criterion for the formation of a condensation due to thermal instability. Field analysed the different possible instability criteria in an infinite, initially stationary uniform medium in the absence of magnetic fields, using the linearized equations. For the equilibrium energy equation, he takes

$$L(\rho_0, T_0) = 0, \qquad (1.31)$$

where L is a genealised heat loss function, defined as energy losses minus energy gains per volume per second. Because the equilibrium temperature is uniform, L does not include thermal conduction.

1.2.: PREVIOUS WORK ON THERMAL INSTABILITY (Contd.)

It can be written as a function of the local values of ρ and T if the gas is optically thin, because then the heat loss function is not complicated by radiative transfer effects. We now perturb the equilibrium in density and temperature while keeping some thermodynamic variable A (e.g. pressure) constant. In the energy equation the entropy S is perturbed to $S_0 + S_1$ and the heat loss function to $L_0 + L_1$, both S_1 and L_1 being calculated at constant A. Then the energy equation becomes

$$-\rho T \frac{dS}{dt} = L_1 \equiv \left(\frac{\partial L}{\partial S}\right)_A S_1 ,$$

so that there is instability if

$$\left(\frac{\partial L}{\partial S}\right)_A < 0 .$$

In an isobaric perturbation A is pressure and $T\,dS = C_p\,dT$ so that the instability criterion becomes

$$\left(\frac{\partial L}{\partial T}\right)_p = \left(\frac{\partial L}{\partial T}\right)_\rho - \frac{\rho_0}{T_0}\left(\frac{\partial L}{\partial T}\right) < 0 , \quad (1.32)$$

the perfect gas law being assumed applicable.
This condition, as Field pointed out, is consistent with the equation of motion because the lack of pressure variations ensures that no forces will destroy the density structure. Hunter (1970) has genealised this stability criterion to include an arbitrary flow in the equilibrium structure and thermal conduction in the heat loss function L.

1.2.: PREVIOUS WORK ON THERMAL INSTABILITY (Contd.)

He shows that there is thermal instability if

$$\rho_u \left(\frac{\partial L}{\partial \rho}\right)_{T_u} - T_u \left(\frac{\partial L}{\partial T}\right)_{\rho_u} + L_u > 0 ,$$

where the subscript u refers to variables in an unperturbed flow. This reduces to Field's criterion in a uniform medium in the absence of effects of thermal conduction, since $L_u = 0$ in that case.

The isochoric perturbation, for which A is density, has the instability criterion,

$$\left(\frac{\partial L}{\partial T}\right)_{\rho} < 0 ,$$

and is the one given by Parker (1953).
If entropy S is kept constant during the perturbations the isentropic instability criterion is

$$\left(\frac{\partial L}{\partial T}\right)_{s} = \left(\frac{\partial L}{\partial T}\right)_{\rho} + \frac{1}{\gamma - 1} \frac{\rho_0}{T_0} \left(\frac{\partial L}{\partial \rho}\right)_{T} < 0 . \quad (1.33)$$

For instance the near-isentropic oscillations in a sound wave are subject to a slight heating during the compression phase, which tends to increase the amplitude of the wave. Hunter (1966) applied this instability to small amplitude disturbances in the chromosphere and suggested that the optical flare event could result from the formation of shock waves when these chromospheric waves became thermally overstable. However, we shall be concerned here only with the condensation mode thermal instability, which is governed by the isobaric criterion equation (1.32).

1.2.: PREVIOUS WORK ON THERMAL INSTABILITY (Contd.)

The thermal instability was applied by Kleczek (1958) and Lust & Zirin (1960) to the theory of active prominences. These loop prominences or 'coronal-rain' prominences seem to condense out of the corona, above active regions, in a few minutes. Kleczek (1958) considered an equilibrium energy equation of the form

$$L = L_{RAD} - G_{COMP} \quad .$$

The coronal matter was first compressed by some undefined process, and then allowed to cool by radiation. Kleczek did not include the effect of thermal conduction and found the time for condensation to be quite long: 10^5 - 10^7 seconds.

Lust & Zirin (1960) pointed out that the temperature in the initial compression would become very high so that conduction becomes an important energy sink. In their work they considered coronal plasma with density n_o, temperature T_o in a magnetic field H. An element of this plasma in some tube of force, is subjected to a radial compression, resulting in a density increase

$$n = n_o (1 + \alpha t) \quad .$$

If this compression is adiabatic then

$$T/T_o = (1 + \alpha t)^{\gamma} \quad ,$$

where

$$\gamma = C_P/C_V = 5/3 \quad .$$

The energy acquired in a unit time by each particle of the plasma due to compression is

$$G_{COMP} = \frac{3}{2} k \frac{dT}{dt} = \frac{3}{2} k T_o \alpha \gamma (1 + \alpha t)^{\gamma - 1} \quad .$$

1.2.: PREVIOUS WORK ON THERMAL INSTABILITY (Contd.)

The energy losses in the compressed tube are due to radiation and thermal conduction. Owing to the magnetic thermal insulation, there is a heat flux only through the end surfaces of the tube, of magnitude

$$\frac{dQ}{dt} = K_0 T^{5/2} \frac{dT}{dr} 2\pi r^2 ,$$

where r is the radius of the tube. Hence the heat loss from thermal conduction for each particle in the plasma per unit time is

$$L_{therm} = \frac{2 \times K_0 T^{5/2} \Delta T}{n \ell^2} ,$$

where $dT/dr \simeq 2\Delta T/\ell$ and ℓ is the length of the tube. Lust & Zirin estimated the energy loss to the plasma by radiation per particle to be

$$L_{RAD} = 1.92 \times 10^{-27} \alpha t T^{1/2} - \frac{1.26 \times 10^{-8} \alpha t}{T} \left[\frac{kT}{2} + 1.08 \times 10^{-10} \right].$$

Hence the energy balance can be written as

$$k \frac{dT}{dt} = G_{COMP} - L_{therm} - L_{RAD} .$$

The solution to this equation, $T(t)$, was found for a series of values of α and T_0. Lust & Zirin found that the temperature first increases to a maximum, T_{max} at a time, t_{max}, due to the initial compression, and then decreases as the increased internal energy is radiated and conducted away. They defined a cooling time, t_{cool}, as the time taken to cool the plasma to a temperature of 2×10^5 °K. The higher the compression rate α, the faster the initial temperature increases, but the subsequent cooling is also faster.

1.2.: PREVIOUS WORK ON THERMAL INSTABILITY (Contd.)

With T_o in the range $1 - 2 \times 10^6$ °K and $n = 10^9 - 10^{10}$ cm^{-3}, values of $10^{-3} - 10^{-2}$ sec^{-1} for α make t_{max} of the order of ½ hour or less and t_{cool} an hour or less, which seems reasonable for the formation of active prominences. However, the means by which compression is achieved is unclear.

Raju (1968) considered an infinitely long cylindrical magnetic flux tube containing an optically thin plasma. He assumed that the plasma is heated by the dissipation of waves propagating up from the chromosphere. Such mechanical heating per unit mass is assumed to have the constant value,

$$G_{mech} = \alpha \,, \qquad (1.34)$$

where α is determined by the thermal equilibrium conditions in the corona. Raju considered the plasma to be cooled by radiation

$$L_{RAD} = \rho\, Q(T) \qquad (1.35)$$

the cooling function Q(T) being more realistic than the one used by Lust & Zirin. Raju used two cooling functions, one by Doherty & Menzel (1965) and the other by Raju (1968).

To produce instability in this case he perturbed the density while holding pressure constant, as in (1.32). An assumption that the total pressure remains constant gives

$$p + (B^2/8\pi) = p_o + (B_o^2/8\pi) \,, \qquad (1.36)$$

where p_o and B_o are the equilibrium values.

1.2.: PREVIOUS WORK ON THERMAL INSTABILITY (Contd.)

The energy equation is

$$\frac{dp}{dt} = \gamma \frac{p}{\rho} \frac{d\rho}{dt} + (\gamma-1)\rho\,[G - L] \qquad (1.37)$$

with $\gamma = \frac{5}{3}$, and

$$p = R \rho T \,. \qquad (1.38)$$

Another equation is still required in order to solve for the four unknowns p, ρ, T, B inside the flux tube. Raju assumed that the plasma and magnetic field would remain uniform inside and outside the cylinder, so any variation in the parameters is one-dimensional and the particle density in the cylinder at any time is inversely proportional to the square of the radius. Thus, from conservation of magnetic flux,

$$\frac{B}{\rho} = \frac{B_0}{\rho_0} \,. \qquad (1.39)$$

Raju solved (1.34) to (1.39) to give, in particular, ρ/ρ_0 as a function of time and found that after an initial perturbation the condensation rate is very slow until some threshold time when the density increases very rapidly. For larger initial perturbations the threshold time was a little smaller. His results depend strongly on

$$\beta \equiv 8\pi p_0 / B_0^2 \,.$$

For $\beta \gg 1$ the magnetic field inhibits the thermal conduction but plays no other role; the density drops by a factor of 60 while temperature drops from 1.5×10^6 to 2.5×10^4 in about 10^6 seconds.

1.2.: PREVIOUS WORK ON THERMAL INSTABILITY (Contd.)

For $\beta > 1$, compression of the cylinder quickly raises the magnetic pressure until the gas pressure p is unimportant in the isobaric condition (1.36). When $\beta = 50$ the density increases only by a factor of 6.7 while the temperature drops from 1.5×10^6 to 3×10^4 in about 1.6×10^6 seconds.

When $\beta \ll 1$ the cylinder behaves as if it were filled with an incompressible fluid. In this case a small percentage increase in magnetic field strength yields a magnetic pressure which can balance even an extreme decrease in interior gas pressure produced by cooling, so that, from (1.39), the density remains almost constant. With a small density perturbation, the density remains almost constant, while the temperature falls from 1.5×10^6 to 3×10^4 in about 3×10^6 seconds.

Raju showed that prominence conditions are reached in about 10^6 seconds, which is a little long compared with the observed formation time of about 10^5 seconds. But he also pointed out that intensification of the magnetic field produced by condensation effectively prevents the density from increasing to prominence values if the final prominence value for the magnetic field is greater than approximately 0.1 Gauss, which is much less than the observed value of 10 Gauss. It should, however be noted that, in this model, Raju has neglected motions along the flux tube, and we would expect, in the strong magnetic field case, that prominence densities could be reached if these motions are included.

1.2.: PREVIOUS WORK ON THERMAL INSTABILITY (Contd.)

Hildner (1974) solved the non-linear time-dependent MHD equations in an attempt to model the formation of solar quiescent prominences by condensation out of the corona. The effects of gravity were included and so the equations were

$$\frac{\partial \rho}{\partial t} + \underline{\nabla}.(\rho \underline{V}) = 0 \ ,$$

$$\rho \frac{d\underline{V}}{dt} = -\underline{\nabla} p + \frac{1}{4\pi}(\underline{\nabla} \wedge \underline{B}) \wedge \underline{B} + \rho \underline{g} \ ,$$

$$\frac{\partial \underline{B}}{\partial t} + \underline{\nabla} \wedge (\underline{V} \wedge \underline{B}) = 0 \ .$$

He wrote his energy equation, for computational reasons, in the form

$$\frac{\partial u}{\partial t} + \underline{\nabla}.S + L = 0 \ ,$$

where the total energy density U, is

$$u = \frac{p}{\gamma - 1} + \frac{1}{2}\rho V^2 + \frac{B^2}{8\pi} + \rho g z$$

and z is the vertical co-ordinate, parallel to gravity The energy flow, S, the Poynting vector, is

$$\underline{S} = \underline{E} \wedge \underline{B} + \left(\frac{\gamma p}{\gamma - 1} + \frac{1}{2}\rho V^2\right)\underline{V} \ .$$

Thermal conduction is not included in the energy equation. In equilibrium the heat loss function L vanishes, where L is a balance between the radiative loss

$$L_{RAD} = \chi \rho^2 T^{\alpha} \ ,$$

defined earlier, and a mechanical heating

$$G_{mech} = \phi_1 \rho + \phi_0 \ ,$$

1.2.: PREVIOUS WORK ON THERMAL INSTABILITY (Contd.)

The constants ψ_1 and ψ_0 are determined by equilibrium conditions in the corona, at temperature $T = 5 \times 10^5$ °K, and in the final prominence with temperature T = 6500°K and with a constant pressure assumption. Initially, he also assumes that there is a uniform magnetic field in the x direction where the $x - z$ plane is perpendicular to the long axis of the prominence and z is parallel to gravity. He considers a two-dimensional geometry in the $x - z$ plane, which is reasonable since the prominence is very much longer than it is high or wide so that y variations are much less important than the other spatial variations.

At the boundary of a rectangular domain in the $x - z$ plane the variables T, ρ and p are held constant at their equilibrium values, while B remains horizontal there. The equilibrium with $\underline{L} = 0$ and $\underline{v} = 0$ is then disturbed by an isobaric 5% density increase in a small region near the centre of the domain of calculation and the resulting cooling is followed by solving the equation numerically.

Hildner considers four particular cases:

(1) $B_0 = g = 0$

In this case the sound speed is very much greater than the Alfvén speed, so that the condensation proceeds isobarically and also, because there are no fields to direct the motion, isotropically.

1.2.: PREVIOUS WORK ON THERMAL INSTABILITY (Contd.)

The inflow is gentle at first but rapidly increases as cooling drives on the instability. The maximum density of condensation, at $t = 3.5 \times 10^4$ sec, is approximately 18 times the initial equilibrium value. The condensation does not reach the final equilibrium because the conditions at the boundary begin to be affected by the condensation.

(2) $B_0 = 0 \quad g \neq 0$

In this case denser matter forms at the centre and falls under gravity, generating vortices as it does so. Again the condensation is isobaric but large condensations are not achieved because the plasma falls more rapidly than it condenses. This indicates that some support for the condensation is required if prominence densities are to be achieved.

(3) $B_0 \neq 0 \quad g = 0$

In this case the condensation proceeds at a similar rate to case (1) but the matter is compelled to flow along the field lines even for fields as small as 0.1 Gauss. The horizontal flow speeds are larger than in Case (1) to compensate for the reduced vertical flow.

(4) $B_0 \neq 0 \quad g \neq 0$

All the effects of cases (1) and (3) are combined in this example. The strength of the field is important in determining the reaction of fluid to the instability.

1.2.: PREVIOUS WORK ON THERMAL INSTABILITY (Contd.)

(4) $B_0 \neq 0$ $g \neq 0$ (contd.)

If the field is so weak that $C_S/C_A > 1$, the denser region falls, accompanied by a vortical flow pattern and the field is deformed by the fluid flow only in the vicinity of the falling condensation. In a strong field ($C_S/C_A < 1$) the vortical motion is suppressed and a slight increase in density causes the fluid to flow down everywhere, so that it reacts as a rigid body. It would have been of interest to take account, if possible, of line-tying at the boundaries.

In all these cases prominence conditions were not achieved, because the disturbance reached the edge of the domain before that was possible. However, the general trend of the thermal instability in the non-linear limit is clearly established. It seems that non-linear dynamical effects, which are included in this numerical study of the problem, make the instability grow more rapidly than in studies where the dynamics of the problem are neglected as, for example, in Raju (1968).

Heyvaerts (1974) considered a uniform, perfect, fully ionized gas with a uniform magnetic field, B_0, in the z direction. He also assumed there was a current $\underline{J}_0$ flowing parallel to $\underline{B}_0$ in this equilibrium state. In order to do this he considered wave numbers k such that

$$\frac{1}{k} \ll L_0 \equiv \frac{B_0}{4\pi J_0} , \qquad (1.40)$$

where zero subscripts refer to the equilibrium state.
The equations he considered are

$$\left.\begin{aligned}
&\underline{\nabla} \wedge \underline{B} = 4\pi \underline{J} \ , \\
&\underline{\nabla} \wedge \underline{E} = -\frac{\partial \underline{B}}{\partial t} \ , \\
&\underline{\nabla} . \underline{B} = 0 \ , \\
&\underline{J} = \underline{\underline{\sigma}} . (\underline{E} + \underline{V} \wedge \underline{B}) \ , \\
&\frac{\partial \rho}{\partial t} + \underline{\nabla} . (\rho \underline{V}) = 0 \ , \\
&\rho \left(\frac{\partial \underline{V}}{\partial t} + (\underline{V} . \underline{\nabla}) \underline{V} \right) = -\underline{\nabla} p + \underline{J} \wedge \underline{B} \ , \\
&\left(\frac{\partial p}{\partial t} + (\underline{V} . \underline{\nabla}) p \right) - \gamma \frac{p}{\rho} \left(\frac{\partial \rho}{\partial t} + (\underline{V} . \underline{\nabla}) \rho \right) = \\
&(\gamma - 1) \left(\frac{J^2}{\sigma} - L(\rho, T) + \underline{\nabla} . (\underline{\underline{K}} . \underline{\nabla} T) \right) .
\end{aligned}\right\} \quad (1.41)$$

In the energy equation, he has included joule heating, thermal condition and an energy loss term defined by

$$L(\rho, T) = -H\rho + \rho^2 Q(T) \ , \quad (1.42)$$

the amount of energy lost per unit time and unit volume due to radiative loss and mechanical heating.
The radiative loss term is that used by Raju (1968).
The equilibrium state is given by

$$\underline{V}_0 = 0 \ , \quad \underline{B}_0 = (0, 0, B_0) \ ,$$

$$J_0^2/\sigma_0 + H\rho_0 - \rho_0^2 Q(T_0) = 0 \ .$$

This state is then perturbed by a small amount, where the perturbed quantities have the form

$$f_1(\underline{r}, t) \propto e^{i(\omega t - \underline{k} . \underline{r})} \ .$$

1.2.: PREVIOUS WORK ON THERMAL INSTABILITY (Contd.)

Equations (1·41) are linearized by ignoring terms of order f_1^2 and then all the variables are eliminated except velocity. This gives a dispersion relation

$$\det. D_{ij}(\omega, K) = 0 \quad ,$$

which is approximated by means of an expansion in terms of order $(kL_0)^{-1} << 1$ by (1·40).

Heyvaerts finds four solutions:

$$\omega = i\omega_1 \quad , \tag{1.43}$$

(for which $V_y \neq 0$ or $V_x \neq 0$ and $V_z \neq 0$)

$$D + \Delta = 0 \, , \tag{1.44}$$

$$\omega^4(\omega - i\omega_1) - \omega^2 k^2 \left[\frac{C_A^2}{D}(\omega - i\omega_1) + C_S^2(\omega - i\omega_2)\right]$$

$$+ k^2 k_{11}^2 \frac{C_A^2 C_S^2}{D}(\omega - i\omega_2) = 0 \, , \tag{1.45}$$

(for which we only have $V_x \neq 0$ and $V_z \neq 0$) and

$$k_{11}^2 C_A^2 - \omega^2 (D + \Delta) = 0 \tag{1.46}$$

(for which $V_y \neq 0$).

The various constants are defined to be

$$\omega_\rho = \frac{L'_\rho \rho_0}{\rho_0} \quad , \qquad k_{11} = k \cos\theta$$

$$\omega_T = \frac{L'_T T_0}{\rho_0} \quad , \qquad k_\perp = k \sin\theta$$

$$\omega_J = \frac{J_0^2}{\sigma_0 \rho_0} \quad ,$$

1.2.: PREVIOUS WORK ON THERMAL INSTABILITY (Contd.)

$$\omega_s = \frac{k^2}{4\pi\sigma_0} \quad ,$$

$$\omega_c = (\underline{k}\,.\,\underline{\underline{K}}\,.\,\underline{k})\,\frac{T_0}{p_0} \quad ,$$

$$\omega_1 = (\gamma-1)\left(-\omega_T - \frac{\partial \log \sigma_0}{\partial \log T_0}\,\omega_J - \omega_c\right) \quad ,$$

$$\omega_2 = \frac{(\gamma-1)}{\gamma}\left(\omega_p - \omega_T - \frac{\partial \log \sigma_0}{\partial \log T_0}\,\omega_J - \omega_c\right) \quad ,$$

$$D \equiv 1 + i\,\frac{k^2}{\omega\, 4\pi\sigma_0} \quad ,$$

which measures the importance of diffusion, and

$$\Delta \equiv 2(\gamma-1)\left(\frac{\partial \log \sigma_0}{\partial \log T_0}\right)\frac{\omega_J}{\omega - i\omega_1}\,\frac{k_\perp^2}{\omega\, 4\pi\sigma_0} \quad ,$$

which measures the importance of the Joule effects.

When $\sigma_0 = \infty$ and no thermal effects are included (so that $\omega_1 = \omega_2 = 0$), equations (1.43) to (1.46) give the usual MHD modes. In this limit, (1.45) becomes

$$\omega^5 - \omega^3\left[C_A^2 + C_S^2\right] + k^4 \cos^2\theta\; C_A^2\, C_S^2\, \omega = 0 \quad ,$$

which has roots

$$\omega^2 = k^2\, C_R^2 \quad ,$$

$$\omega^2 = k^2\, C_L^2 \quad ,$$

$$\omega = 0$$

where C_R and C_L are the fast and slow phase speeds.

1.2.: PREVIOUS WORK ON THERMAL INSTABILITY (Contd.)

Also, when the magnetic and joule effects are neglected (so that $\omega_J = C_A = 0$), equation (1.45) gives Field's modes,

$$\omega^2(\omega - i\omega_1) = k^2 C_s^2 (\omega - i\omega_2) .$$

When $\sigma_0 = \infty$ (so that $D = 1$ and $\Delta = 0$), equation (1.46) gives Alfvén waves,

$$\omega = k_{\parallel} C_A .$$

However, in the diffusion region, an expansion to zero order in the small parameter (ω/ω_s) reduces equation (1.45) to

$$D + \Delta = 0 .$$

This is just equation (1.44) in the diffusion region, and will be considered later.

After pointing out these simple cases, Heyvaerts discusses the solutions to equations (1.43) to (1.46) in general.

$\omega + i\omega_1$ is the purely thermal mode, and its physical nature is determined by whether thermal conductivity is important or not. When thermal conduction dominates (i.e. over short wavelengths)

$$\omega = -i(\gamma-1) \frac{\underline{k} \cdot \underline{\underline{\kappa}} \cdot \underline{k}}{\rho_0} T_0$$

and so the plasma is stable. If thermal conduction is not important (i.e. over long wavelengths), then

$$\omega = i(\gamma-1)\left(-\frac{L_T' T_0}{\rho_0} - \frac{\partial \log \sigma_0}{\partial \log T_0} \frac{J_0^2}{\sigma_0 \rho_0}\right)$$

1.2.: PREVIOUS WORK ON THERMAL INSTABILITY (Contd.)

and so we get instability ($\Im m.(\omega) > 0$) if, using L as defined by (1.42),

$$\frac{dQ_0}{dT_0} < -\frac{J_0^2}{\sigma_0 \rho_0^2} \frac{1}{T_0} \frac{\partial \log \sigma_0}{\partial \log T_0} .$$

The joule term has a stabilizing effect, because σ_0 is proportional to $T_0^{3/2}$, so, if the temperature goes up, the joule heating goes down, thereby restoring the previous thermal balance.

The second set of modes satisfy equation (1.44), which may be written

$$\omega(\omega - i\omega_1) + i\frac{k^2}{4\pi\sigma_0}(\omega - i\omega_1) + 2(\gamma-1)\frac{\partial \log \sigma_0}{\partial \log T_0}\omega_J \frac{k^2 \sin^2\theta}{4\pi\sigma_0} = 0.$$

When $J_0 = 0$, this splits into the thermal mode, $\omega = i\omega_1$, and the mode

$$\omega = -i\frac{k^2}{4\pi\sigma_0} ,$$

which describes field diffusing through the plasma.

When J_0 does not vanish, the two effects are mixed.

Two regimes are of interest:

(1) The Frozen-in regime ($\omega >> \omega_s$) In this case with joule effects dominating and $\theta \simeq \pi/2$

$$\omega = i\frac{k^2}{4\pi\sigma_0}\frac{\sin^2\theta - \cos^2\theta}{\cos^2\theta} .$$

In mainly perpendicular propagation ($\sin^2\theta >> \cos^2\theta$) we have an 'anti-diffusion mode'.

1.2.: PREVIOUS WORK ON THERMAL INSTABILITY (Contd.)

The physics of this mode is that inequalities in the joule heating produce more conductive regions, where the temperature is higher. This causes the currents to flow preferentially in these regions, hence increasing the joule heating. The net effect is to concentrate the currents into thin threads, just like the tearing mode, as if there were an 'anti-diffusion' of the field.

(2) The Diffusion regime ($\omega \ll \omega_s$)

An expansion in ω/ω_s gives

$$\omega = -i(\gamma-1)\left(\frac{p_o^2 Q_o}{p_o} \frac{d\log Q_o}{d\log T_o} + \frac{\underline{k}.\underline{\underline{K}}.\underline{k}}{p_o} T_o - \frac{J_o^2}{\sigma_o p_o} \frac{d\log \sigma_o}{d\log T_o} (\sin^2\theta - \cos^2\theta) \right)$$

When thermal conductivity dominates, the mode is stable ($i\omega < 0$), but when thermal conduction is neglected and $|\omega_T| \ll |\omega_J|$ the mode has cooling properties. So we get a thermal mode driven mainly by joule effects and called by Heyvaerts the "Joule Mode". It is unstable when $\sin^2\theta > \cos^2\theta$ and the thermal conduction is negligible, which occurs in practice only for perpendicular propagation. The effect of the instability is again to form fine structures, aligned to the field, consisting of hot conductive tubes in which most of the current flows, with cold tubes in between. These structures can exist side by side because we are assuming that thermal conductivity is small. Also because the motions are not frozen-in, the instability is not upset at a later stage by non-linear developments.

1.2.: PREVIOUS WORK ON THERMAL INSTABILITY (Contd.)

However, although thermal conductivity perpendicular to the field is small, and has been neglected in this linear analysis, it could become important in the non-linear development, and impede the instability. Heyvaerts points out, however, that these anti-diffusion and joule modes are not important in the normal conditions of the solar atmosphere, because the plasma is very conductive. However, if the resistivity is increased by turbulence, then the growth rate of the instability will also increase. If the resistivity is enhanced by a factor K say, the growth rate would be of the order of

$$\omega_J \simeq \frac{K J_0^2}{\sigma_0 P_0} ,$$

which could be short.

The effect of the anti-diffusion mode in making the fields and currents coalesce instead of diffusing would favour the development of the joule mode. He suggests that these modes may be important in some active phenomena, such as transitory absorbing features (Axisa et al. , 1973), in which observations suggest there are hot emission regions very close to cool absorbing regions. So the hot and cool regions set up by the joule and anti-diffusion modes could be relevant.

1.2.: PREVIOUS WORK ON THERMAL INSTABILITY (Contd.

Lastly we discuss the solutions to equation (1.45), only under frozen-in conditions ($k^2 \omega^{-1} \sigma_0^{-1} \ll 1$), so that D=1, but in two frequency regimes:

(i) $\omega \gg \omega_1, \omega_2$. Four of the high frequency solutions to (1.45) are then

$$\omega = \pm k C_R + i(\omega_1 - \omega_2) \frac{1}{2} \frac{C_R^2 - C_A^2}{C_R^2 - C_L^2} ,$$

$$\omega = \pm k C_L + i(\omega_1 - \omega_2) \frac{1}{2} \frac{C_A^2 - C_L^2}{C_R^2 - C_L^2} ,$$

which are the fast ($\omega = k C_R$) and slow ($\omega = k C_L$) MHD modes, corrected by a thermal effect. At short wavelengths, conduction dominates and so the waves are damped. At larger wavelengths, we have instability, if $(\omega_1 - \omega_2) > 0$, i.e.

$$\omega_1 - \omega_2 \equiv \frac{(\gamma-1)}{C_S^2} \left(\frac{\partial L}{\partial \rho} \right)_S > 0 ,$$

which is the constant entropy condition that Field found (1.33).

A fifth, high frequency solution (1.45) is

$$\omega = i \omega_2 ,$$

which represents thermal conduction at short wavelengths and non-adiabatic effects at larger wavelengths.

1.2.: PREVIOUS WORK ON THERMAL INSTABILITY (Contd.)

It is unstable ($\omega_2 > 0$) when

$$L'_T T_0 - L'_\rho \rho_0 = T \left(\frac{\partial L}{\partial T}\right)_p < 0 \ ,$$

which is Field's constant pressure instability condition (1.32).

(ii) $\omega << \omega_1 , \omega_2$ In the limit of small frequencies equation (1.45) becomes

$$\omega^4 - \omega^2 k^2 \left(C_A^2 + C_S^2 \frac{\omega_2}{\omega_1}\right) + k^2 k_{||}^2 C_A^2 C_S^2 \frac{\omega_2}{\omega_1} = 0 \ , \qquad (1.47)$$

which is the usual dispersion equation for MHD modes, but with C_S^2 replaced by $C_S^2 (\omega_2/\omega_1)$. When $\omega_2/\omega_1 > 0$, (when for example, thermal conduction dominates) then the modes are stable, but when $\omega_2/\omega_1 < 0$ they are unstable. In the latter case the solutions of (1.47) may be written in terms of $C_S^2 \omega_2/\omega_1 = - C_S'^2$ as

$$\omega_R^2 = k^2 \frac{1}{2} \left(\left(\left(C_A^2 - C_S'^2 \right)^2 + 4 C_A^2 C_S'^2 \cos^2\theta \right)^{1/2} + C_A^2 - C_S'^2 \right) \ ,$$

which is a modified fast mode and is always wave-like, and

$$\omega_L^2 = -k^2 \frac{1}{2} \left(\left(\left(C_A^2 - C_S'^2 \right)^2 + 4 C_A^2 C_S'^2 \cos^2\theta \right)^{1/2} - C_A^2 + C_S'^2 \right) \ ,$$

which is the slow mode and is a purely growing, unstable mode.

1.3.: RESISTIVE INSTABILITIES.

The initial comprehensive study of resistive MHD instabilities in a sheet pinch was carried out by Furth, Killeen & Rosenbluth (1963). They assumed that the hydromagnetic approximation is valid and the ion pressure and inertial terms are negligible in Ohm's law. The resistivity η is assumed isotropic, so that the small effect due to the magnetic field is neglected. The fluid is supposed incompressible, $\underline{\nabla}.\underline{v} = 0$, which they justify by saying that the growth rate of the instability is very much less than the hydromagnetic growth rate. To see how this follows, consider the one-dimensional equation of motion, when there is no magnetic field;

$$\rho \frac{\partial v}{\partial t} + \rho v \frac{dv}{dx} = - \frac{dp}{dx} \quad ,$$

so that

$$\rho v \delta v \simeq - \delta p \quad . \qquad (1.48)$$

If we also take p proportional to density ρ, then

$$\delta p = \frac{dp}{d\rho} \delta\rho = c_s^2 \, \delta\rho \quad , \qquad (1.49)$$

where c_s is the sound speed, so that from (1.48) and (1.49),

$$\frac{v}{\rho} \frac{\delta\rho}{\delta v} = \frac{v^2}{c_s} = M^2 \quad ,$$

where M is the Mach number of the flow.

1.3.: RESISTIVE INSTABILITIES (Contd.)

Then, if $M \ll 1$, the variations in density, i.e. the compressibility effect, due to velocity of the flow, is negligibly small and the plasma may be considered incompressible. Now, when there is a magnetic pressure present as well as a gas pressure, we could expect the incompressible conditions to be,

$$\frac{V}{C_A} \ll 1 \quad \text{and} \quad \frac{V}{C_S} \ll 1 \,, \tag{1.50}$$

where C_A is the Alfvén speed. Now $\beta = (C_S/C_A)^2 = 10^{-2}$ to 1.0 in the prominence ($n_e = 5\times10^{10}\,cm^{-3}$, $T = 10^4\,^\circ K$, $B = 10$ Gauss) to the coronal conditions ($n_e = 10^8\,cm^{-3}$, $T = 10^6\,^\circ K$, $B = 1$ Gauss).

Then,

$$\frac{V}{C_S} = \frac{1}{\sqrt{\beta}} \frac{V}{C_A}$$

so that conditions (1.50) are satisfied for $\beta \leq 1$ and the flow is incompressible provided

$$V \ll \sqrt{\beta}\, C_A \,.$$

We know from Furth et al (1963) that the maximum frequency of the tearing mode instability, ω, is $1/(S^{1/2}\tau_A)$, where $S = \tau_R/\tau_A$ the ratio of the resistive to the Alfvénic timescales, so that the maximum velocity associated with the resistive instability $V_{max} = C_A/\sqrt{S}$.

1.3.: RESISTIVE INSTABILITIES (Contd.)

Thus for incompressibility we require

$$S \gg \frac{1}{\beta} .$$

Now S is based on the length scale of magnetic field variations, which for the current sheet we take as the width, such that if the width is small then S can be small, of order 10 say, and then this incompressibility condition could break down if β is small enough, perhaps by having large magnetic field strength.

The relevant equations for resistive instabilities are, the induction equation,

$$\frac{\partial \underline{B}}{\partial t} = \underline{\nabla} \wedge (\underline{v} \wedge \underline{B}) - \underline{\nabla} \wedge \left[(\eta/4\pi)\, \underline{\nabla} \wedge \underline{B} \right] , \qquad (1.15)$$

and the curl of the equation of motion,

$$\underline{\nabla} \wedge \left(\rho \frac{\partial \underline{v}}{\partial t} \right) = \underline{\nabla} \wedge \left[\frac{1}{4\pi} (\underline{\nabla} \wedge \underline{B}) \wedge \underline{B} + \rho \underline{g} \right] . \qquad (1.51)$$

Perturbations in plasma resistivity and $\rho \underline{g}$ are assumed to result from convection, so that

$$\frac{\partial \eta}{\partial t} + (\underline{v} . \underline{\nabla}) \eta = 0 \qquad (1.52)$$

and

$$\frac{\partial (\rho \underline{g})}{\partial t} + (\underline{v} . \underline{\nabla})(\underline{g} \rho) = 0 . \qquad (1.53)$$

The equilibrium magnetic field is

$$\underline{B}_0 = \hat{\underline{x}}\, B_x(y) + \hat{\underline{z}}\, B_z(y) ,$$

which is sheared in the y direction.

1.3.: RESISTIVE INSTABILITIES (Contd.)

The equilibrium velocity,

$$\underline{V}_0 = 0 \ ,$$

so that from the induction equation (1.15),

$$\underline{\nabla} \wedge (\eta_0 \underline{\nabla} \wedge \underline{B}_0) = 0 \ , \qquad (1.54)$$

which they assume holds exactly. The equilibrium pressure can be found from the zero order equation of motion,

$$\underline{\nabla} p_0 = \frac{1}{4\pi} (\underline{\nabla} \wedge \underline{B}_0) \wedge \underline{B}_0 \ ,$$

except when $\underline{B}_0$ is force-free, which, since $\underline{B}_0$ has a general form, except for the restriction (1.54), is possible.

The equations are then linearized by perturbing the variables by small amounts which are denoted by subscript 1. Using $\underline{\nabla} . \underline{B}_1 = \underline{\nabla} . \underline{V}_1 = 0$, we find from (1.15), (1.51) to (1.53),

$$\frac{\partial \underline{B}_1}{\partial t} = (\underline{B}_0 . \underline{\nabla}) \underline{V}_1 - (\underline{V}_1 . \underline{\nabla}) \underline{B}_0 + \frac{1}{4\pi} (\eta_0 \nabla^2 \underline{B}_1 + \eta_1 \nabla^2 \underline{B}_0)$$
$$+ \text{curl } \underline{B}_1 \wedge \underline{\nabla} \eta_0 + \text{curl } \underline{B}_0 \wedge \underline{\nabla} \eta_1 \ , \qquad (1.55)$$

$$\text{curl} \left[\rho_0 \frac{\partial \underline{V}}{\partial t} \right] = \text{curl} \left[\frac{1}{4\pi} [(\text{curl } \underline{B}_0) \wedge \underline{B}_1 + (\text{curl } \underline{B}_1) \wedge \underline{B}_0] + (\rho \underline{g})_1 \right] \ , \qquad (1.56)$$

$$\frac{\partial \eta_1}{\partial t} + (\underline{V}_1 . \underline{\nabla}) \eta_0 = 0 \ , \qquad (1.57)$$

$$\frac{\partial}{\partial t} (\rho \underline{g})_1 + (\underline{V}_1 . \underline{\nabla}) (\rho \underline{g})_0 = 0 \ , \qquad (1.58)$$

1.3.: RESISTIVE INSTABILITIES (Contd.)

All the perturbed quantities are assumed to vary as

$$f_1(x, y, z, t) = f(y) \exp\left[i(k_x x + k_z z) + \omega t\right].$$

The linearized equations (1.55) to (1.58) can then be reduced to

$$\frac{\chi''}{\alpha^2} = \chi\left(1 + \frac{p}{\tilde{\eta}\alpha^2}\right) + \frac{W}{\alpha^2}\left(\frac{F}{\tilde{\eta}} + \frac{\tilde{\eta}' F'}{\tilde{\eta}\, p}\right), \quad (1.59)$$

$$\frac{(\tilde{\rho} W')'}{\alpha^2} = W\left[\tilde{\rho} - \frac{S^2 G}{p^2} + \frac{F S^2}{p}\left(\frac{F}{\tilde{\eta}} + \frac{\tilde{\eta}'}{\tilde{\eta}}\frac{F'}{p}\right) + \chi S^2\left(\frac{F}{\tilde{\eta}} - \frac{F''}{p}\right)\right], \quad (1.60)$$

where dashes denoted differentiation with respect to $\mu \equiv y/a$, a is the scale length of the equilibrium magnetic field, and the normalized variables and parameters are

$$\chi = \frac{B_{1y}}{B_0} \quad , \qquad S = \tau_R/\tau_H \, ,$$

$$W = -i V_{1y} k \tau_R \, , \qquad p = \omega_R \tau_R \, ,$$

$$F = \frac{\underline{k}\cdot\underline{B}_0}{k B_0} \quad , \qquad \tilde{\eta} = \eta_0/\langle\eta\rangle \, ,$$

$$\alpha = ka \quad , \qquad \tilde{\rho} = \rho_0/\langle\rho\rangle \, ,$$

$$k = (k_x^2 + k_z^2)^{1/2}.$$

Also τ_R and τ_H are the characteristic resistive time and the hydromagnetic time,

$$\tau_R = \frac{4\pi a^2}{\langle\eta\rangle} \quad , \quad \tau_H = \frac{a(4\pi\langle\rho\rangle)^{1/2}}{B_0} \, ,$$

where $\langle\eta\rangle$, $\langle\rho\rangle$ are average measures of resistivity and density. G represents the driving force due to gravity and is defined to be

$$G = -\tau_H^2 (g/\rho_0)\, \partial\rho_0/\partial y \, .$$

1.3.: RESISTIVE INSTABILITIES (Contd.)

In dimensionless variables the equilibrium condition (1.54) becomes

$$\tilde{\eta}\, F' = \text{constant}. \qquad (1.61)$$

The magnetic field in (1.59) and (1.60) always appears as $\underline{k}.\underline{B}$ and, since $\underline{B}_0$ possesses shear we can always, for each $\underline{k}$, find a value of μ for which

$$F \equiv \underline{k}.\underline{B}_0 / k B_0 = 0 .$$

At this point diffusion is very important as can be seen from the induction equation (1.15),

$$\frac{\partial B_{1y}}{\partial t} \simeq i(\underline{k}.\underline{B})\, V_{1y} + \frac{\eta_0}{4\pi} \nabla^2 B_{1y} .$$

Near the singular surface $F = \underline{k}.\underline{B}_0 = 0$, the field and plasma are decoupled. Far away from this surface we search for solutions to the equations with $\eta = 0$.

Equations (1.59) and (1.60) may be re-written as,

$$\frac{p^2}{\alpha^2 S^2 F}\left[(\tilde{\rho} W)' + \alpha^2 W\left(\frac{S^2 G}{p^2} - \tilde{\rho}\right)\right] = (\tilde{\rho}\chi + WF)\left[PF' - \frac{F''}{F}\right], \qquad (1.62)$$

$$\frac{p^2}{\alpha^2 S^2 F}\left[(\tilde{\rho} W)' + \alpha^2 W\left(\frac{S^2 G}{p^2} - \tilde{\rho}\right)\right] = P\chi'' - P\chi\left(\alpha + \frac{F''}{F}\right), \qquad (1.63)$$

In the limit $S \to \infty$ $(\eta \to 0)$, (1.62) and (1.63) give

$$P\chi = -FW,$$

and $$\chi'' - \chi\left(\alpha^2 + \frac{F''}{F}\right) - \frac{WG}{PF} = 0 ,$$

or $$\chi'' - \chi\left(\alpha^2 + \frac{F''}{F} - \frac{G}{F^2}\right) = 0 , \qquad (1.64)$$

which is satisfied everywhere except near $F = 0$. Furth et al. find from (1.64) asymptotic solutions to (1.62) and (1.63) which break down at $F = 0$. Then they make a power series expansion of (1.62) and (1.63) around the point $F = 0$. Matching these two sets of solutions at the boundary, where they are both valid, gives the complete solution.

The formal solution does not give much insight into the physical processes at work in the instability. An intuitive derivation for the value of ϵa of the diffusion region width is as follows:

Assume in Ohm's law ($\underline{E} + \underline{V} \wedge \underline{B} = \eta \underline{J}$) that the plasma is moving but the magnetic flux lines are not, so that $\underline{E} = 0$ Thus:

$$\underline{J} = (\underline{V} \wedge \underline{B}) / \eta$$

and there is a Lorentz force which tries to prevent motion across the field,

$$F_s = \underline{J} \wedge \underline{B} = \frac{\underline{B}(\underline{V}.\underline{B}) - \underline{V} B^2}{\eta} .$$

This restoring force is arbitrarily weak near $B=0$ where, for the purposes of the description, B refers to the component $\underline{k}.\underline{B}$. When instability occurs a driving force, F_d, is set up in opposition to F_s and of the same order as it. Thus the rate at which work is done on the plasma in the diffusion region (near $\underline{k}.\underline{B} = 0$) is

$$\underline{V}.\underline{F}_d \simeq -\underline{V}.\underline{F}_s \simeq V_y^2 (B')^2 (\epsilon a)^2 / \eta , \quad (1.65)$$

1.3.: RESISTIVE INSTABILITIES (Contd.)

where B has the value $B'\epsilon a$ near the diffusion region, whose width we suppose to be ϵa .
The driving force gives rise to motions in the $\underline{y}$ and $\underline{k}$ directions, where, from $\underline{\nabla}.\underline{V} = 0$,

$$V_y/\epsilon a \simeq -k V_k .$$

But in general $1/\epsilon a \gg k$, so that the kinetic energy in the $\underline{k}$ direction, $m V_k^2$, dominates. Equating the rate of change of this energy to the driving power, we get

$$\omega \rho_0 V_k^2 = \frac{\omega \rho_0 V_y^2}{(k\epsilon a)^2} = \frac{V_y^2 (B')^2 (\epsilon a)^2}{\eta} .$$

So the width of the diffusion region must be

$$\epsilon a = \left(\frac{\omega \rho_0 \eta}{k^2 B'^2}\right)^{1/4} . \qquad (1.66)$$

We shall now estimate the growth rates of the three resistive instabilities which are possible in a sheet pinch.

(1) Gravitational Mode, which is shown in Figure (4a) page 59 has a driving force of the form

$$\underline{F_d} = \rho_1 \underline{g} = - \frac{V_y \rho_0' \underline{g}}{\omega} .$$

Thus, equating $\underline{F_d}.\underline{V}$ with equation (1.65) gives

$$(B')^2 (\epsilon a)^2/\eta = \rho_0' g/\omega$$

and, using (1.66), we find

$$\omega = \left(\frac{\rho_0' g k \sqrt{\eta/\rho_0}}{B'}\right)^{2/3} ,$$

or, in dimensionless variables,

$$p \simeq (\alpha S G)^{2/3} .$$

1.3.: RESISTIVE INSTABILITIES (Contd.)

(2) Rippling Mode In the rippling mode the circulatory motion of the fluid creates a ridge of lower-resistivity fluid into which the local current is channeled. If we were using an energy equation instead of (1.52), the effect of joule heating would be included and we would also have the 'anti-diffusion' and joule mode thermal instabilities (Heyvaerts), described in section 1.2. To consider the rippling mode descriptively, we must take account of resistivity variations, so that Ohm's law becomes

$$\eta_0 \underline{J}_1 = - \eta_1 \underline{J}_0 + \underline{V} \wedge \underline{B} \quad ,$$

where η_1 is given by the convective law

$$\eta_1 = - \underline{V} . \nabla \eta_0 / \omega \quad .$$

The additional η_1 gives rise to the driving force

$$\underline{F}_d = \underline{J}_1 \wedge \underline{B} = \frac{\underline{V} . \nabla \eta_0 \; \underline{J} \wedge \underline{B}}{\omega \eta_0} \quad ,$$

which changes sign as $\underline{B}$ passes from one side of the null point to the other. Hence F_d is stabilizing on the side of higher resistivity and destabilizing on that of lower resistivity. Equating $\underline{V} . \underline{F}_d$ with (1.65) we have

$$\frac{V_y^2 \eta_0' (B')^2 (\epsilon a)}{4\pi \omega \eta_0} = \frac{V_y^2 (B')^2 (\epsilon a)^2}{\eta_0} \quad ,$$

or

$$\epsilon a \simeq \frac{\eta_0'}{4\pi \omega} \quad .$$

1.3.: RESISTIVE INSTABILITIES (Contd)

Equating this with (1.66) gives

$$\omega = \left[\frac{\eta_0'^4 \, k^2 \, B'^2}{(4\pi)^4 \, \rho_0 \, \eta_0} \right]^{1/5} .$$

The rippling mode thus requires a gradient in resistivity which in turn depends on temperature. The perturbed field and velocities for the rippling mode is shown in Figure (4b) page 59.

(3) Tearing Mode This mode is of particular interest in the formation of quiescent prominences in neutral current sheets (Chapter 2). In this application, the main effect of the instability is to reconnect field lines across the neutral sheet and hence help support the condensing matter. Also, it reduces the magnetic field strength in the diffusion region and so prevents the build-up of magnetic pressure which would inhibit condensation.

The tearing mode is typically a long wavelength rather than a short wavelength mode relative to the dimensions of the current sheet.

The perturbed current is,

$$4\pi \, \underline{J}_{\perp 1} \simeq \frac{\partial \, \underline{B}_{k1}}{\partial y} = - \, \underline{B}_k' ,$$

so that, from $\nabla . \underline{B} = k B_k + B_y' = 0$, we get

$$J_{\perp 1} = \frac{B_y''}{4\pi k} .$$

If $ak \ll 1$, then the more detailed analysis gives

$$B_y'' \simeq \frac{B_y}{(\epsilon k a) \, a^2} .$$

1.3.: RESISTIVE INSTABILITIES (Contd.)

The plasma is not perfectly decoupled even near the diffusion region and the component

$$E_{\perp 1} \simeq \frac{\omega B_y}{k}$$

must be included in Ohm's law

$$\eta_0 \underline{J}_1 = \underline{E}_1 + \underline{v}_1 \wedge \underline{B} \ .$$

The quantity ϵa is chosen so that $\underline{E}_1$ dominates $\underline{v}_1 \wedge \underline{B}$ in the diffusion region. Hence, equating $\eta_0 J_1$ and E_1, we have

$$\frac{\eta_0 B_y}{(\epsilon k a) a^2} \frac{1}{4\pi k} \simeq \frac{\omega B_y}{k} \ ,$$

or

$$\epsilon a \simeq \frac{\eta_0}{4\pi k a^2 \omega} \ .$$

Then from (1.66)

$$\omega = \left[\frac{\eta_0^3 B'^2}{(4\pi)^4 \rho_0 k^2 a^8} \right]^{1/5} \ ,$$

or, in dimensionless variables,

$$p \simeq \left(S/\alpha \right)^{2/5} \ .$$

The flow pattern and the perturbed magnetic field are shown in Figure (4c) page 59 .

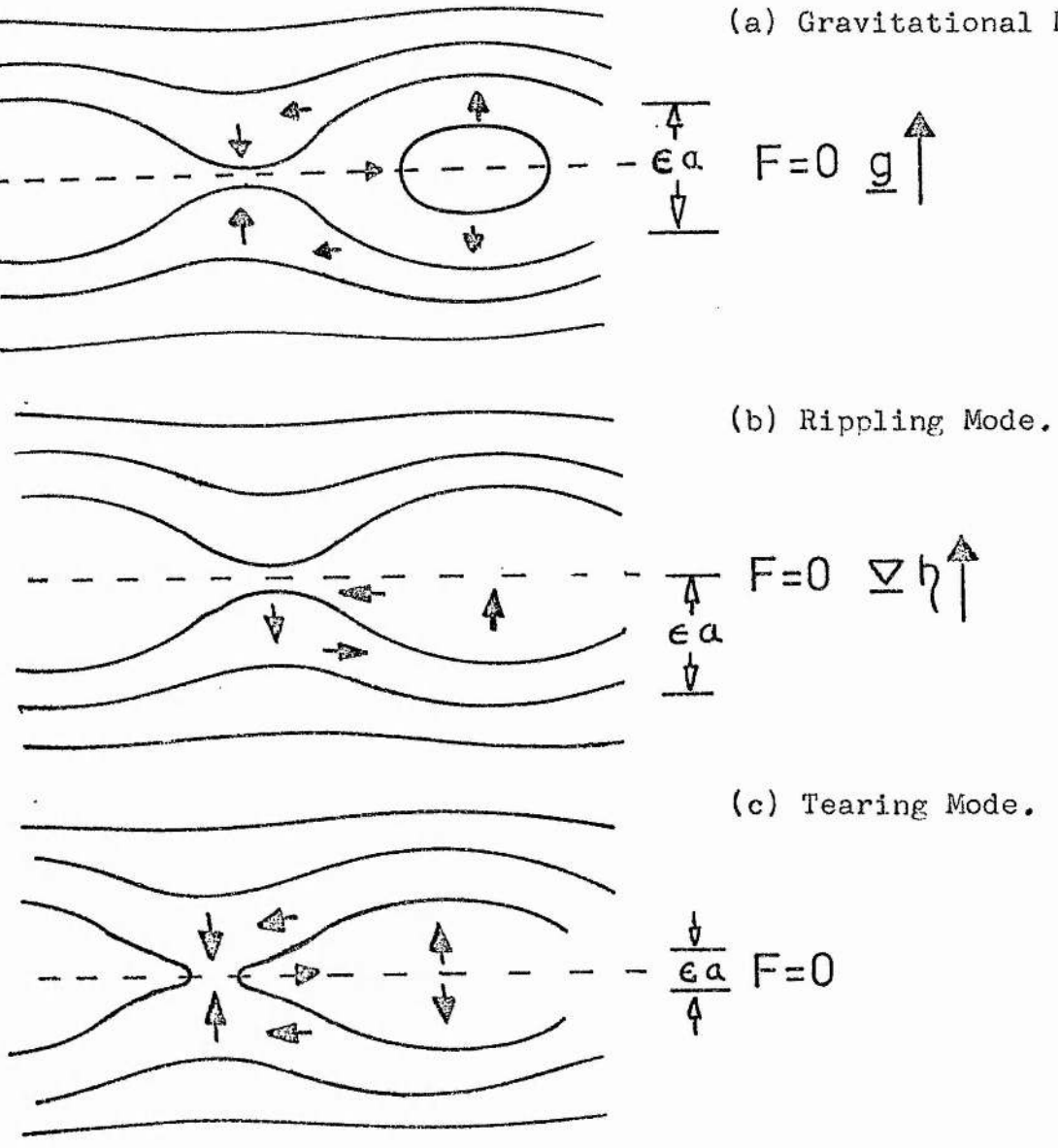

Figure (4). Schematic representation of the perturbed magnetic field and velocities (shown as arrows). In each case ϵa is the width of the diffusion region. In 4(a) is sketched the gravitational mode, with $\underline{g}$ the direction of gravity. In 4 (b) is the rippling mode, with $\underline{\nabla}\,\eta$ the required resistivity gradient, such that the plasma is stable in the upper half plane. In 4 (c) is the tearing mode.

1.3.: RESISTIVE INSTABILITIES (Contd.)

Tearing Mode with Uniform Resistivity

Barston (1969) studied the tearing mode instability in the same equilibrium that Furth et al. chose namely;

$$\underline{B}_o = \hat{\underline{x}}\, B_x(y) + \hat{\underline{z}}\, B_z(y) \quad ,$$

which can, as in the case of Furth et al., either be force-free or can balance a pressure gradient. Also he supposes $\underline{B}_o$ satisfied the induction equation exactly, so that

$$\underline{\nabla} \wedge (\eta_o (\underline{\nabla} \wedge \underline{B}_o)) = 0 \quad ,$$

or, in dimensionless units,

$$\tilde{\eta}\, F' = \text{constant}.$$

Now Barston considered the η = constant case so that

$$F'' = 0 . \qquad (1.67)$$

1.3.: RESISTIVE INSTABILITIES (Contd.)

He then was able to show, using equations (1.59) and (1.60) with the boundary conditions $\chi' = w' = 0$ at $\mu = \pm \infty$, that the plasma was stable.

Van Hoven & Cross (1971) then considered the same problem but used instead the boundary conditions

$$w' = 0 \text{ and } \chi' < \infty \text{ at } \mu = \pm \infty .$$

They were able to show that the plasma was unstable to the tearing mode for small values of α and found the growth rate,

$$p = (\alpha S)^{2/3} \quad , \quad (\text{for } p >> \alpha^2)$$

which is in agreement with the small α case of Furth et al.(1963, Appendix D).

Cross & Van Hoven (1971) then chose to study the tearing mode in a sheared equilibrium magnetic field that was periodic in space and constant in magnitude,

$$\underline{B}_0 = B_0 \left(\hat{\underline{x}} \sin \frac{\pi y}{a} - \hat{\underline{z}} \cos \frac{\pi y}{a} \right) . \qquad (1.68)$$

This sinusoidal variation was chosen to ease the analysis. In this case, unlike the general case of Furth et al, the equilibrium field is force-free, i.e.

$$\underline{J}_0 \wedge \underline{B}_0 = 0 \quad . \qquad (1.69)$$

This time, again unlike Furth et al, the field does not identically satisfy the diffusion equation, so that the field slowly decays at the diffusion rate, $\frac{1}{\tau_R} = \frac{\eta_0}{4\pi a^2}$. Thus they must assume that the growth rate of the instability, ω, satisfies the condition,

$$\omega >> \frac{1}{\tau_R} \quad . \qquad (1.70)$$

1.3.: RESISTIVE INSTABILITIES (Contd.)

Their equilibrium magnetic field (1.68) satisfies in dimensionless form,

$$F'' = -\pi F \quad . \qquad (1.71)$$

Cross (1972) has shown that the tearing mode instability can occur with F satisfying (1.71) if $0 < \alpha < \pi^2$, while, if F satisfies (1.67), then the tearing mode will occur only if

$$\alpha^2 << p \quad .$$

For Cross & Van Hoven's work, the equilibrium temperature T_0 and density ρ_0 are taken uniform in space since no variation is required to satisfy (1.69) also they assumed that the equilibrium velocity is of the order of the resistive diffusion velocity, so that it can be ignored by (1.70).

The MHD equations are linearized, and perturbations of the form

$$B_{1y}(r,t) = \frac{1}{2} \sum_n B_{yn} \cos \frac{n\pi y}{a} \sin kx \, e^{\omega t}$$

and

$$V_{1y}(r,t) = \frac{1}{2} \sum_n V_{yn} \sin \frac{n\pi y}{a} \cos kx \, e^{\omega t} \qquad (1.72)$$

are considered, where the sums run over even n for B_{1y} and odd n for V_{1y}. Incompressibility is assumed so that, since ρ_0 is uniform, we have

$$\rho_1 = 0 \quad .$$

1.3.: RESISTIVE INSTABILITIES (Contd.)

Also, no energy sources or sinks are considered so that, since T_o is uniform and the plasma is incompressible,

$$\eta_1 = 0 \quad .$$

Then, from the $\hat{y}$ component of equation (1.55), we have

$$\omega B_{1y} = B_o k V_{1y} \sin\frac{\pi y}{a} + \frac{\eta_o}{4\pi}\left(B_{1y}'' - k^2 B_{1y}\right) \qquad (1.73)$$

and, from the $\hat{z}$ component of (1.56), we find

$$-\omega\rho_o\left[k V_{1y} + V_{1x}'\right] = \frac{B_o}{4\pi}\sin\frac{\pi y}{a}\left[\left(\frac{\pi^2}{a^2} - k^2\right)B_{1y} + B_{1y}''\right] . \qquad (1.74)$$

We now obtain the coefficients of the Fourier series by multiplying (1.73) by $\cos\frac{n\pi y}{a}$ and (1.74) by $\sin\frac{n\pi y}{a}$ and then integrating from $y = -a$ to $y = +a$, to get

$$\omega B_{yn} = -\frac{\eta_o}{4\pi}\left(k^2 + n^2\frac{\pi^2}{a^2}\right)B_{yn} + \frac{k}{2}B_o\left[V_{y_{n-1}} - V_{y_{n+1}}\right] , \qquad (1.75)$$

$$\frac{4\pi\omega\rho_o}{k}\left(k^2 + \left(\frac{n\pi}{a}\right)^2\right)V_{yn} = \frac{B_o}{2}\left\{\left[k^2 + \frac{\pi^2}{a^2}n(n-2)\right]B_{y_{n-1}} - \left[k^2 + \frac{\pi^2}{a^2}n(n+2)\right]B_{y_{n+1}}\right\} , \qquad (1.76)$$

1.3.: RESISTIVE INSTABILITIES (Contd.)

where we have used $\underline{\nabla} . \underline{V}_1 = 0$ to remove the V_x term. Equations (1.75) and (1.76) then give

$$\left[\frac{4P}{\alpha^2 S^2} (\alpha^2 + n^2 \pi^2) + F_{n+} + F_{n-} \right] V_{yn} - F_{n+} V_{yn+2} + F_{n-} V_{yn-2} = 0 \quad , \qquad (1.77)$$

where $$F_{n\pm} \equiv \frac{\left[\frac{\alpha^2}{\pi^2} + n(n \pm 2) \right]}{\frac{P}{\pi^2} + \frac{\alpha^2}{\pi^2} + (n \pm 1)^2} \quad .$$

Equation (1.77) gives a recurrence relation between the Fourier coefficients of the V_{1y} series. Starting with $n = 1$ we first get, since $V_{y-1} = - V_{y1}$ from (1.72),

$$\frac{V_{y3}}{V_{y1}} = \left(\frac{4P}{\alpha^2 S^2} (\alpha^2 + \pi^2) + F_{1+} + 2 F_{1-} \right) \Big/ F_{1+} \quad .$$

We can then calculate the ratio of successively higher coefficients to V_{y1} by using higher values of n in (1.77). The only unknown in (1.77) is the growth rate P, so that the technique is to put a trial growth rate, Pt, say, in (1.77) and then calculate the ratio of the coefficients V_{yn+2} / V_{y1} for higher and higher values of n . In general the series of terms diverge but for one critical growth rate, Pc, say, they converge.

1.3.: RESISTIVE INSTABILITIES (Contd.)

Since we require the Fourier series to converge, P_c is the value of the instability growth rate. Following Cross & Van Hoven, we plot in Figure (5), page 66, the values of the series for several trial growth rates P_t when $\alpha = 0 \cdot 1 \pi$ and $S = 10^5$. From this we see that when P_t is too high or too low the series diverge but they tend to converge as P_t approach P_c, which in the Figure is 1996.

In Figure (6), page 66, is plotted the growth rate P_c as a function of wave number α, for several values of S which show that there is instability only when $0 < \alpha < \pi$ and that $P \simeq (\alpha S)^{2/3}$

where their assumption of small α $(P \gg \alpha^2)$ in Furth et al. (1963) is similar to the assumption of $P \gg \pi^2$ which is the dimensionless form of (1.70). The growth rate of the fastest growing mode approximately obeys the relation

$$P_{max} = 3 \cdot 4 \, S^{0 \cdot 57} \quad , \text{ when } S > 10^3 .$$

In their small α limit, Furth et al (1963) find $P_{max} \simeq S^{0 \cdot 5}$ so that this result is in good agreement with theirs.

In Chapter 3 we compare these results for a constant field strength, sheared field with those for an equilibrium magnetic field that models a neutral sheet.

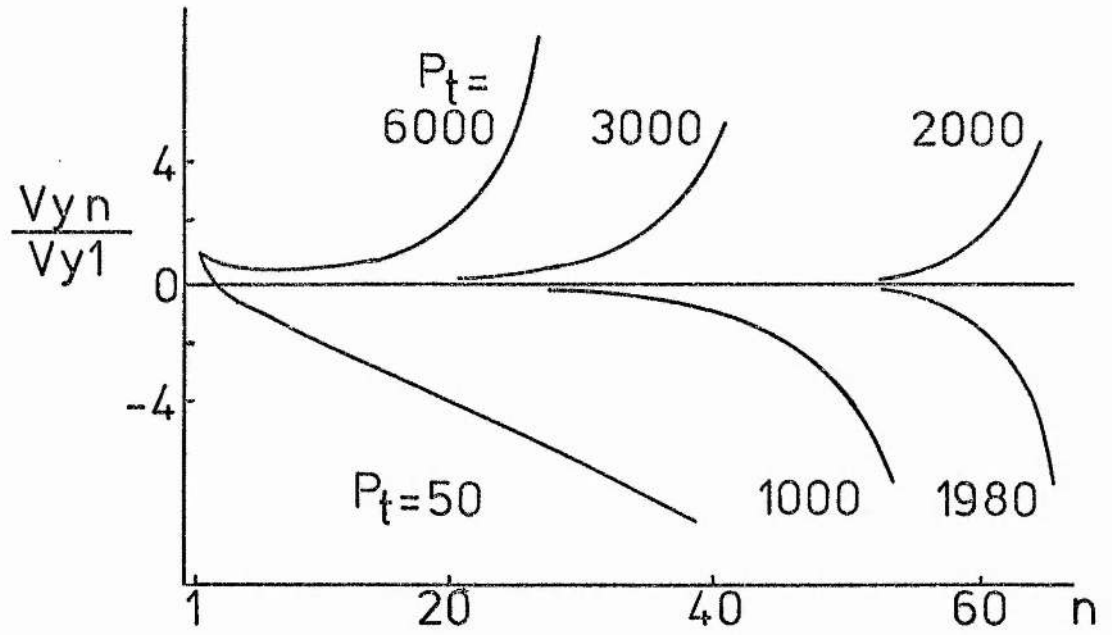

Figure (5). The n^{th} coefficients, Vyn, of the Fourier series of the tearing mode instability in a sheared field as a function of n for several trial values of the growth rate p_t. For this case the ratio of the resistivity to hydromagnetic timescales $S=10^5$, the dimensionless wave number $\alpha = 0{\cdot}1\pi$ and $p_c = 1996$. (From Cross & Van Hoven, 1971).

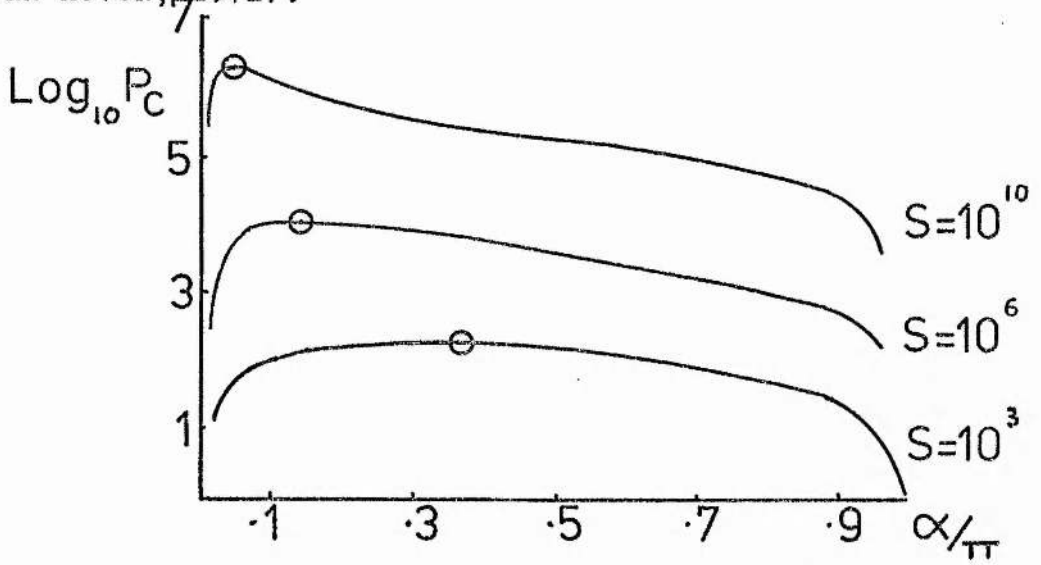

Figure 6. The growth rate Pc for the tearing mode instability in a sheared field as a function of the dimensionless wave number α. Each curve is drawn for a different value of the ratio of resistivity to hydromagnetic time scales, S. The fastest growing mode, P_{max}, is marked by ⊙. (from Cross & Van Hoven, 1971).

1.4.: PROMINENCE OBSERVATIONS

Prominences are cool dense objects situated in the hotter corona. They are called filaments when seen in absorption against the disc but, when seen in emission at the limb of the sun, they are usually called prominences. Many classifications of the observed features of the solar prominences have been made. One of the earliest, by Secchi (1875), divided them into 'quiescent' and 'active' prominences. The long-lived, slowly changing quiescent prominences are normally seen away from active regions, while the short-lived, rapidly changing active prominence is seen in and around active centres. These active prominences can be further sub-divided, for instance in de Jager's (1959) classification, into many types. One of these, the "active region filament" or "active sunspot prominence" may have some features of its formation in common with the quiescent prominence. We shall describe both of these types in this section, while ignoring other ones with which they have little in common.

Basic Data

The quiescent prominence is typically 200,000 km long, 50,000 km high, but only 5,000 km to 10,000 km thick (Tandberg-Hanssen, 1974), so, when seen on the disc it looks like a long, black, meandering ribbon.

1.4.: PROMINENCE OBSERVATIONS (Contd.)

The temperature in the central region of these prominences is about 6,000° K to 7,000° K, determined from the optically thin Balmer lines, while at the edge and top, the temperature is about 12,000° K (Bruzek & Kuperus, 1972). The electron density, obtained from Stark broadening of the high Balmer lines, is in the range of 10^{10} to 5×10^{10} cm^{-3} (Hirayama, 1971). Observed end on, parallel to the long axis, one generally finds that the inner corona surrounding the filament has a region of reduced brightness (Wesley, 1927).

It has been shown that this region of reduced brightness, called the coronal cavity must be due to a reduced electron density (Waldmeier, 1970).

The active region filament looks somewhat like a quiescent prominence but is a factor of three or four smaller. Also it is only seen inside active regions and has one or both ends attached to a sunspot.

The temperature is much the same as in the quiescent prominence but it has a large electron number density, $n_e \gtrsim 10^{11}$ cm^{-3} (Hirayama, 1971).

The lifetimes of solar prominences have a large variation, but averages can be calculated, from the studies made by the d'Azambujas (1948), for both large filaments in active regions and quiescent prominences. For three-quarters of the active region filaments that they studied, it can be deduced (S. Martin, 1973), that the average lifetime is approximately 26 days.

1.4.: PROMINENCE OBSERVATIONS (Contd.)

Also the d'Azambujas found that for quiescent prominences the lifetime varied somewhat with latitude; for low latitude prominences the lifetime is about 3 rotations (51 days) while for those at high latitudes the average duration is 5.1 rotations (138 days). The d'Azambujas found that filaments drift towards the poles at a rate of about 2.3° per rotation, when situated between 0° and 10° latitude, down to 0.8° per rotation, when between 51° and 60° latitude. The decrease in drift rate with increasing latitude along with the increased lifetime of the high latitude quiescent prominences explains why there is frequently a band of long lived filaments appearing to encircle each polar cap. The effect of the differential rotation is to orientate them in an East-West direction, making it possible for some of the filaments to join end to end, an effect which the d'Azambujas called the "polar crown". This drifting of prominences during their lifetime is in the opposite direction to the trend of sunspot appearances during the solar cycle. Along with sunspots, prominences are formed at high latitudes in the early stages of the cycle, but then form at progressively lower latitudes as the solar cycle continues (Kippenheur, 1953).

Observations of the Magnetic Field in Prominences

In his review of the observational data on the magnetic field of prominences, Tandberg-Hanssen (1974) says that the line of sight component of the field, observed at the limb of the sun, $B_{\parallel}$, for quiescent prominences can range from no observable field to 30 or 40 Gauss.

1.4.: PROMINENCE OBSERVATIONS (Contd.)

From a study of 135 quiescent prominences, he finds that the average value of this field, $\langle B_{\parallel} \rangle$, is approximately 7.3 Gauss, with about half the observations in the range $3\ G \leq B_{\parallel} \leq 8\ G$. Rust (1966) found $\langle B_{\parallel} \rangle \simeq 5\ G$ for data from 1965 and Harvey (1969) found $\langle B_{\parallel} \rangle \simeq 6{\cdot}6\ G$ for data from 1967. It is also found by Rust (1967) that the magnetic field strength, $B_{\parallel}$, increases by roughly a factor of $1\frac{1}{2}$ over the height of a quiescent prominence. (Active region prominences, by contrast, have larger values of $B_{\parallel}$, Tandberg-Hanssen (1974) gives a range of 20 G to 70 G .)

Information about the orientation of the magnetic field with respect to the axis of the prominence was given by Tandberg-Hanssen & Anzer (1970), who calculated that the average value of α, the angle between the direction of the field and the long axis of the prominence, was about 15°. In this work it was assumed that the value of the field strength did not affect α. However, observations by Ioshpa (1968) indicate that, while the vector of the field seems to be aligned with the filament in the active regions, the field in the higher, more massive quiescent prominences runs mainly across the filament. From Ioshpa's results, Rust (1972) concludes that there is evidence of a relationship between the strength of the magnetic field and its direction in quiescent prominences of the form,

$$\alpha = 90^{\circ} \left(\frac{B_{max} - B}{B_{max}} \right) ,$$

1.4.: PROMINENCE OBSERVATIONS (Contd.)

where $B_{max} \simeq 30$ Gauss . This, says Rust, is not founded on a detailed study of the data but only on a review of the observation results.

On the disc of the sun, observations of the line-of-sight component of the magnetic field indicate that, for both quiescent prominences (Babcock & Babcock , 1955) and active prominences (Smith & Ramsey, 1967), the filament forms between areas of north and areas of south magnetic field.

Given the normal magnetic field component on the surface of the sun, it is possible to calculate the unique potential field in the atmosphere above. Using this method, Harvey (1969) compared the predicted structure of active region filaments with the observed structure and found that these filaments, unlike some other active filaments, cannot have a potential field. It has been suggested by Raadu & Nakagawa (1971) that a force-free field configuration could represent the magnetic field in these prominences, however, if, as observations suggest, the gas pressure inside the prominence is not negligible, we require a magnetic pressure to balance it, so that the field can not be force-free.

Prominences and their Link with Active Regions.

The strong connection between the evolution of prominences, not only active region filaments but also quiescent prominences, and active regions has been reviewed by S. Martin (1973).

1.4.: PROMINENCE OBSERVATIONS (Contd.)

She discusses three characteristic locations for the formation of prominences: within active regions, between active regions, and in the remnants of old active regions. It was shown by Smith & Ramsey (1967), that all filaments, observed within active regions, formed at the boundary between the areas of positive and negative magnetic field shown on magnetograms, which only displays the line-of-sight component of the field. Smith (1968) has shown that a second condition for the formation of at least some filaments, both in centres of activity and also between adjacent active regions, is that the H_α fibrils (in the chromosphere) align themselves end to end along a path, called a "filament channel", which eventually becomes the filament. The alignment of the chromosphere fibrils within the filament axis supports the observations of Ioshpa (1968) and Harvey (1969) that the magnetic field vector points approximately along the axis.

The process of filament formation between active centres seems to be the same as that within an active centre, except that in the latter case the filament does not form until the boundaries of the two separate magnetic field regions have come into contact. No filament forms as long as there is a zone between the two active centres in which the H_α fibrils have a random orientation. The formation of filaments in the weak fields of remnant active centres is, in many ways, similar to the formation between centres of activity, but there are some differences.

1.4.: PROMINENCE OBSERVATIONS (Contd.)

The timescale for formation of these filaments, as noted by the d'Azambujas (1948), can take several days while, in active centres, the filaments form much more rapidly, the timescale ranging from a few hours to a few days. Also the direction of the H_α fibrils in the adjacent chromosphere is not necessarily along the path which forms the filament. These differences perhaps indicate that the formation is taking place at a greater height above the chromosphere than for filaments within active regions.

In addition to stressing the above three main areas for prominence formation, S. Martin (1973) points out that there are many filaments that form near the boundaries of active regions and display the formation characteristics of each of these areas.

Motions within Prominences.

According to the d'Azambujas (1948), the most common form of quiescent prominences takes the form of a bridge, with one or more supporting arch connecting the prominence with the chromosphere. This, Nakagawa & Malville (1969) interpret as the manifestation of an instability at the interface between the prominence and the plasma beneath it. It is suggested by the d'Azambujas that all prominences would evolve into this form if they lived long enough.

The most common pattern of flow in a quiescent prominence is back and forth horizontally along the axis, with an additional continuous flow down the arches into the chromosphere.

1.4.: PROMINENCE OBSERVATIONS (Contd.)

The velocities range from 0 to 100 km sec^{-1} (Dodson, 1948) However, measurements by Dunn (1960) for quiet quiescent prominences have shown that the vertical velocity is significantly less than the random motions, of 5 to 10 km sec^{-1}, of threads of plasma in the prominence. But, if the quiescent prominence interacts with a sunspot in such a way that matter is streaming out of the prominence into the spot, then the vertical velocities are much higher. Also, within quiet quiescent prominences, there is hardly any mass motion along the axis of the filament and, indeed, this is one of the main differences between the quiescent and the active region filaments. When, however, the quiescent filament interacts with a sunspot, the motions along the axis are greatly increased.

Active region filaments interact more with sunspots than quiescent prominences and so there is much greater activity within them. Most of the motion seems to be out of the prominence into a sunspot, but there is an example of a rarer type in which matter flows out of one spot at about 28 km sec^{-1} , and flows into the other at about 39 km sec^{-1} (Ellison 1937).

The Dissolution of Prominences

Only three types of prominence dissolution have been recognised (Kiepenheuer, 1953): the slow dissolution, the quasi-eruption and the "eruption" or "disparition brusque".

The slow dissolution of a filament occurs when the rate of mass loss, due to material flowing into the chromosphere, is greater than the accumulation of matter into the prominence.

1.4.: PROMINENCE OBSERVATIONS (Contd.)

This often occurs for filaments associated with active regions.

In the quasi-eruptive dissolution, the prominence ascends, breaks into fragments, and then its mass flows into the chromosphere at several places called "centres of attraction" by McMath & Petit (1938). This type is often, but not always, associated with a flare.

The disparition brusque occurs when the whole prominence ascends and disappears, most of the matter rising higher in the corona and the rest flowing back into the disc. The disappearance is permament for about one-third of all cases while, for the rest, the prominence reforms after a period of time ranging from a day to a few weeks, with nearly the same shape as before. This dissolution was considered by d'Azambijas (1948), who observed it in about one half of all low latitude filaments, to be a natural phase in the evolution of the prominence.

1.5.: PROMINENCE FORMATION IN A CURRENT SHEET

In this section we give a background to the work described in Chapter 2.

As already mentioned in section 1.4, the observation of quiescent prominences indicate that they form, sometimes, in regions between active centres which may well be current sheets. Also of interest is the paper by Saito& Tandberg Hanssen (1973), in which many observations are listed of quiescent prominences present at the base of coronal streamers. Such streamers outline the shape of the magnetic field and indicate low lying closed field lines surmounted by an open structure. In this section we shall consider a model which suggests how a condensation can occur in, how its condensation is influenced by, and how the final condensed prominence is supported by the magnetic field of coronal streamer type structure.

Kuperus and Tandberg-Hanssen (1967) proposed a model for the condensation of plasma in a coronal streamer. They assumed that, above an active region, the magnetic field has initially a closed dipole type structure (Figure (7a), page 77). The corona above the centre of activity is more intensely heated than the surrounding corona (Kuperus, 1965), so that the gas pressure in region A becomes higher than at the same level outside the active region. The active coronal region is heated until at some height B the gas pressure exceeds the magnetic pressure.

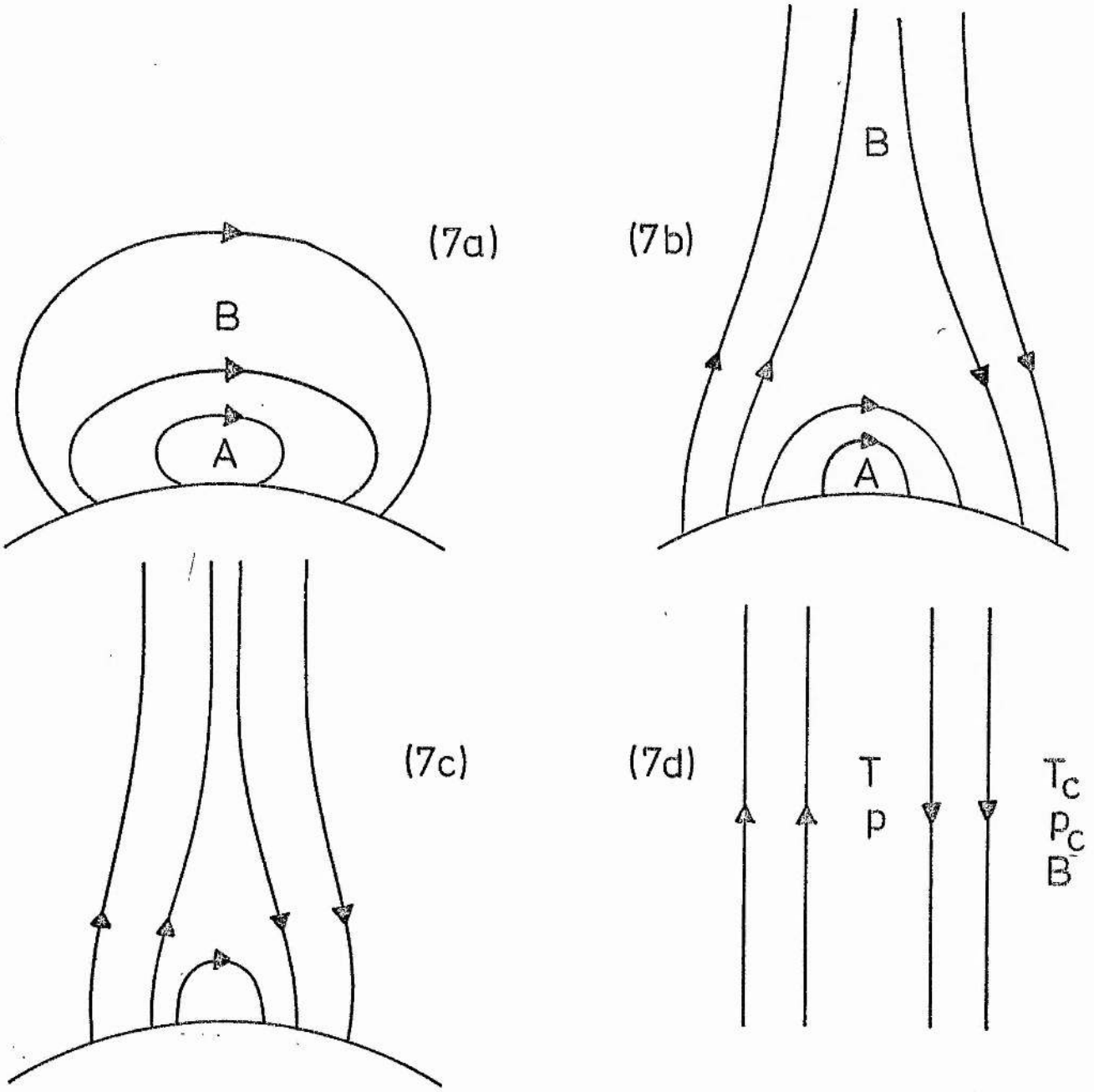

Figure (7). The possible magnetic field configuration over an active region. In 7(a) the plasma in region A is heated more strongly than at the same level outside until at some height B the gas pressure exceeds the magnetic pressure and the field lines open to give 7 (b). After this active phase the field lines come together again as in 7 (c). Approximating for this final magnetic field structure by the parallel straight lines in 7 (d), Kuperus & Tandberg-Hanssen (1967) investigate the thermal instability.

1.5.: PROMINENCE FORMATION IN A CURRENT SHEET (Contd.)

And so the field lines are opened and the matter blown out (Figure (7b), page 77). This is the safety-valve mechanism suggested by Parker (1963).

In region B the field structure is determined by the outward flow, while region A possesses a more or less potential field. After this active phase (Figure (7c)), the outward flow of matter ceases and the field lines are no longer kept open. The region near the plane of symmetry has a very weak field, so that the matter is easily compressed there to maintain lateral pressure equilibrium. The matter near the neutral line has a higher density than the surrounding corona and so loses more energy by radiation. If we assume that the only heat source is mechanical heating, the same both inside and outside the neutral current sheet, then the greater energy loss by radiation in the denser neutral sheet cannot be balanced and so the gas cools down.

The neutral sheet formed in Figure (7c) is approximated by the uniform anti-parallel field lines drawn in Figure (7d).

1.5.: PROMINENCE FORMATION IN A CURRENT SHEET (Contd.)

The coronal conditions, T_c , ρ_c , p_c , B are supposed uniform as are the conditions inside the sheet where we have no magnetic field. Initially the temperature inside the sheet is taken equal to T_c . During the instability it is assumed that the inflow velocity is very much less than the Alfvēn speed, so that, from the equation of motion, there must be lateral pressure balance,

$$p = p_c + B^2/8\pi \quad ,$$

and it is supposed that this pressure remains constant throughout the condensation.

Kupereus & Tandberg-Hanssen took as their energy equation,

$$\frac{d}{dt} p - \gamma \frac{p}{\rho} \frac{d\rho}{dt} = -(\gamma-1) L \quad ,$$

which with the perfect gas law,

$$p = R \rho T \quad , \qquad (1.78)$$

and the fact that the variables have no spatial variation gives,

$$C_p \frac{\partial T}{\partial t} = -\frac{L}{\rho} \quad . \qquad (1.79)$$

1.5.: PROMINENCE FORMATION IN A CURRENT SHEET (Contd.)

In, L, the heat loss per unit time and volume, they include G_{mech} the mechanical heating term and L_{RAD} the energy lost by radiation. Thermal conduction is not includedfor simplicity, but as noted in section 1.2, this is an important effect, which we take account of in Chapter 2. For radiative loss they use the Orrall& Zirker (1961) expression,

$$L_{RAD} = 6{\cdot}3 \times 10^{24} \rho^2 \ \text{ergs cm}^{-3} \text{ sec}^{-1},$$

which is a little low in value at $T = 10^5 {}^{\circ}K$.

For G_{mech} they take the usual expression,

$$G_{mech} = a\rho ,$$

where the constant, a, is determined from the coronal equilibrium condition,

$$L \equiv L_{RAD} - G_{mech} = 6{\cdot}3 \times 10^{24} \rho_c^2 - a\rho_c = 0 .$$

Thus the energy equation (1.79) becomes

$$C_p \frac{\partial T}{\partial t} = 6{\cdot}3 \times 10^{24} (\rho_c - \rho) ,$$

which from (1.78) may be re-written

$$\frac{\partial T}{\partial t} = \frac{6{\cdot}3 \times 10^{24}}{C_p} R \left(\frac{p_c}{T_c} - \frac{p}{T} \right) . \quad (1{\cdot}80)$$

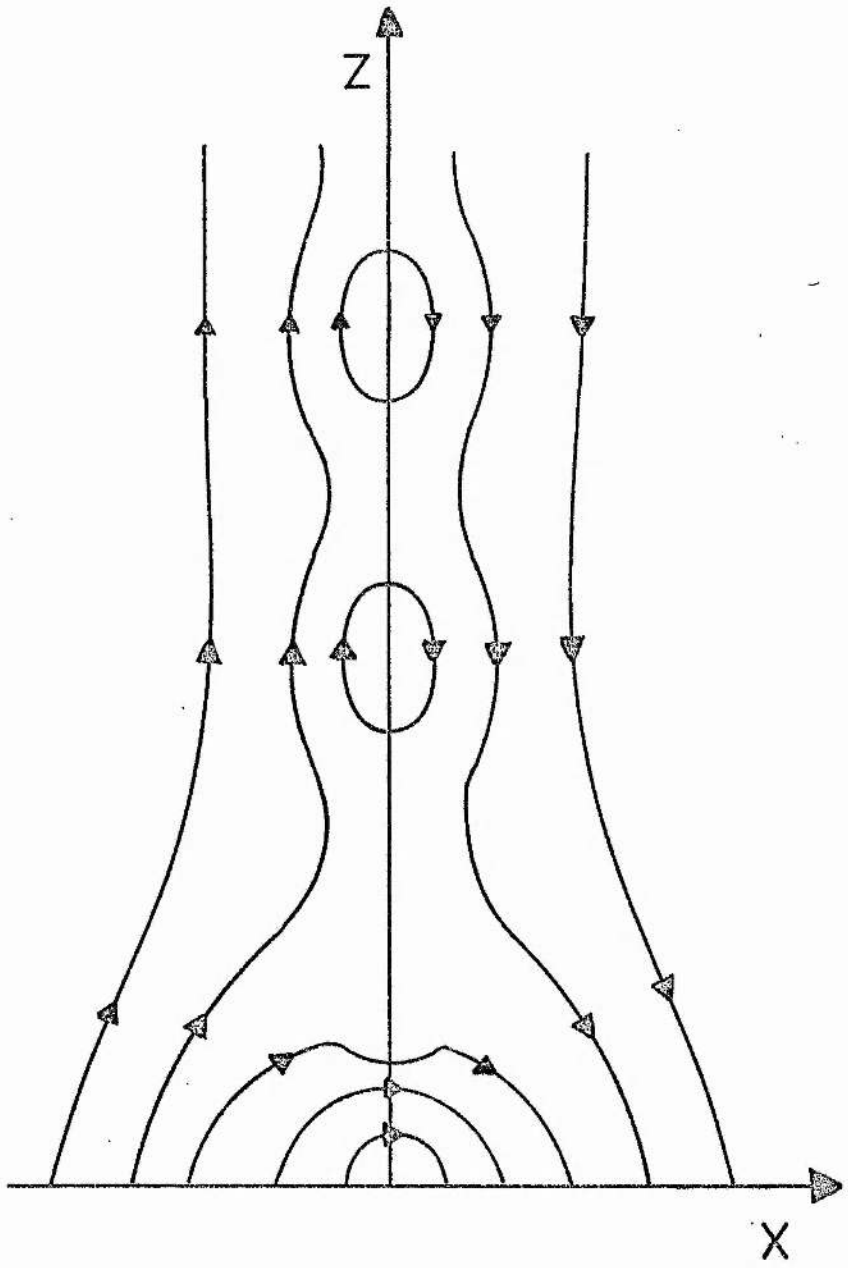

Figure (8). The occurrence of the tearing mode instability in the current sheet of the Kuperus & Tandberg- Hanssen (1967) model. The main effect is to reconnect magnetic field along the neutral line (x=o) reducing the magnetic field strength in that region and forming magnetic loops as shown.

1.5.: PROMINENCE FORMATION IN A CURRENT SHEET (Contd.)

Equation (1.80), in which we assume that pressure remains constant, determines T as a function of time. The result is that the temperature of the neutral sheet drops by a factor of 10 and the density increases by the same factor in about 10^5 seconds from an initial coronal temperature of 10^6 °K . This condensation time gives good agreement with the observed time for prominences to form (d'Azambuja, 1948). It is faster than Raju's time because the build-up of magnetic pressure is, in this case, not considered, so that the condensation is not impeded by magnetic forces. However, because the timescale for the instability is greater than the resistive diffusion time, we would expect magnetic pressure to build up as the condensation increased. However, the neutral sheet configuration is susceptible to resistive instabilities such as the tearing mode, which forms a series of magnetic loops along the neutral line (Figure (8), page 81). At the same time, the magnetic pressure is reduced, allowing the condensation to continue. Also the magnetic field is re-connected across the neutral sheet, so allowing support for the condensing matter. This is essential, as Hildner has shown in his $B_0 = 0$, $\eta \neq 0$ case, where he is unable to get reasonable condensation of the plasma when the denser matter is not supported.

The question of support for the condensing matter in a neutral sheet has been discussed by Kuperus & Raadu (1974). They point out that the separate currents (Figure (8), page 81), which form in the later stages of the condensation process, due to the tearing mode instability will coalesce and form a structure shown in Figure (9) page 84

1.5.: PROMINENCE FORMATION IN A CURRENT SHEET (Contd.)

This may be regarded as the sum of a vertical field, supplying no vertical supporting force and a field structure, shown in Figure (10), page 85, which will supply the upward Lorentz force necessary for support. This field structure can be thought of as being caused by two currents, one, + J, at a height h above the photosphere and the other, - J, at a height -h below the photosphere. The force between these two currents is.

$$F = \frac{J^2}{h} = \frac{B_\varphi^2}{4\pi h} \pi R^2 , \quad (1.81)$$

where B_φ is the azimuthal field at the boundary of the condensed region which we suppose to have a radius R. Thus to support the mass condensed into the filaments, we require,

$$\frac{B_\varphi^2}{4h} R^2 = \rho \pi R^2 g ,$$

which, for $\rho \simeq 10^{-13}$ g cm^{-3}, $g = 2.74 \times 10^4$ cm sec^{-2}, $h = 10^9$ cm, gives $B_\varphi = 6$ Gauss in good agreement with observations (Rust, 1972).

In the calculation we take the initial background field to be vertical. However, as suggested by Figure (8), page 81, there may be components of the field curved downwards near the photosphere and these will tend to pull the plasma down in opposition to the force F in (1.81). The plasma will then fall if this downward force is large enough, but then the plasma could be supported as in Kippenhahn & Schluter model (Figure (13), page 94).

During the condensation process the plasma will bring in the magnetic field lines because they are frozen-in.

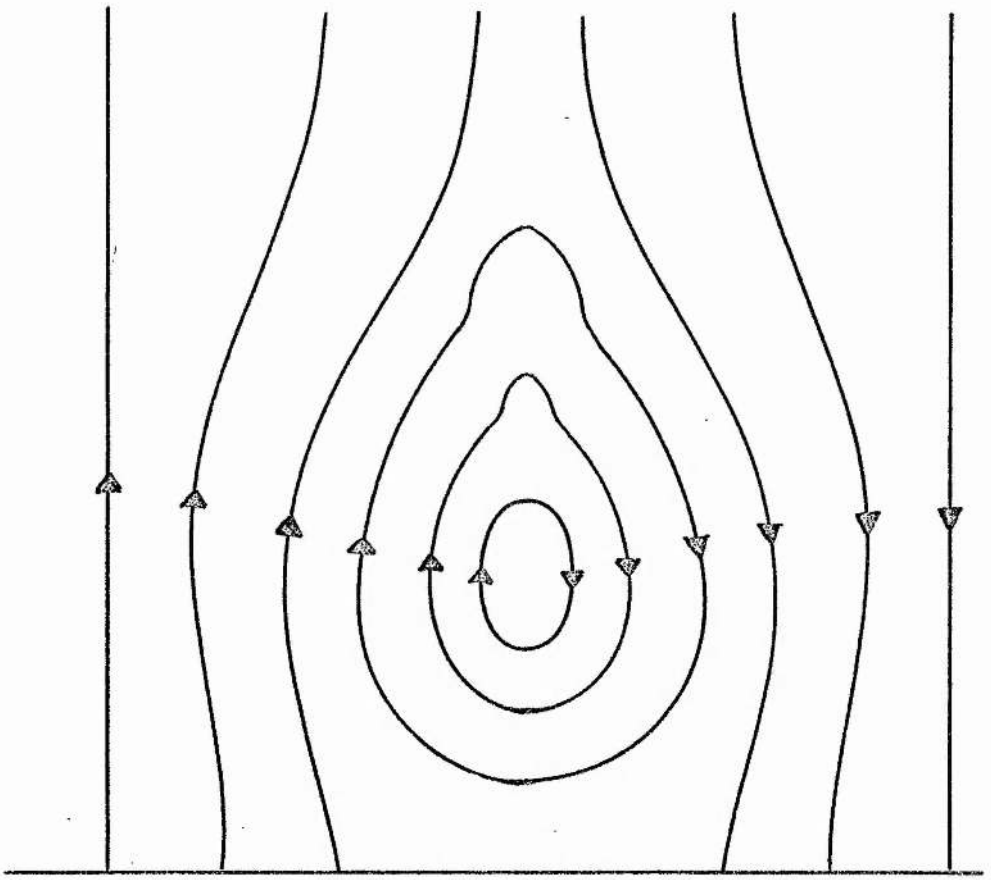

Figure (9). A sketch of the expected coalescence of the currents formed during the tearing mode instability in the current sheet of Figure (8). The magnetic field lines drawn here provide the necessary support, as shown by Kuperus & Raadu (1974), for the condensing matter.

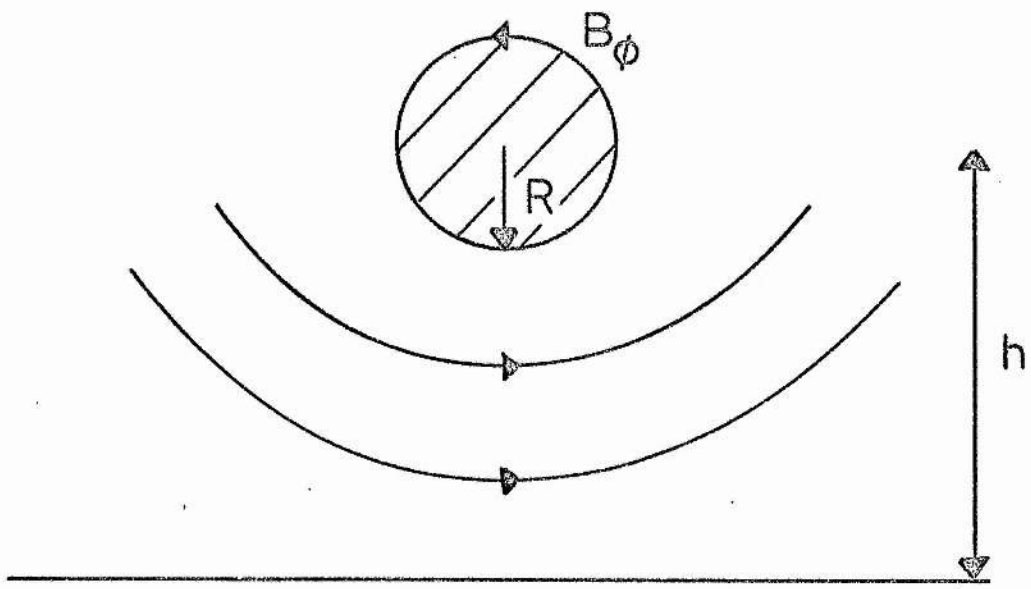

Figure 10. The azimuthal component, B_ϕ , of the magnetic field shown in Figure (9), page 84, which supplies the upward Lorentz force necessary to support the condensed matter, inside the shaded region of radius R, at a height h above the photosphere.

1.5.: PROMINENCE FORMATION IN A CURRENT SHEET (Contd.)

However, these field lines are attached to the photosphere and any magnetohydrodynamic perturbation that travels down the field line is slowed down since the Alfvén speed is proportional to $1/\sqrt{\rho}$. Also the photosphere has a higher inertia than the coronal plasma. Thus the foot-points of the field lines are hardly affected by the condensation process and the field lines will be bent so that Lorentz forces are set up opposing the process. Thus it may seem that this 'line-tying' effect could prevent the condensation from occuring but, as Raadu & Kuperus (1973) show, this is not the case. They consider the field structure drawn in Figure (11), page 87, where it is assumed that the frozen-in plasma pulls in the field lines during the condensation with horizontal velocities. Now, since the field lines are tied to the photosphere there will be no condensation there, but there will be progressively more condensation the higher one goes as the effect of line-tying is reduced. For this reason they expected the condensation to form in a wedge (Figure (12), page 87), so that the variables of the problem depend only on θ.

We expect the condensation to occur more slowly than the Alfvén timescale and so the field and plasma will remain in horizontal force balance,

$$-\frac{\cos\theta}{r}\frac{\partial p}{\partial \theta} + J_z B_y = 0 , \qquad (1.82)$$

where

$$J_z = \frac{1}{4\pi r \cos\theta}\frac{\partial B_y}{\partial \theta} ,$$

and, because the plasma is frozen into the field,

$$\rho/\rho_0 = B_y/B_0 ,$$

where a zero subscript denotes the initial values.

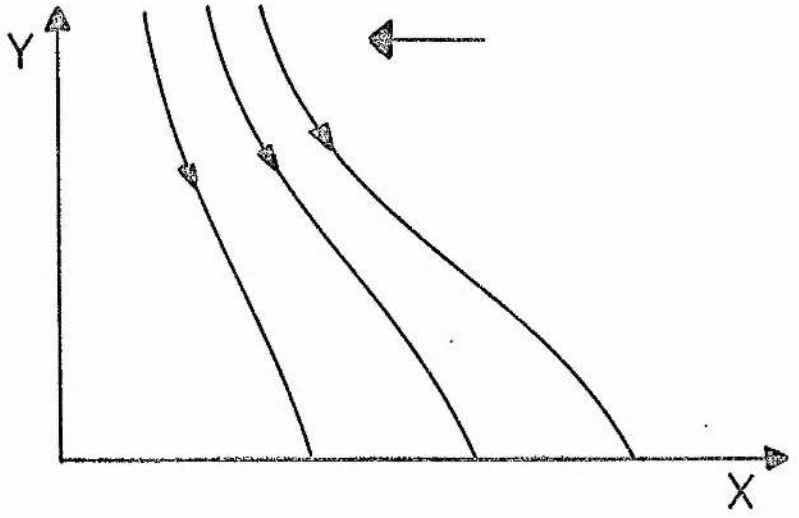

Figure 11. Half of the magnetic field structure in a neutral current sheet with a neutral line at $X=0$. The field lines are attached to the photosphere at $y=0$ and are hardly affected as the condensation process occurs at larger y where the matter flows horizontally, in the direction of the arrow, dragging the field lines with it.

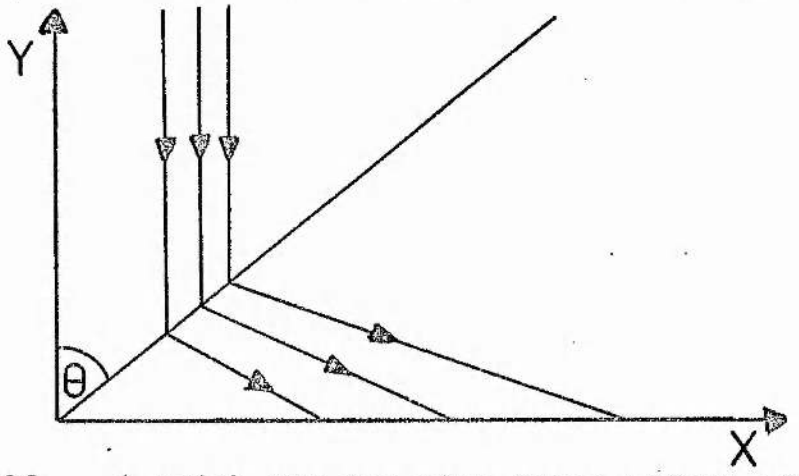

Figure 12. A model for the line-tying effect of Fig.(11) page 87. According to Raadu & Kuperus (1973) they expect the condensation to occur in a wedge formed between the line $X=0$, and the line at an angle θ, but that for angles greater than θ, no condensation occurs.

1.5. : PROMINENCE FORMATION IN A CURRENT SHEET (Contd.)

The energy equation is,

$$\frac{dp}{dt} - \gamma \frac{p}{\rho} \frac{d\rho}{dt} = - L (\gamma - 1) ,$$

where $L = L_{RAD} - G_{mech}$,

$L_{RAD} = \rho^2 q(T)$ ergs cm^{-3} sec^{-1},

and $G_{mech} = \rho \rho_0 q(T_0)$ ergs cm^{-3} sec^{-1}.

Thus

$$\frac{dp}{dt} - \gamma \frac{p}{\rho} \frac{d\rho}{dt} = (\gamma - 1) \rho [\rho_0 q(T_0) - \rho q(T)] . \qquad (1.83)$$

The equilibrium given by (1.82) and by

$$L = 0$$

is perturbed by putting

$$\rho = \rho_0 (1 + \epsilon(\theta) e^{\sigma t}) ,$$

$$p = p_0 + p_1(\theta) e^{\sigma t} .$$

When substituted into (1.82) and (1.83) these give

$$\cos^2\theta \frac{dp_1}{d\theta} + \frac{B_0^2}{4\pi} \frac{d\epsilon}{d\theta} = 0 \qquad (1.84)$$

and $$\sigma p_1 - \gamma p_0 \sigma \epsilon = - \gamma p_0 \delta_p \epsilon + \delta_\rho p_1 , \qquad (1.85)$$

where

$$\delta_p = \frac{1}{c_p T} \left(\frac{\partial L}{\partial \rho} \right)_p = \frac{- \rho}{c_p} \frac{dq}{dT} + \frac{\rho q}{c_p T}$$

and

$$\delta_\rho = \frac{- p}{\rho c_v T} \left(\frac{\partial L}{\partial p} \right)_\rho = - \frac{\rho}{c_v} \frac{dq}{dT}$$

are the growth rates at constant pressure and density, respectively.

Elimination of p_1 from (1.84) and (1.85) gives

$$\left[\gamma p_0 (\sigma - \delta_p) \cos^2\theta + \frac{B_0^2}{4\pi} (\sigma - \delta_\rho) \right] \frac{d\epsilon}{d\theta} = 0 . \qquad (1.86)$$

1.5.: PROMINENCE FORMATION IN A CURRENT SHEET (Contd.)

Thus ϵ is constant except possibly at θ^*, where the term in the bracket vanishes, so that

$$\sigma = \frac{\delta b_\rho + \frac{\gamma p_0 4\pi}{B_0^2} \delta b_p \cos^2\theta^*}{1 + \frac{\gamma p_0 4\pi}{B_0^2} \cos^2\theta^*} \quad . \qquad (1.87)$$

At the photosphere ($\theta = \pi/2$) there is no compression so the solution is

$$\epsilon = \begin{cases} \epsilon_0 & , \theta < \theta^* \\ 0 & , \theta > \theta^* \end{cases} .$$

It is possible to show that the maximum growth rate occurs when $\theta^* = 0$, provided $\delta b_p > \delta b_\rho$, or, for $\gamma = 5/3$, provided

$$\frac{T}{q}\frac{dq}{dT} > -\frac{3}{2} \quad . \qquad (1.88)$$

For the radiative loss function $q(T) = \chi T^\alpha$ (Figure(1), page 14), (1.88) becomes

$$\alpha > -\frac{3}{2} \quad .$$

In the corona, equation (1.27) gives $\alpha = -1.0$ so that this condition holds. Thus the maximum growth rate occurs for $\theta^* = 0$, i.e. for the thinnest wedges.

1.5.: PROMINENCE FORMATION IN A CURRENT SHEET (Contd.)

From these sections we see that a neutral current sheet is a good place in which a thermal instability can occur and cause the condensation of a prominence. In other field configurations, as the plasma condenses, it drags the"frozen-in" magnetic field with it, so the magnetic pressure builds up and inhibits the condensation. Inside a current sheet, on the other hand, magnetic flux can be annihilated by the tearing mode instability, so that the magnetic pressure does not build up so much. Also the tearing mode creates magnetic field loops, which may thermally insulate blobs of plasma and also support, as suggested by Kuperus & Raadu (1974), the condensing plasma. It may have seemed that line-tying would have prevented the instability occuring in a neutral sheet but Raadu & Kuperus(1973) demonstrate that the plasma is still thermally unstable when this effect is considered and that the formation of a thin condensation region is favoured.

1.5.:PROMINENCE FORMATION IN A CURRENT SHEET (Contd.)

THEORIES OF PROMINENCE SUPPORT

In section 1.2 on the discussion of thermal instability we saw that the magnetic field plays two roles. One is to prevent heat conduction into the plasma (so inhibiting the occurrence of the thermal instability) and the other is to support the condensing matter and then allow the condensation to continue.
In the last sub-section we saw how prominence material may be supported in a current sheet. Here we shall look at another magnetic field structure which may support the prominence material.
It is commonly suggested that prominence material is supported against gravity by the Lorentz force. If the magnetic field lines are in a plane perpendicular to the long axis (y direction) of a prominence and a current flows along that axis, the Lorentz force has a vertical ($\pm z$ direction) component opposing gravity.
The plasma is taken to be in mechanical equilibrium under a balance between gravity, pressure gradients and the Lorentz force, so that

$$0 = -\underline{\nabla} p + \rho \underline{g} + \frac{1}{4\pi} (\underline{\nabla} \wedge \underline{B}) \wedge \underline{B} \quad . \qquad (1.89)$$

1.5.: PROMINENCE FORMATION IN A CURRENT SHEET (Contd.)

Any magnetic field component along the prominence is neglected ($B_y = 0$), as are variations of the variables in that direction ($\partial/\partial y = 0$). Also the atmosphere is supposed isothermal so that the perfect gas law gives

$$p = nkT = \rho g H_0 \quad , \qquad (1.90)$$

where the scale height $H_0 = kT/mg$ is constant. Finally, we have

$$\nabla . \underline{B} = 0 \quad . \qquad (1.91)$$

Kippenhahn & Schluter (1957) combined equations (1.89), (1.90) and (1.91) to give

$$B_x \nabla^2 B_z - B_z \nabla^2 B_x + \frac{B_z}{H_0}\left(\frac{\partial B_z}{\partial x} - \frac{\partial B_x}{\partial z}\right) = 0 \quad . \qquad (1.92)$$

Once the magnetic field has been determined, the density distribution follows from the x – component of (1.89)

$$\frac{\partial \rho}{\partial x} = - \frac{m B_z}{4\pi kT}\left[\frac{\partial B_z}{\partial x} - \frac{\partial B_x}{\partial z}\right] \quad . \qquad (1.93)$$

1.5.: PROMINENCE FORMATION IN A CURRENT SHEET (Contd.)

They argued that B_x varies slowly with x in a thin prominence, and so took B_x independent of x .
They also neglect variations of B_x with height so that

$$B_x = \text{constant} .$$

Then by (1.91), B_z is independent of z and (1.92) becomes

$$\frac{\partial^2 B_z}{\partial x^2} + \frac{B_z}{H_0 B_x} \frac{\partial B_z}{\partial x} = 0 \quad . \qquad (1.94)$$

The boundary conditions $B_{z\,(x=0)} = 0$ and $B_{z\,(x \to \infty)} = B_z(\infty)$ give the following solution to (1.94)

$$B_z = B_z(\infty) \tanh\left[\frac{B_z(\infty)}{B_x} \frac{x}{2H_0} \right] . \qquad (1.95)$$

The resulting field lines are sketched in Figure (13), page 94.
Equation (1.93) for the density reduces to

$$\frac{\partial \rho}{\partial x} = - \frac{m}{8\pi kT} \frac{\partial B_z^2}{\partial x}$$

with the solution

$$\rho = - \frac{m B_z(\infty)}{8\pi kT} \left[\tanh^2 \left(\frac{B_z(\infty)}{B_x} \frac{x}{2H_0} \right) - 1 \right] , \qquad (1.96)$$

subject to the boundary condition $\rho = 0$ as $x \to \infty$.

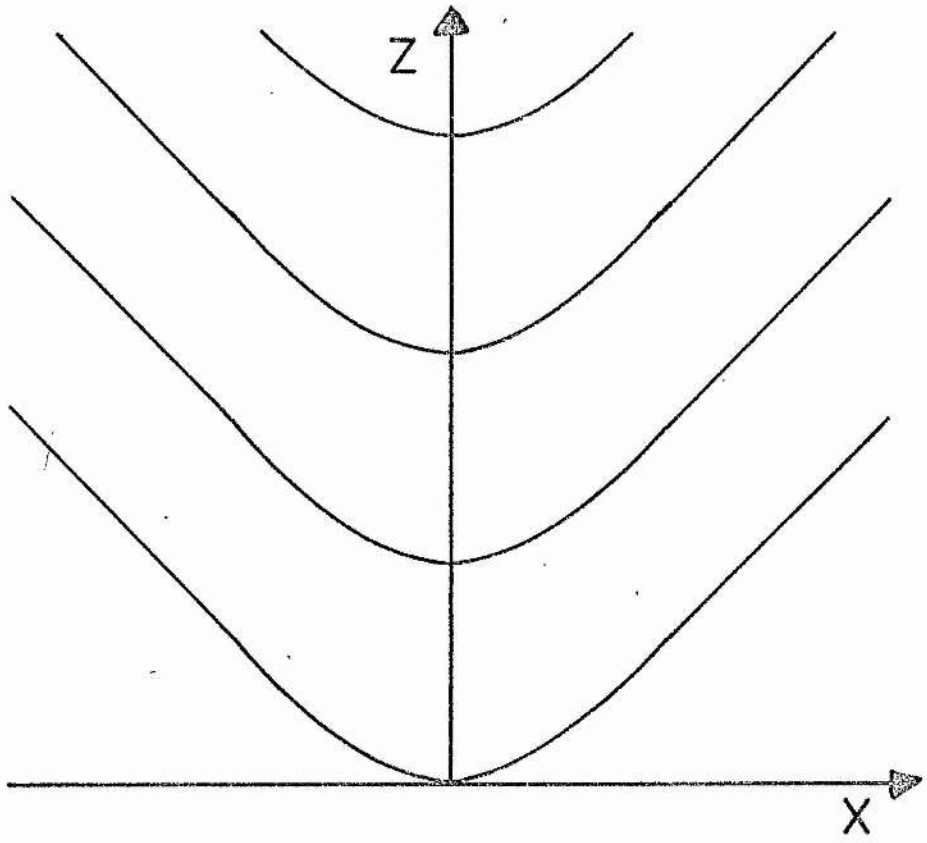

Figure 13. The magnetic field structure which Kippenhahn & Schluter (1957) developed to support the condensed material in a quiescent prominence.

The field structure is given by equation (1.95)..

1.5.: PROMINENCE FORMATION IN A CURRENT SHEET (Contd.)

The density distribution has a fairly sharp maximum at the prominence centre, ($x = 0$), and falls to half its value at $x = \pm 1{\cdot}8\, H_0 \left[B_x / B_z(\infty) \right]$.

If this value of x is interpreted as the width of a prominence we see that the model predicts a width of approximately H_0, the scale height,

$$H_0 = \frac{kT}{m_i g} \simeq 10^9 \text{ cm},$$

where Boltzmann's constant $k = 1{\cdot}38 \times 10^{-16}$ ergs deg^{-1},

the ion mass $m_i = 1{\cdot}67 \times 10^{-24}$ g,

gravitational acceleration $g = 2{\cdot}74 \times 10^4$ cm sec^{-2}

and temperature $T = 10^6\,^\circ$K.

This agrees with the observed values of the width of from 5×10^8 cm to 10^9 cm.

The maximum value of the density $\rho_{max} = m\, B_z(\infty)^2 / 8\pi kT$, which for a prominence with $T = 5 \times 10^3\,^\circ$K, and $B_z(\infty) = 2$ Gauss, gives $\rho_{max} = 5 \times 10^{-13}$ g cm^{-3} or $n_e \simeq 10^{11}$ cm^{-3}, which also agrees with observations.

1.5.: PROMINENCE FORMATION IN A CURRENT SHEET (Contd.)

STABILITY OF THE KIPPENHAHN & SCHLUTER MODEL

At first sight one may suspect that the Kippenhahn & Schluter model is unstable to the interchange instability, since the supporting field lines are concave to the plasma, Anzer (1969), however discussed the stability of the model against arbitrary perturbations and found the model to be stable under certain conditions. He uses an energy principle due to Bernstein et al. (1958), modified to include configurations where the normal component of the magnetic field does not vanish at the discontinuity surface between a plasma and a vacuum. A perturbation, $\underline{\xi}$, of the plasma everywhere produces a change in the potential energy of amount

$$\delta W = -\frac{1}{2}\int \underline{\xi}.\left[\underline{\nabla}\left(\gamma p \underline{\nabla}.\underline{\xi} + \underline{\xi}.\underline{\nabla} p\right) + \underline{J}\wedge \operatorname{curl}\left(\underline{\xi}\wedge\underline{B}\right) - \underline{B}\wedge \operatorname{curl}\operatorname{curl}\left(\underline{\xi}\wedge\underline{B}\right) + \underline{\nabla}.(\rho\underline{\xi}).\underline{\nabla}\phi\right] dV \,, \tag{1.97}$$

the plasma being unstable if there is a particular displacement $\underline{\xi}$ for which $\delta W < 0$.

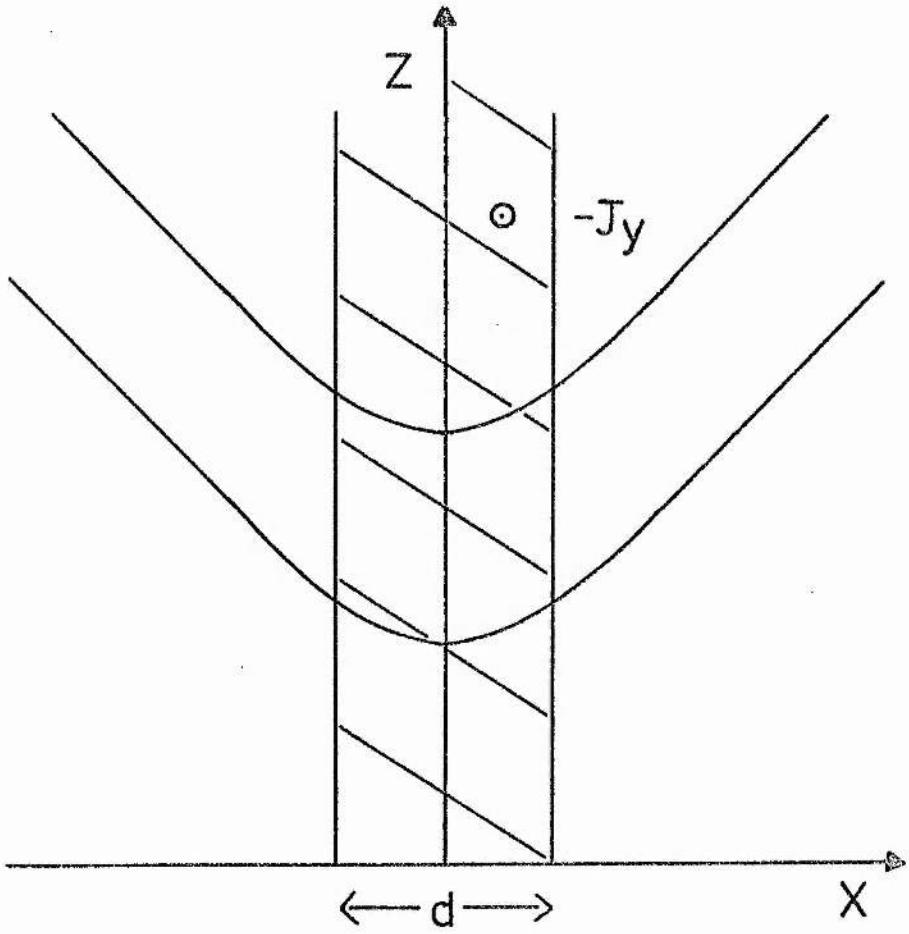

Figure 14. The model of a prominence with width, d, supported by the magnetic field, which Kippenhahn & Schluter (1957) calculated and which was tested for stability to general perturbations by Anzer (1969).

1.5.: PROMINENCE FORMATION IN A CURRENT SHEET (Contd.)

Anzer considered a thin vertical sheet of width d, as shown in Figure(14) page 97, containing a current

$$-J_y(z) = \Delta B_z(z) = (B_z)_{\frac{d}{2}} - (B_z)_{-\frac{d}{2}}$$

In the limit $d \to 0$, with $B_x(x=0) = B_{xo}$ equation (1.97) becomes

$$\delta W = \frac{1}{2}\iint -J_y \frac{dB_{xo}}{dz}\xi_x^2 + B_{xo}\frac{dJ_y}{dz}\xi_z^2\, dy\, dz$$
$$+ \text{positive term},$$

from which we find the following sufficient conditions for stability ($\delta W > 0$):

$$\Delta B_z \frac{dB_{xo}}{dz} \geq 0 \qquad (1.98)$$

and

$$B_{xo}\frac{d\Delta B_z}{dz} \leq 0 \quad . \qquad (1.99)$$

If the mass is supported by the Lorentz force, so that

$$\rho d g = -B_{xo} J_y = B_{xo}\Delta B_z$$

Thus

$$B_{xo}\Delta B_z > 0$$

and (1.99) becomes

$$\Delta B_z \frac{d}{dz}(\Delta B_z) = \frac{1}{2}\frac{d}{dz}(\Delta B_z)^2 = \frac{1}{2}\frac{d}{dz}(J_y)^2 \leq 0\,, \qquad (1.100)$$

1.5.: PROMINENCE FORMATION IN A CURRENT SHEET (Contd.)

so that for stability the current density decreases with height. While measurements indicate that (1.98) is correct in quiescent prominences, direct observational proof of (1.99) is not yet available.

Observations by Rust (1966) and Harvey (1969) that magnetic fields in prominences apparently have no preferred orientation with respect to the prominence axis led Nakagawa to consider the possibility that the shear between the prominence magnetic field and the field below might provide support. Nakagawa & Malville (1969) considered an upper half plane of plasma with a uniform magnetic field B^{p}_{oy} supported against gravity by a magnetic field $(B^{c}_{ox}, B^{c}_{oy}, 0)$ in the vacuum below.

They linearized the MHD equations, neglected radiation and thermal conduction, and investigated the stability of the interface $z = 0$ as a function of the angle between the magnetic fields in the two regions.

The fastest growing unstable mode is obtained from the resulting dispersion relation and predicts a break-up of the prominence plasma into regular spaced sections with a certain wavelength. Nakagawa & Malville suggest that the regular arch structure of many quiescent prominences is produced by such an instability.

The angle of shear between the lower and upper field affects the wavelength at which the instability occurs, and by comparing this wavelength with the observed spacing, they predict this angle to be between 60^{o} and 90^{o}.

1.5.: PROMINENCE FORMATION IN A CURRENT SHEET (Contd.)

THE AIMS OF THE THESIS

We consider two instabilities which can occur in the solar atmosphere, the thermal instability and the tearing mode instability. Both of these instabilities are applied to neutral current sheets in an attempt to understand the processes involved in the formation of prominences within such structures. Also we examine the thermal instability in a magnetic arch structure to see if it could be the cause of condensation in the solar atmosphere.

In chapter 2,we extend the work of Kuperus& Tandberg-Hanssen (1967) on the formation of quiescent prominences in a neutral current sheet. We first set up the equilibrium for current sheet plasma under a balance between radiative loss, constant mechanical heating and thermal conduction, and then investigate its stability. The object is to verify the order of magnitude prediction of section 1.2 that instability occurs when the current sheet length exceeds a certain value and to obtain more accurate values for both this length and the time it takes the plasma to cool to prominence temperatures.

In their paper on the formation of prominences, Kuperus& Tandberg-Hanssen (1967) suggested that the tearing mode instability occurs along with the thermal instability, and so we have examined, in chapter 3, this resistive instability in the neutral current sheet.

1.5.: PROMINENCE FORMATION IN A CURRENT SHEET (Contd.)

As described in section 1.3, Cross & Van Hoven (1971) have developed a numerical technique to calculate the growth rate of the linear stability problem for a sheared field. They search for the unique value of this growth rate which brings about convergence of the Fourier series that describe the perturbations of a spatially periodic equilibrium configuration. We use this method to calculate the growth rate of the tearing-mode instability in a neutral current sheet. In addition, we investigate the influence of a component of the equilibrium magnetic field across the neutral sheet on this growth rate. In particular we want to find how big such a component needs to be to inhibit the tearing-mode, since this is of relevance to a possible trigger mechanism for solar flares.

We expect some types of prominence to form in neutral current sheets, but others may form in closed magnetic field configurations. In chapter 4 we consider a force-free magnetic structure and examine the effects on the thermal instability of moving the feet of the arches and so shearing the field. We expect that, as the shearing increases, so the flux tubes become longer, until thermal conduction is no longer able to prevent the occurrence of a thermal instability. The object is then to verify this intuitive idea and find how much shearing is necessary to initiate a condensation. Presumably at the onset of the instability plasma is sucked up along field lines until enough material is present to allow a new equilibrium in the form of a prominence.

CHAPTER 2.

THERMAL INSTABILITY IN A CURRENT SHEET

In this chapter we present a model for the thermal equilibrium and stability of a current sheet in the corona or upper chromosphere. The energy balance of the neutral sheet is between thermal conduction, radiative loss and a constant mechanical heating. When the length of the sheet is small enough, the plasma in the sheet is kept stable by the dominance of thermal conduction in equalising any potentially unstable temperature differences, but as the length of the sheet increases the effect of thermal conduction is decreased considerably. If the length exceeds a certain maximum value no equilibrium is possible and the plasma cools down. We calculate in this chapter, the values of this maximum length and also the time taken for the unstable plasma to cool down.

We also outline a method originally devised by Cross & Van Hoven (1971) in their study of resistive instabilities, (see Section 1.3) for calculating the linear growth rate of the thermal instability. This may prove to be useful in establishing how the thermal instability interacts with other instabilities, in particular the tearing-mode instability.

2.1.: THE EQUILIBRIUM ENERGY BALANCE IN A CURRENT SHEET

In this section a simple model is set up for the energy balance in the neutral current sheet whose interior field vanishes. The sheet has width ℓ and length L and is bounded by anti-parallel magnetic field lines of uniform field strength B. Equilibrium conditions inside the sheet are characterised by gas pressure P 20, density ρ 20, temperature T 20 and a vanishing magnetic field, while the corresponding values outside are P_1 , ρ_1 , T_1 and B , as indicated in Figure(15) page 104. All these values are assumed uniform so that our simple model takes no account of the spatial structure of the sheet. Plasma motions in the equilibrium state are also neglected, although a more comprehensive treatment would be expected to include them, as well as the vertical pressure gradients produced by gravity.

The neutral sheet is assumed to be in a state of magnetostatic equilibrium under a balance between plasma and magnetic pressure, which gives

$$p_{20} = p_1 + B^2/8\pi \quad . \qquad (2.1)$$

The perfect gas law gives the internal gas pressure as

$$p_{20} = R\,\rho_{20}\,T_{20} \quad . \qquad (2.2)$$

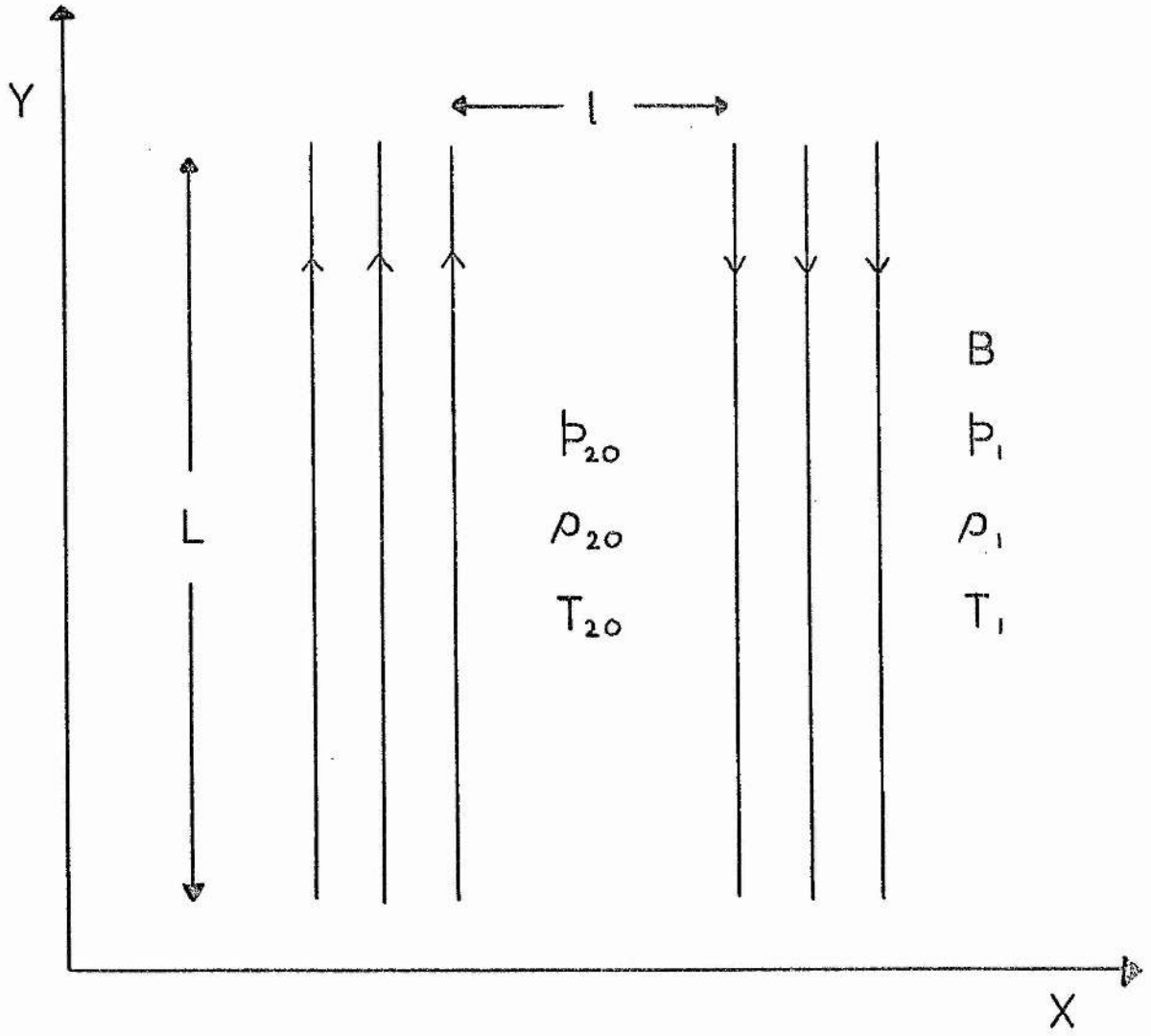

Figure (15). The simple model for a neutral current sheet of width l and length L in equilibrium energy balance. The values of pressure P_{20}, density ρ_{20}, and temperature T 20 inside the sheet, where B=0, are calculated for both coronal and chromosphere values of the corresponding conditions outside the sheet.

2.1.: THE EQUILIBRIUM ENERGY BALANCE IN A CURRENT SHEET (Contd.)

Finally the equilibrium energy balance equation for a unit volume of plasma is

$$-L(\rho,T) + \underline{\nabla}.(\underline{\underline{\kappa}}.\underline{\nabla}T) = 0 , \qquad (2.3)$$

where L is the heat loss function, which is defined (section 1.1) as the difference between the heat lost and heat gained by a unit volume of plasma per unit time due to all sinks and sources in the atmosphere except thermal conduction, and $\underline{\nabla}.(\underline{\underline{\kappa}}.\underline{\nabla}T)$ is the amount of energy conducted into the volume per unit time.
We need to detail the terms which must appear in the energy equation for a plasma in the corona and upper chromosphere. As already mentioned in Chapter 1 (section 1.1), the main heat sources and sinks in the neutral current sheet that we shall consider are the loss of energy by electromagnetic radiation, heat conducted into or out of the sheet, the constant mechanical heating and the joule heating.
In our analysis we shall approximate the conduction of heat into a unit volume per unit time by

$$K_{\parallel}(T_1 - T_{20})/L^2 + K_{\perp}(T_1 - T_{20})/\ell^2 , \qquad (2.4)$$

where L is the length of the sheet in the y direction and ℓ is the width in the x direction. The conduction of heat is affected by the magnetic field, $\underline{B}$, such that the coefficient of thermal conduction parallel to the field, $K_{\parallel}$ is much larger than the coefficient perpendicular to the field, $K_{\perp}$, where from equations (1.22) and (1.23)

$$K_{\parallel} = 2 \times 10^{-6} T_{20}^{5/2} \text{ ergs sec}^{-1} \text{ deg}^{-1} \text{ cm}^{-1} \qquad (2.5)$$

and

$$K_{\perp} = 3 \times 10^{-24} \frac{n^2}{T_{20}^{1/2} B^2} \text{ ergs sec}^{-1} \text{ deg}^{-1} \text{ cm}^{-1} \qquad (2.6)$$

In the sheared magnetic field of a neutral sheet there is an electric current which heats the plasma at a rate J^2/σ , where the current density $J \simeq \frac{B}{\ell 4\pi}$ statamp cm^{-2} and the conductivity $\sigma = 7.7 \times 10^{-15} T_{20}^{3/2}$ e.m.u. from equation (1.4). Thus the joule heating is of order in magnitude

$$J^2/\sigma = 1.3 \times 10^{14} B^2/((4\pi\ell)^2 T_{20}^{3/2}) \qquad (2.7)$$

$$\text{ergs sec}^{-1} \text{ cm}^{-3}$$

Both joule heating and thermal conduction depend on the dimensions of the current sheet while the other main energy term, radiative loss, does not. Thus, to see which terms are important in the quiescent prominence model, we shall compare joule heating and thermal conduction with radiative loss. In fact we shall calculate first the ratio, R_1 , of the radiative loss given by $\chi \rho_{20}^2 T_{20}^{\alpha}$ to the joule heating given by (2.7), and then the ratio, R_2 , of the radiative loss to the thermal conduction parallel to the field which is given by equations (2.4) and (2.5), and lastly the ratio, R_3 , of the radiative loss to the thermal conduction perpendicular to the field, which is given by equations (2.4) and (2.6).

2.1.: THE EQUILIBRIUM ENERGY BALANCE IN A CURRENT SHEET (Contd.)

Thus,

$$R_1 = \frac{\chi \rho_{20}^2 T_{20}^{\alpha} (4\pi\ell)^2 T_{20}^{3/2}}{1.3 \times 10^{14} B^2} ,$$

$$R_2 = \frac{\chi \rho_{20}^2 T_{20}^{\alpha} L^2}{K_{\parallel} (T_1 - T_{20})} ,$$

and $$R_3 = \frac{\chi \rho_{20}^2 T_{20}^{\alpha} \ell^2}{K_{\perp} (T_1 - T_{20})} .$$

We have tabulated R1, R2 and R3 in Table 2 using as the dimension of the quiescent prominence,

$L = 5 \times 10^9$ cm , $\ell = 5 \times 10^8$ cm ,

and with coronal values of temperature and density ,

$T_1 = 10^6$ °K , $n_e = 2 \times 10^8$ cm^{-3}

(corresponding to a height of 3.7×10^9 cms in the Billings & Alvarez model of the corona, Table 1).

It can be seen from Table 2 that, in the coronal current sheet we are considering, the joule heating is very small compared with the radiative loss and so can be neglected. However, in the chromosphere, joule heating can be important, there $T_{20} = T_1/10 \simeq 5 \times 10^3$ °K,

$\rho_1 = 10^{-15}$ g cm^{-3} , $B = 10^2$ Gauss

and, if the width of the current sheet is less than or equal to 5×10^9 cms, then joule heating is as important as the radiative loss term. For this reason joule heating has been included in an energy equation by Heyvaerts & Priest (1976) for their study of a current sheet which forms as new magnetic flux emerges from below the photosphere.

TABLE 1.

The Billings and Alvarez (1975) model for a quiet region of the solar atmosphere. Numbers in parenthesis give the power of ten by which the value has to be multiplied.

HEIGHT (cm.)	LOG T(K)	LOG N(cm^{-3})
2.3804 (8)	4.70	9.98
2.3891 (8)	4.80	9.88
2.3964 (8)	4.90	9.78
2.4000 (8)	4.955	9.73
2.4037 (8)	5.01	9.67
2.4074 (8)	5.06	9.62
2.4115 (8)	5.11	9.57
2.4212 (8)	5.20	9.47
2.4349 (8)	5.30	9.37
2.4566 (8)	5.40	9.27
2.4950 (8)	5.50	9.17
2.5724 (8)	5.60	9.07
2.7477 (8)	5.70	8.97
3.2014 (8)	5.80	8.86
4.5649 (8)	5.90	8.74
9.3620 (8)	6.00	8.60
1.6320 (9)	6.05	8.50
3.7199 (9)	6.10	8.31
2.0440(10)	6.135	7.46

In their model atmosphere, Billings & Alvarez measure height from the centre of the transition region ($T \simeq 10^5$°K) and so, in order to give the height relative to the photosphere, it has been assumed that this point in the transition region is 2.4×10^8 cm. above the photosphere (Vernazza, Avrett & Loeser, 1973).

TABLE 2.

The size of the various heating terms relative to the radiative loss term in a structure with the dimensions, $L = 5 \times 10^9$ cm and $\ell = 5 \times 10^8$ cm, of a prominence and surrounded by coronal plasma at a temperature of $T_1 = 10^6$ °K and a density of $n_e = 2 \times 10^8$ cm^{-3}

	R_1			R_2			R_3		
Magnetic Field Strength (Gauss)	The ratio of the rad. loss over the joule heating.			The ratio of the rad. loss over the conduction of heat parallel to B.			The ratio of the rad. loss over the conduction of heat perpendicular to B.		
	The temp. inside the sheet.			The temp. inside the sheet.			The temp. inside the sheet.		
	$T_{20}=T_1$	$T_{20}=\frac{T_1}{10}$	$T_{20}=\frac{T_1}{100}$	$T_{20}\simeq T_1$	$T_{20}=\frac{T_1}{10}$	$T_{20}=\frac{T_1}{100}$	$T_{20}\simeq T_1$	$T_{20}=\frac{T_1}{10}$	$T_{20}=\frac{T_1}{100}$
0.1	7.1×10^{10}	3.7×10^{12}	10^{10}	6×10^{-2}	7×10^{4}	8×10^{5}	5.4×10^{5}	2.8×10^{6}	1.9×10^{5}
1.0	2.1×10^{9}	1.1×10^{11}	2.9×10^{8}	1.7×10^{-1}	1.1×10^{5}	2.4×10^{6}	6.8×10^{7}	2.8×10^{8}	6.0×10^{5}
10.0	3.7×10^{10}	2.0×10^{12}	5.0×10^{9}	3×10^{2}	1.7×10^{8}	4.1×10^{9}	4.2×10^{9}	2.4×10^{10}	9.8×10^{8}
100	3.7×10^{12}	2.0×10^{14}	5.2×10^{11}	3.0×10^{6}	1.6×10^{12}	4.1×10^{13}	4.3×10^{11}	2.4×10^{12}	9.8×10^{10}

2.1.: THE EQUILIBRIUM ENERGY BALANCE IN A CURRENT SHEET (Contd.)

It can also be seen from Table 2 that the heat conducted across the sheet is small compared to the radiative loss in a structure with the dimensions of a prominence, where for the case $T_{20} \simeq T_1$ we have put $(T_{20} - T_1) \simeq T_1$ in both R2 and R3. In what follows, therefore, thermal conduction across the sheet will not be included in the energy equation. From the values of R3 we see that the heat conducted along the field lines is important when $T_{20} \simeq T_1$ and $B \leq 10$ Gauss, so we include it in the energy equation.

For neutral current sheets in the corona and upper chromosphere, the terms which we are including in the energy equation (2.3) are the radiative loss, thermal conduction along the field, and a constant mechanical heating, so that (2.3) reduces to

$$b\rho_{20} - \chi \rho_{20}^2 T_{20}^{\alpha} + \frac{K_{11}(T_1 - T_{20})}{L^2} = 0 \quad (2.8)$$

If the mechanical heating rate per unit mass inside the sheet is the same as that outside, where it balances a radiative loss alone, b is determined to be $b = \chi_1 \rho_1 T_1^{\alpha_1}$, so using (2.5) for K_{11}, (2.8) becomes

$$\chi_1 \rho_1 T_1^{\alpha_1} - \chi \rho_{20} T_{20}^{\alpha} + \frac{2\times10^{-6} T_{20}^{5/2}(T_1 - T_{20})}{\rho_{20} L^2} = 0 \quad (2.9)$$

The three equations (2.1), (2.2) and (2.9) are solved for the three unknowns ρ_{20}, P_{20}, and T_{20} with L and B as parameters.

2.1.: THE EQUILIBRIUM ENERGY BALANCE IN A CURRENT SHEET (Contd.)

In particular the results for L as a function of T 20 for various values of B are shown in Figures (16), page 112 and (17), page 113. Figure (16) is plotted for coronal conditions ($T_1 = 10^6 °K$, $n_e = 10^8 cm^{-3}$). It shows that as the length L of the sheet increases, so the equilibrium solution moves along a curve from the bottom right-hand corner; the temperature T20 inside the sheet decreases slightly from the coronal value ($10^6 °K$). Eventually, where the length exceeds the maximum value L max (which, when B = 1 Gauss, is approximately the height of a quiescent prominence (5×10^9 cms)), there is no longer any neighbouring equilibrium. It can also be seen that for values of L between this maximum and a certain minimum, there are in fact three possible values of T20. Figure (17), page 113 is plotted for the upper chromosphere case ($T_1 = 10^5 °K$, $n_e = 10^9 cm^{-3}$) where we have included the high temperature solution ($T_1 > 10^5 °K$). This solution also exists in the coronal case but the values of L are too large to be relevant to the formation of quiescent prominences. This can be seen in Figure (18), page 114, where we have plotted the minimum value of length , L_{min}, for these high temperature solutions as a function of height, using the Billings & Alvarez model atmosphere (Table 1.). The values of L_{min} in this model are greater than 10^{12} cms. in the corona but drop to more reasonable values in the upper chromosphere.

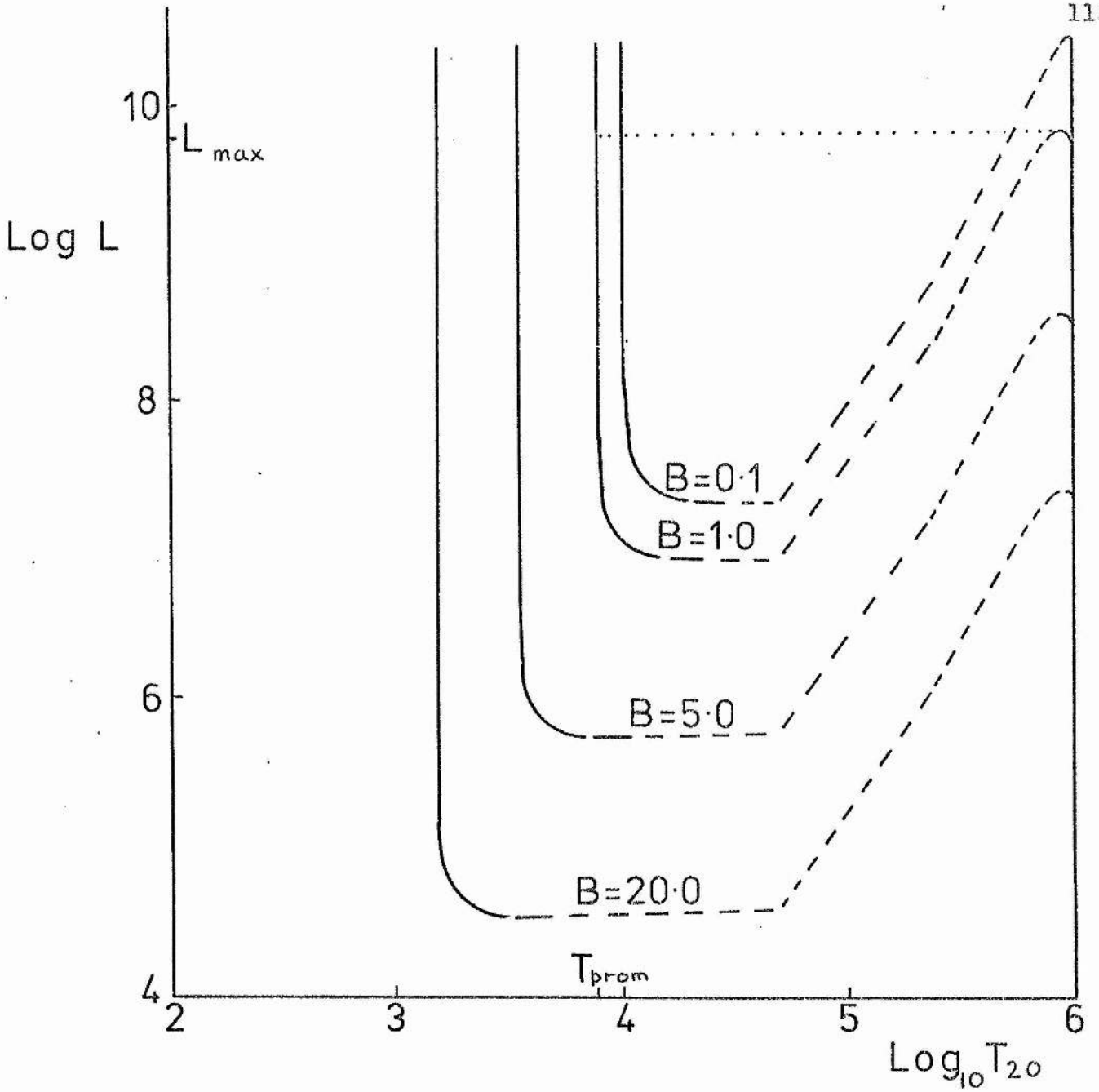

Figure (16). The length of a neutral sheet in thermal equilibrium in the corona (with ambient temperature $T_1 = 10^6\,^{\circ}K$) as a function of the temperature, T 20, inside the sheet for several values of the external magnetic field B (Gauss). The solid parts of the curves represent stable equilibria, while the dashed parts indicate unstable equilibria. If the length of the neutral sheet is increased beyond L_{max} (shown here for the particular case B=1 Gauss) then the plasma becomes unstable and cools down along the dotted line to a new equilibrium value of temperature T_{prom}.

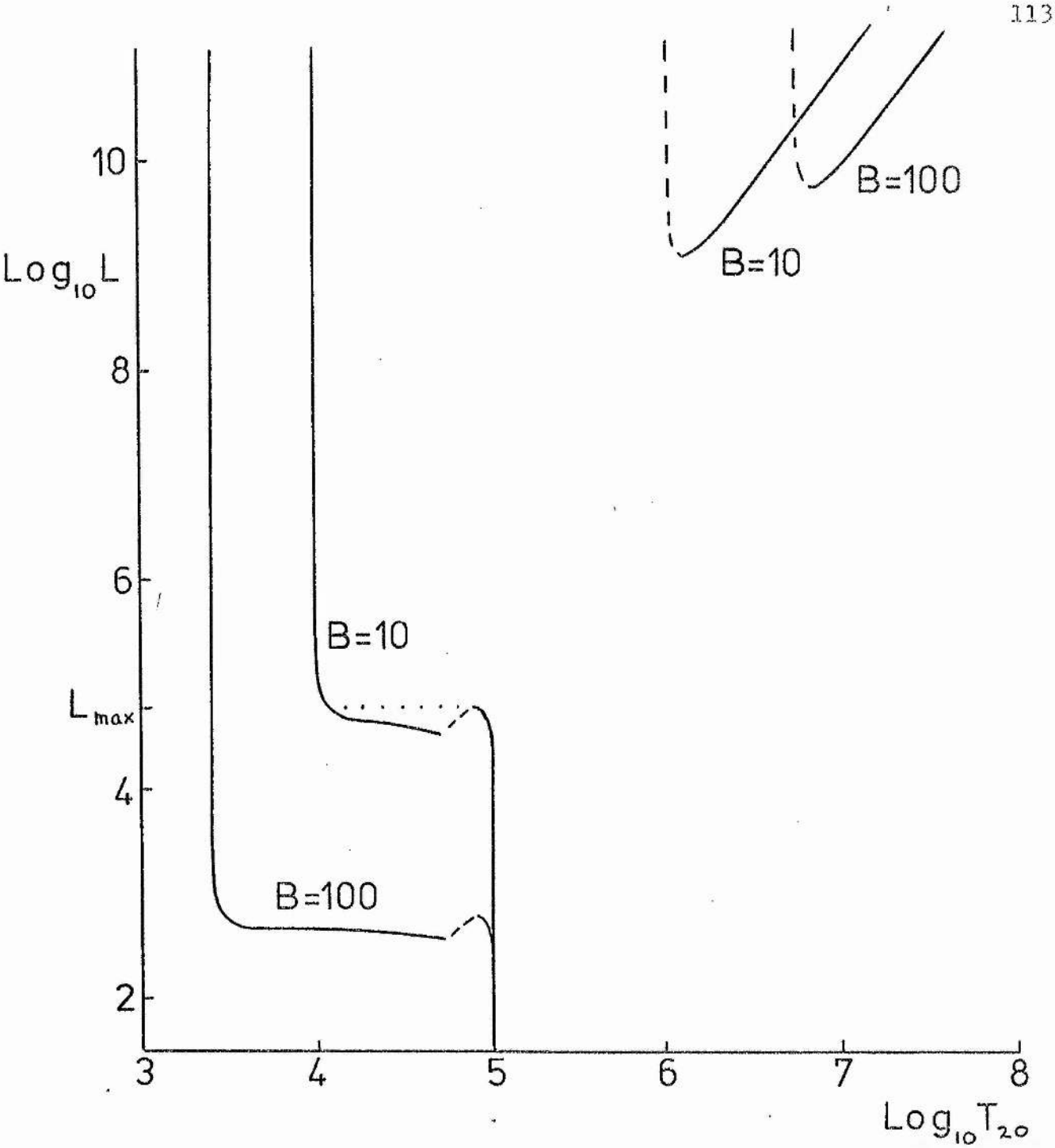

Figure (17). The length of a neutral current sheet in thermal equilibrium in the chromosphere (with ambient temperature $T_1 = 10^5$°K as a function of the temperature T 20, inside the sheet for several values of the external magnetic field, B (Gauss). (_____ stable equilibria, - - - - - unstable equilibria ..... instability path when B-10 Gauss and L → L max).

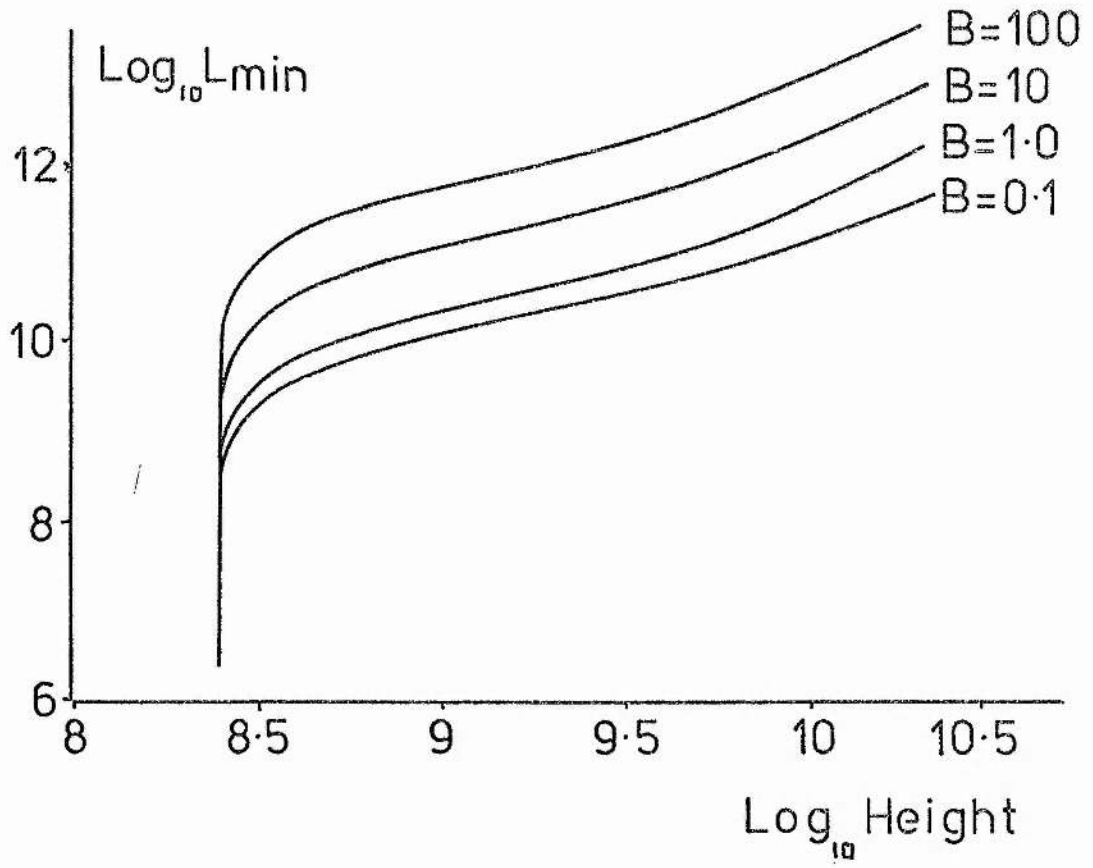

Figure (18). The minimum length for a stable sheet, Lmin (cms) (see Figure (17) page 113, when $T_{20} > 10^5 °K$) as a function of the height (cms) in the atmosphere model given in Table I for several values of the external magnetic field B (Gauss)

2.1.: THE EQUILIBRIUM ENERGY BALANCE IN A CURRENT SHEET (Contd.)

In Figures (16) and (17) pages 112 and 113, the discontinuities in slope at 2.5×10^5 °K and 5×10^4 °K are due to corresponding jumps in the values of γ and α which are present in the approximation to the radiative loss term.

The slope and turning points of the curves in Figures (16) and (17), for the equilibrium temperature, T20, are determined by the size and sign of the temperature gradients of thermal conduction and radiative loss. To see this we will consider the heat gain function, which is defined as,

$$H = \gamma_1 \rho_1 T_1^{\alpha_1} - \gamma \rho_2 T_2^{\alpha} + 2 \times 10^{-6} T_2^{5/2} \frac{(T_1 - T_2)}{\rho_2 L^2} \quad . \quad (2 \cdot 10)$$

In an equilibrium neutral sheet we have $T_2 = T_{20}$ and $\rho_2 = \rho_{20}$, where from (2.1) and (2.2)

$$\rho_{20} = \rho_1 \frac{T_1}{T_{20}} \left(1 + \frac{1}{\beta}\right)$$

and

$$\beta = \frac{p_1 8\pi}{B^2} \quad .$$

The equilibrium value of H , H_0 say, can thus be written in terms of L and T20 only as

$$H_0(L, T_{20}) = \gamma_1 \rho_1 T_1^{\alpha_1} - \gamma \rho_1 T_1 T_{20}^{\alpha - 1} \left(1 + \frac{1}{\beta}\right) + \frac{2 \times 10^{-6} T_{20}^{7/2} (T_1 - T_{20})}{\rho_1 T_1 \left(1 + \frac{1}{\beta}\right) L^2} \quad . \quad (2 \cdot 11)$$

It is the equilibrium condition, $H_0(L, T_{20}) = 0$, that gives the curves L = L (T20) that are plotted in Figures (16) and (17). Thus

$$0 = \frac{dH_0}{dT_{20}} = \frac{\partial H_0}{\partial T_{20}} + \frac{\partial H_0}{\partial L} \frac{dL}{dT_{20}} \quad ,$$

or

$$\frac{dL}{dT_{20}} = - \frac{\partial H_0 / \partial T_{20}}{\partial H_0 / \partial L} \quad . \quad (2 \cdot 12)$$

2.1.: THE EQUILIBRIUM ENERGY BALANCE IN A CURRENT SHEET (Contd.)

Now from (2.11)

$$\frac{\partial H_0}{\partial L} \begin{cases} > 0 & \text{when } T_1 < T_{20}, \\ < 0 & \text{when } T_1 > T_{20}, \end{cases} \qquad (2.13)$$

so that an increase in L leads to a decrease in the heat conducted out of the plasma when $T_1 < T_{20}$ and an increase when $T_1 > T_{20}$. Thus (2.12) gives a direct relationship between the slope and turning points of the equilibrium curves and the value of $\partial H_0 / \partial T_{20}$, which from (2.11) is determined by the size and sign of the temperature gradients of thermal conduction and radiative loss. (2.12) is used in the next section to help determine the stability of each part of the equilibrium curves in Figures (16) and (17) pages 112 and 113.

2.2.: THE STABILITY OF THE CURRENT SHEET

We now set up the equations which govern the condensation and cooling in the current sheet as the temperature falls along the dotted line in Figure (16) page 112, (when B=1 Gauss). First of all, the transverse component of the equation of motion is

$$\rho \frac{dv_x}{dt} = - \frac{\partial}{\partial x} (p + B^2/8\pi) \cdot$$

But the x - component of the plasma velocity may be ignored, because the representative velocity $v = \ell/\tau$ $\simeq 10^4$ cm sec^{-1} (τ - cooling time $\simeq 10^5$ sec ; ℓ - width of the sheet $\simeq 10^9$ cm) is very much less than the Alfvén speed $v_A = \sqrt{(B^2/4\pi\rho)} \simeq 10^7$ cm sec^{-1} ($B = 1$ Gauss, $\rho = 10^{-16}$ g cm^{-3}).

Thus the equation of motion reduces to

$$p_2 = p_1 + B^2/8\pi \quad , \qquad (2.14)$$

since the magnetic field vanishes inside the sheet.

The rate of flow of energy in a unit volume is

$$\frac{1}{(\gamma-1)} \frac{dp_2}{dt} - \frac{\gamma}{(\gamma-1)} \frac{p_2}{\rho_2} \frac{d\rho_2}{dt} = b\rho_2 - \chi \rho_2^2 T_2^{\alpha} + \frac{\partial}{\partial y}\left(K_{11} \frac{\partial T_2}{\partial y}\right) , \qquad (2.15)$$

where $\gamma = C_p / C_v$ is the ratio of the specific heats. Using the perfect gas law $p_2 = R \rho_2 T_2$ and approximating the right-hand side of (2.15) as in the previous section, the rate of energy flow into a unit mass becomes

$$C_p \frac{\partial T_2}{\partial t} = \chi_1 \rho_1 T_1^{\alpha_1} - \chi \rho_2 T_2^{\alpha} + 2\times 10^{-6} \frac{T_2^{5/2} (T_1 - T_2)}{\rho_2 L^2} , \qquad (2.16)$$

2.2.: THE STABILITY OF THE CURRENT SHEET (Contd.)

where the total derivative d/dt is approximated by the partial derivative $\partial/\partial t$ since we are not taking account of the structure of the sheet in our simple model. Equation (2.16) may be written, using the heat gain function from (2.10), in the form

$$C_p \frac{\partial T_2}{\partial t} = H(L, T_2) \quad . \qquad (2.17)$$

Since the value of the sheet temperature T_2 which satisfies the equilibrium energy equation (2.9) is denoted by T_{20}, the equilibrium condition may be written

$$H_0(L, T_{20}) = 0 \quad .$$

Now suppose that the equilibrium temperature is perturbed in time to a value

$$T_2 = T_{20} + A e^{\sigma t} \quad ,$$

where A is constant. The stability of the equilibrium is governed by the value of σ ; a positive σ implies instability and a negative σ implies stability. By expanding equation (2.17) in a Taylor's series about T=T20 we find that

$$\sigma = \partial H_0 / \partial T_{20} \quad , \qquad (2.18)$$

or using (2.12)

$$\sigma = - \frac{\partial H_0}{\partial L} \frac{dL}{dT_{20}} \quad , \qquad (2.19)$$

2.2.: THE STABILITY OF THE CURRENT SHEET (Contd.)

where the sign of $\partial H_0 / \partial L$ is determined by (2.13). Thus the stability of the equilibrium to linear perturbations in temperature is directly related to the slope of the L- T20 curves, as indicated in Figures (16) and (17) pages 112 and 113, where the unstable parts of the curves are shown dashed and the stable parts solid. We have shown that the slope of the L-T20 curve, and hence the stability of the sheet, depends on the size and sign of the temperature gradients of both the rate of heat loss per unit mass by radiation and the rate of heat gain by conduction per unit mass (equations (2.18) and (2.11)). These energy terms do not both have the same effect on the stability of the sheet for all values of T 20 for

$$\sigma = \frac{\partial H_0}{\partial T_{20}} = -(\alpha-1)\chi\rho_1 T_1 T_{20}^{\alpha-2}\left(1+\frac{1}{\beta}\right) + \frac{2\times10^{-6}\, T_{20}^{5/2}\left(\frac{7}{2}T_1 - \frac{9}{2}T_{20}\right)}{\rho_1 T_1 \left(1+\frac{1}{\beta}\right) L^2}$$

$$\equiv -\frac{\partial}{\partial T_{20}}(L_{RAD}) + \frac{\partial}{\partial T_{20}}(C_{11}), \text{ say}.$$

The $\partial(C_{11})/\partial T_{20}$ term is negative, and hence stabilizing, when $T_{20} > \frac{7}{9} T_1$ and positive, and hence destabilizing when $T_{20} < \frac{7}{9} T_1$. The sign of the temperature gradient of the radiative loss depends only on α. When $T \geq 5\times10^4\,^\circ K$, then $\alpha \leq 0$, so that $[-\partial(L_{RAD})/\partial T_{20}]$ is positive and hence destabilizing. But, when $T < 5\times10^4\,^\circ K$, $\alpha = 4\cdot37$, so that $[-\partial(L_{RAD})/\partial T_{20}]$ is negative and hence stabilizing.

2.2.: THE STABILITY OF THE CURRENT SHEET (Contd.)

Thus we see that in the temperature range $5 \times 10^4 {}^\circ K < T_{20} < \frac{7}{9} T_1$ both $[-\partial(L_{RAD})/\partial T_{20}]$ and $\partial(C_{11})/\partial T_{20}$ are positive and hence destabilizing.

When, however, $T_{20} < 5 \times 10^4$ we find $[-\partial(L_{RAD})/\partial T_{20}] < 0$ while $\partial(C_{11})/\partial T_{20} > 0$, so that it is the radiative loss which gives stability at these low temperatures.

But when $T_{20} > \frac{7}{9} T_1$ the opposite is true; $\partial(C_{11})/\partial T_{20} < 0$ and $[-\partial(L_{RAD})/\partial T_{20}] > 0$ so that, when T 20 is near the temperature of the surrounding plasma, the thermal conduction is stabilizing and the radiative loss is destabilizing the plasma.

The equilibrium is neutrally stable ($\sigma = 0$) at $\partial H_0/\partial T_{20} = 0$ which occurs, according to (2.12), at $dL/dT_{20} = 0$. In other words, the maximum and minimum points of the curves are neutrally stable. If these points are given a second order temperature perturbation the energy equation (2.17) gives

$$C_p \frac{\partial T_2}{\partial t} \simeq \frac{1}{2} (T_2 - T_{20})^2 \partial^2 H_0/\partial T_{20}^2 \quad , \qquad (2.20)$$

where from (2.11)

$$\frac{\partial^2 H_0}{\partial T_{20}^2} = \frac{(\chi \rho_{20} T_{20}^{\alpha} - \chi_1 \rho_1 T_1^{\alpha_1})}{T_{20}^2 (T_1 - T_{20})} \left[T_1 \left(-(\alpha-2)\frac{7}{2} + \frac{35}{4} \right) + T_{20} \left((\alpha-2)\frac{9}{2} - \frac{45}{4} \right) \right] , \qquad (2.21)$$

where we have used $H_0 = \partial H_0 / \partial T_{20} = 0$.

Now we are only interested in $\partial^2 H_0 / \partial T_{20}^2$ at the turning points of the curves, which can occur only when $T_{20} > \frac{7}{9} T_1$ from the stability considerations given earlier.

2.2.: THE STABILITY OF THE CURRENT SHEET (Contd.)

Thus, in equation (2.21) the term in the square bracket is negative. The term outside the square bracket is positive when $T_{20} > \frac{7}{9} T_1$, because from the stability arguments given earlier $\partial(L_{RAD})/\partial T_{20}$ is negative in this temperature range. Thus, since the radiative loss inside the sheet, $\chi \rho_{20} T_{20}^{\alpha}$, equals the radiative loss outside the sheet, $\chi_1 \rho_1 T_1^{\alpha_1}$, when $T_1 = T_{20}$, our constant pressure assumption implies that $\chi \rho_{20} T_{20}^{\alpha} > \chi_1 \rho_1 T_1^{\alpha_1}$ when $T_1 > T_{20}$ and vice versa. Thus we can see that $\partial^2 H_0/\partial T_{20}^2$ is negative at both of the turning points. If the temperature is increased above T 20, it will return to its equilibrium value, but if the temperature is decreased below T 20 it will continue to fall since $\partial T_2/\partial t$ becomes negative from equation (2.20). Hence the turning points are unstable to quadratic perturbations in temperature and the gas cools down at these points.

For the formation of quiescent prominences in the corona, the neutral sheets are expected to develop along the equilibrium curves T 20 (Figure (16) page 112). Begin at the bottom right-hand corner of Figure (16) with T 20 $\lesssim T_1$ and a small sheet length L. As the sheet lengthens, one moves along the curve through a series of equilibria characterised by slightly lower temperatures inside the sheet, since less heat is conducted into the sheet for larger values of L.

2.2.: THE STABILITY OF THE CURRENT SHEET (Contd.)

If L remains less than Lmax, the gas keeps in stable equilibrium. Since it is found from the equilibrium curves (Figures (16) and (17), pages 112 and 113), L_{max} is a more accurate measure than L_{crit} (given by (1.30)) of the longest stable sheet. The variation of (L_{max} / L_{crit}) with β is shown in Figure (19) page 123, where the two curves represent different ambient temperature ranges. It can be seen that L_{max} is always less than L_{crit}. For instance, when $\beta = 1$, $L_{max} \simeq L_{crit}/10$. The extent to which L_{crit} overestimates the maximum length of a stable sheet becomes greater as β decreases, the reason being that the approximation $p_1 = p_{20}$ becomes more inaccurate. From Figures (3) and (19) the value of L_{max} can be found at any height in the Billings & Alvarez model atmosphere for $10^{-4} \leq \beta \leq 10^{3}$.

If the length of the sheet increases beyond L_{max}, the plasma becomes unstable. It cools down, under the influence of the radiative loss term in the energy equation, along the line which is shown dotted for one illustrative magnetic field value in each of Figures (16) and (17) until it reaches a new stable equilibrium temperature value. In the coronal case, when B=1 Gauss and $p_1 = 2{\cdot}8 \times 10^{-2}$ dynes cm^{-2}, this new temperature is approximately 8×10^{3} °K ; inside the current sheet p_{20}, which we assume remains constant throughout the condensation process, is by equation (2.1) approximately 7×10^{-2} dynes cm^{-2}, so that the final number density is 3×10^{10} cm^{-3} from the perfect gas law.

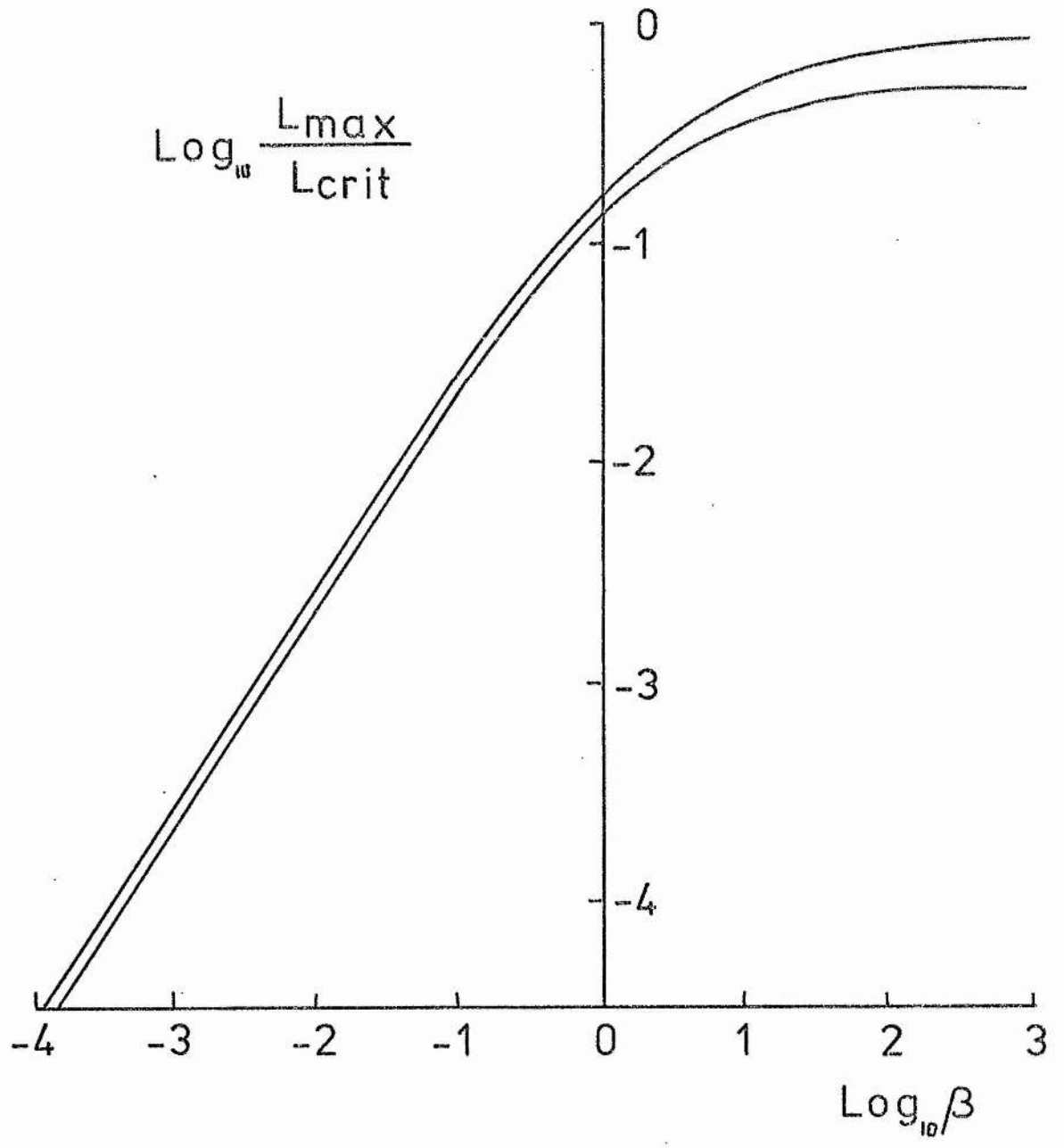

Figure (19). The maximum length for a stable sheet, L_{max} (see Figure (17) page 113), divided by the approximate value L_{crit} (from equation (1·30)), as a function of β, the coronal pressure, $p_1 = 2 \cdot 8 \times 10^{-2}$ dynes cm^{-2}, divided by the magnetic pressure. The upper and lower curves apply to the ambient temperature ranges $T_1 > 2 \cdot 5 \times 10^5 {}^\circ K$ and $5 \times 10^4 {}^\circ K < T_1 < 2 \cdot 5 \times 10^5 {}^\circ K$ respectively.

2.2.: THE STABILITY OF THE CURRENT SHEET (Contd.)

Observed values of these quantities are $T = 6{,}000^{\circ}K$ to $7{,}000^{\circ}K$ and $n_e = 10^{10} cm^{-3}$ to $5 \times 10^{10} cm^{-3}$, so that $p_1 = 1{\cdot}7 \times 10^{-2}$ dynes cm^{-2} to $9{\cdot}7 \times 10^{-2}$ dynes cm^{-2} (Bruzek & Kuperus, 1972). Thus the estimated values are in good agreement with the observed values, considering the approximate nature of the calculation, for example the inaccurate form of the radiative loss function at the lower end of the temperature range.

The fact that the equilibrium position at L_{max} is unstable has already been mentioned, but, if one assumes that the sheet has a gradually increasing length, the actual development of the instability depends on the length $L_{max}(1 + \epsilon)$ which the sheet has attained before the instability gets under way. The resulting approximate dependence of the temperature on time is thus found by integrating equation (2.17), while keeping L constant at $L_{max}(1 + \epsilon)$; this gives

$$t = C_p \int_{T_{max}}^{T_2} \frac{dT_2}{H(L, T_2)} \quad , \qquad (2{\cdot}22)$$

where T_{max} is the value of T_2 at L_{max}, H is given by (2.11) and we find p_2 from (2.1) and (2.2) to be

$$p_2 = p_1 \frac{T_1}{T_2} \left(1 + \frac{1}{\beta}\right) .$$

The temperature as a function of time is drawn in Figure (20) page 125, for $\beta = 1{\cdot}0$ ($B = 0{\cdot}8$ Gauss, $p_1 = 2{\cdot}8 \times 10^{-2}$ dynes cm^{-2}) and several values of ϵ. It gives a decay time τ (the time taken for the temperature to fall to the lower stable equilibrium temperature) of between 10^4 sec and 10^5 sec depending on the size of ϵ.

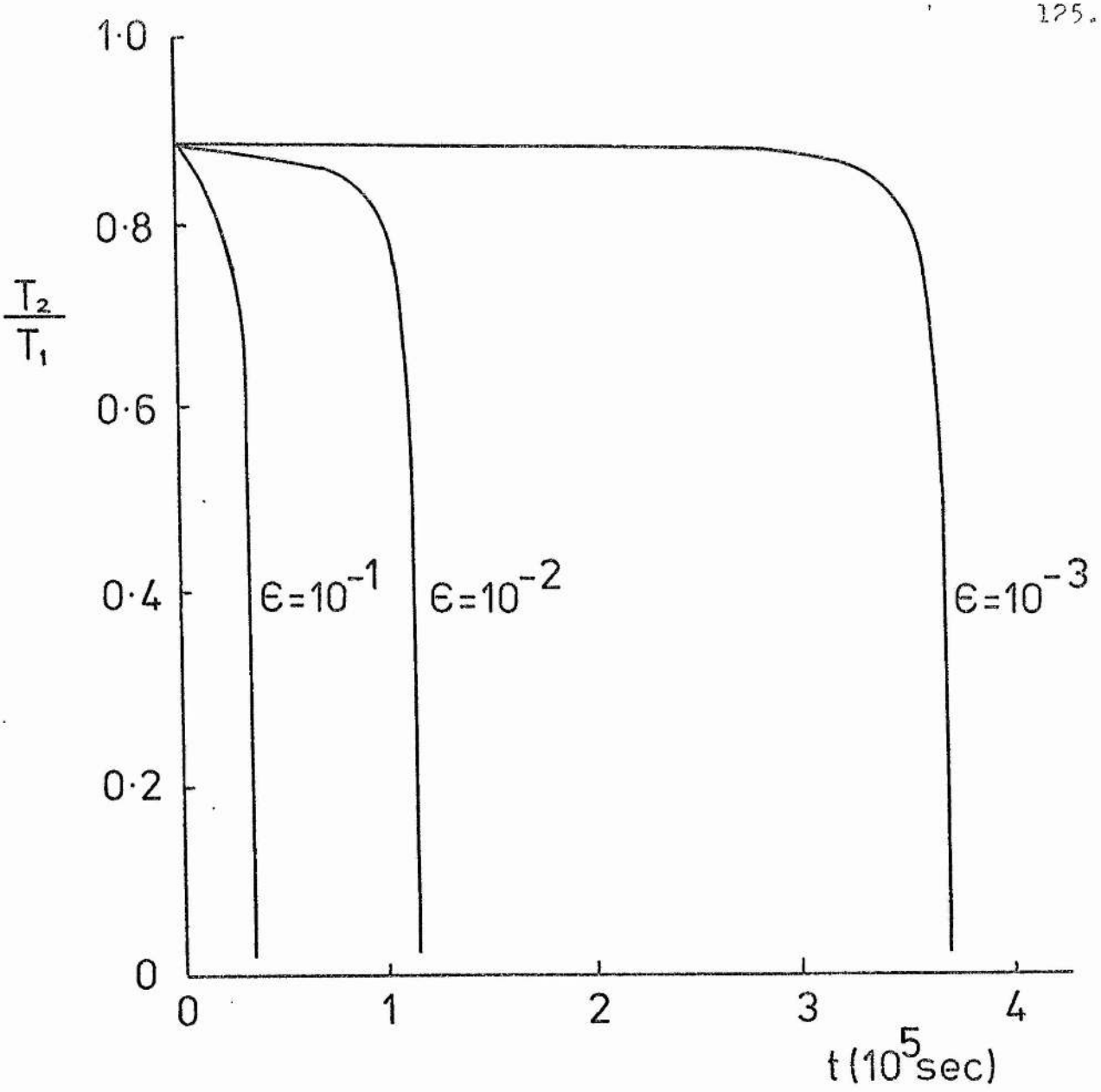

Figure (20). The time development of the temperature T_2 inside a neutral sheet which has been made unstable by increasing its length from L_{max} to $L_{max}(1+\epsilon)$. T_1 is the ambient coronal temperature (10^{6}°K) and β, the ratio of gas to magnetic pressure, is unity. The calculation is stopped when T_2 reaches the new equilibrium temperature value T_{prom} (see Figure (16), page 112).

2.2.: THE STABILITY OF THE CURRENT SHEET (Contd.)

In these temperature decay curves the temperature stays almost constant until the time is close to τ and then suddenly falls. This feature is noticeable in other temperature decay curves associated with thermal instabilities (e.g. Raju, 1968 and Hildner, 1971) and is more pronounced the smaller the value of ϵ .

The solution of equation (2.22), shown in Figure (20), page 125 was calculated numerically; however, it is possible to get an approximate, analytic solution with which to compare these results. Since the length of the sheet is kept constant at $L_{max}(1+\epsilon)$, the heat gain function H is a function of T_2 only so that we may expand it in a Taylor's series about $T = T_{max}$.

$$H(L_{max}(1+\epsilon), T_2) \simeq a_1 f(\epsilon) + (T_2 - T_{max}) a_2 f(\epsilon) + (T_2 - T_{max})^2 a_3 \quad , \tag{2.23}$$

where

$$a_1 = -\chi_1 \rho_1 T_1^{\alpha_1} + \chi \rho_1 T_1 T_{max}^{\alpha-1} \left(1 + \frac{1}{\beta}\right) ,$$

$$a_2 = (\alpha-1) \chi \rho_1 T_1 T_{max}^{\alpha-2} \left(1 + \frac{1}{\beta}\right) ,$$

$$a_3 = \frac{1}{2} \left[-(\alpha-1)(\alpha-2) \chi \rho_1 T_1 T_{max}^{\alpha-3} \left(1 + \frac{1}{\beta}\right) + \frac{2 \times 10^{-6} T_{max}^{3/2} \left(\frac{35}{4} T_1 - \frac{63}{4} T_{max}\right)}{\rho_1 T_1 \left(1 + \frac{1}{\beta}\right) L_{max}^2 (1+\epsilon)^2} \right] ,$$

$$f(\epsilon) = \frac{-\epsilon(2+\epsilon)}{(1+\epsilon)^2} \quad .$$

2.2.: THE STABILITY OF THE CURRENT SHEET (Contd.)

Now substitute the approximate form (2.23) for H, in equation (2.22) to give

$$t = C_p \int_0^{T_{max} - T_2} \frac{-d\overline{T}}{a_3 \overline{T}^2 - a_2 f(\epsilon)\overline{T} + a_1 f(\epsilon)} ,$$

where

$$\overline{T} = T_{max} - T_2 .$$

Performing the integration, we have

$$t = \frac{-2 C_p}{g(\epsilon)} \left[\tan^{-1}\left(\frac{2 a_3 \overline{T} - a_2 f(\epsilon)}{g(\epsilon)} \right) + \tan^{-1}\left(\frac{a_2 f(\epsilon)}{g(\epsilon)} \right) \right] , \quad (2.24)$$

where

$$g(\epsilon) = \sqrt{(4 a_3 a_1 f(\epsilon) - a_2^2 f^2(\epsilon))} .$$

When T_2 as a function of t, as determined by (2.24), is plotted on Figure (20) page 125, the result is indistinguishable from the numerical solutions.

We shall now calculate an approximate value for the decay time, τ, the time taken in equation (2.24) for T to go to zero, that is $\overline{T} \to T_{max}$.

We consider $\epsilon << 1$ and also $2 a_3 T_{max} > 10$, which, we shall show later, is true. Also, we only use $\alpha = \alpha_1$, so that from equation (2.24)

$$\tau \simeq \frac{2 C_p}{g(\epsilon)} \left[\frac{\pi}{2} - \tan^{-1}\left(\frac{a_2 f(\epsilon)}{g(\epsilon)} \right) \right] ,$$

since

$$| 2 a_3 T_{max} | > 10 \chi_1 \beta_1 T_1^{\alpha_1} >> a_2 f(\epsilon) ,$$

or, approximating further,

$$\tau \simeq \frac{\pi C_p}{\sqrt{(-8 a_3 a_1 \epsilon)}} \quad (2.25)$$

since

$$\epsilon << 1 .$$

2.2.: THE STABILITY OF THE CURRENT SHEET (Contd.)

Equation (2.25) shows how τ depends on ϵ, now if we let $T_{max} = 0.9\,T_1$, we can see how $\hat{\tau}$ depends on β. With these approximations we find that, for large β

$$a_1 = \chi_1 \rho_1 T_1^{\alpha_1} \left(0.34 + 1.34\tfrac{1}{\beta}\right) ,$$

$$a_2 = -\chi_1 \rho_1 T_1^{\alpha_1} \left(4.2\left(1+\tfrac{1}{\beta}\right)\right) ,$$

$$a_3 = \chi_1 \rho_1 T_1^{\alpha_1} \left(-20 - 54\tfrac{1}{\beta}\right) ,$$

$$f(\epsilon) = -2\epsilon ,$$

so we see that, as we assumed earlier,

$$|2a_3 T_{max}| > 10 >> a_2 f(\epsilon) .$$

Then

$$\hat{\tau} \simeq \frac{\pi C_p}{\chi_1 \rho_1 T_1^{\alpha_1} \sqrt{\left(\left(56 + 367\tfrac{1}{\beta} + 579\tfrac{1}{\beta^2}\right)\epsilon\right)}} . \qquad (2.26)$$

In Figure (20) page 125, we see that for $t < \hat{\tau}$ the temperature T is approximately equal to T_{max}, but when $t \simeq \hat{\tau}$ the gradient of the curve is very large. We will now show this effect by calculating an approximation to the gradients using equation (2.24) and comparing these values with the gradients of the full solution. Equation (2.24) may be written

$$t = -\frac{2\hat{\tau}}{\pi}\left\{\tan^{-1}(A_1 - A_2) + \tan^{-1}(A_2)\right\} , \qquad (2.27)$$

where

$$A_1 = \frac{2a_3\overline{T}}{g(\epsilon)} \simeq \frac{-\left(40 + 108\tfrac{1}{\beta}\right)}{\sqrt{\left(\left(56 + 367\tfrac{1}{\beta} + 579\tfrac{1}{\beta^2}\right)\epsilon\right)}} \simeq \frac{-5\overline{T}}{\sqrt{\epsilon}}$$

$$A_2 = \frac{a_2 f(\epsilon)}{g(\epsilon)} \simeq \frac{8\left(1+\tfrac{1}{\beta}\right)\epsilon}{\sqrt{\left(\left(56 + 367\tfrac{1}{\beta} + 579\tfrac{1}{\beta^2}\right)\epsilon\right)}} \simeq \sqrt{\epsilon} .$$

2.2.: THE STABILITY OF THE CURRENT SHEET (Contd.)

To calculate the approximate value of the gradient when $\overline{T} \simeq \overline{T}_{max}$ we use the fact that $A_1 < 1$ and $A_2 < 1$ to get

$$t_1 \simeq -\frac{2\tau}{\pi} A_1 = \frac{10\overline{T}}{\pi\sqrt{\epsilon}}\tau \ ,$$

so that the gradient

$$G_1 = \frac{-\overline{T}}{t_1} = \frac{-\pi\sqrt{\epsilon}}{10\tau} \ .$$

This is compared with the gradients, G, calculated using (2.24)

ϵ	β	$\overline{T}$	t	τ	G	G_1
10^{-3}	2	0·883	$1·3\times10^{6}$	$1·67\times10^{6}$	$-1·4\times10^{-8}$	$-5·9\times10^{-9}$
	0·2	0·852	$1·9\times10^{5}$	$2·6\times10^{5}$	$-9·0\times10^{-8}$	$-3·8\times10^{-8}$
10^{-1}	2	0·865	$5·8\times10^{4}$	$1·6\times10^{5}$	$-6·2\times10^{-7}$	$-6·2\times10^{-7}$
	0·2	0·835	$7·6\times10^{3}$	$2·5\times10^{4}$	$-4·5\times10^{-6}$	$-4·0\times10^{-6}$

where T is the temperature at a time t on the temperature decay curve and G is the measured gradient, while G_1 is the approximated gradient. We see that G and G_1 are in reasonable agreement and their values are typical of this slowly varying initial phase of the decay.

2.2.: THE STABILITY OF THE CURRENT SHEET (Contd.)

To calculate the gradient at the final phase of the decay, when $t \simeq \hat{\tau}$, we assume that $\overline{T}$ is sufficiently large and ϵ sufficiently small that

$$|A_1| \gg A_2 \quad \text{and that} \quad A_2 < 1 .$$

Then in (2.27)

$$t = -\frac{2\hat{\tau}}{\pi}\left(\frac{\pi}{2} + \frac{1}{A_1}\right) .$$

The approximate value of the gradient G_2 is

$$G_2 = \frac{-T}{\hat{\tau} - t} = \frac{-T\ 5\pi\overline{T}}{2\hat{\tau}\sqrt{\epsilon}}$$

and is compared with the gradients, G, calculated from (2.24).

ϵ	β	T	t	$\hat{\tau}$	G_T	G_2
10^{-3}	2	0·6	$1{\cdot}66\times10^{6}$	$1{\cdot}67\times10^{6}$	$-9{\cdot}1\times10^{-5}$	$-2{\cdot}7\times10^{-5}$
	0·2	0·6	$2{\cdot}56\times10^{5}$	$2{\cdot}59\times10^{5}$	$-2{\cdot}3\times10^{-4}$	$-1{\cdot}7\times10^{-4}$
10^{-1}	2	0·6	$1{\cdot}49\times10^{5}$	$1{\cdot}6\times10^{5}$	$-5{\cdot}6\times10^{-5}$	$-2{\cdot}8\times10^{-5}$
	0·2	0·6	$2{\cdot}29\times10^{4}$	$2{\cdot}5\times10^{4}$	$-2{\cdot}6\times10^{-4}$	$-1{\cdot}6\times10^{-4}$

where the gradients G are measured from T = 0.6 at time t to T=0 at time $\hat{\tau}$. We can see that the gradients are much larger when t is close to $\hat{\tau}$ and this is followed closely by the approximate value of the gradient G_2 .

2.2.: THE STABILITY OF THE CURRENT SHEET (Contd.)

From the numerical solutions, the dependence of the temperature decay time τ on ϵ is given in Figure(21), page 133, for several values of β ($\beta = 10^{2}$ to 10^{-4} i.e. $B = 0{\cdot}08$ to $B = 83$ Gauss where $p_1 = 2{\cdot}8 \times 10^{-2}$ dynes cm^{-2}).

A decrease in β reduces the decay time for the following reason. From (2.14) and the perfect gas law, for given values of p_1 and T_2 , a decrease in β leads to a higher value of ρ_2 , which in turn increases the radiative loss term and decreases the conductive term in (2.16). Thus $-\partial T_2 / \partial t$ increases and the decay becomes more rapid. The fact that a decrease in β reduces the decay time can be seen in (2.26). Another feature of the curve is that an increase in ϵ above about 10 hardly affects the decay time, since the conduction term in (2.16) becomes negligible. Furthermore, as ϵ decreases, so the decay time increases. In fact, in the limit as ϵ approaches zero, τ becomes infinite. This effect of ϵ on the decay time can be seen in the approximate solution (2.25). So the decay time increases like $1/\sqrt{\epsilon}$ as ϵ approaches zero, which agrees with the variation found in Figure (21).

The decay time τ depends crucially on the value of ϵ, so the problem arises as to which value of ϵ to choose. In the above analysis we supposed that the sheet length jumps instantaneously from L_{max} to $L_{max}(1 + \epsilon)$.

2.2.: THE STABILITY OF THE CURRENT SHEET (Contd.)

It may be assumed instead that the length increases at a uniform rate above L_{max}, so that $L = L_{max}(1 + (d\epsilon/dt)t)$, where $d\epsilon/dt$ = constant. In view of the time profiles in Figure (20), page 125, we then expect the sheet temperature to remain approximately constant until $t = \tau^*$, say (and $\epsilon = (d\epsilon/dt)\,\tau^*$) at which time the temperature falls sharply. The relevant decay time τ^* in this case can therefore be estimated from the intersection of an $\epsilon - \tau$ curve in Figure (21), page 133, with the straight line $\epsilon = (d\epsilon/dt)\,\tau$ for each value of β and $d\epsilon/dt$. The result is given in Figure (22) page 134, for several values of β.

($\beta = 10^{2}$ to 10^{-4} i.e. $B = 0.08$ to $B = 83$ Gauss where $p_1 = 2.8 \times 10^{-2}$ dynes cm^{-2}).

Quiescent prominences are formed over a period of about 10^5 seconds, which from the graph, requires a very small value for the rate $d\epsilon/dt$ at which the sheet length is increasing, namely 10^{-7} - 10^{-5} for $\beta \simeq 1$ to 0.1.

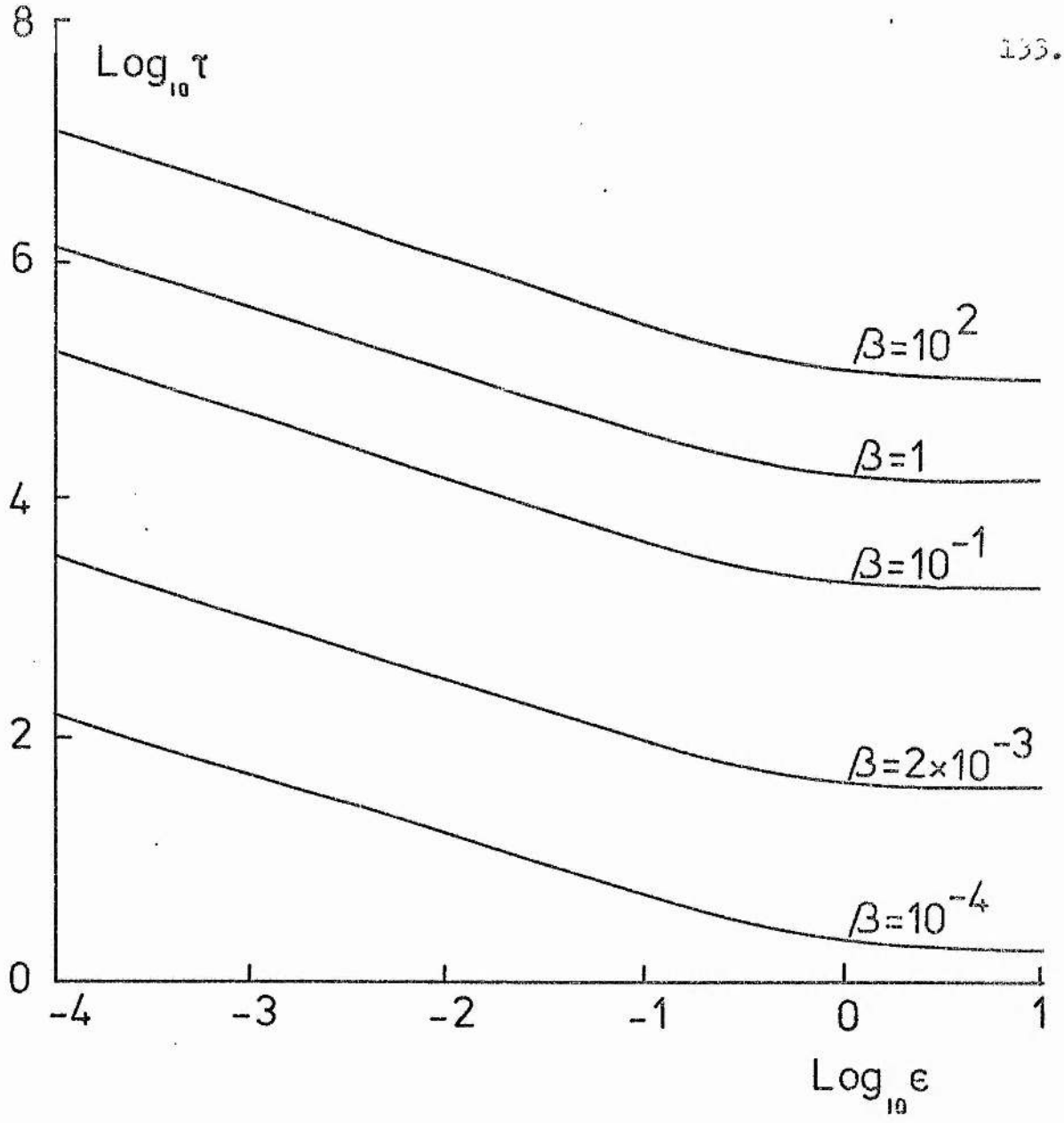

Figure (21). The decay time τ for an unstable coronal neutral sheet whose length has been increased to $L_{max}(1+\epsilon)$ as a function of ϵ for several values of β, the ratio of gas to magnetic pressure.

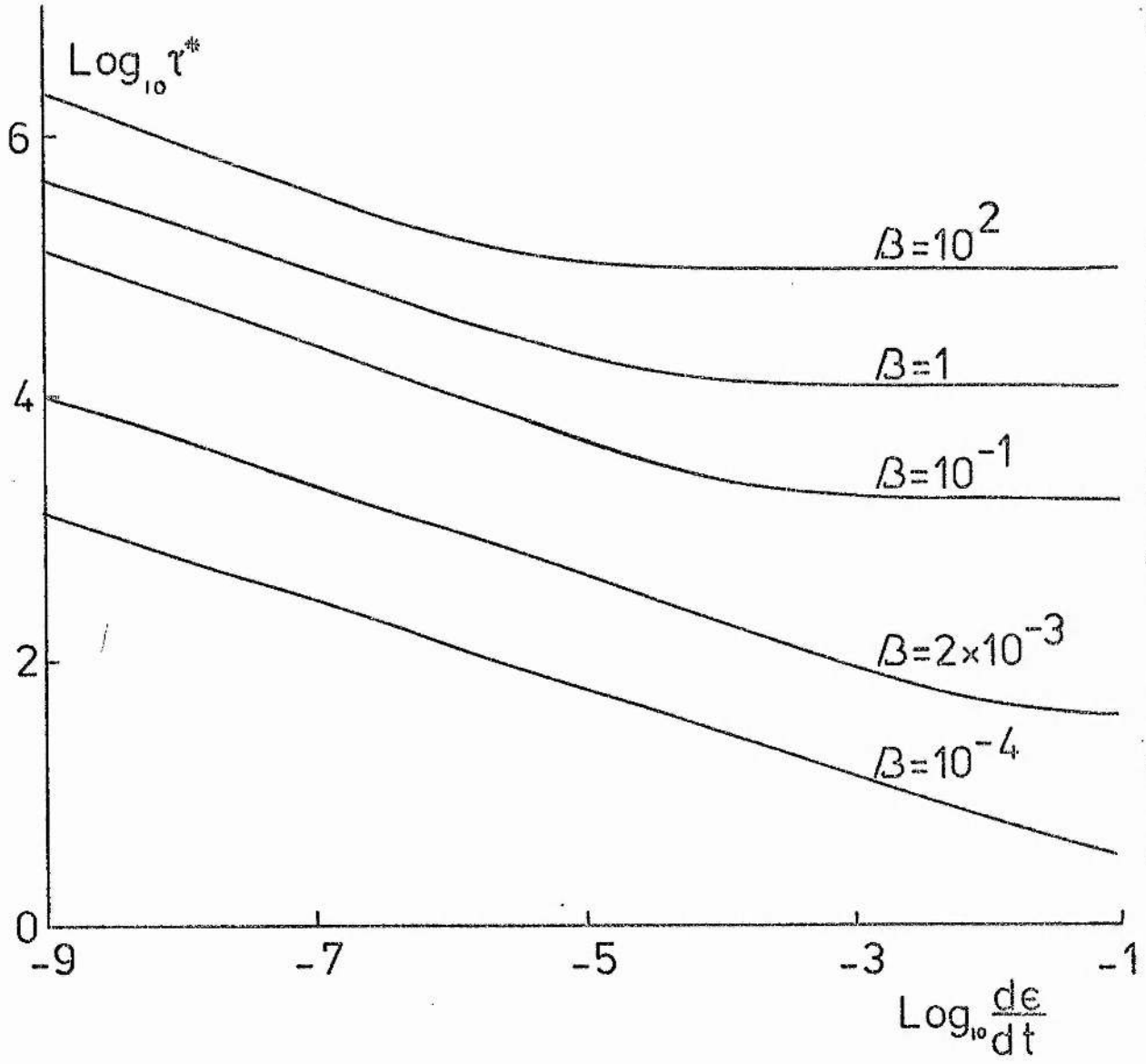

Figure (22). The variation of the decay time τ^* with $d\epsilon/dt$, for a neutral sheet with a uniformly increasing length $L_{max}(1 + (d\epsilon/dt)t)$, for several values of the ratio β of gas to magnetic pressure.

2.3.: ATTEMPT AT A MORE DETAILED ANALYSIS OF THE THERMAL INSTABILITY IN A CURRENT SHEET.

In this section we describe a method we employed to try to calculate the linear growth rate of the thermal instability in a neutral current sheet. The method was developed by Cross & Van Hoven (1971) and used to study the tearing mode instability in a sheared magnetic field, as described in Chapter 1, section 1.3. We had already successfully applied their method to the study of the tearing mode instability in a neutral current sheet, (see Chapter 3). We had hoped to study the thermal instability first by itself, when, by suitable choice of parameters, it was the fastest instability in the neutral sheet, and then coupled with the tearing mode instability, when, by changing the parameters, both these instabilities were important. However, as outlined in this section, we were unable to calculate the growth rate for the thermal instability itself.

The Initial Equilibrium

We model the neutral sheet by taking the following equilibrium magnetic field

$$\underline{B}_0 = B \sin \frac{\pi y}{a} \hat{\underline{x}} \qquad (2.28)$$

where the zero subscript denotes an equilibrium variable.

2.3.: ATTEMPT AT A MORE DETAILED ANALYSIS OF THE THERMAL INSTABILITY IN A CURRENT SHEET. (Contd.)

From the induction equation, with the equilibrium velocity $\underline{V}_0 = 0$, we get

$$\underline{\nabla} \wedge [\eta_0 (\underline{\nabla} \wedge \underline{B}_0)] = 0 ,$$

which is only valid, with the equilibrium field given in equation (2.28), when the time scale of the thermal instability is very much less than the diffusion time of the equilibrium magnetic field.

From the equation of motion, we get

$$\underline{\nabla} p_0 = \frac{1}{4\pi} (\underline{\nabla} \wedge \underline{B}_0) \wedge \underline{B}_0 \quad . \qquad (2.29)$$

Equation (2.29) with the equation of state for a perfect gas $p_0 = R \rho_0 T_0$, gives

$$\rho_0 = \frac{p_{20}}{R T_0} \left(1 - \frac{1}{\beta} \sin^2 \frac{\pi y}{a} \right) \qquad (2.30)$$

The energy equilibrium is established by a balance between the constant mechanical heating and radiative loss,

$$0 = b \rho_0 - \rho_0^2 \chi T_0^{\alpha} \quad , \qquad (2.31)$$

where the constant, b, is found by assuming an equilibrium balance in the corona. In order to satisfy equation (2.30) the density ρ_0 must vary with y and then equation (2.31) implies that T_0 varies with y.

2.3.: ATTEMPT AT A MORE DETAILED ANALYSIS OF THE THERMAL INSTABILITY IN A CURRENT SHEET (Contd.)

However, in (2.31), T_0 is raised to a non integer power α and the method developed by Cross & Van Hoven involving the Fourier transform of such functions, is unable to deal with this awkward variation and so we are forced to take T_0 uniform. With this condition we can satisfy (2.31) only if ρ_0 is uniform, which implies, in (2.30) that

$$\beta >> 1$$

When the equilibrium is perturbed by a small amount, the linearized equations become

$$\frac{\partial \rho_1}{\partial t} + \rho_0 \underline{\nabla} . \underline{v}_1 = 0 \quad , \tag{2.32}$$

$$\frac{\partial \underline{B}_1}{\partial t} = \underline{\nabla} \wedge (\underline{v}_1 \wedge \underline{B}_0) - \frac{1}{4\pi} \underline{\nabla} \wedge \left[\eta_1 (\underline{\nabla} \wedge \underline{B}_0) + \eta_0 (\underline{\nabla} \wedge \underline{B}_1) \right] , \tag{2.33}$$

$$\rho_0 \frac{\partial \underline{v}_1}{\partial t} = -\underline{\nabla} p_1 + \frac{1}{4\pi} \left[(\underline{\nabla} \wedge \underline{B}_1) \wedge \underline{B}_0 + (\underline{\nabla} \wedge \underline{B}_0) \wedge \underline{B}_1 \right] , \tag{2.34}$$

$$C_v \rho_0 \left[\frac{\partial T_1}{\partial t} + (\gamma - 1) T_0 (\underline{\nabla} . \underline{v}_1) \right] = b \rho_1 - \rho_0^2 \chi \alpha T_0^{\alpha - 1} T_1 - 2 \rho_0 \chi T_0^{\alpha} \rho_1 \quad , \tag{2.35}$$

$$\eta_1 = -\frac{3}{2} \eta_0 T_1 / T_0 \quad , \tag{2.36}$$

$$p_1 = R (\rho_0 T_1 + T_0 \rho_1) \quad , \tag{2.37}$$

where spatial variations in the equilibrium are negligible when $\beta >> 1$.

If, in the linearized energy equation (2.35), we choose the equilibrium variables such that the radiative loss terms are negligible, then we find that $T_1 = 0$, if the flow is incompressible. These conditions will give us the tearing mode instability, which is dealt with in greater detail later.

2.3.: ATTEMPT AT A MORE DETAILED ANALYSIS OF THE THERMAL INSTABILITY IN A CURRENT SHEET (Contd.)

However, if the radiative loss term is important in the energy equation, the thermal instability will occur more quickly. From order of magnitude considerations we have shown in Chapter 1, section 1.2, that the thermal instability time scale is $\tau_T \simeq \frac{C_p}{\chi \rho_0 T_0^{\alpha-1}}$ which is also the time scale we get from (2.35) apart from the factor $\frac{C_v}{\alpha C_p}$, when the radiative loss term is included in (2.35). If the growth rate of the instability $\omega \gg \frac{1}{\tau_T}$ then we get the tearing mode instability, while if $\omega \simeq \frac{1}{\tau_T}$ we expect the thermal instability.

Following the method of Cross & Van Hoven we take perturbations with the form

$$\left.\begin{aligned} B_x(x,y,t) &= e^{\omega t} \cos kx \sum_{n=2}^{\infty} B_{xn} \sin \frac{n\pi y}{a} \\ B_y(x,y,t) &= e^{\omega t} \sin kx \sum_{n=2}^{\infty} B_{yn} \cos \frac{n\pi y}{a} \end{aligned}\right\} \quad n \text{ is even.}$$

$$\left.\begin{aligned} V_x(x,y,t) &= e^{\omega t} \sin kx \sum_{n=1}^{\infty} V_{xn} \cos \frac{n\pi y}{a} \\ V_y(x,y,t) &= e^{\omega t} \cos kx \sum_{n=1}^{\infty} V_{yn} \sin \frac{n\pi y}{a} \\ \rho(x,y,t) &= e^{\omega t} \cos kx \sum_{n=1}^{\infty} \rho_n \cos \frac{n\pi y}{a} \\ T(x,y,t) &= e^{\omega t} \cos kx \sum_{n=1}^{\infty} T_n \cos \frac{n\pi y}{a} \end{aligned}\right\} \quad n \text{ is odd.}$$

Equations for the Fourier coefficients are found by taking the appropriate Fourier transform of the linearized equations (2.32) to (2.37). This gives us, as will be seen Chapter 3, where the solution for the tearing mode instability is calculated in detail, six equations for the six coefficients B_{xn}, B_{yn}, V_{xn}, V_{yn}, ρ_n, T_n in terms of coefficients with index less than n.

2.3.: ATTEMPT AT A MORE DETAILED ANALYSIS OF THE THERMAL INSTABILITY IN A CURRENT SHEET (Contd.)

However, a problem arises, as it does in the tearing mode case, with the coefficients with n at its smallest value, $n = 3$. Here the equations relate the coefficients B_{x3}, B_{y3}, V_{x3}, V_{y3}, ρ_3 and T_3 to the corresponding coefficients with 3 replaced by 1 but, since n cannot be made smaller, there are no more equations from which we can calculate the first terms of the Fourier series, B_{x1}, B_{y1}, V_{x1}, V_{y1}, ρ_1 and T_1 and so we must make an assumption about these terms in order to find them.

We assume that

$$V_{x1} + \frac{\overline{\eta}}{ak} V_{y1} = d$$

where the constant d is zero when these coefficients obey the incompressible equation, as we assume in the tearing mode case, but will not be zero in the thermal instability case. It can be shown that this assumption is sufficient to solve for all the coefficients of the Fourier series by using the Fourier transformed, linearized equations (2.32) to (2.37).

We then calculate these coefficients for several trial values of the unknown growth rate, ω_t, to find that value for which the coefficients converge as n is increased. The unique value of ω will then be the growth rate of the thermal instability. However, we were unable, for several values of d, to find a value of ω for which the Fourier series converged.

2.3.: ATTEMPT AT A MORE DETAILED ANALYSIS OF THE THERMAL INSTABILITY IN A CURRENT SHEET (Contd.)

The typical behaviour of the coefficients is shown in Table 3 where the values of V_{yn}/V_{y_1}, are shown for several values of n and ω' (where $\omega' = \frac{\omega}{\omega_{TM_1}} 10^6$ and $\omega_{TM_1} = \left(ak \frac{\hat{\tau}_R}{\hat{\tau}_A}\right)^{2/3}$, the value that Furth, Killeen & Rosenbluth (1963) found for the growth rate of the tearing mode instability), also d is chosen such that the first coefficient of the ρ_n sequence, $\rho_1 = 1{\cdot}0$. (when $\beta \gg 1$ the continuity equation for the first terms is

$$V_{x_1} + \frac{\pi}{ak} V_{y_1} = - \frac{\omega \hat{\tau}_A}{ak} \rho_1 ,$$

so that we are taking $d = - \frac{\omega \hat{\tau}_A}{ak}$).

TABLE 3

Values of V_{yn}/V_{y_1}

n \ ω'	10^{-3}	10^{-2}	1	5·4	5·6	10	10^2
1	1·0	1·0	1·0	1·0	1·0	1·0	1·0
3	0·8	4×10	4×10^5	2×10^8	-4×10^8	-6×10^6	-3×10^6
5	-2×10^3	9×10^2	2×10^{11}	2×10^{15}	-4×10^{15}	-2×10^{14}	8×10^{12}
7	6×10^9	6×10^9	2×10^{17}	2×10^{22}	-5×10^{22}	-3×10^{21}	-3×10^{19}
9	-2×10^{16}	-2×10^{16}	10^{23}	3×10^{29}	-6×10^{28}	-5×10^{28}	10^{26}

2.3.: ATTEMPT AT A MORE DETAILED ANALYSIS OF THE THERMAL INSTABILITY IN A CURRENT SHEET (Contd.)

We see in Table 3 that, for large or small ω', the terms of the sequence change sign alternately, but for the range in between we find, as did Cross & Van Hoven (1971). that for values of ω' on one side of some critical value, ω'_c (here $\omega'_c \simeq 5{\cdot}5$) the sequence has positive terms, and that they are negative on the other side. However, unlike Cross & Van Hoven we find that, as we get closer to ω'_c, the sequences diverge and so we are unable to find a value of ω for which the terms of the Fourier series converge.

2.4.: SUMMARY.

In this Chapter we have presented a simple model for the thermal equilibrium and stability of a neutral current sheet in the corona and upper chromosphere. We have shown that in a current sheet, with approximately the size of a quiescent prominence (L = height $\simeq 5\times10^9$ cm, ℓ = width $\simeq 5\times10^8$ cm), the main terms in the energy equilibrium are mechanical heating, radiative loss, and thermal conduction.

It is found that as the length of the sheet increases it passes through a series of stable equilibria until a certain value, L_{max}, is reached, when the sheet cools down to a new equilibrium. We also find, for temperatures in the sheet that are approximately equal to the temperature of the surrounding plasma, that the stable sheet is kept stable under the influence of the thermal conduction, but that the radiative loss is a destabilizing influence, while at the lower equilibrium the plasma is kept stable by the radiative loss term and this time the conduction is destabilizing.

For an unstable sheet with length $L_{max}(1+\epsilon)$, we calculate numerically the value of temperature as a function of time and also find an approximate analytic solution which agrees closely with the computed solution. For coronal conditions, the values of L_{max} and the cooling time(for small ϵ) are in fair agreement with the observed values for prominence formation.

2.4.: SUMMARY (Contd.)

Using both the numerical and the analytical solution we calculate the decay time for the unstable plasma to cool down to the lower equilibrium. This shows that the decay time depends on both ϵ and β the ratio of gas to magnetic pressure, in such a way that a decrease in ϵ or an increase in β will increase the decay time.

After considering the neutral sheet with a static length we look at the effect of allowing the length to vary with time, and show that the constant rate of change of the length must be very small for reasonable decay times.

In the last section of this Chapter we have outlined a method for calculating the linear growth rate of the thermal instability, which may prove to be useful in establishing how the thermal instability interacts with other instabilities and, in particular, the tearing mode instability.

CHAPTER 3.

TEARING MODE INSTABILITY (T.M.I.) IN A CURRENT SHEET

In section 3.1 we calculate the growth rate of the tearing mode instability (T.M.I.) in a neutral current sheet using a technique that Cross & Van Hoven (1971) devised to study the T.M.I. in a sheared magnetic field with constant magnetic field strength. We find that their force-free equilibrium configuration gives somewhat different results to our case where, in the equilibrium, the gas pressure is required to balance the magnetic pressure. Comments on an alternative equilibrium structure and the possibility of an ideal instability are presented in section 3.2 and 3.3. Next, in section 3.4 the effect on the T.M.I. of adding a transverse magnetic field component, B_t, is studied numerically; in particular we find how the strength of B_t affects the growth rate. An analytic treatment is given in section 3.5 for comparison.

3.1.: THE LINEAR GROWTH RATE OF THE T.M.I.

In this section the growth rate of the T.M.I. is calculated for a plasma inside a neutral current sheet, using the method devised by M.A. Cross & G. Van Hoven (1971). We first set up the equilibrium configuration, a typical variable being f_0, say. (A zero subscript is used to denote an equilibrium value). The stability is then tested by perturbing the variables to $f_0 + f_1$ and assuming $f_1 \ll f_0$, so that squares and products of small quantities can be neglected and the equations linearized.

The M.H.D. equations, in electromagnetic units, governing the tearing mode instability are the continuity equation,

$$\frac{\partial \rho}{\partial t} + \underline{\nabla} \cdot (\rho \underline{v}) = 0 ,$$

the induction equation, $$\frac{\partial \underline{B}}{\partial t} = \underline{\nabla} \wedge (\underline{v} \wedge \underline{B}) - \frac{1}{4\pi} \underline{\nabla} \wedge [\eta (\underline{\nabla} \wedge \underline{B})] ,$$

and the momentum equation,

$$\rho \left(\frac{\partial \underline{v}}{\partial t} + (\underline{v} \cdot \underline{\nabla}) \underline{v} \right) = -\underline{\nabla} p + \frac{1}{4\pi} (\underline{\nabla} \wedge \underline{B}) \wedge \underline{B} .$$

In this section, we neglect energy sources or sinks, under the assumption that the time scale for the T.M.I. is much less than the time scale for conduction, radiation and mechanical heating in the corona. Joule heating is assumed to be unimportant in the energy balance. So the energy equation is,

$$\frac{\partial T}{\partial t} + (\underline{v} \cdot \underline{\nabla}) T + (\gamma - 1) T (\underline{\nabla} \cdot \underline{v}) = 0 .$$

3.1. : THE LINEAR GROWTH RATE OF THE T.M.I. (Contd.)

For a perfect gas, the pressure is given by

$$p = R\rho T ,$$

and for a fully-ionized gas, the Coulomb resistivity is given by

$$\eta = 6{\cdot}53 \times 10^{12} \frac{\ell n.\Lambda}{T^{3/2}} \quad \text{e.m.u.},$$

where $\gamma = C_p/C_v$, the ratio of the specific heats,

R is the universal gas constant,

and $\ell n.\Lambda$ is the Coulomb logarithm (page 11).

The Equilibrium Configuration

We expect the T.M.I. to occur in a neutral current sheet, which we represent by the equilibrium magnetic field

$$\underline{B}_0 = B_a \sin \frac{\pi y}{a} \hat{x} , \quad (|y| \leq \frac{a}{2}) \qquad (3{\cdot}1)$$

where a is the width of the sheet. The equilibrium field is drawn in Figure (23), page 148, where we have noted that coronal conditions are assumed at $y = \pm \frac{a}{2}$ so that $p_0 = p_a$, $\rho_0 = \rho_a$ and $|B_0| = B_a$ there.

The zero order equilibrium equations are

$$\underline{V}_0 = 0 , \qquad (3{\cdot}2)$$

$$\nabla \wedge (\eta_0 (\nabla \wedge \underline{B}_0)) = 0 , \qquad (3{\cdot}3)$$

$$\nabla p_0 = \frac{1}{4\pi} (\nabla \wedge \underline{B}_0) \wedge \underline{B}_0 , \qquad (3{\cdot}4)$$

$$T_0 = \text{constant} , \qquad (3{\cdot}5)$$

$$p_0 = R \rho_0 T_0 , \qquad (3{\cdot}6)$$

and

$$\eta_0 = 6{\cdot}53 \times 10^{12} \frac{\ell n.\Lambda}{T_0^{3/2}} . \qquad (3{\cdot}7)$$

3.1. : THE LINEAR GROWTH RATE OF THE T.M.I. (Contd.)

From (3.4) and (3.1) we have

$$0 = -\underline{\nabla} p_0 - \underline{\hat{y}} \frac{1}{8\pi} \frac{d}{dy} \left(B_a^2 \sin^2 \frac{\pi y}{a} \right) ,$$

with components $$\frac{\partial p_0}{\partial x} = \rho \quad ,$$

and $$\frac{\partial}{\partial y} \left(p_0 + \frac{B_a^2}{8\pi} \sin^2 \frac{\pi y}{a} \right) = 0 ,$$

so that $$p_0 + \frac{B_a^2}{8\pi} \sin^2 \frac{\pi y}{a} = p_a + \frac{B_a^2}{8\pi} .$$

Note that (3.3) is not in fact satisfied by the assumed equilibrium magnetic field (3.1), which must therefore be varying slowly with time. However, this time variation can be ignored provided that the growth time, τ_{TMI}, of the tearing mode instability is very much less than the resistive diffusion time scale, τ_R / π^2, for the zero order magnetic field,

$$\text{i.e.} \quad \tau_{TMI} \ll \tau_R / \pi^2 \quad , \qquad (3.8)$$

where $\tau_R \equiv 4\pi a^2 / \eta_0$.

Thus, the zero order equilibrium, which we take, is characterised by

$$T_0 = \text{constant} ,$$

$$p_0 + \frac{B_a^2}{8\pi} \sin^2 \frac{\pi y}{a} = p_a + \frac{B_a^2}{8\pi} ,$$

$$\rho_0 = p_0 / (R T_0) \quad , \qquad (3.9)$$

$$\underline{B}_0 = B_a \sin \frac{\pi y}{a} \hat{\underline{x}} \quad ,$$

and $$\underline{v}_0 = 0$$

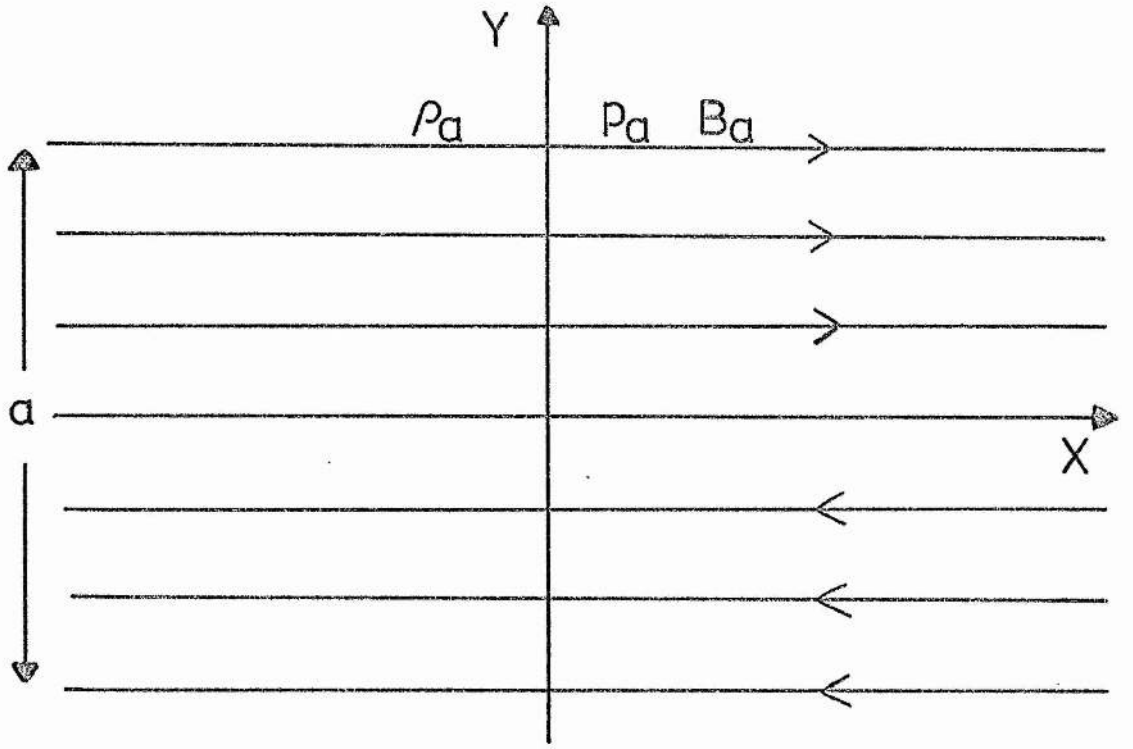

Figure (23). The equilibrium magnetic field $\underline{B}_o = B_a \sin\frac{\pi y}{a}\,\hat{x}$ which is perturbed to calculate the growth rate of the tearing mode instability. Coronal conditions are assumed at $y = \pm\frac{a}{2}$ where we suppose $p_o = p_a$, $\rho_o = \rho_a$ and $|B_o| = B_a$

3.1.: THE LINEAR GROWTH RATE OF THE T.M.I. (Contd.)

The Linearized Equations for the perturbed Variables.

We now write $\rho = \rho_0 + \rho_1$, $T = T_0 + T_1$, $p = p_0 + p_1$,

$\underline{v} = \underline{v}_1$, $\underline{B} = \underline{B}_0 + \underline{B}_1$, $\eta = \eta_0 + \eta_1$

with departures from equilibrium values indicated by a subscript of unity. After neglecting squares and products of small quantities, the basic equations reduce to

$$\frac{\partial \rho_1}{\partial t} + \rho_0 (\underline{\nabla} . \underline{v}_1) + (\underline{v}_1 . \underline{\nabla}) \rho_0 = 0 \quad , \tag{3.10}$$

$$\frac{\partial \underline{B}_1}{\partial t} = \underline{\nabla} \wedge (\underline{v}_1 \wedge \underline{B}_0) - \frac{1}{4\pi} \underline{\nabla} \wedge [\eta_1 (\underline{\nabla} \wedge \underline{B}_0) + \eta_0 (\underline{\nabla} \wedge \underline{B}_1)] \quad , \tag{3.11}$$

$$\rho_0 \frac{\partial \underline{v}_1}{\partial t} = -\underline{\nabla} p_1 + \frac{1}{4\pi} [(\underline{\nabla} \wedge \underline{B}_1) \wedge \underline{B}_0 + (\underline{\nabla} \wedge \underline{B}_0) \wedge \underline{B}_1] \quad , \tag{3.12}$$

$$\frac{\partial T_1}{\partial t} + (\gamma - 1) T_0 (\underline{\nabla} . \underline{v}_1) = 0 \quad , \tag{3.13}$$

$$p_1 = R [\rho_0 T_1 + \rho_1 T_0] \quad , \tag{3.14}$$

$$\eta_1 = -\frac{3}{2} \eta_0 \frac{T_1}{T_0} \quad . \tag{3.15}$$

Following the standard method for the solution of linear stability problems, we next assume the perturbations take the form

$$f_1 (x, y, t) = f(y) \, e^{\omega t + ikx} \quad , \tag{3.16}$$

3.1.: THE LINEAR GROWTH RATE OF THE T.M.I. (Contd.)

where the physical perturbation is the real part of $f_1(x,y,t)$. We are assuming that there is no variation with Z.

The object of the analysis is to solve (3.10) to (3.15) for ω, the linear growth rate of the instability, as a function of k, the wave number of the perturbation.

It is possible to assume f_1 is proportioned to e^{ikx} and so remove the x-variation because the variable x does not appear explicitly in (3.10) to (3.15).

The boundary conditions on the variables $\rho, T, \underline{v}$ and $\underline{B}$, that they remain finite as $X \to \pm\infty$, imply that k is real.

It is assumed the ω is real, so that we are looking for purely growing unstable modes and not overstable modes.

The next stage in the solution is to expand $f(y)$ in a Fourier series,

$$f(y) = \frac{f_0}{2} + \sum_{n=1}^{\infty} f_n \cos\frac{n\pi y}{a} + g_n \sin\frac{n\pi y}{a},$$

where $f(y)$ is defined, at this stage only, over the range $-a \le y \le a$.

Now it is possible, from previous work (e.g. Furth et al, 1963) to say whether the variables $f(y)$ are symmetric or anti-symmetric about the neutral line of the current sheet $y = 0$, so that it is necessary to define $f(y)$ only over the half-range $0 \le y \le a$ and specify it as an even or odd function in the other half-range. In this way the variables $f(y)$ can be approximated by a sine or cosine series only, as follows

$$\left.\begin{aligned} B_{x}(y) &= \sum_{n=0}^{\infty} B_{xn} \sin\frac{n\pi y}{a}\,, \\ B_{y}(y) &= \sum_{n=0}^{\infty} B_{yn} \cos\frac{n\pi y}{a}\,, \\ V_{x}(y) &= \sum_{n=0}^{\infty} V_{xn} \cos\frac{n\pi y}{a}\,, \\ V_{y}(y) &= \sum_{n=0}^{\infty} V_{yn} \sin\frac{n\pi y}{a}\,, \\ \rho(y) &= \sum_{n=0}^{\infty} \rho_{n} \cos\frac{n\pi y}{a}\,, \\ T(y) &= \sum_{n=0}^{\infty} T_{n} \cos\frac{n\pi y}{a}\,. \end{aligned}\right\} \qquad (3.17)$$

The z components of $\underline{B}_1$ and $\underline{V}_1$ are decoupled from (3.10) to (3.15), because we assume that there are no variations with z, so they need not be considered. The range of y of interest to us is only $0 \le y \le \frac{a}{2}$ since the current sheet has half-width $\frac{a}{2}$. Thus we are free to define $\rho(y)$, over the range $0 \le y \le a$, as either symmetric or anti-symmetric about $y = a/2$. If we assume that $\rho(y)$ and $T(y)$ are anti-symmetric over this range then we see from (3.17) that only odd values of n appear in their Fourier series, which is equivalent to choosing boundary conditions $\rho_n = T_n = 0$ at $y = a/2$, the edge of the current sheet, so that the equilibrium is not perturbed there. When this condition is applied to the Fourier transformed equations, it can be shown that only even values of n appear for $B_x(y)$ and $B_y(y)$ while there are only odd values for $V_x(y)$ and $V_y(y)$.

3.1.: THE LINEAR GROWTH OF THE T.M.I. (Contd.)

We have so far used only 6 boundary conditions on the variables as functions of x, namely that each of

$$\rho,\ T,\ V_x,\ V_y,\ B_x \text{ and } B_y$$

be finite as $x \to \infty$. However, in (3.10) to (3.13), the sum of the orders of the differential equations with respect to x is 8 and so we need to choose two more boundary conditions. The ones we take are that

$$B_{1y}(0,y,t) = V_{1x}(0,y,t) = 0 \quad \text{at } x=0,$$

from the expected nature of the tearing mode instability. Then, bearing in mind the form in (3.16) we see that the real variables $B_{1y}(x,y,t)$ and $V_{1y}(x,y,t)$ need to be proportional to $\sin kx$.

The Fourier transformed equations then imply that

$$B_{1x}(x,y,t),\ V_{1y}(x,y,t),\ \rho_1(x,y,t)$$

and $T_1(x,y,t)$ are each proportional to $\cos kx$.

So the final form for the perturbations is,

$$\left.\begin{aligned} B_{1x}(x,y,t) &= e^{\omega t}\cos kx \sum_{n=2}^{\infty} B_{xn} \sin\frac{n\pi y}{a} \\ B_{1y}(x,y,t) &= e^{\omega t}\sin kx \sum_{n=0}^{\infty} B_{yn} \cos\frac{n\pi y}{a} \end{aligned}\right\} \quad n \text{ is even.}$$

$$\left.\begin{aligned} V_{1x}(x,y,t) &= e^{\omega t}\sin kx \sum_{n=1}^{\infty} V_{xn} \cos\frac{n\pi y}{a} \\ V_{1y}(x,y,t) &= e^{\omega t}\cos kx \sum_{n=1}^{\infty} V_{yn} \sin\frac{n\pi y}{a} \\ \rho_1(x,y,t) &= e^{\omega t}\cos kx \sum_{n=1}^{\infty} \rho_n \cos\frac{n\pi y}{a} \\ T_1(x,y,t) &= e^{\omega t}\cos kx \sum_{n=1}^{\infty} T_n \cos\frac{n\pi y}{a} \end{aligned}\right\} \quad n \text{ is odd.}$$

3.1.: THE LINEAR GROWTH OF THE T.M.I. (Contd.)

The approximate form of the magnetic field, once the equilibrium field is perturbed, is shown in Figure (24) page 154. The perturbations in this form, and the equilibrium magnetic field, density and temperature structure are then substituted into equations (3.10) to (3.13), whose Fourier transforms give the following set of equations for the coefficients of the Fourier series.

$$\bar{\rho}_n = A_1 \bar{V}_{xn} + A_2 [\bar{V}_{x(n-2)} + \bar{V}_{x(n+2)}] + n A_3 \bar{V}_{yn} + n A_4 [\bar{V}_{y(n-2)} + \bar{V}_{y(n+2)}], \quad (3.18)$$

$$\bar{B}_{x(n+1)} = [\bar{V}_{y(n+2)} - \bar{V}_{yn}](n+1) B_{1(n+1)} + [\bar{\bar{T}}_{(n+2)} + \bar{\bar{T}}_n](n+1) B_{2(n+1)}, \quad (3.19)$$

$$\bar{B}_{y(n+1)} = -\frac{\bar{k}}{(n+1)\pi} \bar{B}_{x(n+1)}, \quad (3.20)$$

$$0 = \bar{V}_{xn} A_5 + [\bar{V}_{x(n-2)} + \bar{V}_{x(n+2)}] A_6 + \bar{k} \bar{\rho}_n + A_7 \bar{\bar{T}}_n + A_8 [\bar{\bar{T}}_{n+2} + \bar{\bar{T}}_{n-2}] + A_9 \left[\frac{\bar{B}_{x(n+1)}}{n+1} + \frac{\bar{B}_{x(n-1)}}{n-1} \right], \quad (3.21)$$

$$0 = \bar{V}_{yn} A_5 + [\bar{V}_{y(n-2)} + \bar{V}_{y(n+2)}] A_6 + n\pi \bar{\rho}_n + n A_{10} \bar{\bar{T}}_n + n A_{11} [\bar{\bar{T}}_{n+2} + \bar{\bar{T}}_{n-2}] + \left[A_{12_n} + \frac{A_{13}}{n+1} \right] \bar{B}_{x(n+1)} - \left[A_{12_n} + \frac{A_{13}}{n-1} \right] \bar{B}_{x(n-1)}, \quad (3.22)$$

$$A_{14} \bar{\bar{T}}_{n+2} = \bar{k} \bar{V}_{x(n+2)} + (n+2)\pi \bar{V}_{y(n+2)}. \quad (3.23)$$

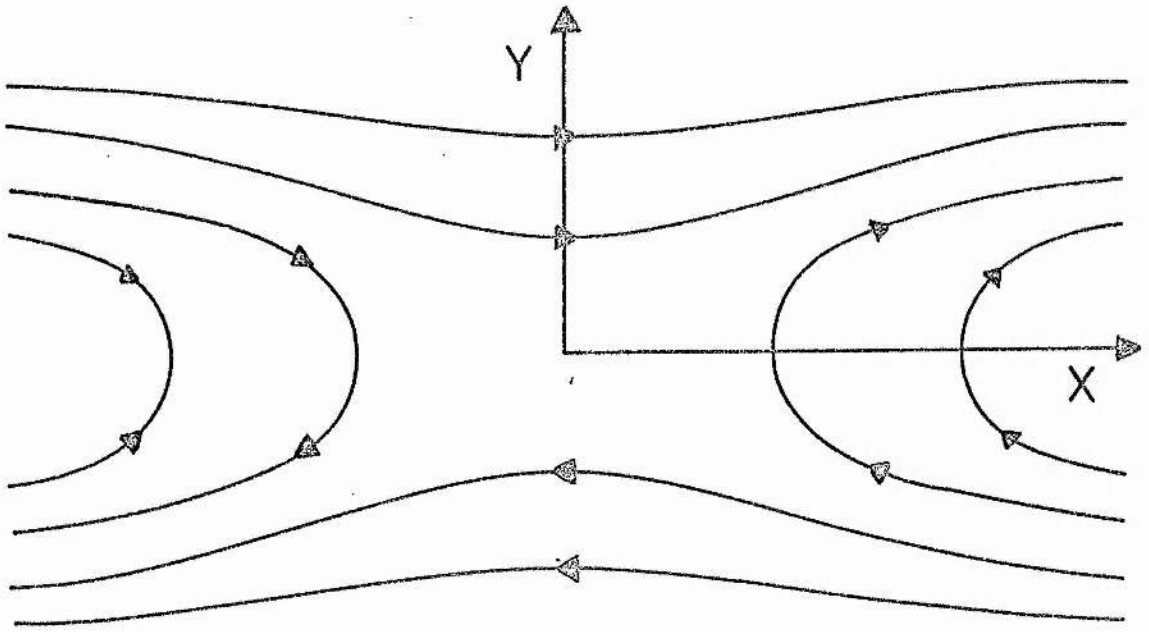

Figure (24). The approximate form of the magnetic field once the equilibrium field, given by (3.1) is perturbed.

(3.20) is a result of $\nabla . \underline{B} = 0$ and has been used to eliminate B_{y_n} from the other equations. (3.14) and (3.15) have been employed to eliminate p_1 and η_1 .

The variables in (3.18) to (3.23) are dimensionless, defined by

$$\overline{B}_x = \frac{B_x}{B_a} \quad , \quad \overline{B}_y = \frac{B_y}{B_a} \quad , \quad \overline{\rho} = \frac{\rho}{\rho_0(y=0)}$$

where $\rho_0(y=0)$ is the value of the equilibrium density ρ_0, at $y=0$,

$$\overline{V}_x = \frac{V_x}{V_A} \quad , \quad \overline{V}_y = \frac{V_y}{V_A} \quad , \quad \overline{T} = \frac{T}{T_0} \quad , \quad \overline{\omega} = \omega \tau_R$$

and $\overline{k} = a k$.

The coefficients appearing (3.18) to (3.23) are

$$A_1 = -\overline{k}\,\frac{S}{\overline{\omega}}\left(1 - \frac{1}{2(1+\beta)}\right) \quad , \quad A_2 = -\frac{\overline{k}}{4(1+\beta)}\,\frac{S}{\overline{\omega}} \quad ,$$

$$A_3 = \frac{\overline{\Pi}}{\overline{k}}\,A_1 \quad , \quad A_4 = \frac{\overline{\Pi}}{\overline{k}}\,A_2 \quad ,$$

$$A_5 = -\frac{\overline{\omega}}{S}\,\frac{2}{\beta}\left(1 - \frac{1}{2(1+\beta)}\right) \quad , \quad A_6 = -\frac{\overline{\omega}}{S}\,\frac{1}{2\beta(1+\beta)} \quad ,$$

$$A_7 = \overline{k}\left(1 - \frac{1}{2(1+\beta)}\right) \quad , \quad A_8 = \frac{\overline{k}}{4(1+\beta)} \quad ,$$

$$A_9 = \frac{-\overline{k}}{(1+\beta)} \quad , \quad A_{10} = \overline{\Pi}\left(1 - \frac{1}{2(1+\beta)}\right) \quad ,$$

$$A_{11} = \frac{\pi}{4(1+\beta)} \quad , \quad A_{12n} = \frac{n\pi}{(1+\beta)}$$

$$A_{13} = \frac{\bar{k}^2}{\pi(1+\beta)} \quad , \quad A_{14} = \frac{-\bar{\omega}}{(\gamma-1)S} \quad ,$$

$$B_{1n} = \frac{\frac{\pi}{2}S}{\bar{\omega} + \bar{k}^2 + (n\pi)^2} \quad , \quad B_{2n} = \frac{3}{2}\pi \frac{B_{1n}}{S} \quad .$$

The dimensionless parameters are

$$\beta = p_a 8\pi / B_a^2 \quad ,$$

$$\text{and} \quad S = \tau_R / \tau_A \quad , \qquad (3.24)$$

where $\tau_R = 4\pi a^2/\eta_0$ and $\tau_A = a/V_A = a(4\pi\rho_a)^{1/2}/B_a$ are the resistive diffusion and Alfvén time scales.

We can solve (3.18) to (3.23) for the six unknowns

$$V_{x(n+2)} \, , \; V_{y(n+2)} \, , \; B_{x(n+1)} \, , \; B_{y(n+1)} \, , \; T_{(n+2)} \text{ and } p_n$$

once we know the values of the Fourier coefficients with indices less than these. Any negative values are determined by $f_n = -f_{-n}$ for the Fourier coefficients of the sine series and $f_n = f_{-n}$ for the cosine series. In order to begin the recurrence relations at $n=1$, it is necessary to specify the 2 starting values V_{x1} and V_{y1}. (We already know that $B_{x0} = 0$ from the assumption that $B_x(x,y,t)$ is antisymmetric in y about $y = 0$.) Cross (1972) also had to devise extra conditions to determine starting values when he looked at the effect of heating on the T.M.I.

3.1.: THE LINEAR GROWTH OF THE T.M.I.(Contd.)

Following him, we note firstly that the perturbations $f_1(x,y,t)$ satisfy linear equations so we are free to choose one of the coefficients arbitrarily, say

$$V_{y_1} = 1 \qquad (3.25)$$

Furthermore, from previous work (Furth et. al., 1963) we know that the time scale of the T.M.I. is very much greater than both the Alfvēnic time scale and, (if β is not too small) the sound speed time scale, so that the fluid behaves incompressibly (see section 1.3). Until now we have not assumed incompressibility, but we now do so for the first terms of the Fourier series. From $\underline{\nabla} . \underline{V}_1 = 0$ we get

$$V_{x_1} = -\frac{\pi}{ak} V_{y_1} \qquad (3.26)$$

This assumption is justified, in part, by the computations which show that $V_{x_n} = -\frac{n\pi}{ak} V_{y_n}$ for a converging series of coefficients. A result of this assumption is that with $n=-1$, (3.23) gives

$$T_1 = 0 \qquad . \qquad (3.27)$$

We find from the computations that T_n is very much less than V_{x_n} and V_{y_n}, for a converging series of coefficients. With the two extra equations, (3.26) and (3.27), as starting values, we can find all the coefficients of the Fourier series from (3.18) to (3.23).

3.1.: THE LINEAR GROWTH OF THE T.M.I. (Contd.)

The aim is to find the value of $\bar{\omega}$ for which the coefficients of the Fourier series converge as n is increased. Since the perturbation functions must have convergent Fourier series, we conclude that the value of the frequency found in this way is the frequency of the T.M.I. For general values of $\bar{\omega}$ the series will not converge but as $\bar{\omega}$ gets closer to the actual value of the frequency then the convergence of the series improves and so it is possible to find the growth rate of the T.M.I. to any desired accuracy.

In Table 4 we show how the sequence of coefficients V_{yn}/V_{y_1}, with $S = 10^5$ and $\bar{k} = \pi/10$, converges as we get closer to a value $\bar{\omega}_c \simeq 1842.4120726$.

TABLE 4

Values of V_{yn}/V_{y_1}

n \ $\bar{\omega}$	1842·40.	1842·4120726	1842·41207261	1842·41
1	1·0	1·0	1·0	1·0
3	0·3	0·3	0·3	0·3
5	0·2	0·2	0·2	0·2
7	0·1	0·1	0·1	0·1
9	0·2	0·09	0·09	0·09
11	− 50	0·07	0·07	0·2
13	2×10^5	0·05	0·03	− 60
15	-8×10^6	−2·0	5·6	2×10^4
17	3×10^9	8×10^2	-2×10^3	-10^7
19	-10^{12}	-3×10^5	9×10^5	4×10^9

3.1.: THE LINEAR GROWTH OF THE T.M.I. (Contd.)

T A B L E 4 (Contd.)

When $\bar{\omega}$ is far from $\bar{\omega}_c$ then the sequence diverges and oscillates such that, for values of $\bar{\omega}$ on one side of $\bar{\omega}_c$, the coefficients oscillate with n in one sense, but on the other side of $\bar{\omega}_c$ they oscillate in the opposite sense. As we get closer to $\bar{\omega}_c$ more terms of the sequence converge and in this way we calculate $\bar{\omega}_c$ to any desired accuracy. We find that in order to get convergence for the first seven terms of the sequence we require $\bar{\omega}_c$ to fourteen figures, which is on the limit of the accuracy of the computations and so we are unable to find more than the first seven coefficients of the Fourier series. In their case Cross & Van Hoven found it much easier to obtain convergence.

Results:

The general shape of the dispersion relation, $\bar{\omega}$ against $\bar{k}$, is shown in Figure (25) page 160, for the values $S = 10^{10}, 10^{8}$ and 10^{5} and $\beta = 10^{6}$. Since we have followed the method of Cross & Van Hoven in calculating $\bar{\omega}$ it is interesting to compare the similarities and differences between the two sets of results.
Qualitatively, the shape of the $\bar{\omega}/\bar{k}$ graph is similar, with $\bar{\omega} = 0$ at $\bar{k} = 0$ and $\bar{k} \gtrsim \pi$ and with one maximum value of $\bar{\omega}$ in between. For small values of $\bar{k}$ we find that the value of $\bar{\omega}$ is close to $(\bar{k}S)^{2/3}$ in agreement with their results (Cross & Van Hoven, 1971) and the original analytic ones of Furth et.al. (1963, Appendix D).

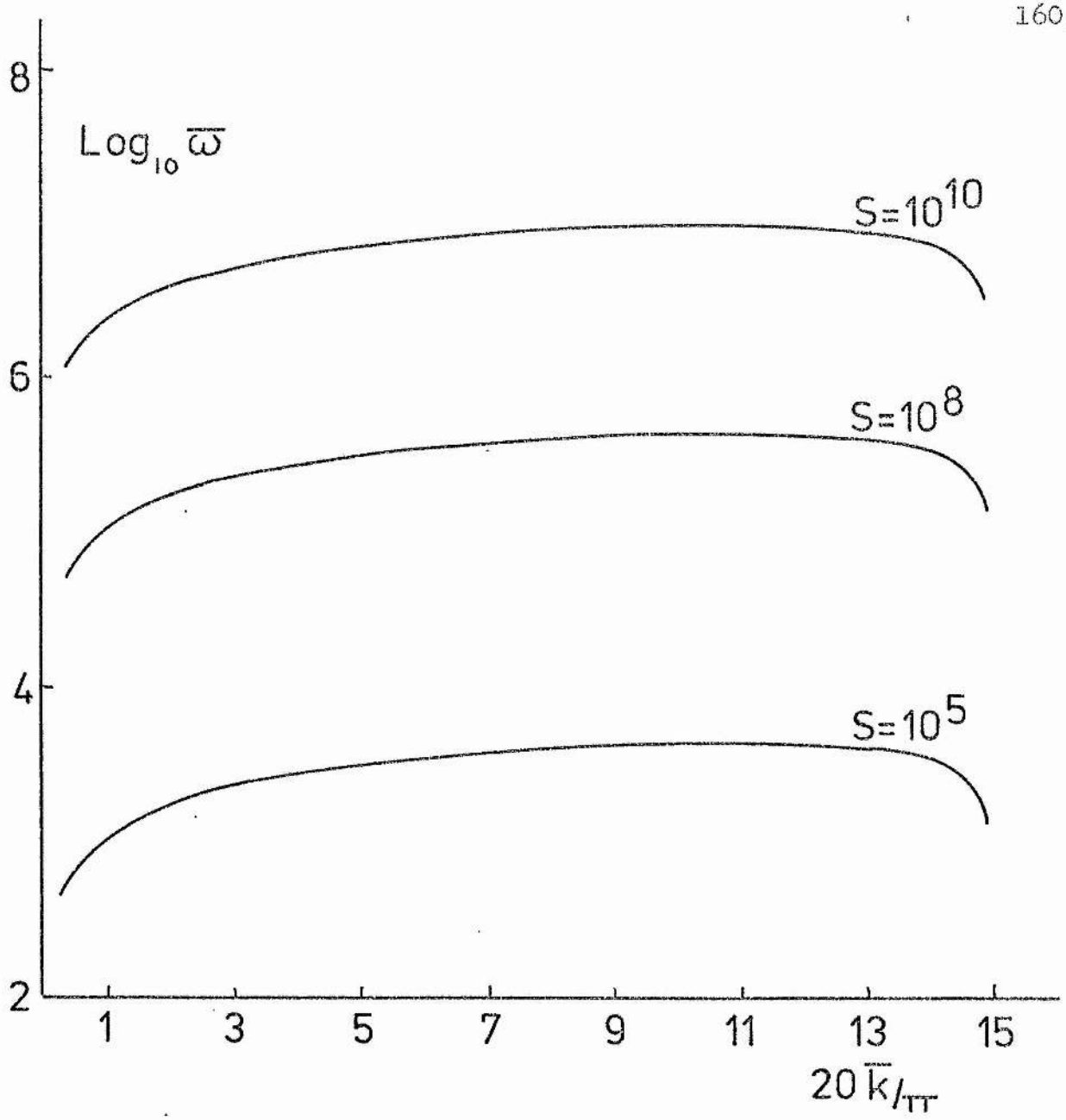

Figure (25). The variation of $\overline{\omega}$, the growth rate of the tearing mode instability, with $\overline{k}$, the wave number of the perturbation, for several values of S, the ratio of the resistive time scale to the Alfvénic time scale.

3.1.: THE LINEAR GROWTH OF THE T.M.I. (Contd.)

As $\bar{k}$ increases, $\bar{\omega}$ becomes less than $(\bar{k}S)^{2/3}$, again in agreement with Cross & Van Hoven. But our maximum value for $\bar{\omega}$ is somewhat larger than their value and it occurs at a value of $\bar{k}$, $\bar{k}_{max}$ say, which depends on β but is independent of S (when $\beta = 10^6$, for instance, $\bar{k}_{max} = \pi/2$). Cross & Van Hoven find instead that $\bar{k}_{max}$ decreases as S increases. The dependence of $\bar{k}_{max}$ on β is drawn on Figure (26), page 162.

For given values of S and β there is a maximum value of $\bar{\omega}$, $\bar{\omega}_{max}$, say, which has been plotted in Figure (27) page 163, for $\beta = 10^6, 1{\cdot}0, 10^{-2}$.
We find that

$$\bar{\omega}_{max} = \begin{cases} 2{\cdot}1\, S^{0.67} & \text{for } \beta = 10^6 \\ 1{\cdot}5\, S^{0.67} & \text{for } \beta = 1{\cdot}0 \\ 0{\cdot}2\, S^{0.67} & \text{for } \beta = 10^{-2} \end{cases}$$

So that, as β is reduced, $\bar{\omega}_{max}$ falls equally for all values of S considered.

Cross & Van Hoven find that

$$\bar{\omega}_{max} = 3{\cdot}4\, S^{0.57} \qquad (S > 10^3)$$

and Furth et.al.(1963) found that $\bar{\omega}_{max} \propto S^{0.5}$, which is in reasonable agreement. The frequency that is likely to occur naturally is the fastest growing one so that, although there is close agreement between our results and those of Cross & Van Hoven for small values of $\bar{k}$, we would find in practice that the frequency at which the T.M.I. occurred would, in our case, be faster than theirs for a given value of S by up to an order of magnitude.

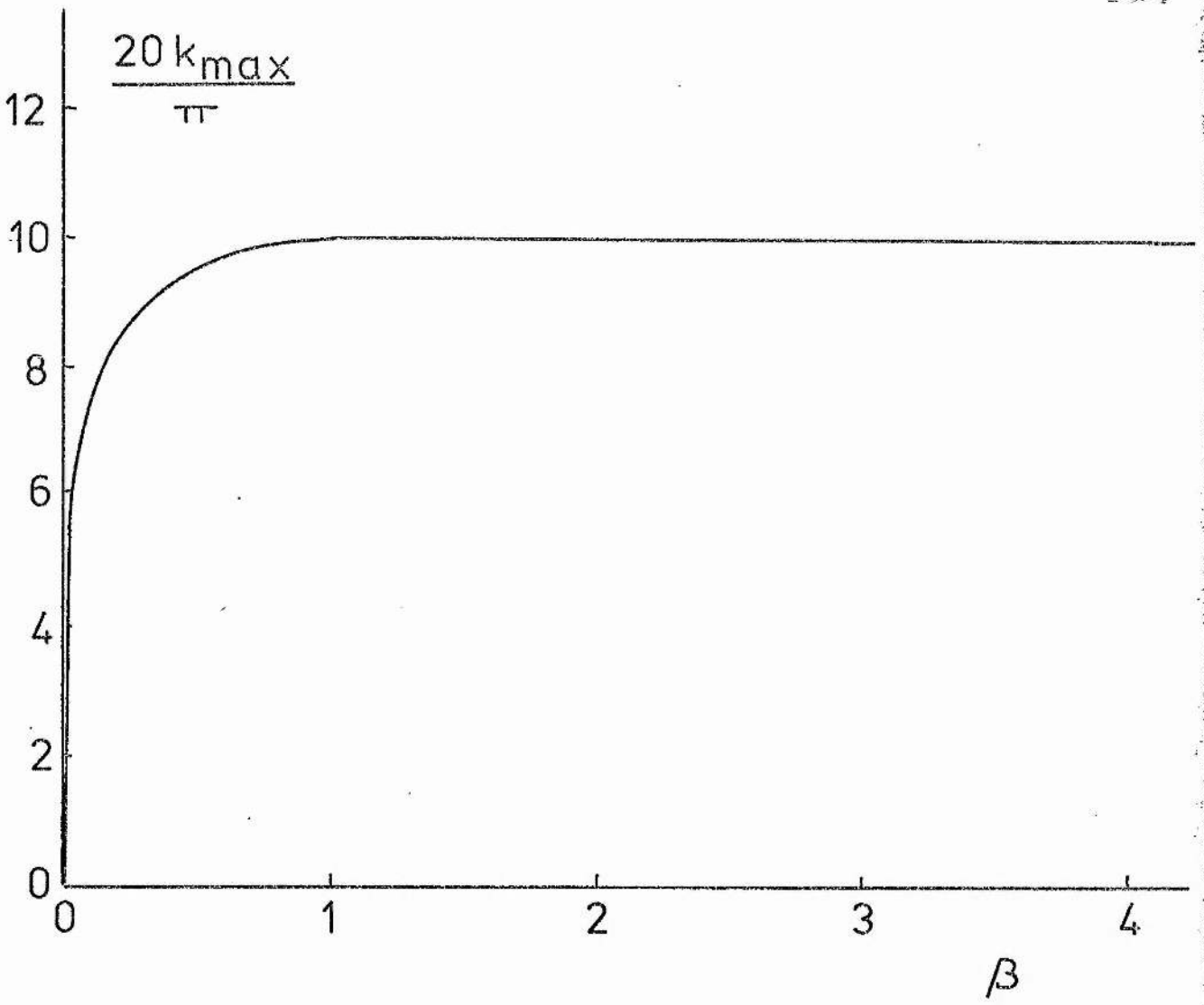

Figure (26). The dependence of $\overline{k}_{max}$, the value of $\overline{k}$ at the maximum of an $\overline{\omega}/\overline{k}$ curve for a given S, (Figure (25)), as a function of β, the ratio of the gas to the magnetic pressure.

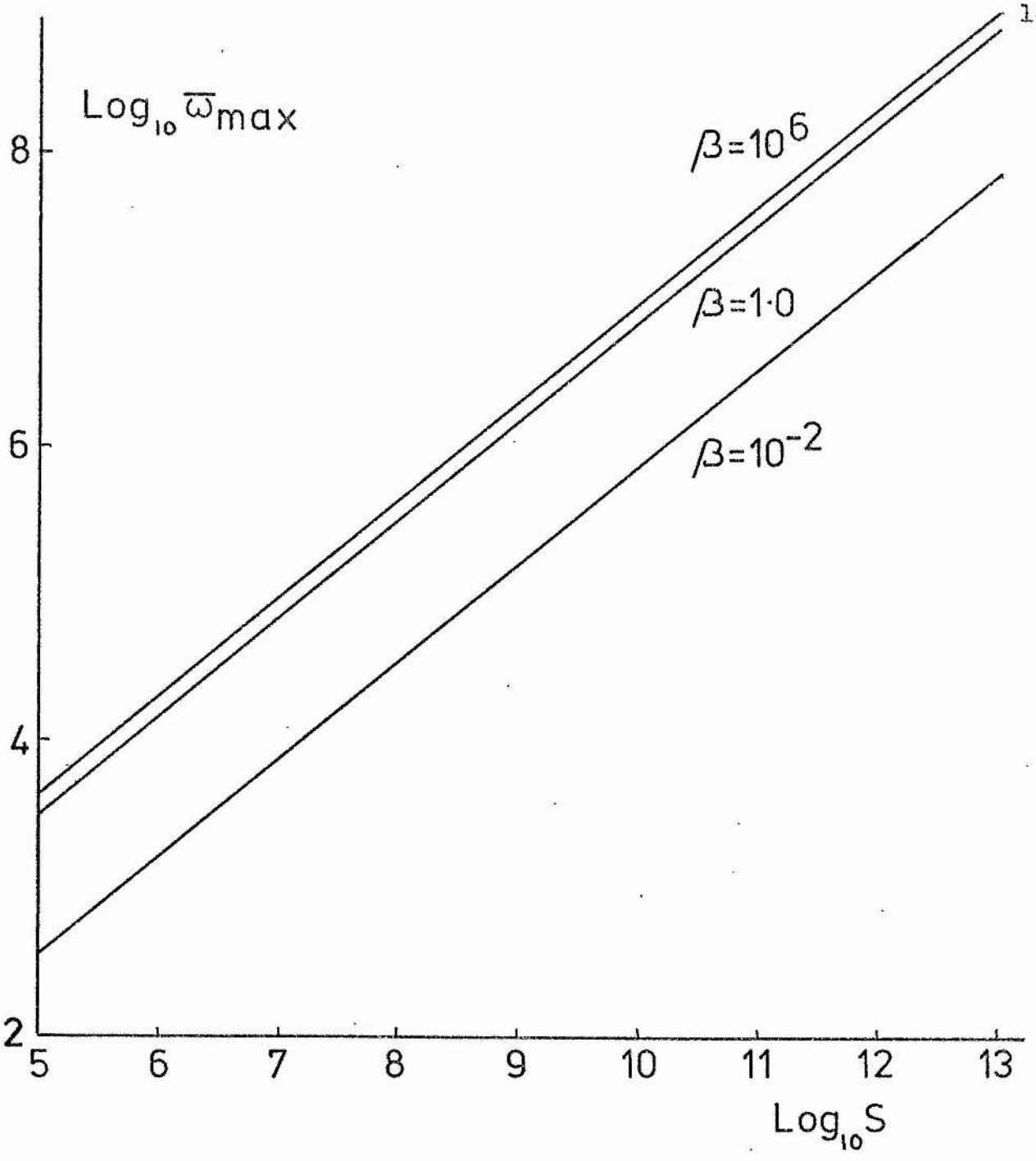

Figure (27). The variation of $\overline{\omega}_{max}$, the maximum value of $\overline{\omega}$ for a given value of S, on the $\overline{\omega}(\overline{k})$ curve, Figure (25) page 160, with S, the ration of the resistive diffusion time scale to the Alfvénic time scale, for several values of β, the ratio of the gas to magnetic pressure.

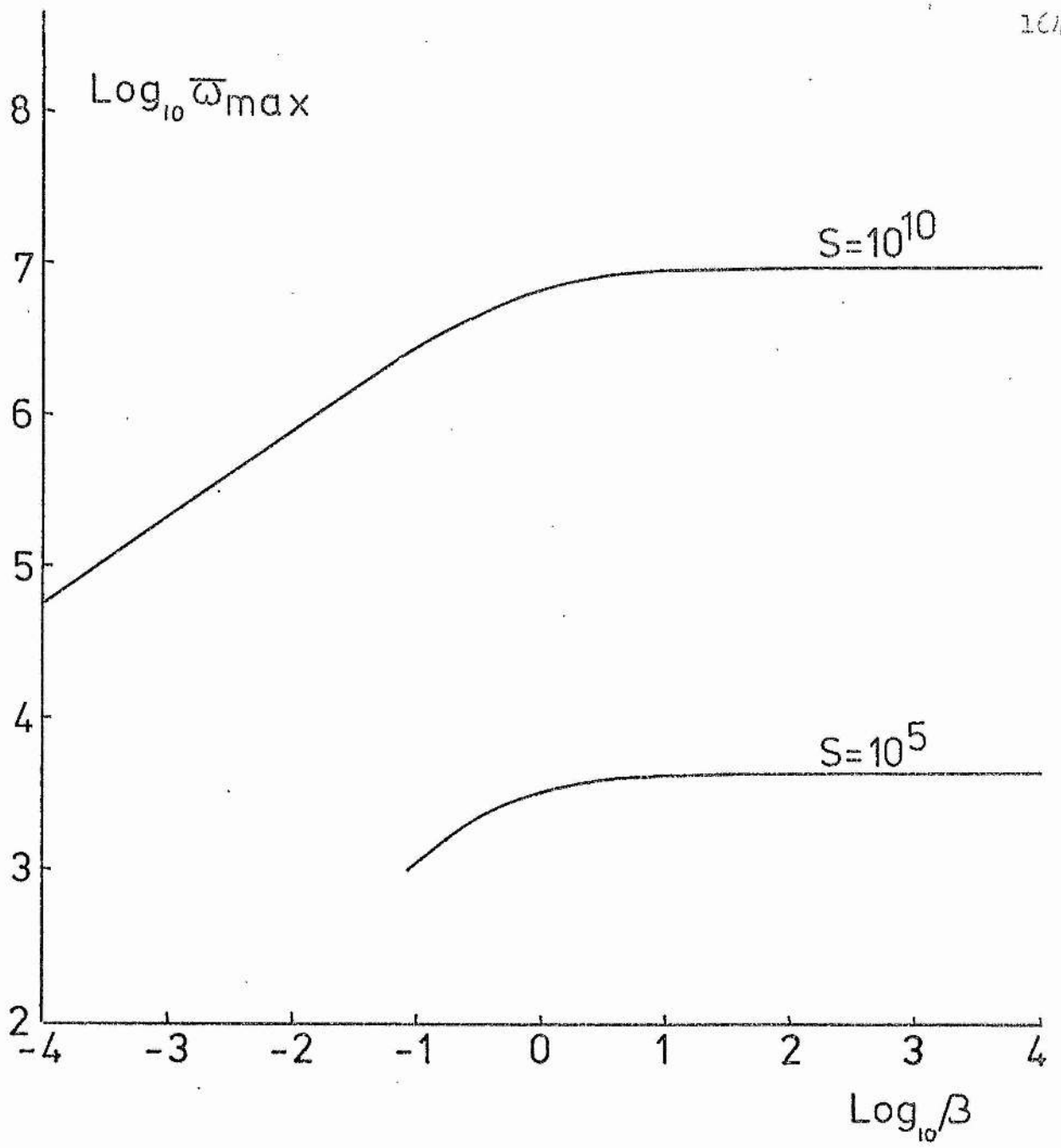

Figure (28). The dependence of $\overline{\omega}_{max}$, the maximum value of $\overline{\omega}$ for a given value of S, on the $\overline{\omega}(\overline{k})$ curve, Figure (25), page 160 on β the ratio of the gas to magnetic pressure, for two values of S, the ratio of the resistive diffusion time scale to the Alfvénic time scale.

3.1.: THE LINEAR GROWTH OF THE T.M.I. (Contd.)

The way in which the value of β affects $\bar{\omega}_{max}$ is shown in Figure (28) page 164, for $S = 10^{10}$ and 10^{5}; we stopped the calculation when $\bar{\omega}_{max} \leq 10^{3}$, because then condition (3.8) is no longer valid, i.e. $\bar{\omega} \not\gg \pi^2$. A possible reason why $\bar{\omega}_{max}$ is an increasing function of β for constant S, is as follows. In the works of Furth et. al. and Cross & Van Hoven, $\bar{\omega}$ is found in terms of $\langle S \rangle$, an average value of S calculated from (3.24) using average values of density and resistivity. But in our case when $\beta < 1$, S, defined at the edge of the sheet, is not an average value. From the definition in (3.24) we see that $S \propto \left(\frac{1}{\rho_a}\right)^{1/2}$ where ρ_a is the density at the edge of the sheet and is related to the value $\rho_0 (y=0)$ at the centre by

$$\rho_a / \rho_0(y=0) = \beta/(1+\beta) .$$

Thus ρ_a, and hence S, is only an average value when $\beta > 1$, while with $\beta << 1$ the average value $\langle S \rangle$ is much less than S. The effect of reducing β is therefore to reduce the average value $\langle S \rangle$ and so we would expect from Furth et. al. and Cross & Van Hoven, that $\bar{\omega}$ would be reduced also. That this effect is occurring in our case is confirmed, in part, by the fact that it is only when $\beta << 1$ that $\bar{\omega}_{max}$ is reduced substantially from its large β results, as shown in Figure (28), page 164.

3.1.: THE LINEAR GROWTH OF THE T.M.I. (Contd.)

To summerize, we find that our T.M.I. results are qualitatively similar to those of previous authors, but that we find significantly higher maximum values of $\overline{\omega}$. The differences are due to the different equilibrium magnetic field taken in each case. In our work the equilibrium field structure is that of a current sheet, whereas the others were considering a sheared magnetic field of constant magnitude.

3.2.: AN ALTERNATIVE EQUILIBRIUM STRUCTURE WHEN $\beta >> 1$

We have so far considered a simple equilibrium current sheet structure, which we refer to as model A and which has a constant temperature T_o throughout the sheet. In reality, however, the temperature may well vary greatly across the sheet, its form being determined by an energy equation, whose most important terms may vary considerably from one situation to another. The method we are employing demands that the equilibrium variables have fairly simple forms, but an alternative structure, which we can treat and which we refer to as model B, possesses a constant density ρ_o , so that its temperature varies with y in order to preserve constancy of total pressure. Furthermore, we are able to demonstrate below that model B gives a growth rate that is independent of β and is identical with that already found for $\beta >> 1$ with model A. In the model we have considered, in section 3.1, for the T.M.I. the zero order equilibrium variables are

$$T_o = \text{constant} ,$$

$$p_o + \frac{B_a^2}{8\pi} \sin^2 \frac{\pi y}{a} = p_a + \frac{B_a^2}{8\pi} ,$$

$$\rho_o = p_o / R T_o ,$$

$$\eta_o = 6{\cdot}53 \times 10^{12} \frac{\rho_m \cdot \Lambda}{T_o^{3/2}} ,$$

$$\underline{B}_o = B_a \sin \frac{\pi y}{a} \hat{\underline{x}} .$$

3.2.: AN ALTERNATIVE EQUILIBRIUM STRUCTURE WHEN $\beta >> 1$ (contd.)

In the limit $\beta \equiv \frac{8\pi p_a}{B_a^2} >> 1$ these equations reduce to

$$\left.\begin{aligned} T_o &= \text{constant}, \\ p_o &= p_a + \frac{B_a^2}{8\pi}, \\ \rho_o &= p_o / R T_o, \\ \eta_o &= 6.53 \times 10^{12} \frac{\ln \Lambda}{T_o^{3/2}}, \\ \underline{B}_o &= B_a \sin \frac{\pi y}{a} \underline{\hat{x}}. \end{aligned}\right\} \quad \text{MODEL A}$$

Consider now, the model

$$\left.\begin{aligned} T_o &= T_o(y), \\ p_o &= p_o(y), \\ \rho_o &= \text{constant}, \\ \eta_o &= \text{constant}, \\ \underline{B}_o &= B_a \sin \frac{\pi y}{a} \underline{\hat{x}}. \end{aligned}\right\} \quad \text{MODEL B}$$

We can show that for any positive β, model B gives the same growth rate for the T.M.I. that model A gives when $\beta >> 1$. For model A, the linearized equations (3.10) to (3.15), with the perturbed variables proportional to $e^{\omega t}$, reduce to the following set, in the limit $\beta >> 1$.

$$\rho_1 = 0, \qquad (3.28)$$

$$T_1 = 0, \qquad (3.29)$$

$$p_1 = 0, \qquad (3.30)$$

$$\eta_1 = 0, \qquad (3.31)$$

$$\omega \underline{B}_1 = \underline{\nabla} \wedge (\underline{v}_1 \wedge \underline{B}_o) - \frac{\eta_o}{4\pi} \underline{\nabla} \wedge (\underline{\nabla} \wedge \underline{B}_1), \qquad (3.32)$$

$$\omega \rho_o \underline{v}_1 = \frac{1}{4\pi} \left[(\underline{\nabla} \wedge \underline{B}_o) \wedge \underline{B}_1 + (\underline{\nabla} \wedge \underline{B}_1) \wedge \underline{B}_o \right], \qquad (3.33)$$

3.2.: AN ALTERNATIVE EQUILIBRIUM STRUCTURE WHEN $\beta >> 1$ (contd.)

so that (3.32) and (3.33) determine $\underline{B}_1$ and $\underline{V}_1$. An alternative way to derive (3.28) to (3.33) is to make the incompressibility assumption, $\underline{\nabla} \cdot \underline{V}_1 = 0$ based on previous work. The $\hat{z}$ component of the curl of (3.33) then becomes

$$\omega \rho_0 \left(\frac{\partial V_{1y}}{\partial x} - \frac{\partial V_{1x}}{\partial y} \right) = \frac{1}{4\pi} \hat{z} \cdot \left\{ \underline{\nabla} \wedge \left[(\underline{\nabla} \wedge \underline{B}_0) \wedge \underline{B}_1 + (\underline{\nabla} \wedge \underline{B}_1) \wedge \underline{B}_0 \right] \right\} , \quad (3.34)$$

where

$$\frac{\partial V_{1y}}{\partial y} + \frac{\partial V_{1x}}{\partial x} = 0 , \quad (3.35)$$

and (3.32), (3.34) and (3.35) can be solved for $\underline{B}_1$, V_{1x} and V_{1y}.

For model B on the other hand, the linearized equations with the perturbed variables proportional to $e^{\omega t}$ become

$$\rho_1 = 0 , \quad (3.36)$$

$$\omega T_1 + (\underline{V}_1 \cdot \underline{\nabla}) T_0 = 0 , \quad (3.37)$$

$$p_1 = R \rho_0 T_1 , \quad (3.38)$$

$$\eta_1 = 0 , \quad (3.39)$$

$$\omega \underline{B}_1 = \underline{\nabla} \wedge (\underline{V}_1 \wedge \underline{B}_0) - \frac{\eta_0}{4\pi} \underline{\nabla} \wedge (\underline{\nabla} \wedge \underline{B}_1) , \quad (3.40)$$

$$\rho_0 \omega \underline{V}_1 = -\underline{\nabla} p_1 + \frac{1}{4\pi} \left[(\underline{\nabla} \wedge \underline{B}_1) \wedge \underline{B}_0 + (\underline{\nabla} \wedge \underline{B}_0) \wedge \underline{B}_1 \right] , \quad (3.41)$$

3.2.: AN ALTERNATIVE EQUILIBRIUM STRUCTURE WHEN $\beta \gg 1$ (Contd.)

so that (3.37), (3.38), (3.40) and (3.41) determine $T_1, p_1, \underline{B}_1$ and $\underline{V}_1$. However, the equations for $\underline{V}_1$ and $\underline{B}_1$ can be decoupled from the rest by taking the $\hat{z}$ component of curl (3.41) and using $\underline{\nabla} \cdot \underline{V}_1 = 0$. This gives

$$\rho_0 \omega \left(\frac{\partial V_{1y}}{\partial x} - \frac{\partial}{\partial y} V_{1x} \right) = \frac{1}{4\pi} \hat{z} \cdot \underline{\nabla} \wedge \left[(\underline{\nabla} \wedge \underline{B}_1) \wedge \underline{B}_0 + (\underline{\nabla} \wedge \underline{B}_0) \wedge \underline{B}_1 \right], \quad (3.42)$$

$$\text{where} \quad \frac{\partial V_{1y}}{\partial y} + \frac{\partial V_{1x}}{\partial x} = 0, \quad (3.43)$$

so that we can solve (3.40), (3.42) and (3.43) for $\underline{B}_1$, V_{1x} and V_{1y} and then solve (3.37) and (3.38) for T_1 and p_1. The equations for $\underline{B}_1$, V_{1x} and V_{1y} in the two models A and B are identical, so the values of $\underline{B}_1$, V_{1x} and V_{1y} and the resulting frequency will be the same. It is only the resulting perturbed pressure and density which differ.

The advantages of Model A over Model B are that one does not need to impose the condition $\underline{\nabla} \cdot \underline{V}_1 = 0$ and a more realistic value of the resistivity is assumed. Model B however holds for all values of β.

3.3.: THE POSSIBILITY OF AN IDEAL INSTABILITY

In the results of the T.M.I. we found that, as β is reduced from 10^6, the frequency falls in value. The question arises as to whether this reduced frequency still corresponds to the T.M.I. It certainly cannot be one of the other two resistive instabilities, the rippling mode and the gravitational mode, because the former requires a gradient in the equilibrium resistivity, and the latter requires a gravitational force, both of which are not included on the model. However, it is necessary to demonstrate that an infinite conductivity instability is not playing a part. To do this we show that, when $\eta_0 = 0$, the plasma is stable to the perturbations we prescribe.

We first solved, numerically, equations (3.18) to (3.23) with $\eta_0 = 0$, but found no convergence for the coefficients of the Fourier series taking several values of S and $0 < \omega \leq S$. This suggests that the configuration is stable to perturbations of the form (3.17). For confirmation of this numerical result we next calculated $\bar{\omega}$ analytically when $\eta_0 = 0$. Equation (3.11) and curl (3.12) become, when the effects of resistivity are ignored by neglecting terms of order S^{-1};

$$\bar{\omega}\bar{B}_y + \bar{V}_y \bar{B}_{x0} - \frac{\bar{B}''_{x0}}{\bar{B}_{x0}} \bar{B}_y = 0 \quad , \qquad (3.44)$$

and

$$\bar{B}''_y - \bar{B}_y \left(\bar{k}^2 + \frac{\bar{B}''_{x0}}{\bar{B}_{x0}} \right) = 0 \quad , \qquad (3.45)$$

where a dash represents differentiation with respect to $\bar{y} \equiv y/a$.

3.3.: THE POSSIBILITY OF AN IDEAL INSTABILITY (Contd.)

Then, using (3.1) for $\underline{B}_0$, we find

$$\bar{\omega}\,\bar{B}_y + \bar{V}_y \sin\frac{\pi y}{a} + \pi^2 \bar{B}_y = 0 \,, \qquad (3.46)$$

$$\bar{B}_y'' - \bar{B}_y(\bar{k}^2 - \pi^2) = 0. \qquad (3.47)$$

In this section we are following the description of section 3.1 as closely as possible to see if there is instability when resistivity is ignored. In that section we assume that B_y is symmetric about $y=0$, so the boundary condition is

$$\frac{\partial B_y}{\partial y} = 0 \quad \text{at} \quad y = 0 \,.$$

The solution to (3.47) for $-1/2 \le \bar{y} \le 1/2$ with this boundary condition is

$$\bar{B}_y = A \cosh(\bar{k}^2 - \pi^2)^{1/2}\,\bar{y} \,, \qquad (3.48)$$

where A is constant. Now in (3.46) at $\bar{y} = 0$ we have

$$(\bar{\omega} + \pi^2)\,\bar{B}_y = 0 \,,$$

so that

$$\bar{\omega} + \pi^2 = 0$$

or

$$\bar{B}_y = 0 \quad \text{at} \quad \bar{y} = 0.$$

If we take $\bar{B}_y = 0$ at $\bar{y} = 0$ as the solution, then (3.48) implies $A = 0$, so that $\bar{B}_y = 0$ for all $\bar{y}$ in the range $-1/2 \le \bar{y} \le 1/2$.

If we choose the solution $\bar{B}_y = 0$ then (3.46) implies $\bar{V}_y = 0$ in that range and so we get the simple uninformative solution to (3.44) and (3.45). Thus more generally $\bar{\omega} = -\pi^2$. However, this valuc

3.3.: THE POSSIBILITY OF AN IDEAL INSTABILITY (Contd.)

of $\bar{\omega}$ does not satisfy (3.8), and so there are no instabilities in this model which have time scales much less than the diffusion time scale and are unstable tothe particular perturbations taken.

Although there is no instability in this case, it has been shown that a T.M.I. does exist when $\eta = 0$ if we use the complete Ohm's law. Furth et.al. suggested and Cross (1972) has shown, that the inertial terms in the generalized Ohm's law support the electric field driving the current, and thus, give rise to a T.M.I.

Our analysis, and the computations, indicate that there is no T.M.I. when resistivity is zero, that is susceptible to the perturbations taken here, so that we are left with the conclusion that the frequencies calculated in the previous section are those of the T.M.I. reduced when β is reduced. It is possible for instability to occur if other perturbations are chosen, in particular if the neutral sheet is perturbed by a wave form in the z direction it is unstable to the interchange mode (Uchida and Sakurai, 1977).

3.4.: T.M.I. IN A CURRENT SHEET WITH A TRANSVERSE MAGNETIC FIELD

In this section we investigate the stability of the equilibrium magnetic field (3.1) with a constant component B_t superimposed transverse to the sheet, namely

$$\underline{B}_0 = B_a \sin\frac{\pi y}{a}\,\hat{\underline{x}} + B_t\,\hat{\underline{y}} \qquad (3.49)$$

We also suppose that

$$\left.\begin{aligned} &T_0 = \text{constant}\ , \\ &\eta_0 = 6{\cdot}53\times 10^{12}\,\frac{\ln\Lambda}{T_0^{3/2}}\ , \\ &\underline{V}_0 = 0\ , \\ &\text{and}\quad p_0 = R\rho_0 T_0 . \end{aligned}\right\} \qquad (3{\cdot}50)$$

The equilibrium force balance between the pressure gradient and Lorentz force, has components

$$\frac{\partial}{\partial y}\left(p_0 + \frac{B_a^2}{8\pi}\sin^2\frac{\pi y}{a}\right) = 0\ , \qquad (3{\cdot}51)$$

and

$$\frac{\partial}{\partial x}(p_0) = \frac{1}{4\pi} B_t \frac{\partial}{\partial y}\left(B_a \sin\frac{\pi y}{a}\right). \qquad (3{\cdot}52)$$

Equations (3.52) and (3.50) imply a density gradient in the x direction. In order to be able to solve the equations using the Fourier series technique of Cross and Van Hoven, no such gradients of the equilibrium variables in the x direction are allowed. However, this density gradient is ignorable if in the continuity equation

$$\rho_0 \frac{\partial v_x}{\partial x} \gg v_x \frac{\partial \rho_0}{\partial x}\ , \qquad (3{\cdot}53)$$

But $\frac{1}{\rho_0}\frac{\partial \rho_0}{\partial x} = \frac{1}{p_0}\frac{\partial p_0}{\partial x} = \frac{B_a^2}{8\pi p_a}\frac{2\pi}{a}\frac{B_t}{B_a}\cos\frac{\pi y}{a} \simeq \frac{1}{\beta}\frac{B_t}{B_a}\frac{2\pi}{a}$

by (3.52), so (3.53) implies

$$k \gg \frac{1}{\beta}\frac{B_t}{B_a}\frac{2\pi}{a}$$

3.4.: T.M.I. IN A CURRENT SHEET WITH A TRANSVERSE MAGNETIC FIELD (Contd.)

or $$\frac{B_t}{B_a} << \beta \frac{ak}{2\pi} .$$

In other words, we are restricted to transverse fields so small that the scale for pressure variations along the sheet exceeds the wavelength of the instability.

The pressure balance in the y direction, (3.51), then gives

$$p_o = p_a \left(1 + \frac{1}{\beta} \cos^2 \frac{\pi y}{a}\right) , \qquad (3.54)$$

$$\rho_o = p_o / RT_o , \qquad (3.55)$$

where $$\beta = \frac{8\pi p_a}{B_a^2} .$$

Also, as before, we require the time scale of the instability to be much shorter than the diffusion time scale of the equilibrium magnetic field (3.49) so

$$\frac{\tau_R}{\tau_{TMI}} >> \pi^2 .$$

The linearized equations for the perturbed variables are, as given in the first section, (3.10) to (3.15). Following the method used in that section we write each of the perturbations in the form

$$F_1(x,y,t) = Re \left\{ e^{\omega t + ikx} F(y) \right\} , \qquad (3.56)$$

where $F(y)$ is a Fourier sine or cosine series.

3.4.: T.M.I. IN A CURRENT SHEET WITH A TRANSCERSE MAGNETIC FIELD (Contd.)

Either

$$F(y) = \sum_{n=0}^{\infty} F_n \operatorname{Sin} \frac{n\pi y}{a}$$

$$\text{or} \quad F(y) = \sum_{n=0}^{\infty} F_n \operatorname{Cos} \frac{n\pi y}{a} \quad , \qquad (3.57)$$

depending whether the particular variable is assumed to be symmetrical or anti-symmetrical. The Fourier transform of (3.10) to (3.15), together with the equilibrium conditions (3.50) and (3.54), gives a set of equations for the Fourier coefficients F_n.

By contrast with the case $B_t = 0$, it is necessary to allow F_n to be complex so that (3.57) and (3.56) imply

$$F_1(x,y,t) = e^{\omega t}\left[\operatorname{Cos} kx\, F_R(y) + \operatorname{Sin} kx\, F_i(y)\right] .$$

The need for both $\operatorname{Cos} kx$ and $\operatorname{Sin} kx$ variations when $B_t \neq 0$ can be seen as follows. Previously, with $B_t = 0$, we had $B_y(0, y, t) = 0$ which implied that $B_y(x,y,t)$ is proportional to $\operatorname{Sin} kx$ and that all the other variables are proportional to either $\operatorname{Cos} kx$ or $\operatorname{Sin} kx$. However, when $B_t \neq 0$, $B_y(0,y,t) \neq 0$ and so an extra $\operatorname{Cos} kx$ variation is needed for $B_y(x,y,t)$.

The case $B_t = 0$ can be obtained from the present case by imposing the extra boundary condition $B_y(0,y,t) = 0$, which eliminates either F_R or F_i.

3.4.: T.M.I. IN A CURRENT SHEET WITH A TRANSVERSE MAGNETIC FIELD (Contd.)

The form of the perturbations taken is thus,

$$B_{1x}(x,y,t) = e^{\omega t}\left\{ \cos kx \sum_{n=0}^{\infty} B_{xRn} \sin \frac{n\pi y}{a} + \sin kx \sum_{n=0}^{\infty} B_{xin} \sin \frac{n\pi y}{a} \right\},$$

$$B_{1y}(x,y,t) = e^{\omega t}\left\{ \cos kx \sum_{n=0}^{\infty} B_{yRn} \cos \frac{n\pi y}{a} + \sin kx \sum_{n=0}^{\infty} B_{yin} \cos \frac{n\pi y}{a} \right\},$$

$$V_{1x}(x,y,t) = e^{\omega t}\left\{ \cos kx \sum_{n=0}^{\infty} V_{xRn} \cos \frac{n\pi y}{a} + \sin kx \sum_{n=0}^{\infty} V_{xin} \cos \frac{n\pi y}{a} \right\},$$

$$V_{1y}(x,y,t) = e^{\omega t}\left\{ \cos kx \sum_{n=0}^{\infty} V_{yRn} \sin \frac{n\pi y}{a} + \sin kx \sum_{n=0}^{\infty} V_{yin} \sin \frac{n\pi y}{a} \right\},$$

$$\rho_1(x,y,t) = e^{\omega t}\left\{ \cos kx \sum_{n=0}^{\infty} \rho_{Rn} \cos \frac{n\pi y}{a} + \sin kx \sum_{n=0}^{\infty} \rho_{in} \cos \frac{n\pi y}{a} \right\},$$

$$T_1(x,y,t) = e^{\omega t}\left\{ \cos kx \sum_{n=0}^{\infty} T_{Rn} \cos \frac{n\pi y}{a} + \sin kx \sum_{n=0}^{\infty} T_{in} \cos \frac{n\pi y}{a} \right\}.$$

3.4.: T.M.I. IN A CURRENT SHEET WITH A TRANSVERSE MAGNETIC FIELD (Contd.)

The equations for the Fourier coefficients are

$$\rho_{Rn} = A_1 V_{xin} + A_2 [V_{xi(n+2)} + V_{xi(n-2)}] + n A_3 V_{yRn} + n A_4 [V_{yR(n+2)} + V_{yR(n-2)}] , \quad (3.58)$$

$$\rho_{in} = -A_1 V_{xRn} - A_2 [V_{xR(n+2)} + V_{xR(n-2)}] + n A_3 V_{yin} + n A_4 [V_{yi(n+2)} + V_{yi(n-2)}] , \quad (3.59)$$

$$B_{xRn} = [V_{yR(n+1)} - V_{yR(n-1)}] n B_{1n} + [T_{R(n+1)} + T_{R(n-1)}] n B_{2n} + V_{xRn} n B_{3n} , \quad (3.60)$$

$$B_{xin} = [V_{yi(n+1)} - V_{yi(n-1)}] n B_{1n} + [T_{i(n+1)} + T_{i(n-1)}] n B_{2n} + V_{xin} n B_{3n} , \quad (3.61)$$

$$0 = A_5 V_{xin} + A_6 [V_{xi(n+2)} + V_{xi(n-2)}] + \bar{k} \rho_{Rn} + A_7 T_{Rn} + A_8 [T_{R(n+2)} + T_{R(n-2)}] + A_9 \left[\frac{B_{xR(n+1)}}{n+1} + \frac{B_{xR(n-1)}}{n-1} \right] + \frac{B_t}{B_a} \frac{2}{1+\beta} \left(n\pi + \frac{\bar{k}^2}{n\pi} \right) B_{xin} , \quad (3.62)$$

$$0 = A_5 V_{xRn} + A_6 [V_{xR(n+2)} + V_{xR(n-2)}] - \bar{k} \rho_{in} - A_7 T_{in} + A_8 [T_{i(n+2)} + T_{i(n-2)}] - A_9 \left[\frac{B_{xi(n+1)}}{n+1} + \frac{B_{xi(n-1)}}{n-1} \right] + \frac{B_t}{B_a} \frac{2}{(1+\beta)} \left(n\pi + \frac{\bar{k}^2}{n\pi} \right) B_{xRn} , \quad (3.63)$$

$$0 = A_5 V_{yRn} + A_6 [V_{yR(n+2)} + V_{yR(n-2)}] + n\pi \rho_{Rn} + T_{Rn} n A_{10} + n A_{11} [T_{R(n+2)} + T_{R(n-2)}] + B_{xR(n+1)} \left[A_{12n} + \frac{A_{13}}{n+1} \right] - B_{xR(n-1)} \left[A_{12n} + \frac{A_{13}}{n-1} \right] , \quad (3.64)$$

$$0 = A_5 V_{yin} + A_6 [V_{yi(n+2)} + V_{yi(n-2)}] + n\pi \rho_{in} + T_{in} n A_{10} + n A_{11} [T_{i(n+2)} + T_{i(n-2)}] + B_{xi(n+1)} \left[A_{12n} + \frac{A_{13}}{n+1} \right] - B_{xi(n-1)} \left[A_{12n} + \frac{A_{13}}{n-1} \right] , \quad (3.65)$$

$$A_{14} T_{R(n+2)} = \bar{k} V_{xi(n+2)} + (n+2)\pi V_{yR(n+2)} , \quad (3.66)$$

$$A_{14} T_{i(n+2)} = -\bar{k} V_{xR(n+2)} + (n+2)\pi V_{yi(n+2)} , \quad (3.67)$$

where coefficients A_1 to A_{14} and B_{1n} and B_{2n} are given on page 155, and

$$B_{3n} = \frac{-\pi S B_t / B_a}{\bar{\omega} + \bar{k}^2 + (n\pi)^2}$$

3.4.: T.M.I. IN A CURRENT SHEET WITH A TRANSVERSE MAGNETIC FIELD (Contd.)

The Fourier series representations (3.57) are periodic over a width 2a, but we are interested only in the region $0 \leq y \leq a/2$. Conditions of symmetry or anti-symmetry about $a/2$ can be imposed, as in the $B_t = 0$ case, where the effect was to restrict n to either odd or even values. For consistency with the $B_t = 0$ case, we assume that V_{xin}, V_{yRn}, ρ_{Rn} and T_{Rn} take only odd values and B_{xRn} only even values of n.

We now assume that this even or odd nature is retained in these terms when $B_t \neq 0$. For simplicity we assume B_{xin}, V_{xRn}, V_{yin}, ρ_{in} and T_{in} take only odd values of n.

These conditions split the equations (3.58) to (3.67) into two independent sets, one of which can be solved for V_{xi}, V_{yR}, ρ_R, T_R, B_{xi} and B_{xR} while the other can be solved for V_{xR}, V_{yi}, ρ_i, T_i, B_{xR} and B_{xi}. We shall now solve for the first group only and, indeed, it can be shown that the solution for the other group gives $V_{Rn} = V_{yin} = \rho_{in} = T_{in} = 0$, while B_{xn} remains complex, so that it is through B_x that B_t affects the T.M.I. When these conditions are applied to (3.58) to (3.67) we find

$$\rho_{Rn} = A_1 V_{xin} + A_2 [V_{xi(n+2)} + V_{xi(n-2)}] + n A_3 V_{yRn} + n A_4 [V_{yR(n+2)} + V_{yR(n-2)}] , \qquad (3.68)$$

$$B_{xR(n+1)} = [V_{yR(n+2)} - V_{yRn}] (n+1) B_{1(n+1)} + [T_{R(n+2)} + T_{Rn}] (n+1) B_{2(n+1)} , \qquad (3.69)$$

3.4.: T.M.I. IN A CURRENT SHEET WITH A TRANSVERSE MAGNETIC FIELD (Contd.)

$$B_{xin} = V_{xin}\, n\, B_{3n} \quad , \tag{3.70}$$

$$0 = A_5 V_{xin} + A_6 \left[V_{xi(n+2)} + V_{xi(n-2)} \right] + \bar{k}\, \rho_{Rn} + A_7 T_{Rn} + A_8 \left[T_{R(n+2)} + T_{R(n-2)} \right] + A_9 \left[\frac{B_{xR(n+1)}}{n+1} + \frac{B_{xR(n-1)}}{n-1} \right] + \frac{B_t}{B_a} \frac{2}{1+\beta} \left(n\pi + \frac{\bar{k}^2}{n\pi} \right) B_{xin} \quad , \tag{3.71}$$

$$0 = A_5 V_{yRn} + A_6 \left[V_{yR(n+2)} + V_{yR(n-2)} \right] + n\pi\, \rho_{Rn} + n A_{10} T_{Rn} + n A_{11} \left[T_{R(n+2)} + T_{R(n-2)} \right] + B_{xR(n+1)} \left[A_{12n} + \frac{A_{13}}{n+1} \right] - B_{xR(n-1)} \left[A_{12n} + \frac{A_{13}}{n-1} \right] \quad , \tag{3.72}$$

$$A_{14} T_{R(n+2)} = \bar{k}\, V_{xi(n+2)} + (n+2)\pi\, V_{yR(n+2)} \quad . \tag{3.73}$$

Equations (3.68) to (3.73) can be solved for $V_{xi(n+2)}$, $V_{yR(n+2)}$, $T_{R(n+2)}$, ρ_{Rn}, $B_{xR(n+1)}$, B_{xin} once the starting values have been specified. (We already know that $B_{xR0} = 0$ because $B_{xR}(x, y, t)$ is antisymmetric in y about $y = 0$). As in the $B_t = 0$ case we may put

$$V_{yR1} = 1 \quad , \tag{3.74}$$

since the amplitude of the perturbations is arbitrary. Also the incompressible condition gives

$$V_{xi1} = -\frac{\pi}{ak} V_{yR1} = -\frac{\pi}{ak} \quad . \tag{3.75}$$

((3.73) then implies $T_{R1} = 0$).

3.4.: T.M.I. IN A CURRENT SHEET WITH A TRANSVERSE MAGNETIC FIELD (Contd.)

Equations (3.68) to (3.73) are then solved for the coefficients of the Fourier series for several values of n. As before we search for the value of $\bar{\omega}$ at which the series converge, this being the value at which the instability occurs.

Results

In this problem we consider only the case $\beta = 10^6$ but, as shown in section 3.2, it gives the same growth rate as model B in which ρ and η are both constant, and β takes any value.

The variation of $\bar{\omega}$ with $\bar{k}$ is the same as in the $B_t = 0$ case (Figure 25) page 160, except that increasing B_t moves the whole curve down without changing it in any other way. The curves thus have a maximum frequency $\bar{\omega}_{max}$ which we draw in Figure (29) page 182, as a function of B_t/B_a for $10^4 \leq S \leq 10^{10}$. We see that for a given S, when B_t/B_a is small enough (much less than $S^{-1/2}$) $\bar{\omega}_{max}$ is constant, $\bar{\omega}_o$ say, and we find that

$$\bar{\omega}_o(S) = 2{\cdot}1\, S^{0{\cdot}67}, \qquad (3{\cdot}76)$$

the same variation that was found when $B_t = 0$, in section 3.1.

An order of magnitude calculation indicates that the tearing mode instability is unaffected if B_t is small enough. The effect of B_t is to allow the transport of energy across the sheet by Alfven waves, so if the growth rate of the tearing mode instability is very much greater than the growth rate of the transport of energy across the sheet then B_t will not affect the tearing mode instability.

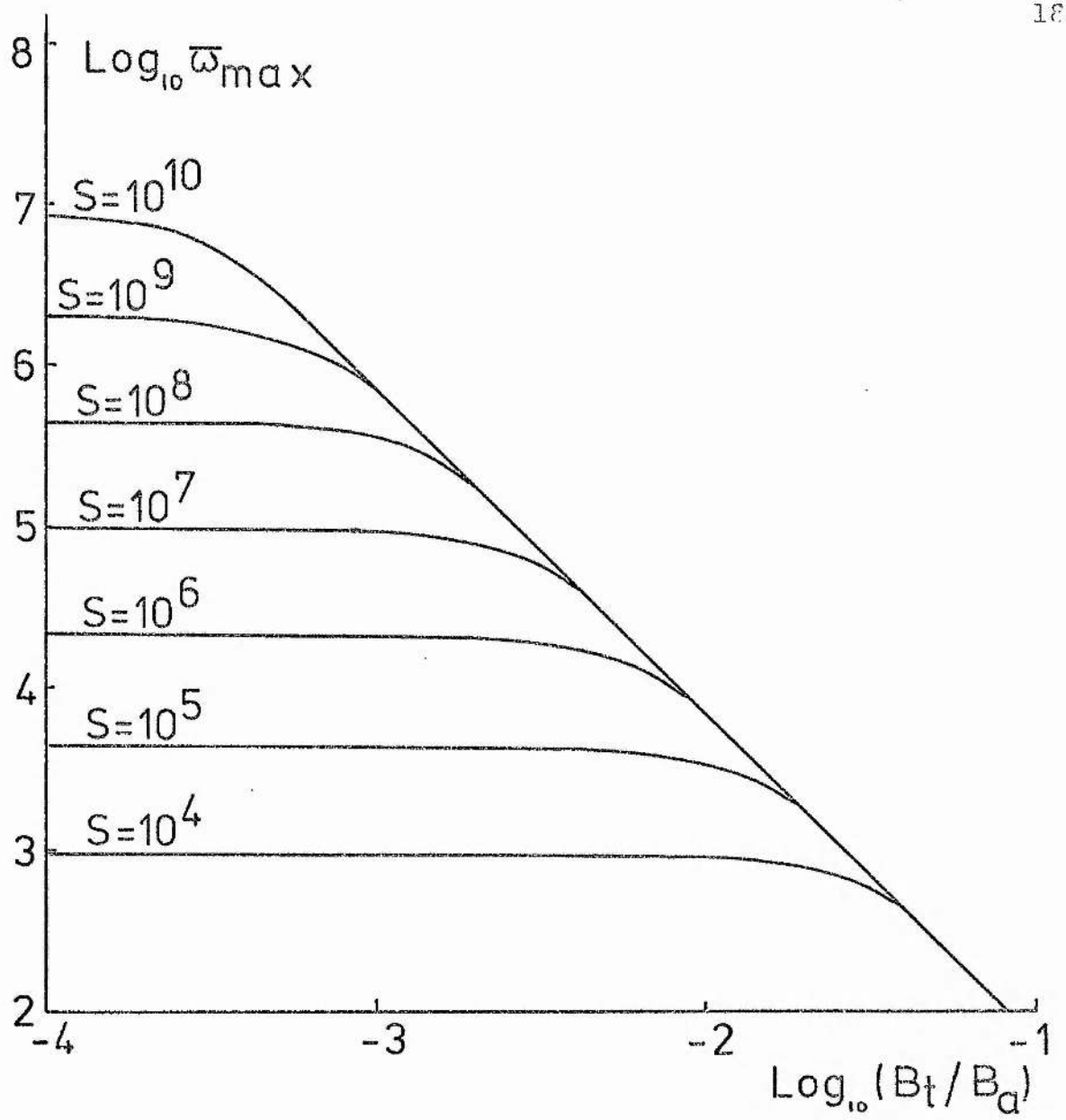

Figure (29). The variation of $\overline{\omega}_{max}$ the maximum growth rate of the tearing mode instability in a neutral current sheet with a component of magnetic field, B_t, transverse to the neutral line, as a function of B_t/B_a, where the constant, B_a, is the value of the magnetic field strength at the edge of the neutral current sheet.

The curves are drawn for several values of S, the ratio of the diffusion time scale to the Alfvénic time scale.

3.4.: T.M.I. IN A CURRENT SHEET WITH A TRANSVERSE MAGNETIC FIELD (Contd.)

The time scale for energy transport by Alfvén waves across the sheet is $\tau_{At} \simeq \frac{a}{V_{At}}$ and the time scale for the tearing mode instability with $B_t = 0$, is, from Furth et al (1963) $\tau_{TMI} \simeq (\tau_D \tau_{Ao})^{1/2}$ where τ_D is the diffusion time scale and τ_{Ao} the Alfvén time scale when $B_t = 0$. The effect of B_t is ignorable if

$$\tau_{TMI} << \tau_{At} \Rightarrow \frac{V_{At}}{V_{Ao}} << \left(\frac{V_o}{V_{Ao}}\right)^{1/2}$$

$$\Rightarrow \frac{B_t}{B_a} << S^{-1/2}.$$

This order of magnitude calculation is confirmed in Figure (29), page 182, where the tearing mode instability is unaffected when $B_t/B_a << S^{-1/2}$.

We did not calculate the variation of $\bar{\omega}_{max}$ with B_t/B_a for $S < 10^4$, because then $\bar{\omega}_{max} < 10^3$ so that $\bar{\omega}_{max}$ is not very much greater than π^2 and the diffusion of the equilibrium magnetic field becomes important.

As B_t/B_a is increased we find that $\bar{\omega}_{max}$ falls in value until $\bar{\omega}_{max} \simeq \pi^2$, where the method breaks down because the T.M.I. time scale is approximately equal to the diffusion time scale of the equilibrium magnetic field. When B_t/B_a is large enough, $\bar{\omega}_{max}$ decreases linearly with B_t/B_a on the log-log plot. Further, the linear curve that is approached is independent of S; it has the equation

$$\log_{10} \bar{\omega}_{max} = 2 \log_{10} \left\{ \frac{(B_t/B_a)_1}{(B_t/B_a)} \right\}, \quad (3.77)$$

where

$$\frac{B_t}{B_a} = \left(\frac{B_t}{B_a}\right)_1 \quad \text{at} \quad \bar{\omega} = 1$$

and $(B_t/B_a)_1 = 10^{-0.13} = 0.74$ from the intersection of the curve in Figure (29), page 182 with the $\log_{10} \bar{\omega}_{max} = 0$ axis.

3.4.: T.M.I. IN A CURRENT SHEET WITH A TRANSVERSE MAGNETIC FIELD (Contd.)

As B_t / B_a is increased, so $\bar{\omega}_{max}$ falls in value and the question arises as to what value of B_t, $B_{t\,crit}$ say, inhibits the tearing mode. The answer depends on whether we want the value of B_t/B_a which reduces $\bar{\omega}_{max}$ to a certain fixed value $\bar{\omega}_1$ say, or the value which reduces $\bar{\omega}_{max}$ to a certain fraction of $\bar{\omega}_o(S)$, say $\bar{\omega}_o(S)/n$.

In the first case, suppose $\bar{\omega}_1$ is less than 10^3, then the graph in Figure (29) is linear, independent of S, and so from (3.77) the minimum value of B_t which inhibits the tearing mode is given by

$$\log_{10}(B_{t\,crit}/B_a) = -0.13 - \tfrac{1}{2}\log_{10}\bar{\omega}_1 , \qquad (3.78)$$

Or, in the limit as $\bar{\omega}_1$ approaches 1,

$$B_{t\,crit} / B_a = 0.74 .$$

In the second case, we require the value of B_t/B_a which makes $\bar{\omega}_{max}$ equal to $\frac{\bar{\omega}_o}{n}$, or from (3.76),

$$\bar{\omega}_{max} = \frac{2.1\, S^{0.67}}{n} . \qquad (3.79)$$

Now provided $n \geq 3$ we can use (3.77) to estimate $\bar{\omega}_{max}$ so (3.79) reduces to

$$-0.26 - 2\log_{10}\left(\frac{B_{t\,crit}}{B_a}\right) = \log_{10}\frac{2.1}{n} + 0.67\log S ,$$

$$\text{or} \quad B_{t\,crit}/B_a = \frac{\sqrt{n}}{3.8}\,\frac{1}{S^{0.34}} . \qquad (3.80)$$

Again, when B_t exceeds $B_{t\,crit}$, the tearing mode can be said to be significantly inhibited by the presence of the transverse field.

3.5.: ANALYTIC TREATMENT OF THE TEARING MODE INSTABILITY WITH A TRANSVERSE MAGNETIC FIELD COMPONENT PRESENT.

The method used in this section is based on the analysis of the T.M.I. by Priest (1969) in which the growth rate is calculated for an equilibrium magnetic field that has no transverse field component.
We approximate the equilibrium current sheet magnetic field by

$$\underline{B}_o = \hat{\underline{x}}\, B_{xo}(y) + \hat{\underline{y}}\, B_{yo} = \begin{cases} B\frac{y}{a}\,\hat{\underline{x}} + B_{yo}\,\hat{\underline{y}} , & |y| < a \\ B\,\hat{\underline{x}} + B_{yo}\,\hat{\underline{y}} , & y > a \\ -B\,\hat{\underline{x}} + B_{yo}\,\hat{\underline{y}} , & y < -a \end{cases} \qquad (3.81)$$

where B and B_{yo} are constants. This magnetic field satisfies the equilibrium condition that

$$\underline{\nabla} \wedge [(\underline{\nabla} \wedge \underline{B}_o) \wedge \underline{B}_o] = 0$$

in a piecewise manner. The equilibrium velocity $\underline{V}_o$ is assumed to be zero.
The linearized equations, from (3.11) and curl (3.12), for small perturbations $\underline{V}_1$ and $\underline{B}_1$, are

$$\frac{\partial \underline{B}_1}{\partial t} = \underline{\nabla} \wedge (\underline{V}_1 \wedge \underline{B}_o) + \frac{\eta}{4\pi} \nabla^2 \underline{B}_1 , \qquad (3.82)$$

$$\rho_o \frac{\partial}{\partial t}(\underline{\nabla} \wedge \underline{V}_1) = \frac{1}{4\pi} \underline{\nabla} \wedge [(\underline{\nabla} \wedge \underline{B}_o) \wedge \underline{B}_1 + (\underline{\nabla} \wedge \underline{B}_1) \wedge \underline{B}_o] , \qquad (3.83)$$

$$\underline{\nabla} . \underline{B}_1 = \underline{\nabla} . \underline{V}_1 = 0 . \qquad (3.84)$$

If we next assume $\underline{V}_1$ and $\underline{B}_1$ to be proportional to

$e^{\omega t + ikx}$, the y-component of (3.82) gives

$$\omega B_y = B_{yo} \frac{dV_y}{dy} + B_{xo} ikV_y + \frac{\eta}{4\pi}\left(-k^2 B_y + \frac{d^2 B_y}{dy^2}\right) , \qquad (3.85)$$

3.5.: ANALYTIC TREATMENT OF THE TEARING MODE INSTABILITY WITH A TRANSVERSE MAGNETIC FIELD COMPONENT PRESENT. (Contd.)

while the z component of (3.83) reduces (after using (3.85) and (3.84)) to

$$\left(1+\frac{B_{yo}^2}{\omega\rho\eta}\right)\frac{d^2V_y}{dy^2} = k^2V_y\left(1+\frac{B_{xo}^2}{\eta\omega\rho}\right)+\frac{\omega}{\eta}\frac{B_{yo}}{\omega\rho}\frac{dB_y}{dy}$$
$$+ik\left[-\frac{dV_y}{dy}\left(\frac{2B_{xo}B_{yo}}{\eta\omega\rho}\right)-V_y\left(\frac{B_{yo}}{\omega\rho\eta}\frac{dB_{xo}}{dy}\right)\right.$$
$$\left.+\frac{B_y}{4\pi\omega\rho}\left(-\frac{d^2B_{xo}}{dy^2}+\frac{\omega 4\pi B_{xo}}{\eta}\right)\right]. \quad (3.86)$$

In terms of the dimensionless variables

$$\bar{B}=B/B_0\,,\quad \bar{V}_y=-V_y\,ik\tau_R\,,\quad \bar{k}=ak\,,\quad \bar{\omega}=\omega\tau_R$$

$$\bar{y}=y/a\,,\quad S=\tau_R/\tau_A\,,\quad \tau_R=4\pi a^2/\eta\,,\quad \tau_A=a(4\pi\rho)^{1/2}/B\,,$$

the two equations (3.85) and (3.86) for V_y and B_y become

$$\bar{B}_y'' = \bar{B}_y(\bar{\omega}+\bar{k}^2)+\bar{V}_y\bar{B}_{xo}+\frac{\bar{V}_y'}{i\bar{k}}\bar{B}_{yo}\,, \quad (3.87)$$

$$\bar{V}_y''\left(1+\frac{S^2\bar{B}_{yo}^2}{\bar{\omega}}\right)=\bar{k}^2\bar{V}_y\left(1+\frac{S^2\bar{B}_{xo}}{\bar{\omega}}\right)-i\bar{k}S^2\bar{B}_{yo}\bar{B}_y'$$
$$+\bar{k}^2\bar{B}_y\frac{S^2}{\bar{\omega}}(\bar{\omega}\bar{B}_{xo}-\bar{B}_{xo}'')$$
$$-i\bar{k}\left[\bar{V}_y'\left(\frac{2S^2\bar{B}_{xo}\bar{B}_{yo}}{\bar{\omega}}\right)+\bar{V}_y\left(\frac{S^2\bar{B}_{yo}\bar{B}_{xo}'}{\bar{\omega}}\right)\right]\,, \quad (3.88)$$

where a dash denotes differentiation with respect to $\bar{y}$. Equations (3.87) and (3.88) can be solved for $\bar{B}_y$ and $\bar{V}_y$ for given values of $\bar{\omega}$, $\bar{k}$ and S. Solutions are obtained in two regions, an outer region ($\bar{y}>\epsilon_o$, say) and an inner region ($0<\bar{y}<\epsilon_o$) and then matched at the boundary ($\bar{y}=\epsilon_o$). In the outer region the resistive terms are neglected so that the magnetic field is "frozen into" the plasma, while on the inner region diffusion is important.

3.5.: ANALYTIC TREATMENT OF THE TEARING MODE INSTABILITY WITH A TRANSVERSE MAGNETIC FIELD COMPONENT PRESENT (Contd.)

It is because of diffusion that the magnetic field can reconnect across the neutral sheet and allow the T.M.I. to occur, so that it is in the inner region that the small transverse field component, B_{y_0}, will have most influence on the instability. In order to simplify the analysis, while still retaining the essential elements, we shall assume that B_{y_0} is so small that it does not influence the dynamics in the outer region but still remains important in the inner region.

Outer Region: $(\bar{y} \gg \epsilon_0)$

In this region where diffusion is unimportant we neglect terms of order $1/S$ in (3.87) and (3.88), which become

$$\bar{B}_y'' = \bar{B}_y(\bar{\omega} + \bar{k}^2) + \bar{V}_y \bar{B}_{x_0} + \frac{\bar{V}_y'}{i\bar{k}} \bar{B}_{y_0} \quad , \quad (3.89)$$

$$\bar{V}_y'' \frac{\bar{B}_{y_0}^2}{\bar{\omega}} = \bar{k}^2 \bar{V}_y \frac{\bar{B}_{x_0}^2}{\bar{\omega}} - i\bar{k} \bar{B}_{y_0} \bar{B}_y' + \frac{\bar{k}^2}{\bar{\omega}} \bar{B}_y (\bar{\omega} \bar{B}_{x_0} - \bar{B}_{x_0}'') - i\bar{k} \left[\bar{V}_y' \left(\frac{2 \bar{B}_{x_0} \bar{B}_{y_0}}{\bar{\omega}} \right) + \bar{V}_y \left(\frac{\bar{B}_{x_0}'}{\bar{\omega}} \bar{B}_{y_0} \right) \right] . \quad (3.90)$$

In general $\bar{B}_y$ and $\bar{V}_y$ are complex, $\bar{B}_y = \bar{B}_{y_R} + i B_{y_i}$ say, so rewriting (3.89) and (3.90) in their real and imaginary parts, assuming $\bar{\omega}$ and $\bar{k}$ are real (i.e. we are looking for a purely growing instability which is susceptible to a perturbation with an oscillatory X variation), we find

$$\bar{B}_{y_R}'' = \bar{B}_{y_R}(\bar{\omega} + \bar{k}^2) + \bar{V}_{y_R} \bar{B}_{x_0} + \bar{V}_{y_i}' \frac{\bar{B}_{y_0}}{\bar{k}} \quad , \quad (3.91)$$

$$\bar{B}_{y_i}'' = \bar{B}_{y_i}(\bar{\omega} + \bar{k}^2) + \bar{V}_{y_i} \bar{B}_{x_0} - \bar{V}_{y_R}' \frac{\bar{B}_{y_0}}{\bar{k}} \quad , \quad (3.92)$$

$$\bar{V}_{y_R}'' \frac{\bar{B}_{y_0}^2}{\bar{\omega}} = \bar{V}_{y_R} \frac{\bar{k}^2 \bar{B}_{x_0}^2}{\bar{\omega}} + \bar{B}_{y_i}' \bar{k} \bar{B}_{y_0} + \bar{B}_{y_R} \frac{\bar{k}^2}{\bar{\omega}} (\bar{\omega} \bar{B}_{x_0} - \bar{B}_{x_0}'') + \bar{k} \left[\bar{V}_{y_i}' \frac{2 \bar{B}_{x_0} \bar{B}_{y_0}}{\bar{\omega}} + \bar{V}_{y_i} \frac{\bar{B}_{x_0}' \bar{B}_{y_0}}{\bar{\omega}} \right] \quad , \quad (3.93)$$

3.5.: ANALYTIC TREATMENT OF THE TEARING MODE INSTABILITY WITH A TRANSVERSE MAGNETIC FIELD COMPONENT PRESENT (Contd.)

$$\bar{V}_{yi}'' \frac{\bar{B}_{yo}^2}{\bar{\omega}} = \bar{V}_{yi} \frac{\bar{k}^2 \bar{B}_{xo}^2}{\bar{\omega}} - \bar{B}_{yR}' \bar{k} \bar{B}_{yo} + \bar{B}_{yi} \frac{\bar{k}^2}{\bar{\omega}} (\bar{\omega} \bar{B}_{xo} - \bar{B}_{xo}'')$$

$$- \bar{k} \left[\bar{V}_{yR}' \frac{2 \bar{B}_{xo} \bar{B}_{yo}}{\bar{\omega}} + \bar{V}_{yR} \frac{\bar{B}_{xo}' \bar{B}_{yo}}{\bar{\omega}} \right] . \qquad (3.94)$$

To ignore the effect of $\bar{B}_{yo}$ in (3.91) to (3.94) we require

$$\bar{B}_{yo} << k \epsilon_o \bar{B}_{xo} , \qquad (3.95)$$

provided the real and imaginary parts of each component are the same in order of magnitude. But from (3.81) the minimum value of $\bar{B}_{xo}$ in the outer region is ϵ_o, so (3.95) becomes

$$\bar{B}_{yo} << \bar{k} \epsilon_o^2 .$$

With this assumption (3.91) and (3.93) become

$$\bar{B}_{yR}'' = \bar{B}_{yR} (\bar{\omega} + \bar{k}^2) + \bar{V}_{yR} \bar{B}_{xo} , \qquad (3.96)$$

$$0 = \bar{V}_{yR} \frac{\bar{k}^2 \bar{B}_{xo}^2}{\bar{\omega}} + \bar{B}_{yR} \frac{\bar{k}^2}{\bar{\omega}} (\bar{\omega} \bar{B}_{xo} - \bar{B}_{xo}'') , \qquad (3.97)$$

where $\bar{B}_{xo}'' = 0$ except at $\bar{y} = \pm 1$. They are then decoupled from (3.92) and (3.94) which have the same forms.

Elimination of $\bar{V}_{yR}$ between (3.96) and (3.97) gives

$$\bar{B}_{yR}'' = \bar{B}_{yR} (\bar{k}^2 + \bar{B}_{xo}'' / \bar{B}_{xo}) . \qquad (3.98)$$

The solution of (3.98) which becomes zero as $\bar{y} \to \infty$ is

$$B_{yR} = \begin{cases} \alpha_1 \sinh \bar{k}\bar{y} + \beta_1 \cosh \bar{k}\bar{y} , & 0 \le \bar{y} < 1 \\ \alpha \exp(-\bar{k}\bar{y}) , & \bar{y} > 1 \end{cases}$$

where the constants of integration, α_1 and β_1 are found in terms of α by the following two conditions at $\bar{y} = 1$:

3.5.: ANALYTIC TREATMENT OF THE TEARING MODE INSTABILITY WITH A TRANSVERSE MAGNETIC FIELD COMPONENT PRESENT (Contd.)

(i) $\bar{B}_y$ is continuous ,

(ii) $\int_{1-}^{1+} \bar{B}_y''/\bar{B}_y \, d\bar{y} = -1$.

Condition (ii) is a result of (3.98) and the definition of $\bar{B}_{xo}$, (3.81), together with the fact that $\bar{B}_{xo}$ is roughly constant when $\bar{y}$ is close enough to unity. These two conditions give

$$\alpha_1 = \alpha \left[e^{-\bar{k}} \frac{\cosh \bar{k}}{\bar{k}} - 1 \right] ,$$

$$\beta_1 = \alpha \left[1 - e^{-\bar{k}} \sinh \bar{k} \right] .$$

Assuming symmetry about the neutral line so that $\bar{B}_{yR}(\bar{y}) = \bar{B}_{yR}(-\bar{y})$ we can evaluate the quantity

$$\Delta \equiv \left(\frac{\bar{B}'_{yR}}{\bar{B}_{yR}} \right)_{0+} - \left(\frac{\bar{B}'_{yR}}{\bar{B}_{yR}} \right)_{0-} = 2 \left(\frac{\bar{B}'_{yR}}{\bar{B}_{yR}} \right)_{0+} = \frac{2\alpha_1 \bar{k}}{\beta_1}$$

In other words, substituting for α_1 and β_1

$$\Delta = \frac{2\bar{k} \, (1 - \bar{k} - \bar{k} \tanh \bar{k})}{\bar{k} - (1 - \bar{k}) \tanh \bar{k}} , \qquad (3.99)$$

or, in the limit $\bar{k} << 1$, $\Delta = \frac{2}{\bar{k}}$. (3.100)

Inner Region: ($\bar{y} \leq \epsilon_o$)

Define new variables $\bar{\bar{y}} = \bar{y}/\epsilon$, $\bar{\bar{v}}_y = \bar{v}_y (4\epsilon/\bar{\omega})$,

where $\epsilon^4 = \bar{\omega}/(4 \bar{k}^2 S^2)$. (3.101)

Equations (3.89) and (3.90) then become, with $\bar{B}_{xo} = \bar{\bar{y}} \epsilon$,

$$\ddot{\bar{B}}_y = \bar{B}_y \epsilon^2 (\bar{\omega} + \bar{k}^2) + \dot{\bar{\bar{v}}}_y \frac{\bar{\omega}}{4} \frac{\bar{B}_{yo}}{i\bar{k}} + \bar{\bar{v}}_y \bar{\bar{y}} \frac{\epsilon^2}{4} \bar{\omega} , \qquad (3.102)$$

3.5.: ANALYTIC TREATMENT OF THE TEARING MODE INSTABILITY WITH A TRANSVERSE MAGNETIC FIELD COMPONENT PRESENT (Contd.)

$$\ddot{\bar{V}}_y \left(1 + \frac{\bar{B}_{yo}^2}{4\bar{k}^2\epsilon^4}\right) = \bar{V}_y \left(\bar{k}^2\epsilon^2 + \frac{\bar{\bar{y}}^2}{4}\right) - \frac{i\bar{B}_{yo}}{\bar{k}\epsilon^2}\dot{\bar{B}}_y + \bar{\bar{y}}\bar{B}_y$$

$$- \frac{i\bar{B}_{yo}}{4\bar{k}\epsilon^2}\left(\dot{\bar{V}}_y 2\bar{\bar{y}} + \bar{V}_y\right) \quad , \qquad (3.103)$$

where a dot denotes differentiation with respect to $\bar{\bar{y}}$.

(3.102) and (3.103) determine $\bar{B}_y$ and $\bar{V}_y$ in the inner region, whereas in the outer region the revelant equations are (3.89) and (3.90), which reduce, when $\bar{B}_{yo} << \bar{k}\epsilon_o^2$, to (3.96) and (3.97), together with the corresponding equations for the imaginary parts. In terms of the inner region variables, the latter become

$$\ddot{\bar{B}}_y = \bar{B}_y \bar{k}^2 \epsilon^2, \qquad (3.104)$$

$$\bar{B}_y + \frac{\bar{\bar{V}}_y}{4}\bar{\bar{y}} = 0 \quad , \qquad (3.105)$$

At $\bar{\bar{y}} = \epsilon_o/\epsilon$, the boundary between the inner and outer regions, equations (3.102), (3.103), (3.104) and (3.105) all apply. From them we can deduce a lower limit for ϵ_o/ϵ as follows,

(3.103) and (3.105) at $\bar{\bar{y}} = \frac{\epsilon_o}{\epsilon}$, are approximately

$$\bar{\bar{V}}_y \frac{\epsilon^2}{\epsilon_o^2} \simeq \bar{V}_y\left[\frac{\epsilon_o^2}{\epsilon}\frac{1}{4} - \frac{i\bar{B}_{yo}}{4\bar{k}\epsilon^2}3\right] + \bar{B}_y\left[-\frac{i\bar{B}_{yo}}{\bar{k}\epsilon^2}\frac{\epsilon}{\epsilon_o} + \frac{\epsilon_o}{\epsilon}\right] , \qquad (3.106)$$

and

$$\bar{B}_y = -\frac{\bar{\bar{V}}_y}{4}\frac{\epsilon_o}{\epsilon} \quad . \qquad (3.107)$$

Since (3.106) and (3.107) apply simultaneously we need

$$\left(\frac{\epsilon_o}{\epsilon}\right)^2 >> \frac{i\bar{B}_{yo}}{\bar{k}\epsilon^2} \qquad (3.108)$$

and

$$\left(\frac{\epsilon_o}{\epsilon}\right)^4 >> 1 \quad .$$

3.5.: ANALYTIC TREATMENT OF THE TEARING MODE INSTABILITY WITH A TRANSVERSE MAGNETIC FIELD COMPONENT PRESENT (Contd.)

If, for instance, we choose $\frac{\epsilon_0}{\epsilon} = 10^{1/2}$, then (3.108) gives

$$\bar{B}_{y0} << 10\, \bar{k}\, \epsilon^2 ,$$

which gives an upper bound on the value of $\bar{B}_{y0}$ for which our method works.

Now let $b = \frac{i\bar{B}_{y0}}{\bar{k}\epsilon^2}$, so that the equations (3.102) and (3.103) become

$$\ddot{\bar{B}}_y = \bar{B}_y \epsilon^2 (\bar{\omega} + \bar{k}^2) - \dddot{\bar{V}}_y \frac{\bar{\omega}\epsilon^2}{4} b + \ddot{\bar{V}}_y \frac{\bar{y}}{4} \bar{\omega}\epsilon^2 , \quad (3.109)$$

$$\dddot{\bar{V}}_y (1 - b^2/4) = \ddot{\bar{V}}_y (\bar{k}^2\epsilon^2 + \bar{y}^2/4) - b\dot{\bar{B}}_y + \bar{y}\bar{B}_y - \frac{b}{4}(\dddot{\bar{V}}_y 2\bar{y} + \ddot{\bar{V}}_y) , \quad (3.110)$$

which give, after eliminating $\dot{\bar{B}}_y$,

$$\ddddot{\bar{V}}_y (1 - b^2/4) = \dddot{\bar{V}}_y \left(-\frac{2b\bar{y}}{4} + \frac{\bar{y}}{b}\left(\frac{b^2}{4} - 1\right)\right) + \ddot{\bar{V}}_y \left(\bar{k}^2\epsilon^2 + \frac{\bar{y}^2}{4} - \frac{3}{4}b + \frac{\bar{\omega}\epsilon^2}{4}b^2 - \frac{\bar{y}}{2}\right) + \dot{\bar{V}}_y \left(\frac{\bar{y}}{2} - \frac{\bar{y}}{4}\bar{\omega}\epsilon^2 b + \frac{\bar{y}}{b}\left(\bar{k}^2\epsilon^2 + \frac{\bar{y}^2}{4} - \frac{b}{4}\right)\right) + \bar{B}_y \left(1 - b\epsilon^2(\bar{\omega} + \bar{k}^2) + \frac{\bar{y}^2}{b}\right) . \quad (3.111)$$

We note that, even although $\bar{B}_{y0}$ can be ignored in the outer region, its presence is required in the inner region, since at some point there $\bar{y}$ becomes less than b.

Equation (3.111) is solved for $\ddot{\bar{V}}_y$, following the method of Furth et al. (1963), by assuming $\bar{B}_y$ = constant across the inner region. The boundary condition for (3.111) are

(a) $\ddot{\bar{V}}_y$ is antisymmetric so that $\dddot{\bar{V}}_y = 0$ at $\bar{y} = 0$;

(b) $\ddot{\bar{V}}_y$ is continuous at the inner-outer region boundary, so $\ddot{\bar{V}}_y\left(\frac{\epsilon_0}{\epsilon}-\right) = \ddot{\bar{V}}_y\left(\frac{\epsilon_0}{\epsilon}+\right) = 4\bar{B}_y\frac{\epsilon}{\epsilon_0}$ from (3.105);

(c) $\bar{B}_y$ is symmetric, so that $\dot{\bar{B}}_y = 0$ at $\bar{y} = 0$ or by (a) and (3.110) $\dddot{\bar{V}}_y = 0$ at $\bar{y} = 0$.

3.5.: ANALYTIC TREATMENT OF THE TEARING MODE INSTABILITY WITH A TRANSVERSE MAGNETIC FIELD COMPONENT PRESENT (Contd.)

The solution to (3.111) is found as a series

$$\bar{\bar{V}}_y = \sum_{n=0}^{3} a_n \bar{\bar{V}}_y^n$$

under the assumptions (i) $\bar{B}_y$ = constant = $\bar{B}_y\left(\frac{\epsilon_0}{\epsilon}\right)$,

(ii) $|b|^2 \ll 1$,

(iii) $|\bar{\omega}\,\epsilon^2 b^2| \ll 1$,

(iv) $\bar{k}^2 \ll \bar{\omega}$,

the latter two of which are justified later.

The result is

$$\bar{\bar{V}}_{yR} = \bar{B}_{yR}\left[\left(-\frac{31}{15} - \frac{b}{i}\left(-\frac{31}{12} + \frac{5}{3}\bar{\omega}\,\epsilon^2\right)\right)\bar{\bar{y}} + \frac{\bar{\bar{y}}^3}{10}\left(\frac{5}{3} - \frac{b}{i}\left(\frac{31}{12} - \frac{5}{3}\bar{\omega}\,\epsilon^2\right)\right)\right], \tag{3.112}$$

$$\bar{\bar{V}}_{yi} = \bar{B}_{yR}\left[\left(-\frac{31}{15} - \frac{b}{i}\left(-\frac{31}{12} + \frac{5}{3}\bar{\omega}\,\epsilon^2\right)\right)\bar{\bar{y}} + \frac{\bar{\bar{y}}^3}{10}\left(\frac{5}{3} + \frac{b}{i}\left(\frac{31}{12} - \frac{5}{3}\bar{\omega}\,\epsilon^2\right)\right)\right]. \tag{3.113}$$

Now the inner and outer regions are matched by requiring that the quantity Δ, estimated in (3.100) for the outer region, has the same value here. The real part of (3.109) gives, using $\bar{k}^2 \ll \bar{\omega}$,

$$\dot{\bar{\bar{B}}}_{yR} = \bar{B}_{yR}\,\bar{\omega}\,\epsilon^2 - i\,\dot{\bar{\bar{V}}}_{yi}\,\frac{\bar{\omega}\,\epsilon^2 b}{4} + \bar{\bar{V}}_{yR}\,\frac{\bar{\bar{y}}\,\bar{\omega}\,\epsilon^2}{4},$$

so that, from (3.112) and (3.113), we find

$$\Delta \equiv 2\left(\frac{\bar{B}'_{yR}}{\bar{B}_{yR}}\right)_{\bar{\bar{y}}=\epsilon_0} = \frac{2}{\epsilon}\left(\frac{\dot{\bar{B}}_{yR}}{\bar{B}_{yR}}\right)_{\bar{\bar{y}}=\epsilon_0/\epsilon}$$

$$= 2\bar{\omega}\,\epsilon\sqrt{10}\left[1/9 + ib\left(-0.7611 + \bar{\omega}\,\epsilon^2/1.8\right)\right]$$

$$= \bar{\omega}^{5/4}\sqrt{\frac{20}{S\bar{k}}}\left[\frac{1}{9} - \frac{\bar{B}_{y0}}{\bar{k}\,\epsilon^2}\left(-0.7611 + \frac{\bar{\omega}\,\epsilon^2}{1.8}\right)\right]. \tag{3.114}$$

3.5.: ANALYTIC TREATMENT OF THE TEARING MODE INSTABILITY WITH A TRANSVERSE MAGNETIC FIELD COMPONENT PRESENT (Contd.)

The condition that $\bar{B}_y'$ be continuous at the boundary between the inner and outer regions means that we must equate the values of Δ given by (3.100) and (3.114), which in the limit $\bar{k} \ll 1$ gives the dispersion relation

$$\bar{\omega}^{5/4} = \sqrt{\frac{S}{5\bar{k}}} \frac{1}{\left[1/9 + \frac{\bar{B}_{y0}}{\bar{k}\epsilon^2}\left(0.7611 - \frac{\bar{\omega}\epsilon^2}{1.8}\right)\right]} , \qquad (3.115)$$

where $\epsilon^4 = \bar{\omega}/(4\bar{k}^2 S^2)$ from (3.101). We note that provided $\bar{\omega}\epsilon^2 \lesssim 1$, the effect of increasing $\bar{B}_{y0}$ in (3.115) is to make $\bar{\omega}$ decrease. The maximum value of $\bar{\omega}$ at $\bar{B}_{y0} = 0$, is

$$\bar{\omega}^*_{max} = (16\, S/\bar{k})^{2/5} \qquad (3.116)$$

which compares with Furth et al. (1963) who get $\bar{\omega}$ proportional to $(S/\bar{k})^{2/5}$.

The solution (3.115) is no longer valid when $\bar{k}$ is too small. In deriving the growth rate we assumed that $\bar{B}_y$ is constant in the inner region, which is true if the length scale over which $\bar{B}_y$ varies is greater than the width of the inner region. In other words

$$\epsilon_0 \left| \frac{\bar{B}_y'}{\bar{B}_y} \right| < 1 . \qquad (3.117)$$

But according to (3.100), when $\bar{k} \ll 1$, $|\bar{B}_y'/\bar{B}_y| \simeq 1/\bar{k}$ so the condition (3.117) becomes

$$\max|\Delta| < \frac{1}{\epsilon_0} < \frac{1}{\epsilon} ,$$

Thus

$$\bar{k} > 2\epsilon$$

$$\text{or} \quad \bar{k} > (4\bar{\omega}/S^2)^{1/6} . \qquad (3.118)$$

(3.118) and (3.116) imply that

$$\bar{\omega}^*_{max} < S^{1/2} . \qquad (3.119)$$

3.5.: ANALYTIC TREATMENT OF THE TEARING MODE INSTABILITY WITH A TRANSVERSE MAGNETIC FIELD COMPONENT PRESENT (Contd.)

Thus by (3.101), $\bar{\omega}\,\epsilon^2 = \frac{\bar{\omega}^{3/2}}{2S\bar{k}} < \left(\frac{\bar{\omega}^2}{4S}\right)^{2/3} < 1$

and so we see that assumption (iii) is justified provided (ii) is valid.

From (3.116), (3.118) and (3.119) we have

$$S^{2/5} << \bar{\omega}^*_{max} < S^{1/2} .$$

Since $S >> 1$ this implies that

$$1 << \bar{\omega}^*_{max} << S ,$$

so that the instability frequency lies between the resistive diffusion and Alfvén wave frequencies. This implies, from section 1.3, that the plasma is incompressible provided

$$\frac{1}{S} << \beta .$$

Thus we find that the dispersion relation for the tearing mode instability in a neutral current sheet with a transverse component of magnetic field is

$$\bar{\omega}^{5/4} = \sqrt{\frac{S}{5}}\;\frac{1}{\left[\frac{\sqrt{\bar{k}}}{9} + \frac{\bar{B}_{y0}}{\sqrt{\bar{k}}\,\epsilon^2}\left(0.7611 - \frac{\bar{\omega}\,\epsilon^2}{1.8}\right)\right]} , \qquad (3.115)$$

where

$$\epsilon^4 = \bar{\omega}/(4\bar{k}^2 S^2)$$

The assumptions made to derive this relationship are

(1) $\frac{\bar{B}_{y0}}{\bar{k}\,\epsilon_0^2} << 1$ which gives the maximum value of $\bar{k}$ for which the solution is valid.

(2) $\bar{k}^2 << 1$,

(3) $|\bar{\omega}\,\epsilon^2 b^2| << 1$,

(4) $|b^2| = \bar{B}_{y0}^2/(\bar{k}^2\epsilon^4) << 1$,

(5) $\bar{B}_y = \text{constant} = \bar{B}_y\left(\frac{\epsilon_0}{\epsilon}\right)$ in the inner region.

(6) $\bar{k} > 2\epsilon = (4\bar{\omega}/S^2)^{1/6}$.

3.5.: ANALYTIC TREATMENT OF THE TEARING MODE INSTABILITY WITH A TRANSVERSE MAGNETIC FIELD COMPONENT PRESENT (Contd.)

We can see the approximate behaviour of $\bar{\omega}$ with $\bar{B}_{y_0}$ if we assume $\bar{\omega}$ is almost equal to $\bar{\omega}^*_{max}$, given in (3.116), and then substitute $\bar{\omega}$ with $\bar{\omega}^*_{max}$ in the right hand side of (3.115). This gives

$$\bar{\omega}^{\frac{5}{4}} \simeq \sqrt{\frac{S}{5}} \frac{1}{\left[\frac{\sqrt{\bar{k}}}{9} + \frac{\bar{B}_{y_0} 2 S^{4/5}}{16^{1/5}} 0.7611 \bar{k}^{7/10} - \frac{\bar{B}_{y_0} (16S)^{2/5}}{1.8\ \bar{k}^{9/10}}\right]} \qquad (3.120)$$

We differentiate this equation with respect to $\bar{k}$ to see if there are any turning points

$$\frac{5}{4}\bar{\omega}^{1/4}\frac{d\bar{\omega}}{d\bar{k}} = -\sqrt{\frac{S}{5}} \frac{\left[\frac{1}{18}\frac{1}{\sqrt{\bar{k}}} + \frac{7}{10}\frac{2}{16^{1/5}}\frac{0.7611\bar{B}_{y_0}S^{4/5}}{\bar{k}^{3/10}} + \frac{9}{10}\frac{16^{2/5}}{1.8}\frac{\bar{B}_{y_0}S^{2/5}}{\bar{k}^{19/10}}\right]}{\left[\frac{\sqrt{\bar{k}}}{9} + \frac{\bar{B}_{y_0}2}{16^{1/5}}S^{4/5}0.7611\bar{k}^{7/10} - \frac{\bar{B}_{y_0}(16S)^{2/5}}{1.8\ \bar{k}^{9/10}}\right]^2},$$

so that there are no turning points and $d\bar{\omega}/d\bar{k} < 0$ implying that the maximum value of $\bar{\omega}$, $\bar{\omega}_{max}$ say, occurs at the smallest value of $\bar{k}$. This is, from (3.118)

$$\bar{k}_{min} = \left(4\bar{\omega}/S^2\right)^{1/6},$$

or

$$\bar{k}_{min} = \sqrt{2}/S^{2/9}$$

Substituting this value of $\bar{k}$ into (3.120) gives

$$\left(\bar{\omega}_{max}\right)^{5/4} = \frac{S^{11/18}}{0.295 + \bar{B}_{y_0} S^{32/45}\left(2.49\, S^{2/45} - 2.75\right)},$$

so we see that $\bar{\omega}_{max}$ gradually falls as $\bar{B}_{y_0}$ increases, but that $\bar{\omega}_{max}$ does not reach zero for finite values of $\bar{B}_{y_0}$, unlike the more accurate numerical solution found in section 3.4.

3.6.: SUMMARY

In this chapter we examine the T.M.I. in a current sheet and compare the results with those derived by Cross & Van Hoven (1971) for the T.M.I. in a sheared magnetic field of constant magnitude. We find that the growth rate can be much larger in our case. We also examine the effect of a transverse component, B_t, of the magnetic field on the T.M.I. in a current sheet and show that, if B_t is large enough, the instability is significantly inhibited.

In section 3.1, we calculated the growth of the T.M.I. in a neutral current sheet using a method devised by Cross & Van Hoven (1971). In the equilibrium current sheet we assume a pressure balance across the sheet with temperature constant, so that the density will vary to keep the total pressure constant. We assume that there is no equilibrium velocity, and that there are no energy sources or sinks, so that the temperature remains constant during the instability. The equilibrium magnetic fielddecays by diffusion and so we require the instability time scale to be much less than the diffusion time scale. The equilibrium is then perturbed by a small quantity so that, by ignoring products of the small perturbations, the equations are linearized. The perturbations take the form

$$f_1 = e^{\omega t + ikx} f(y) ,$$

3.6.: SUMMARY (Contd.)

where $f(y)$ is represented by the sum of a cosine or sine Fourier series, e.g.

$$f(y) = \sum_{n=0}^{\infty} f_n \cos \frac{n\pi y}{a} .$$

The Fourier transformed, linearized equations can then be solved to give a recurrence relationship for the Fourier coefficients, f_n. After choosing the initial terms, f_1, for the sequence of Fourier coefficients, we calculate values for larger n and show that in general they diverge but that for a particular value of frequency they converge. This value must then be the growth rate of the instability since we require the Fourier series to converge. We then calculate the dependence of this growth rate, $\bar{\omega}$, on the wave number, $\bar{k}$, of the perturbation, and show that it is similar to that found by Cross & Van Hoven (1971) in their study of a sheared magnetic field, and in particular that it has a maximum growth rate $\bar{\omega}_{max}$. Our value of $\bar{\omega}_{max}$ is somewhat larger than theirs and it occurs at a value of $\bar{k}$, $\bar{k}_{max}$, which depends on β but not on S. Cross & Van Hoven find that $\bar{k}_{max}$ decreases as S increases. We calculate the dependence of $\bar{\omega}_{max}$ on S for several values of β and find that

$$\bar{\omega}_{max} \propto S^{0.67}$$

for the range of β considered.

3.6.: SUMMARY (Contd.)

This is to be compared with $\overline{\omega}_{max} \propto S^{0.57}$ found by Cross & Van Hoven, showing that our results can be up to an order of magnitude larger than theirs since S can be as large as 10^{10}. The effect of β on $\overline{\omega}_{max}$ is shown for two values of S and in both cases we find that, as β is reduced, $\overline{\omega}_{max}$ is constant until $\beta < 1$ when $\overline{\omega}_{max}$ falls linearly, on the log-log scale, as β is reduced further.

In section 3.1 we considered a model for the neutral current sheet in which the temperature, T_0, was constant, in section 3.2 we compare this with a model in which T_0 is varying. In order to keep the equilibrium fairly simple we keep the density constant so that T_0 varies across the sheet to preserve a constant total pressure. We are able to show that the second model gives the same growth rate, independent of β, as the model used in 3.1 does for $\beta \gg 1$. This is done by showing that the perturbed variables, $\underline{B}_1$, V_{1x} and V_{1y} satisfy the same equations in both models.

The fact that $\overline{\omega}_{max}$ falls as β falls may have been due to another, infinite conductivity, instability. But we show in section 3.3 that this is not the case. We try to find the growth rate of an instability using the technique of 3.1 with $\eta = 0$, but are unable to find a value of $\overline{\omega}$ for which the sequence of Fourier coefficients converge.

3.6.: SUMMARY (Contd.)

Then we calculated the growth rate analytically, of any instability which may occur when $\eta = 0$ but again we found that, for the types of perturbation considered (i.e. those used in 3.1) there were no instabilities with time scales much less than the diffusion time scale. Thus we show that the T.M.I. in 3.1 is not influenced by any infinite conductivity instability; this does not mean, however, that the current sheet is stable in the limit of infinite conductivity and, indeed, Uchida & Sakurai (1977) have shown that such instabilities do occur if the neutral sheet is perturbed in the z direction.

In section 3.4. we investigate the T.M.I. in the neutral current sheet with a transverse component, B_t, of the magnetic field, by using similar techniques to those used in 3.1. We calculate the growth rate, $\bar{\omega}$, but only for $\beta = 10^6$, and show that the variation of $\bar{\omega}$ with $\bar{k}$, the wave number, is the same as in 3.1 but that, as B_t increases, the whole curve is reduced. When $B_t/B_a \ll S^{-1/2}$ where B_a is the field strength at the edge of the current sheet in section 3.1, we find that B_t does not affect the problem and we get the results found in 3.1. However, when B_t is large enough, $\bar{\omega}_{max}$, the maximum value of $\bar{\omega}$ in the $\bar{\omega}/\bar{k}$ curve, is proportional to $(B_a/B_t)^2$.

3.6.: SUMMARY (Contd.)

As B_t is increased then $\bar{\omega}$ falls in value and the question arises as to what value of B_t, $B_{t\,crit}$ say, inhibits the T.M.I. The value of B_t which reduces $\bar{\omega}$ to 1 is $B_{t\,crit} = 0{\cdot}74\, B_a$. The value of B_t which reduces the value of $\bar{\omega}$ when $B_t = 0$, $\bar{\omega}_o$ say, to some fraction of this value e.g. $\frac{\bar{\omega}_o}{n}$, is given by

$$B_{t\,crit} = \frac{\sqrt{n}}{3{\cdot}8} \frac{B_a}{S^{0{\cdot}34}}$$

In both cases, when B_t exceeds $B_{t\,crit}$, the T.M.I. can be said to be significantly inhibited by the presence of the transverse field.

Finally, we consider an analytic treatment of the T.M.I. in a current sheet with a transverse component of the magnetic field. The equilibrium magnetic field is

$$\underline{B}_o = \begin{cases} B\frac{y}{a}\hat{\underline{x}} + B_{yo}\hat{\underline{y}} & , \ |y| < a \\ B\hat{\underline{x}} + B_{yo}\hat{\underline{y}} & , \ y > a \\ -B\hat{\underline{x}} + B_{yo}\hat{\underline{y}} & , \ y < -a \end{cases}$$

where B and B_{yo} are constants. As in section 3.4 we ignore energy sources and sinks, assume that the equilibrium temperature is constant and the equilibrium velocity is zero. Also we assume that the fluid is incompressible during the instability, which we later show is allowable if $\beta \gg 1/S$.

3.6.: SUMMARY (Contd.)

The equilibrium is then perturbed by a small amount and, by ignoring products of these small terms, we derive the linearized equations for these perturbations.
The solution is found in two regions; an outer region where the field is "frozen-into" the plasma so that resistivity is neglected and an inner region where the field diffuses through the plasma. Then the solutions are matched at the boundary to establish the dispersion relation between $\bar{\omega}$ and $\bar{k}$ with S and B_{y_0} as parameters. In order to establish the solution we must make several assumptions and in particular that B_{y_0} is very small, so that it is ignored in the outer region but retained in the inner region.
We find that $\bar{\omega}$ falls as B_{y_0} is increased, as we found in section 3.4, so that the maximum value, $\bar{\omega}^*_{max}$ occurs at $B_{y_0}=0$, where $\bar{\omega}^*_{max} \propto (S/\bar{k})^{2/5}$, as found by Furth et al. (1963). Also, as $\bar{k}$ is increased we find that $\bar{\omega}$ falls, so that the maximum value, $\bar{\omega}_{max}$ occurs at the smallest $\bar{k}$ allowed by the method, $\bar{k}_{min} = (4\bar{\omega}/S)^{1/6}$. We find that

$$(\bar{\omega}_{max})^{5/4} = \frac{1}{a + \bar{B}_{y_0} b}$$

where a and b are constant for a given value of S, so that $\bar{\omega}_{max}$ falls as $\bar{B}_{y_0}$ increases but does not reach zero for finite values of $\bar{B}_{y_0}$, unlike the more accurate numerical solutions of section 3.4 where $\bar{B}_{y_0} = B_c / B_a$.

CHAPTER 4

PROMINENCE FORMATION IN A SHEARED MAGNETIC FIELD

In this section a simple model is presented for the way that prominences may form by a thermal instability in a sheared field. The instability occurs for a similar reason to that for the neutral current sheet instability, described in chapter 1. It takes place when,

$$t_{\parallel} > t_{cool} \quad , \qquad (4.1)$$

where $t_{\parallel} = (L^2 C_p T)/(\kappa_{\parallel} \Delta T)$ is the time taken to conduct heat into a region, and $t_{cool} = C_p T /(a \rho^2)$ is the time taken to radiate heat out of the region, where the constant $a = 6.3 \times 10^{24}$ ergs cm^3 g^{-2} sec^{-1} (Orrall & Zirker, 1961) In this case L is the length measured along a field line in a sheared field. As the field becomes more sheared, so L increases possibly to such an extent that (4.1) is satisfied and the plasma becomes thermally unstable.

In the first section we discuss, in detail, the force-free magnetic field structure that we will use in this chapter. Such a force-free configuration is valid in the corona only if the magnetic field strength is large enough that the gas pressure is dominated by the magnetic pressure.

In our model we are including the effects of gravity, which, in particular, implies that the density decreases with height. This reduces the effectiveness with which the radiative loss can try to destabilize the plasma, since the higher a field line reaches the larger will be the value of t_{cool} in (4.1). However, for field lines that reach greater heights, the length L increases so that $t_{\parallel}$ also increases, tending to make the plasma unstable. Thus we see that for field lines reaching higher and higher into the atmosphere both $t_{\parallel}$ and t_{cool} increase.

PROMINENCE FORMATION IN A SHEARED MAGNETIC FIELD (Contd.)

In section 4.2 we shall, in an order of magnitude calculation, investigate the manner in which this ratio changes with height. The object is to see if there is a maximum value of t_u/t_{cool} in excess of unity, which, by (4.1) would imply that the plasma is thermally unstable for some height range.

In section 4.3 we investigate in more detail the ideas developed in the order of magnitude calculations of section 4.2. The force-free magnetic field structure discussed in 4.1 and the plasma are assumed to be in mechanical equilibrium under a balance between gravity and a vertical pressure gradient, and in thermal equilibrium under a balance between thermal conduction and radiative loss. We assume the order of magnitude form of this thermal balance that we used when investigating the thermal instability in a current sheet in chapter 2. For the mechanical balance we assume that the temperature variations are not important, so that the pressure gradient implies that the density is reduced with height, thus the density effect discussed in section 4.2 is present. The other effect, the increasing length scale for thermal conduction, is supplied by increasing the shear angle which, as we show in section 4.1, increases the length of the field lines. We take an approximate form for the dependence of the length of the field line on the sheer angle and solve the equations of mechanical and thermal balance with the equation of state, for the temperature at the top of a flux tube as a function of h, the height to which that flux tube reaches. We show how this variation depends on the shear angle and on the value of two other parameters, g' and $\bar{\delta}$, which are defined in terms of the values of the density and temperature at the base of the magnetic field region and on the scale length of that region

PROMINENCE FORMATION IN A SHEARED MAGNETIC FIELD (Contd.)

We then look at the same problem in section 4.4, but with mechanical heating added to the thermal balance. Again we calculate the temperature at the top of the field line as a function of the height to which that field line reaches and show how this variation depends on the shear angle.

In section 4.5 we examine the problem discussed in section 4.3: the thermal equilibrium balance between radiative loss and thermal conduction in the force-free field and the mechanical equilibrium balance between gravity and a vertical gradient in that magnetic field, but, this time, we solve the full equations numerically. We are able to find the temperature variation along each field line and establish how this variation depends on the height to which the field line reaches. As in section 4.3, we examine the effect of changing the shear angle and another parameter of the problem, $\overline{\gamma}$. In this fashion we are able to confirm, in a more and more rigorous fashion, the idea that is developed in section 4.2.

4.1.: THE MAGNETIC FIELD STRUCTURE

If, in the magnetostatic equation $\nabla p = \underline{J} \wedge \underline{B}$ we have

$$\beta << 1 , \qquad (4.2)$$

where $\beta = 8\pi p / B^2$, then it reduces to

$$\underline{J} \wedge \underline{B} = 0 \qquad (4.3)$$

This implies that $\nabla \wedge \underline{B} = \alpha \underline{B}$ (4.4)

where $(\underline{B}.\nabla)\alpha = 0$ (α is constant along a magnetic field line). One method that has been used for simplicity is to suppose α = constant everywhere, so that curl (4.4) gives

$$(\nabla^2 + \alpha^2)\underline{B} = 0 .$$

In the corona $p = 2.8 \times 10^{-2}$ dynes cm^{-2}, from the perfect gas law $p = R\rho T$, $\rho = 1.7 \times 10^{-16}$ g cm^{-3} and $T = 10^6$ °K , thus (4.2) becomes $B >> 0.1$ Gauss which holds in active regions and may also be true near quiescent prominences.

Solutions of (4.3), subject to specified shearing motions is very difficult in general. We circumvent this problem by looking for simple solutions, which have the form of a sheared field in which prominences may form. Suppose that $\underline{B} = \underline{B}(x,z)$, then (4.3) may be written

$$\nabla(\tfrac{1}{2}B^2) = (\underline{B}.\nabla)\underline{B},$$

which has components

$$\left.\begin{aligned} \frac{\partial}{\partial x}\left(\tfrac{1}{2}B^2\right) &= \left(B_x\frac{\partial}{\partial x} + B_z\frac{\partial}{\partial z}\right)B_x , \\ \frac{\partial}{\partial z}\left(\tfrac{1}{2}B^2\right) &= \left(B_x\frac{\partial}{\partial x} + B_z\frac{\partial}{\partial z}\right)B_z , \\ 0 &= \left(B_x\frac{\partial}{\partial x} + B_z\frac{\partial}{\partial z}\right)B_y . \end{aligned}\right\} \qquad (4.5)$$

4.1.: THE MAGNETIC FIELD STRUCTURE (Contd.)

Now, in particular, search for solutions in which

$$\left.\begin{aligned} B_x &= A_1 \cos kx\ e^{-\ell z}\ , \\ B_y &= A_2 \cos kx\ e^{-\ell z}\ , \\ B_z &= B_0 \sin kx\ e^{-\ell z}\ , \end{aligned}\right\} \qquad (4.6)$$

where $\ell^2 = k^2 - \alpha^2$, so that B_x vanishes at $x = \pm \frac{\pi}{k}$ and B_z vanishes at $x = 0$ as indicated in Figure (30a), page 207. Also field lines in the x-z plane are straight lines as shown in Figure (30b) page 207. Thus the field will rise if the foot-points in the photosphere have a shearing motion parallel to the y-axis in such a way that the shear in velocity is linearly proportional to the distance from the y-axis. Note, however, that we have no guarantee that field with such a linkage of foot-points and the normal component, B_z, at the photosphere, is unique. Substituting (4.6) into (4.5) gives

$$A_1 = -(\ell/k)\, B_0 \ ,$$

and

$$A_2^2 = B_0 (1 - \ell^2/k^2) \ .$$

In other words, the field that we take is

$$\left.\begin{aligned} B_x &= -\frac{\ell}{k} B_0 \cos kx\ e^{-\ell z}\ , \\ B_y &= B_0 (1 - \ell^2/k^2) \cos kx\ e^{-\ell z}\ , \\ B_z &= B_0 \sin kx\ e^{-\ell z}\ . \end{aligned}\right\} \qquad (4.7)$$

It was first considered by Nakagawa & Tanaka (1974).

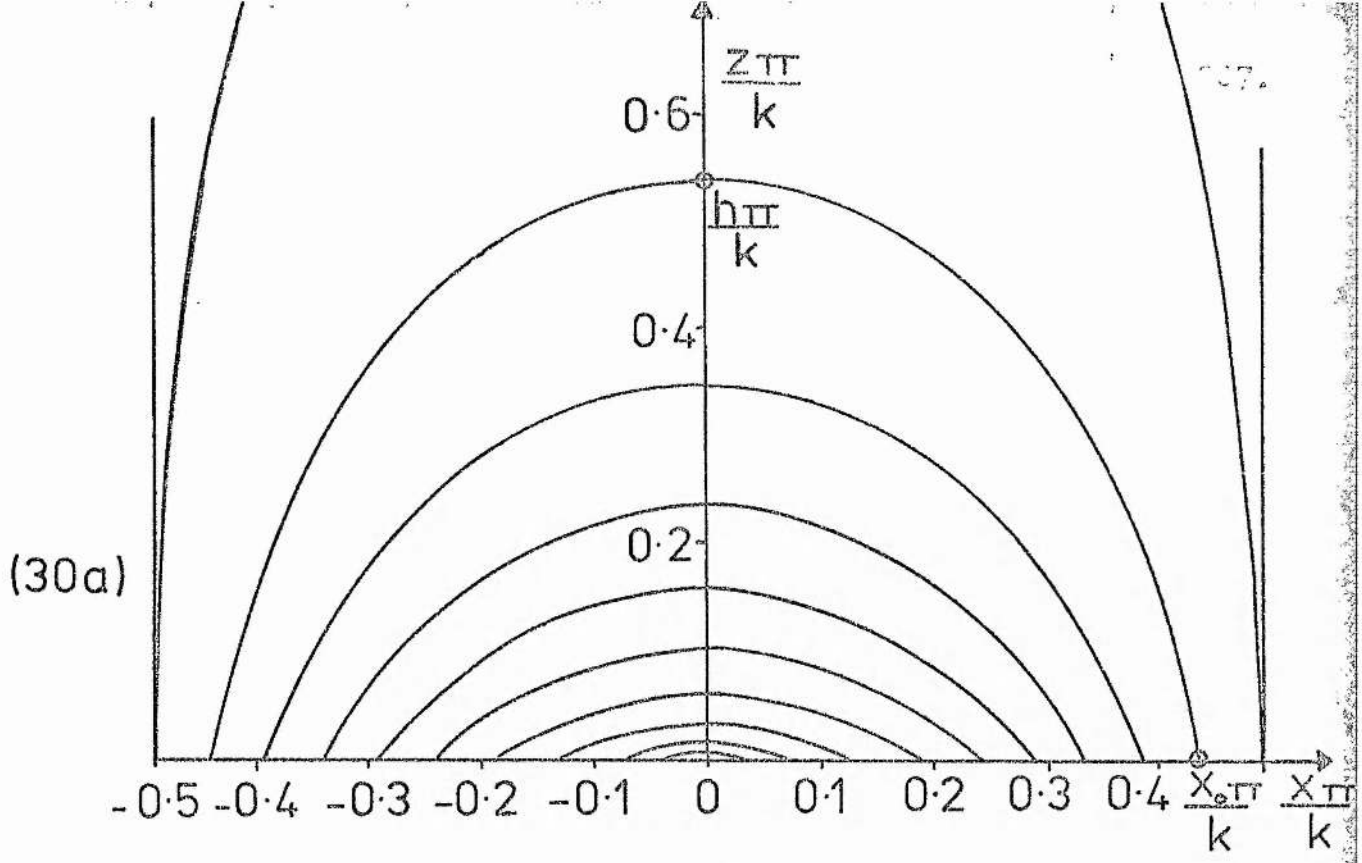

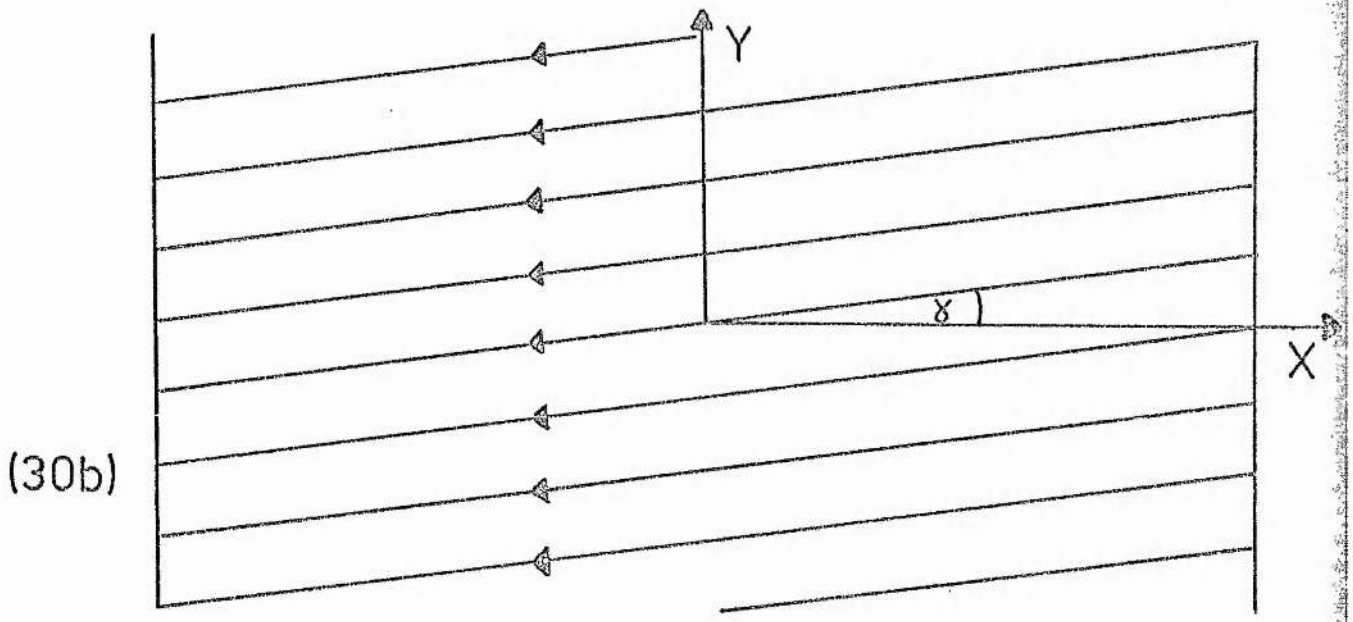

Figure 30. A constant α force-free magnetic field structure given by equation (4.7) where $\alpha = k \sin\gamma$. Figure (30 a) shows that the magnetic field lines in a vertical plane have an arch structure with vertical field lines at the edge of the region, $X = \pm \frac{\pi}{2k}$. A field line that starts a distance X_o from $X = 0$ on the x-axis reaches to a height h. Figure (30 b) shows that the projection of the magnetic field on the x-y plane gives a set of straight lines inclined at an angle, γ , the shear angle, to the x-axis.

4.1.: THE MAGNETIC FIELD STRUCTURE (Contd.)

We note from $\underline{J} = \text{curl}\,\frac{\underline{B}}{4\pi}$, that

$$J_x = -k\left(1 - \ell^2/k^2\right)^{1/2} B_x \ ,$$

$$J_y = -k\left(1 - \ell^2/k^2\right)^{1/2} B_y \ ,$$

$$J_z = -k\left(1 - \ell^2/k^2\right)^{1/2} B_z \ .$$

so that the field is a constant-α force-free field with $\alpha^2 = k^2 - \ell^2$. The field lines in the x-y plane are inclined at an angle, to the x-axis, of

$$\gamma = \tan^{-1}\left(\frac{B_y}{B_x}\right) = \tan^{-1}\left(\frac{k^2}{\ell^2} - 1\right)^{1/2} \ ,$$

so $$\frac{\ell}{k} = \cos\gamma$$

and $$\alpha = k \sin\gamma \ .$$

Thus, as α increases in value from zero, where the field is potential, to k , so the shear angle, γ , goes from zero to $\pi/2$.

The equation of the field line in the x- z plane through $(x_0, 0)$ is given by the solution of $dx/B_x = dz/B_z$, namely

$$z = \frac{1}{\ell} \log_e\left(\frac{\cos kx}{\cos kx_0}\right) \ .$$

Thus the maximum height of the field line through $(x_0, 0)$ is

$$h = -\frac{1}{\ell} \log_e(\cos kx_0) \ , \qquad (4.8)$$

or

$$\frac{hk}{\pi} = -\frac{\log_e(\cos kx_0)}{\pi \cos\gamma} \ .$$

4.1.: THE MAGNETIC FIELD STRUCTURE (Contd.)

We plot from this equation, the graph of the dimensionless variable, (hk/π), where, from Figure(30 a), page 207, π/k is the width, in the X-Z plane, of the magnetic field region, as a function of $x_o \frac{k}{\pi}$, for several values of the shear angle γ, in Figure(31a), page 210. This shows how the top of a field line, height h, reaches higher and higher as the footpoint of the line, at x_o, gets close to the edge of the magnetic field region, at $x_o = \pi/k$. The effect of changing the shear angle, γ, shown in Figure(31a), is shown more clearly in Figure(31b), where we plot the variation of the maximum height of a field line, h, as a function of the shear angle γ, for several values of x_o, the footpoint of the field line. The field line rises into the atmosphere as the shear angle is increased and the rise is particularly rapid near $\gamma = 90^\circ$.

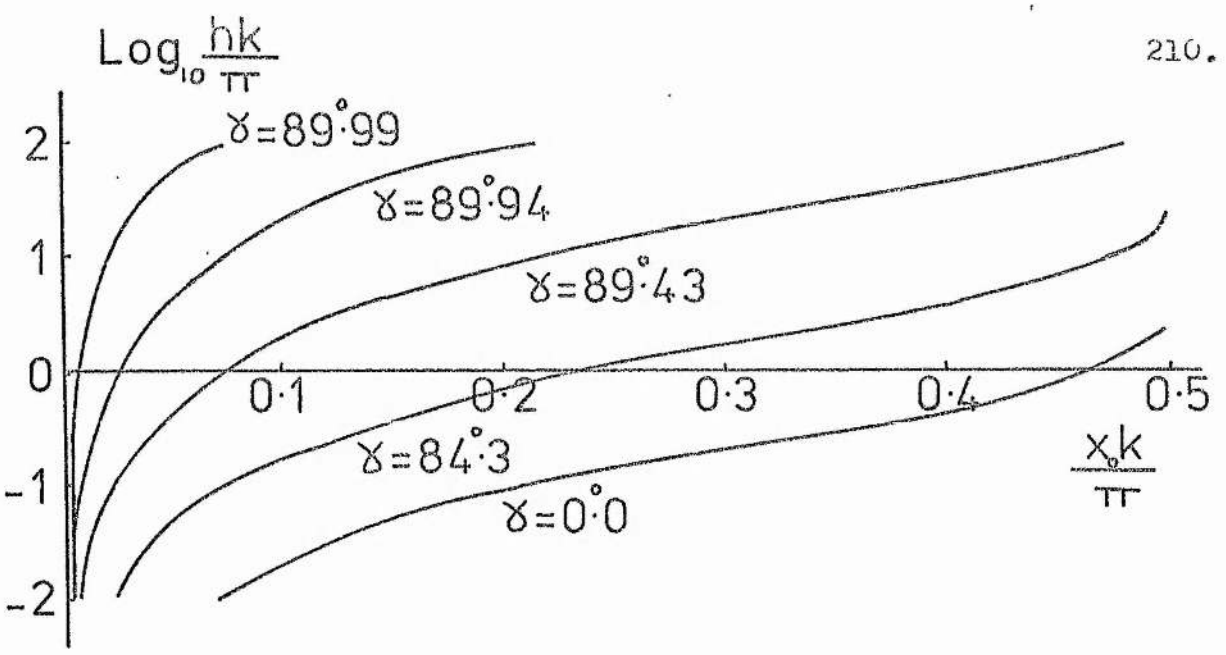

Figure 31a. The maximum height h of a magnetic field line as a function of X_o for several values of the shear angle γ.

X_o is the point on the x axis shown in Figure(30a) page 207 at which the field line crosses the $Z=0$ line. The variables h and X_o are written in terms of the width of the magnetic field region, $\frac{\pi}{k}$,.

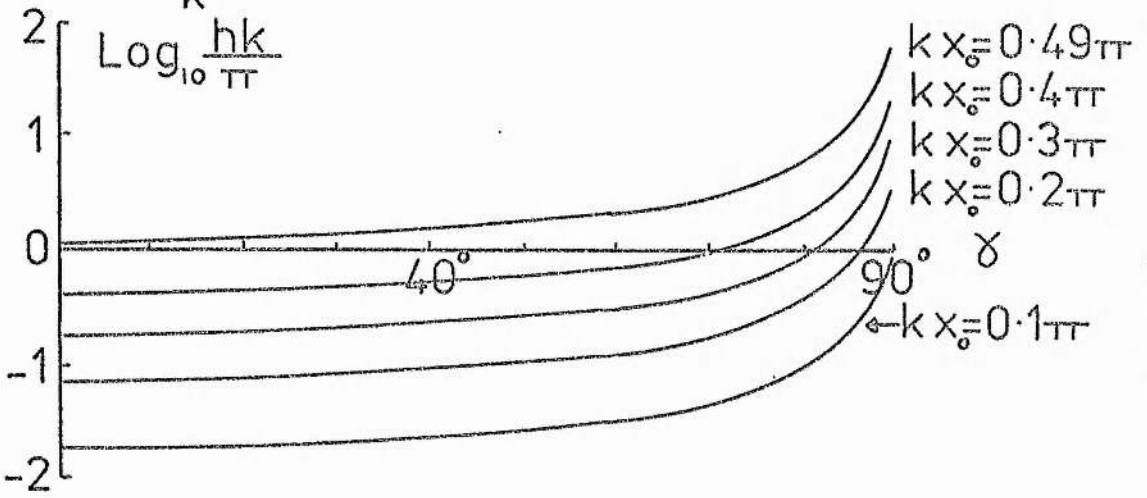

Figure 31b. The maximum height h of a magnetic field line as a function of the shear angle γ for several values of X_o . The variables h and X_o are written in terms of the width of the magnetic field region, $\frac{\pi}{k}$, shown in Figure(30a).

4.2.: ORDER OF MAGNITUDE ESTIMATE

We are interested in the conduction of heat a distance L along a field line in a magnetic structure such as that considered above. As one goes to higher and higher locations in the structure, so the length L of the field lines increases which tends to increase $t_{\parallel}/t_{cool}$. But, at the same time, the density ρ decreases which tends to decrease the value of $t_{\parallel}/t_{cool}$. It is the competition, between the destabilizing effect of increasing a flux tube's length and the stabilizing effect of decreasing the density therein, which determines whether or not the thermal instability sets in. Let us consider this competition roughly, before proceeding with a discussion of the numerical solution.

In order to balance the force of gravity, the density at the top, $z = h$, of a field line will decrease with height h, such that approximately

$$\rho = \rho_0 e^{-h/\Lambda} ,$$

where the scale height $\Lambda = 2 k_B T/(m_i g)$. Then we have from (4.1) that

$$\frac{t_{\parallel}}{t_{cool}} = \frac{\alpha \rho_0^2}{K_{\parallel} \Delta T} L^2 e^{-2h/\Lambda} ,$$

which, once L and ΔT are specified as function of h, determines the variation of the ratio $t_{\parallel}/t_{cool}$ with height. For simplicity let us suppose ΔT is constant and $L = nh$, say. Then

$$\frac{t_{\parallel}}{t_{cool}} = \frac{\alpha \rho_0^2}{K_{\parallel} \Delta T} n^2 h^2 e^{-2h/\Lambda} ,$$

4.2.: ORDER OF MAGNITUDE ESTIMATE (Contd.)

so that as h increases, $t_{\parallel}/t_{cool}$ first increases from zero, passes through a maximum value, at $h=\Lambda$, of

$$\left(\frac{t_{\parallel}}{t_{cool}}\right)_{max} = \frac{a\rho_0^2}{K_{\parallel}\Delta T} n^2 \Lambda^2 e^{-2} \qquad (4.9)$$

and then decreases to zero as h approaches infinity. In order of magnitude, if this ratio exceeds unity we expect thermal instability to occur and, furthermore, the instability will be first manifested at a height of $h = \Lambda$.

For the sake of illustration, let us adopt the following values, characteristic of a coronal condensation from which some prominences form: density $\rho_0 = 1.7 \times 10^{-15}$ g cm^{-2}, temperature $T = 10^6$ °K, $\Delta T = 5 \times 10^5$ °K, the coefficient of thermal conduction along a field line $K_{\parallel} = 2 \times 10^{-6} T^{5/2}$ from equation (1.22), the constant $a = 6.3 \times 10^{24}$ ergs cm^3 g^{-2} sec^{-1} (Orrall & Zirker, 1961) and the scale height $\Lambda = 2 k_B T / m_i g = 6 \times 10^9$ cm, where Boltzmann's constant $k_B = 1.4 \times 10^{-16}$ erg deg^{-1}, the mass of a proton $m_i = 1.7 \times 10^{-24}$ g, and the gravitational acceleration $g = 2.74 \times 10^4$ cm sec^{-2} at the solar surface. Then (4.9) becomes

$$\left(t_{\parallel}/t_{cool}\right)_{max} = 0.1\, n^2 .$$

Note that away from coronal condensations, where the density is a factor of 10 lower, this ratio is smaller by a factor of 100 so the thermal instability is far less likely to take place. When the field is not sheared, so that $n \simeq 1$, we see that $(t_{\parallel}/t_{cool})_{max} < 1$ and the plasma is thermally stable.

4.2.: ORDER OF MAGNITUDE ESTIMATE (Contd.)

But, as the field becomes sheared, so the length of the field lines tend to increase. For a given height, h, the field lines therefore have greater lengths than unsheared field lines and so n exceeds unity. If the shearing (and consequently the value of n) is large enough we see that $(t_{\parallel} / t_{cool})_{max}$ may exceed unity, so giving thermal instability. It is the purpose of the following sections to work these ideas out more precisely.

4.3.: THE THERMAL AND HYDROSTATIC EQUILIBRIUM OF THE PLASMA IN THE SHEARED MAGNETIC CONFIGURATION.

Within the force-free magnetic structure given by (4.7) we shall suppose the equilibrium values of density and temperature to be given by the equations

$$\frac{d}{dz}(R\rho T) = -\rho g \quad , \tag{4.10}$$

$$\underline{\nabla}.(\underline{\underline{K}}.\underline{\nabla}T) = \chi \rho^2 T^{\alpha} \quad . \tag{4.11}$$

Equation (4.10) expresses hydrostatic equilibrium along field lines, while the thermal equilibrium is assumed to be governed by a balance between thermal conduction and radiation, as expressed in (4.11). This may arise if heat is dumped at some location, say the top or bottom of the field lines, and then conducted into the rest of the structure. The more general case, of significant mechanical heating throughout the configuration, will be considered in 4.4. We are considering conduction only along the field lines because, as shown earlier, the heat conducted across the field is very much less in structures the size of quiescent prominences. In addition we assume that the acceleration due to gravity, g, is constant and that it equals the value on the solar surface, $g_\odot$, for all heights. ($g_\odot = G M_\odot / R_\odot^2 = 2{\cdot}7 \times 10^4$). Over the height of a prominence (5×10^9 cm), g is reduced by a factor of only 0.9 so that the effect of height variations on g is small enough to be neglected.

4.3.: THE THERMAL AND HYDROSTATIC EQUILIBRIUM OF THE PLASMA IN THE SHEARED MAGNETIC CONFIGURATION. (Contd.)

In this section the field structure of Figure (30) page 207 is approximated by straight lines, Figure (32), page 216, such that in the x-z plane along a field line $B_z/B = h/L$ = constant. Then (4.10) and (4.11) reduce to

$$\frac{d}{dz}(R\rho T) = -\rho g \,, \tag{4.12}$$

$$\frac{h^2}{L^2}\frac{d}{dz}\left(K_{\parallel}\frac{dT}{dz}\right) = \chi \rho^2 T^{\alpha} \,, \tag{4.13}$$

where

$$K_{\parallel} = K_0 T^{5/2} \,. \tag{4.14}$$

In order to solve (4.12), we further assume that T is constant along the field line, i.e. $T=T_T$, the value of temperature at the top of a loop. This gives

$$\rho = \rho_0 e^{-z/\Lambda} \,, \tag{4.15}$$

where the scale height $\Lambda = 2 k_B T/(m_i g)$, so that the value of density at the top of the loop is

$$\rho_T = \rho_0 e^{-\frac{h}{\Lambda_0}\frac{T_T}{T_0}} \,,$$

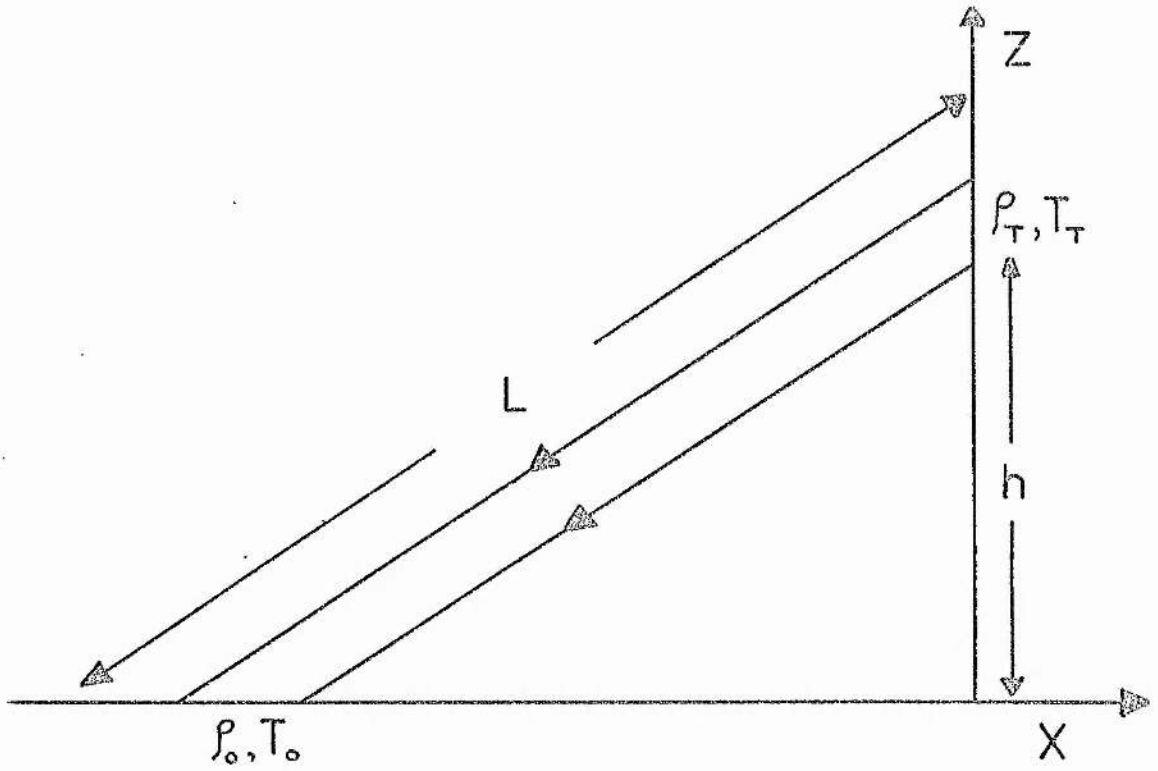

Figure (32). The straight line representation of the magnetic field structure drawn in Figure (30a) page 207,
With this representation we approximate in section 4.3 the amount of heat conducted along a field line, of length L, from the surrounding plasma, at density ρ_o and temperature T_o , to the top of the loop, a height, h, above the base of the magnetic field region, where the density is ρ_T and temperature T_T .

4.3.: THE THERMAL AND HYDROSTATIC EQUILIBRIUM OF THE PLASMA IN THE SHEARED MAGNETIC CONFIGURATION. (Contd.)

where $\Lambda_0 = 2k_B T_0/(m_i g)$. Next, to solve (4.13), we approximate the thermal conduction term, as in chapter 1, so that (4.13) becomes

$$\frac{h^2}{L^2} K_0 T_T^{5/2} \frac{(T_T - T_0)}{L^2} = -\chi \rho^2 T_T^{\alpha}$$

or, substituting for ρ from (4.15),

$$\frac{h^2}{L^2} K_0 T_T^{5/2} \frac{(T_0 - T_T)}{L^2} = \chi \rho_0^2 T_T^{\alpha} \exp\left(-\frac{2hT_T}{\Lambda_0 T_0}\right) . \quad (4.16)$$

To make (4.16) dimensionless, put

$$T_T = T_0 T_T' , \quad h = h' \frac{\pi}{k} , \quad L = L' \frac{\pi}{k} ,$$

giving $$T_T'^{(\frac{5}{2}-\alpha)}(1 - T_T') = \bar{\gamma} \frac{L'^4}{h'^2} \exp(-2h'g'T_T') , \quad (4.17)$$

where $$\bar{\gamma} = \frac{\chi \rho_0^2 T_0^{\alpha}}{K_0 T_0^{7/2}} \left(\frac{\pi}{k}\right)^2 ,$$

and $$g' = \frac{\pi}{\Lambda_0 k} .$$

We therefore need to solve (4.17) for T_T' as a function of h', with $L' = L'(h')$ given below.

According to (4.8), the footpoint of a field line (Figure (33) page 218), whose maximum height is h, is located a distance

$$x_0 = \frac{1}{k} \cos^{-1}(\exp(-hk\cos\gamma)) \quad (4.18)$$

from the y-axis. We approximate the length of such a field line by the length of the dashed straight line on Figure (33), namely

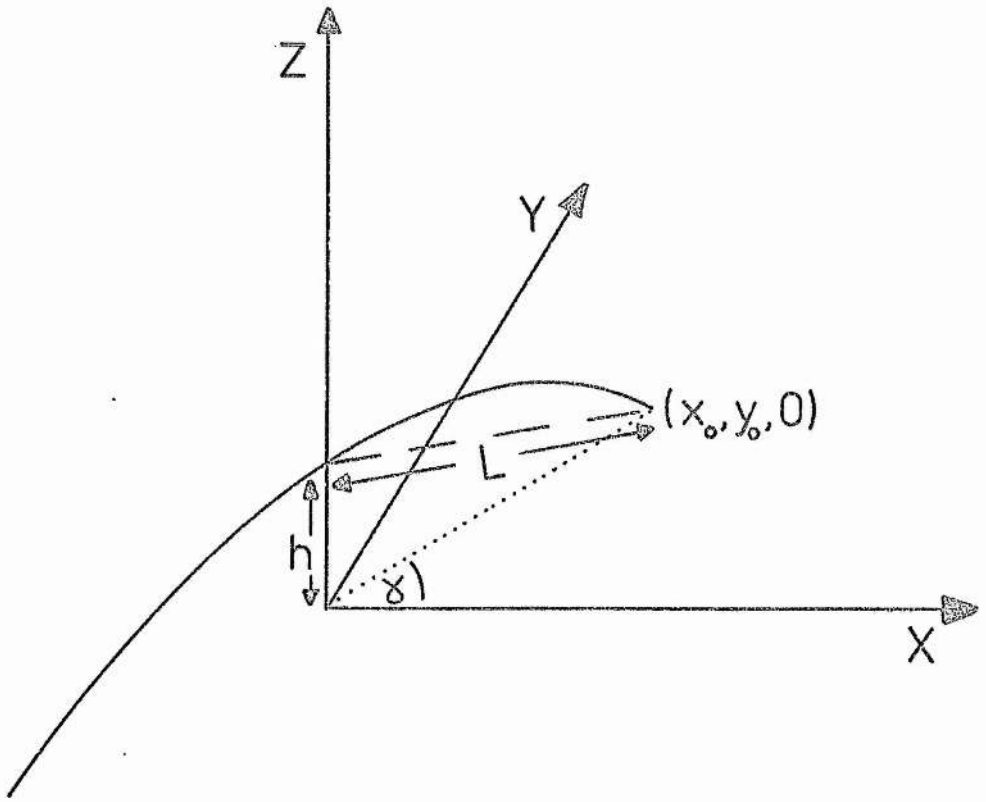

Figure(33). A curved field line of the magnetic structure drawn in Figures (30a) and (30b) page 207.

In section 4.3 we approximate the length of the field line from the foot point at (X_o , y_o , Z_o) to the top of the arch at $(0, 0, h)$, by the straight line of length L shown dashed in the figure. The angle, γ, also shown in the Figure (30b) gives the amount by which the field is sheared.

4.3.: THE THERMAL AND HYDROSTATIC EQUILIBRIUM OF THE PLASMA IN THE SHEARED MAGNETIC CONFIGURATION (Contd.)

$$L^2 = x_o^2 + y_o^2 + h^2 = x_o^2 \sec^2\gamma + h^2 ,$$

or, using (4.18) for x_o,

$$L^2 = \frac{\sec^2\gamma}{k^2}\left[\cos^{-1} e^{-hk\cos\gamma}\right]^2 + h^2 .$$

In dimensionless form this is

$$L'^2 = \frac{\sec^2\gamma}{\pi^2}\left[\cos^{-1} e^{-h'\pi\cos\gamma}\right]^2 + h'^2 , \qquad (4.19)$$

which gives L' as a function of h' for a given shear angle γ. So, from (4.17) and (4.19) we have

$$\frac{T_T'^{(\frac{5}{2}-\alpha)}(1-T_T')}{\bar{\gamma}\exp(-2h'g'T_T')} = \frac{\left[\frac{\sec^2\gamma}{\pi^2}\left(\cos^{-1}e^{-h'\pi\cos\gamma}\right)^2 + h'^2\right]^2}{h'^2} . \qquad (4.20)$$

Equation (4.20) determines the temperature at the top of the loop, T_T', as a function of the height of the loop, h', with parameters γ (the shear angle), $\bar{\gamma}$ (the ratio of radiation to thermal conduction) and g' (the ratio of the width of the structure to the scale height). In Figure (34), page 220, (calculated numerically from (4.20)), we have plotted $T_T'(h')$ for coronal values of $\bar{\gamma}$ and g' ($\bar{\gamma} = 3.74\times10^{-4}$, $g' = 0.4$ where we have used $\frac{\pi}{k} = 5\times10^9$ cm, the approximate height of a quiescent prominence, $\rho_o = 1.7\times10^{-16}$ g cm^{-3} and $T_o = 2\times10^6$ °K) and several values of the shear angle γ. These graphs imply the occurrence of a thermal instability when γ is large enough.

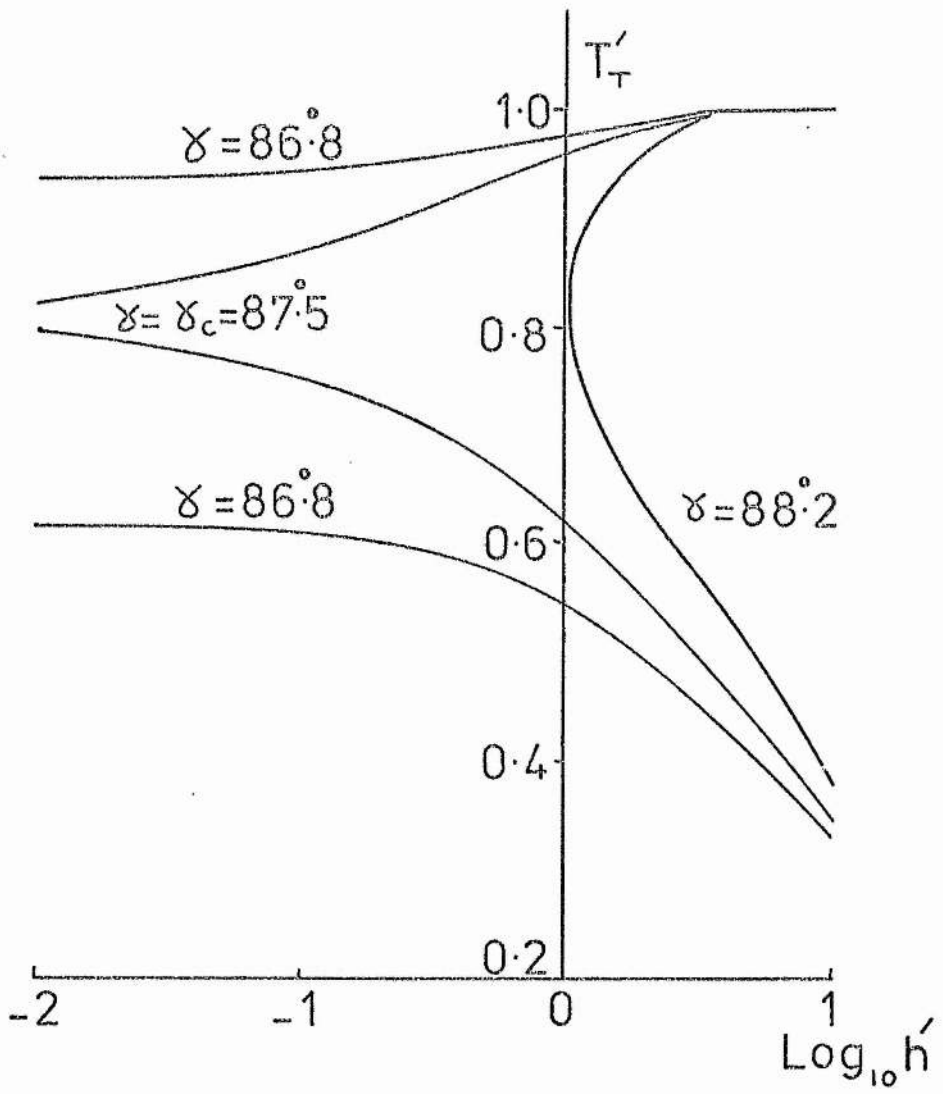

Figure (34). The equilibrium curves of the temperature T'_T at the top of a magnetic field arch, as a function of h', the height of the top of the arch above the base of the magnetic field region. These are drawn for several values of the shear angle, γ, and in particular for the critical value of the shear angle γ_c. For $\gamma > \gamma_c$ there is a region of h' in which the only equilibrium temperatures are very low ($T'_T < 10^{-4}$) so that the plasma initially at coronal equilibrium temperatures has become unstable.

4.3.: THE THERMAL AND HYDROSTATIC EQUILIBRIUM OF THE PLASMA IN THE SHEARED MAGNETIC CONFIGURATION (Contd.)

When γ is small there are three equilibrium values of T_T' for all values of h'. One of the equilibrium solutions occurs at $T_T' < 10^{-4}$ so that the curve of T_T' as a function of h' is, in this scale of graph, coincident with the h'-axis. However, when γ is greater than some critical value, γ_c say, there is a region of h' in which the equilibrium values have $T_T' < 10^{-4}$, so that the plasma with the higher equilibrium temperatures become unstable as γ_c is exceeded. This region of h' increases from $h' \ll 1$ when $\gamma \gtrsim \gamma_c$ until there are no equilibrium values of h' at all when $\gamma = \pi/2$. We expect that the initially hot plasma, in this non-equilibrium range of heights, cools down rather than heats up, because the thermal conduction has become negligible in the energy balance as the shear γ and length scale L' have increased. Thus the energetics of the plasma are dominated by the radiative loss. As in the case of thermal instability in a neutral current sheet (chapter 2), we expect that the plasma will cool down locally in about a day, to the third equilibrium solution and in the process new plasma is drawn up into the region along the field lines. The temperature of this third equilibrium is very low ($T_T' < 10^{-4}$) and is unrealistic in practice since the radiative loss used in this thesis (Figure 1) is not accurate for temperatures below about 10^5°K because of the radiative transfer effects that have been ignored in its derivation.

4.3.: THE THERMAL AND HYDROSTATIC EQUILIBRIUM OF THE PLASMA IN THE SHEARED MAGNETIC CONFIGURATION (Contd.)

Also, the equations we have used are no longer valid for the final equilibrium in which β may no longer be small.

Solutions at Low Heights.

In the corona this thermal instability occurs when h is small, so that we can confirm the numerical solutions, and perhaps understand the onset of instability better, by looking more closely at equation (4.20) with h' small. When $h' \ll \frac{\sec\gamma}{\pi}$ and $h' g' T_T' < 1$, equation (4.20) becomes, to lowest order

$$T_T'\left(\tfrac{5}{2}-\alpha\right)\left(1-T_T'\right) = \frac{4\sec^2\gamma}{\pi^2}\,\overline{\gamma} \quad . \tag{4.21}$$

Its solution is given from the intersections of the two curves shown in Figure (35), page 223, where we define

$$F\left(T_T'\right) = T_T'^{\left(\frac{5}{2}-\alpha\right)}\left(1-T_T'\right) \quad . \tag{4.22}$$

F vanishes at $T_T' = 1$ and approaches infinity as T_T' approaches zero. It possesses a maximum of 0.08 at

$$T_T' = \frac{\frac{5}{2}-\alpha}{\frac{7}{2}-\alpha} = 0.8 \quad \text{(with } \alpha = -1.8 \text{ from Figure (1))} \, .$$

In Figure (34) we found only the low temperature solution for T_T' at small h' when γ exceeds the critical value γ_c. This effect can be seen in Figure (35), page 223, where, for small values of γ there are three solutions, one near $T_T' = 0$, one near $T_T' = 1$, and the other in between.

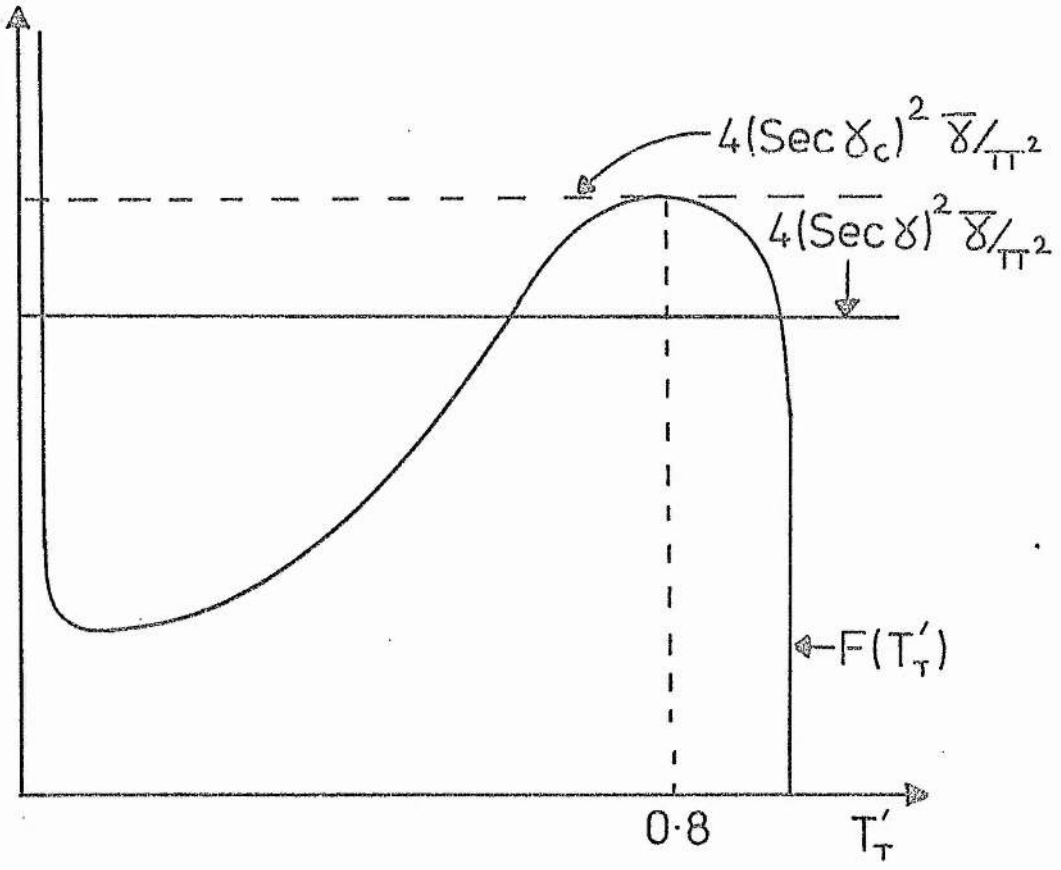

Figure 35. The two curves $F(T_T')$ (defined in (4.22)) and $4(\mathrm{Sec}\,\gamma)^2\,\overline{\gamma}/_{\pi^2}$, whose intersections represent the equilibrium solutions T_T', the temperature at the top of the magnetic field line shown in Figure (32) page 216. γ is the shear angle, shown in Figure (30b) page 207, and the parameter $\overline{\gamma}$ is the ratio of radiative loss to thermal conduction at the base of the magnetic field.

4.3.: THE THERMAL AND HYDROSTATIC EQUILIBRIUM OF THE PLASMA IN THE SHEARED MAGNETIC CONFIGURATION (Contd.)

As γ increases, the $4\frac{\sec^2\gamma}{\pi^2}\bar{\gamma}$ line increases until, at $\gamma=\gamma_c$, it just touches the maximum of the $F(T_T')$ curve, where $T_T' = T_c = 0\cdot8$.

If $\gamma > \gamma_c$ then the curves only intersect at the lower temperature so that there is no higher temperature solution.

The critical value γ_c is determined by putting $T_T' = 0\cdot8$ in (4.21), so that

$$\sec\gamma_c = \left(\frac{\pi^2}{4\bar{\gamma}}\,0\cdot08\right)^{1/2}. \qquad (4.23)$$

For coronal values ($\rho_0 = 1\cdot7\times10^{-16}$ g cm^{-3} , $T_0 = 2\times10^6$ °K and $\pi/k = 5\times10^9$ cm) $\bar{\gamma} = 3\cdot74\times10^{-4}$ and $\gamma_c = \pi/2\cdot06 = 87^\circ$.

Figure (36), page 225, gives the variation of the critical shear angle with $\bar{\gamma}$; the other parameter of the problem, g' has no effect on γ_c. A restriction on the validity of Figure (36) is that $T_0 > 10^5$ °K , since we have used the value $\alpha = -1\cdot8$ in the radiative loss function. When $T_0 < 10^5$ °K, however, we expect no thermal instability to occur because of the shape of the more accurate radiative loss function as given for example by Cox & Tucker (1969).

The parameter $\bar{\gamma}$ is defined by

$$\bar{\gamma} = \frac{\chi\,\rho_0^2\,T_0^{\alpha}}{K_0\,T_0^{7/2}}\left(\frac{\pi}{k}\right)^2. \qquad (4.24)$$

Thus we see that the effect of increasing the scale (π/k) of the structure or of increasing the density, ρ_0, is to raise the value of $\bar{\gamma}$ and so from Figure (36), page 225, to destabilize the plasma at smaller shear angles γ_c.

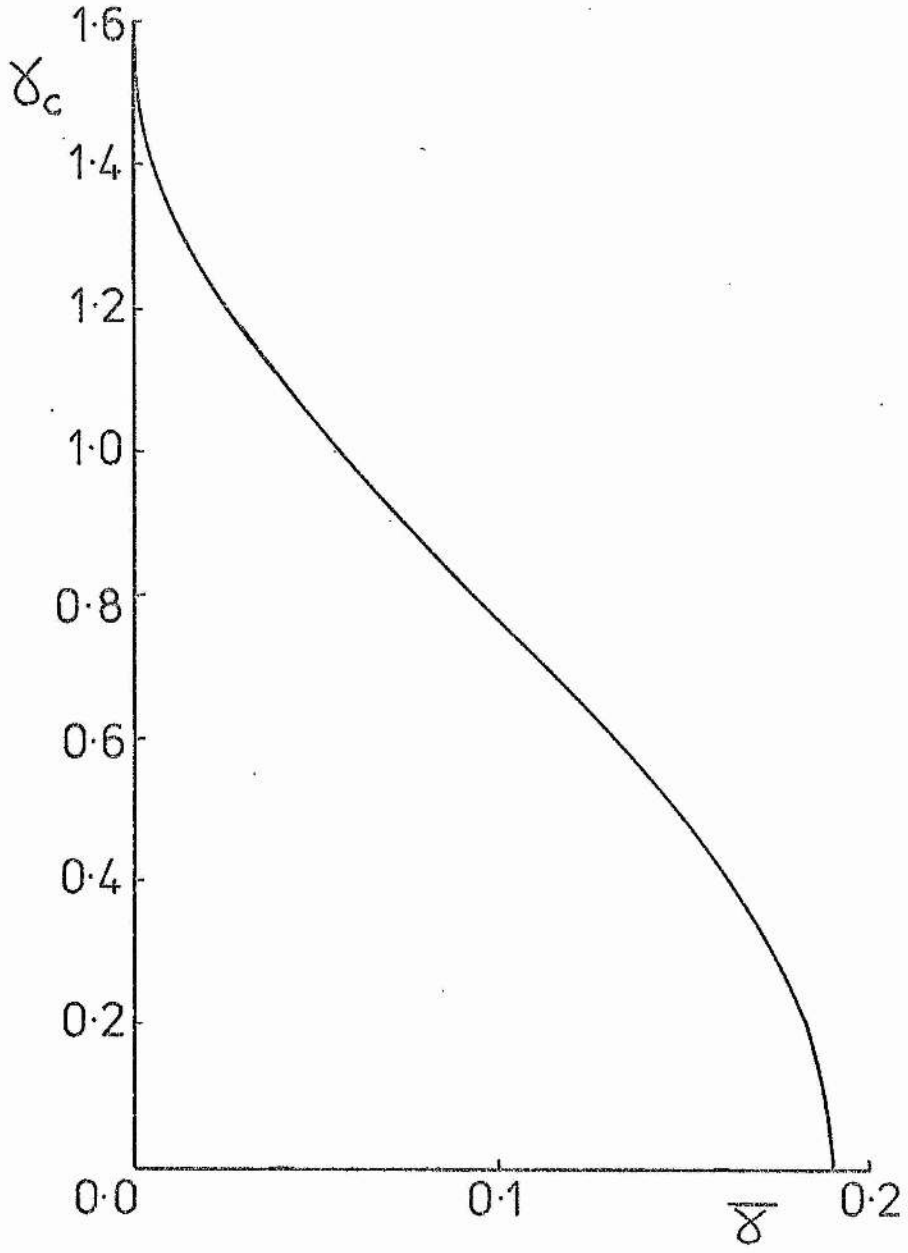

Figure 36. The variation of the critical shearing angle γ_c as a function of the parameter $\bar{\gamma}$, which, given by (4.24), is the ratio of the radiative loss to thermal conduction at the base of the magnetic field. If the shear angle, γ, shown on Figure (30b) page 207, is greater than γ_c, then there is a region of height, h', in which there are no hot equilibrium solutions, as shown in Figure (34) page 220.

If, for example, the density were a factor of 10 higher, as it may be in coronal condensations, so that $\rho_0 = 1{\cdot}7 \times 10^{-15}$ g cm^{-3} then $\bar{\gamma} = 3{\cdot}7 \times 10^{-2}$ and the corresponding value of γ_c is 63° from Figure (36), page 225. If, in addition to the above increase in density we doubled the scale length (π/k) to 10^{10} cms. then $\bar{\gamma} = 0.15$ and the corresponding value of γ_c is 29°. The value of $\bar{\gamma}$ is also sensitive to temperature; if, for example, we reduce T_0 to 10^6 °K then $\bar{\gamma} = 1{\cdot}5 \times 10^{-2}$ and the value of γ_c is 73°. Thus we see that much smaller values of γ_c can be found by reasonable changes in the density, scale length or temperature.

It can also be seen from Figure (36), page 225, that if $\bar{\gamma}$ is greater than $\bar{\gamma}_{max} \simeq 0.19$, then $\gamma_c = 0$, so that the plasma has no hot equilibrium values for all shear angles. This value, $\bar{\gamma}_{max}$, corresponds, for a temperature $T_0 = 2 \times 10^6$, to a density $\rho_{max} = \left(\frac{3{\cdot}6 \times 10^{-10}}{(\pi/k)^2}\right)^{1/2}$ g cm^{-3}. If the plasma density is greater than ρ_{max} then the plasma is unstable even when there is no shear, $\gamma = 0$. If, for instance, $(\pi/k) = 5 \times 10^9$ cm, the approximate height of a quiescent prominence, then $\rho_{max} = 3{\cdot}8 \times 10^{-15}$ g cm^{-3}, giving a number density 2×10^9 cm^{-3}.

We have found in Figure (34), page 220, that for $\gamma > \gamma_c$, there is a height range over which only a low temperature solution for T_T' exists and that the range increases with γ.

4.3.: THE THERMAL AND HYDROSTATIC EQUILIBRIUM OF THE PLASMA IN THE SHEARED MAGNETIC CONFIGURATION (Contd.)

This effect can be shown analytically, from (4.20), as follows. The derivative of (4.20) is

$$\frac{dF}{dT_T'}\frac{dT_T'}{dh'} \simeq \bar{\gamma}\,\frac{8\,\mathrm{Sec}\,\gamma}{\pi}\left[-g T_T' \frac{\mathrm{Sec}\,\gamma}{\pi} + 1\right] + O(k) \qquad (4.25)$$

where, from (4.22),

$$\frac{dF}{dT_T'} = 0 \qquad \text{at } T_T' = T_c = \frac{\frac{5}{2}-\alpha}{\frac{7}{2}-\alpha}$$

and $\frac{dF}{dT_T'} \gtrless 0$ when $T_T' \lesseqgtr T_c$.

Thus, if $g' T_T' \frac{\mathrm{Sec}\,\gamma}{\pi} > 1$ (for $\rho_0 = 1.7\times10^{-16}$ g cm^{-3}, $T_0 = 2\times10^6$ °K and $\pi/k = 5\times10^9$ cm $g'T_T'/\pi = 0.1$ so that we require $\mathrm{Sec}\,\gamma > 10$ i.e. $\gamma > 84^\circ$ which is satisfied since, in this particular case, we are only interested in γ near $\gamma_c = 87^\circ$), we see from (4.25) that

$$\frac{dT_T'}{dh'} > 0 \quad \text{if } T_T' > T_c ,$$

$$\frac{dT_T'}{dh'} = -\infty \quad \text{if } T_T' = T_c ,$$

and

$$\frac{dT_T'}{dh'} < 0 \quad \text{if } T_T' < T_c ,$$

so that the graph of $T_T' = T_T'(h')$ must have the form shown in Figure (37), page 228. The critical height, h_c', below which no equilibrium exists is given by putting $T_T' = T_c$ in (4.20). When $h_c' \ll \frac{\mathrm{Sec}\,\gamma}{\pi}$, (4.20) becomes, retaining terms of order h_c',

$$F(T_c) = \bar{\gamma}\,\frac{4\,\mathrm{Sec}^2\gamma}{\pi^2}\left[1 + h_c'\left(\frac{\pi}{3\,\mathrm{Sec}\,\gamma} - 2g' T_c\right)\right] , \qquad (4.26)$$

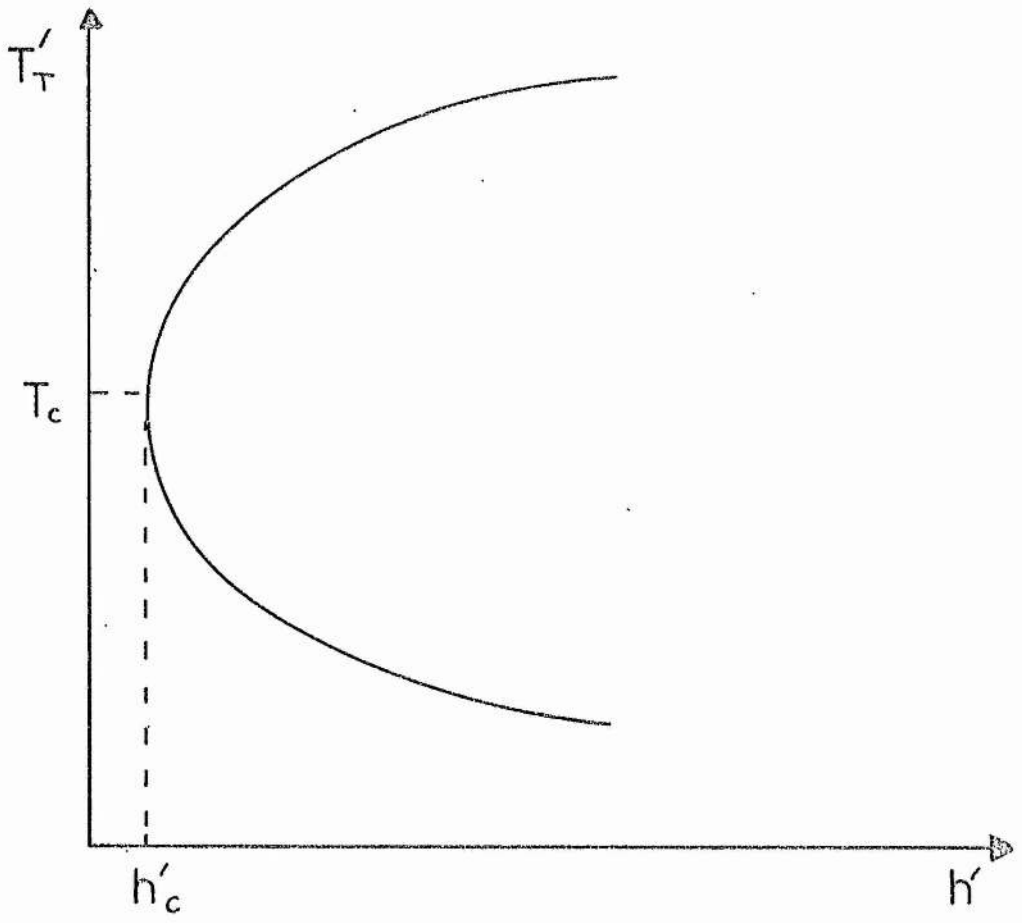

Figure 37. The approximate shape of the equilibrium curve T'_T the temperature at the top of a field line, as a function of h' the height of the top of the field line above the base of the magnetic field region. The critical height, h'_c, is such that there are no equilibrium solutions for $h' < h'_c$, and T'_c is the value of T'_T when $h' = h'_c$.

4.3.: THE THERMAL AND HYDROSTATIC EQUILIBRIUM OF THE PLASMA IN THE SHEARED MAGNETIC CONFIGURATION (Contd.)

from which we see that, if $\gamma = \gamma_c$, equation (4.23), then $h'_c = 0$, and that, as γ increases above γ_c, so h'_c increases so that an unstable region develops extending from $h' = 0$ up to $h' = h'_c$. The thermal instability thus sets in at $h' = 0$ in the present approximation and the unstable region spreads to larger heights as γ increases.

Solution at Large Heights.

The numerical solutions to equation (4.20), which we have presented in Figure (34), page 220, show the thermal instability starts at low heights; but with different values for the parameters $\bar{\gamma}$ and g', it is possible that stability may first break down at greater heights. To test this possibility we consider here the solution at large heights such that

$$h' >> (\mathrm{Sec}\,\gamma)/\pi .$$

Equation (4.20) then reduces to

$$f(T'_T) = g(x) ,$$

where $x = T'_T h'$, $f(T'_T) = T'^{(\frac{q}{2}-\alpha)}_T (1 - T'_T)$

and $g(x) = x^2 \bar{\gamma} \exp(-2 g' x)$.

The three possible types of solution are sketched in Figure (38), page 230, where the graphs of $f(T'_T)$ and $g(x)$ are plotted on the left hand side and the solution T'_T as a function of h' is plotted on the right hand side.

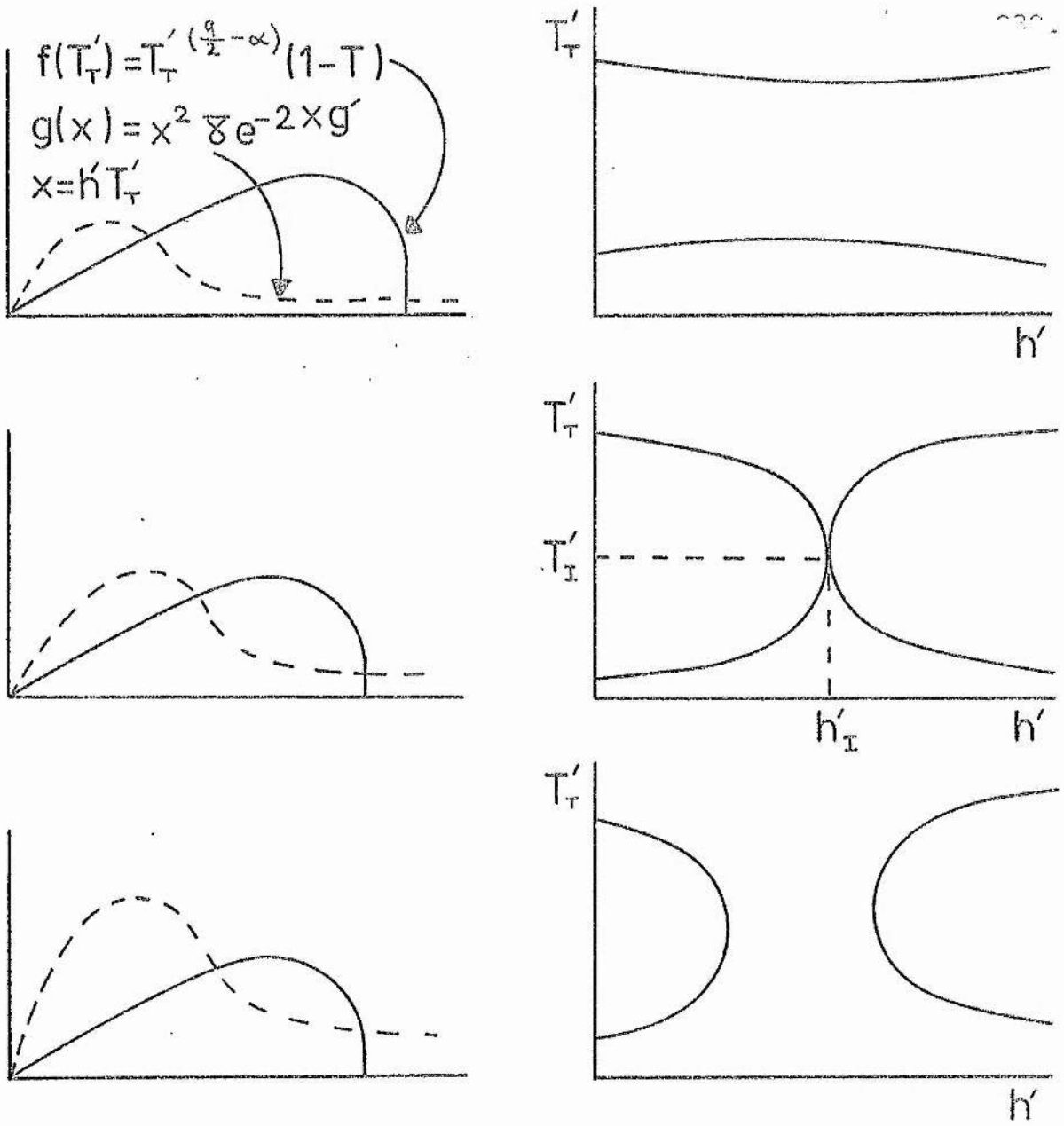

Figure 38. The equilibrium equation (4.20) for large h', the height at the top of a field arch, can be represented by $f(T_T') = g(x)$; these curves are shown on the left hand side of this figure and the corresponding solution, T_T' , the temperature at the top of a field line, as a function of h' is drawn in the right hand side. If the maximum of $g(x)$ is greater than the maximum of $f(T_T')$ then a region develops in which there are no equilibrium solution ; this first occurs when $T_T' = T_I'$ and $h' = h_I'$

4.3.: THE THERMAL AND HYDROSTATIC EQUILIBRIUM OF THE PLASMA IN THE SHEARED MAGNETIC CONFIGURATION. (Contd.)

As the maximum of $g(x)$ is increased above the maximum of $f(T_T')$, there occurs a region of h' in which there is no equilibrium solution. The maximum of $f(T_T')$ (namely $f(T_T') = (T_T')^{9/2-\alpha}(1-T_T') = 0.05$) occurs at $T_T' = \frac{4.5-\alpha}{5.5-\alpha} = 0.86$ (for $\alpha = -1.8$), and the maximum of $g(x)$ (namely $\bar{\gamma}e^{-2}/g'^2 = 2.9\times10^{-4}$) at $x = \frac{1}{g'} = 2.4$. Thus the height h_I' and temperature T_I' at which instability first occurs are given by

$$T_I' = \frac{4.5-\alpha}{5.5-\alpha} \tag{4.27}$$

and

$$h_I' = \frac{1}{g' T_I'} \tag{4.28}$$

At $h' = h_I'$ the maxima of the two curves are equal, so that

$$\frac{\bar{\gamma}}{g'^2} e^{-2} = (T_I')^{\frac{9}{2}-\alpha}(1-T_I'),$$

which on substituting for T_I' gives a critical value of $\bar{\gamma}$, say $\bar{\gamma}^*$, above which instability takes place:

$$\frac{\bar{\gamma}^*}{g'^2} = 0.05\, e^2 \tag{4.29}$$

By comparison, we found in (4.9) that instability occurs when (in dimensionless variables)

$$\frac{\bar{\gamma}}{g'^2} > n^{-2} e^2,$$

so that (4.29) may be regarded as a more accurate version of criterion (4.9). We further note that the parameter $\bar{\gamma}/g'^2$ does not depend on the shear angle γ or the lengthscale π/k.

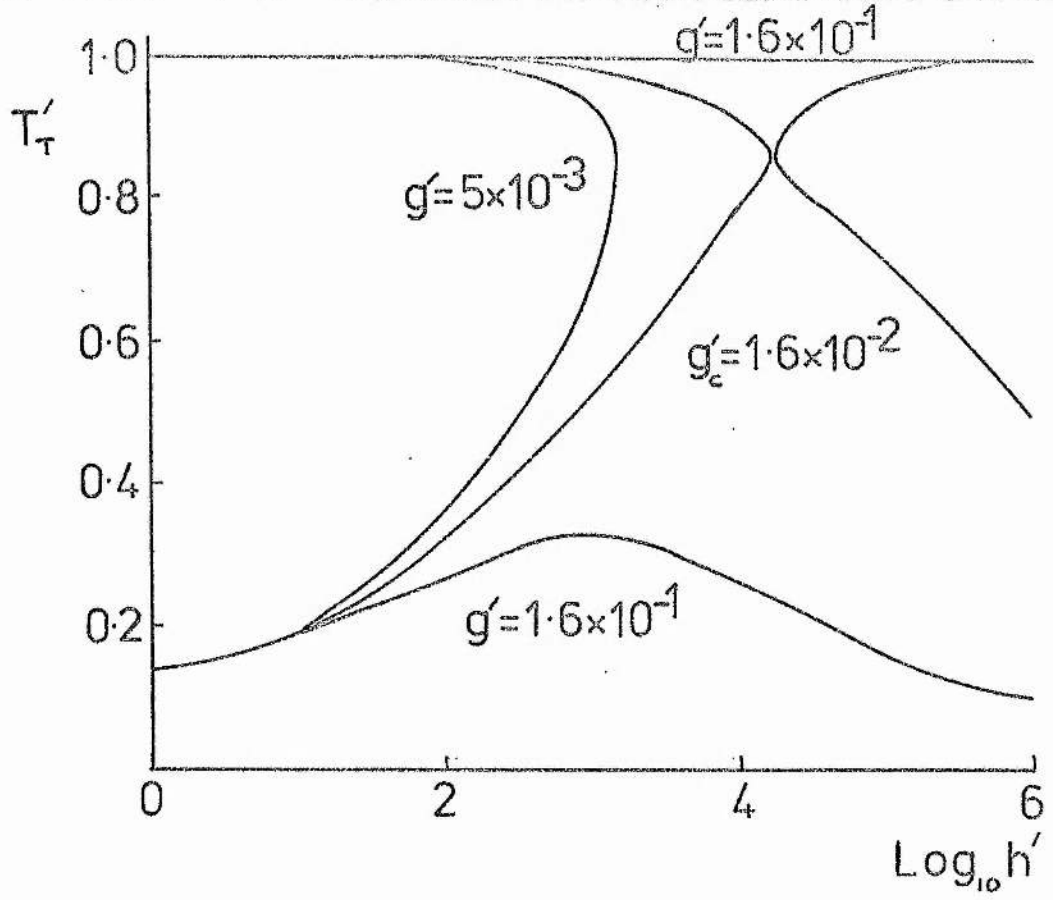

Figure 39. The numerical solution to the equilibrium equation (4.20) for T'_τ, the temperature at the top of the magnetic field line as a function of h', the height of the top of the field line above the base of the magnetic region. This is drawn for several values of the parameter g', which is the ratio of the width of the magnetic field region to the scale height . The shear angle is $\gamma = 0$ and the parameter $\overline{\gamma}$ the ratio of the radiative loss to the thermal conduction at the base of the magnetic region, is $\overline{\gamma} = 10^{-4}$. The critical value g'_c satisfies (4.29) and is such that if $g' < g'_c$ a region develops in which there are no hot equilibrium solutions.

4.3.: THE THERMAL AND HYDROSTATIC EQUILIBRIUM OF THE PLASMA IN THE SHEARED MAGNETIC CONFIGURATION. (Contd.)

It is, in dimensionless variables

$$\frac{\bar{\gamma}}{g'^2} = \frac{\varkappa \rho_0^2 T_0^{\alpha}}{K_0 T_0^{7/2}} \Lambda_0^2 ,$$

so that whether the magnetic structure (4.7) has an unstable region, or not, at large h', depends only on the values of ρ_0 and T_0. Normal coronal values of $T_0 = 10^6\,^{\circ}K$ and $n_e = 10^8\ cm^{-3}$ make

$$\frac{\bar{\gamma}}{g'^2} = 2{\cdot}2 \times 10^{-3} ,$$

so that the plasma is stable at large heights. For $T_0 = 10^6\,^{\circ}K$ one needs $\rho_0 > 2{\cdot}3 \times 10^{-15}\ g\ cm^{-3}$ $(n_e > 10^9\ cm^{-3})$ in order for the unstable region to occur.

To show that the unstable region, that we are predicting for large heights, can occur we solved the full equation (4.20) numerically and plotted T_T' as a function of h' in Figure (39), page 232 for the case where $\gamma = 0$, $\bar{\gamma} = 10^{-4}$ and $g' = 1{\cdot}58 \times 10^{-1}$, $1{\cdot}58 \times 10^{-2}$ and 5×10^{-3}, where $g' = 1{\cdot}58 \times 10^{-2}$ is the value of g' which satisfies (4.29). Note, however, that this instability is occurring at very large heights, $h \simeq 10^4 \frac{\pi}{k}$ so that it will not be relevant with these particular parameters. But this indicates the possibility of instability occurring at a realistic height for other values of $\bar{\gamma}$ and g'. From (4.28) and (4.27) we see that the height at which instability occurs is

$$h_I' = \frac{1}{0{\cdot}86\, g'} = \frac{\pi/k}{0{\cdot}86\, \Lambda_0} ,$$

where $\Lambda_0 = 2 k_B T_0/(m_i g) = 6 \times 10^9\ cm$, is the scale height.

4.3.: THE THERMAL AND HYDROSTATIC EQUILIBRIUM OF THE PLASMA IN THE SCHLÜTER MAGNETIC CONFIGURATION (Contd.)

Thus, by choosing suitably large values of g', h'_I can be more reasonable. For instance, $\pi/k = 1{\cdot}4 \times 10^{10}$ cm makes $g' = 0{\cdot}6$ so the height at which instability occurs is $h'_I = 2$. However, it should be noted that smaller values of h' invalidate the approximation $h' \gg (\mathrm{Sec}\,\chi)/\pi$.

4.4.: THE ADDITION OF A MECHANICAL HEATING TERM.

The corona is heated by presumably the dissipation of waves that propagate up from below, but the details of the mechanism are not yet worked out. In order to investigate the effect on the equilibrium solutions of a continuous heating throughout the sheared field, we assume that the heating is proportional to density and is unaffected by the magnetic field. The equations for the temperature and density are then

$$\frac{d}{dz}(R\rho T) = -\rho g \quad , \tag{4.30}$$

$$\frac{h^2}{L^2}\frac{d}{dz}\left(K_0 T^{5/2}\frac{dT}{dz}\right) = \chi\rho^2 T^{\alpha} - a\rho \quad . \tag{4.31}$$

The constant, a, can be specified by assuming, for instance, that the heating balances the radiative loss at the base of the magnetic field, so

$$a = \chi \rho_0 T_0^{\alpha} \quad .$$

By approximating for the conductive heating term and the magnetic field, as in section 4.3, equations (4.30) and (4.31) give us a modified version of (4.20), namely

$$\frac{T_T'^{\left(\frac{5}{2}-\alpha\right)}\left(1-T_T'\right)}{\bar{\gamma}\, L'^4\, e^{-(h'g'T_T')}} = \frac{e^{-(h'g'T_T')} - T_T'^{-\alpha}}{h'^2} \tag{4.32}$$

where $L' = L'(h')$ is given by (4.19). The solution to (4.32) for T_T' as a function of h' for several values of the shear angle, γ, is plotted in Figure (40) page 237, for $\bar{\gamma} = 3.74\times10^{-4}$ and $g' = 0.4$ (which correspond to coronal values $\rho_0 = 1.7\times10^{-16}$ g cm^{-3}, $T_0 = 2\times10^6$ °K and $\frac{\pi}{k} = 5\times10^9$ cm).

4.4.: THE ADDITION OF A MECHANICAL HEATING TERM. (Contd.)

It can be seen that the temperature T_T' increases as the shear angle γ increases, and that there are equilibrium solutions for all values of h'. It seems that heating of such a size prevents the thermal instability occurring. This is to be expected since, if the thermal conduction is made negligible in the energy equation (4.31) by increasing L', through an increase in γ, then the mechanical heating will now be able to balance the radiative loss. We note that this time the temperature in the upper solution rises as γ is increased unlike the case when mechanical heating was neglected, where the temperature fell.

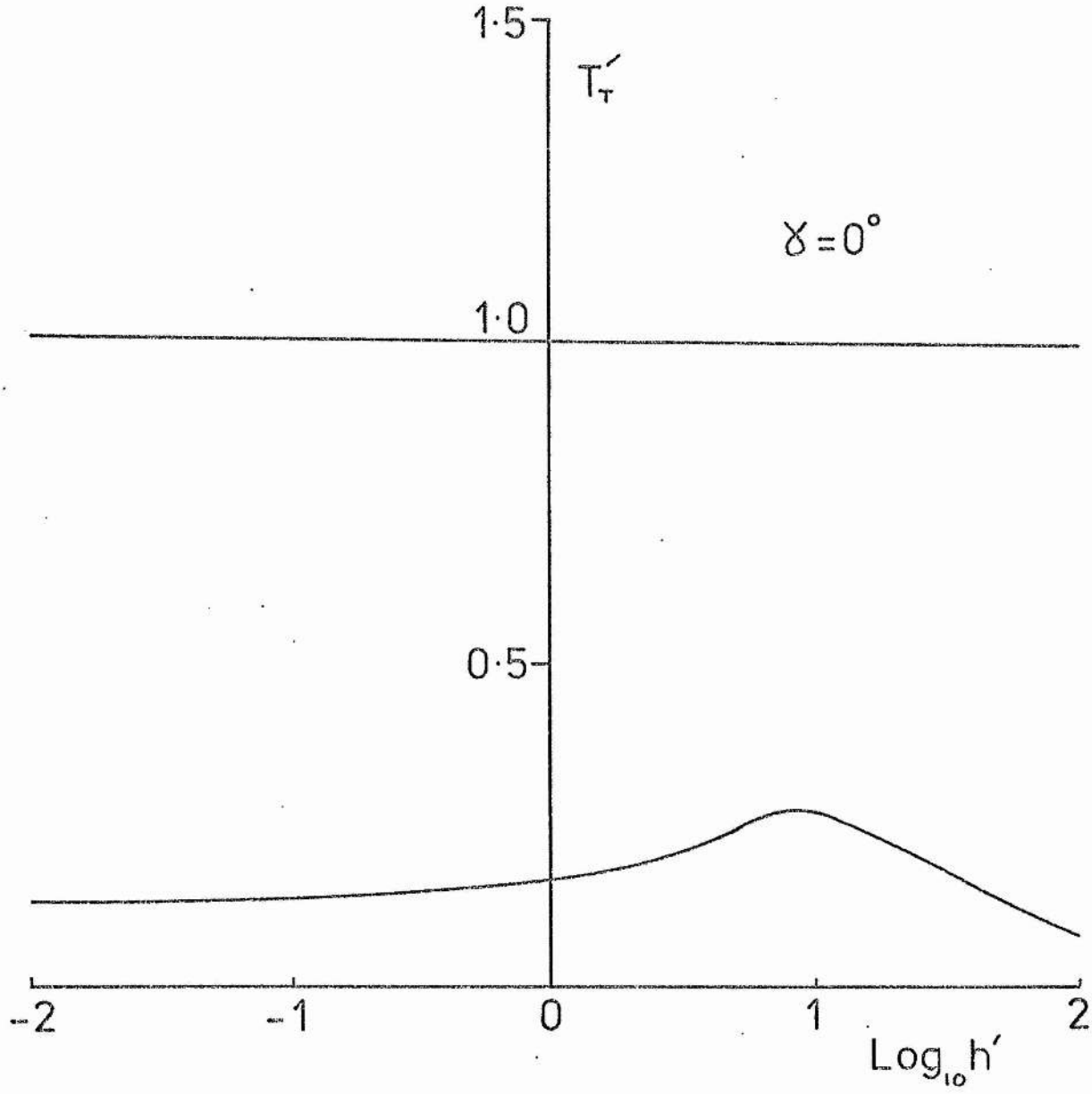

Figure (40a) The solution of (4.32) for T_T', the temperature at the top of a field line, as a function of h' the height of the top of the field line above the base of the magnetic field region.

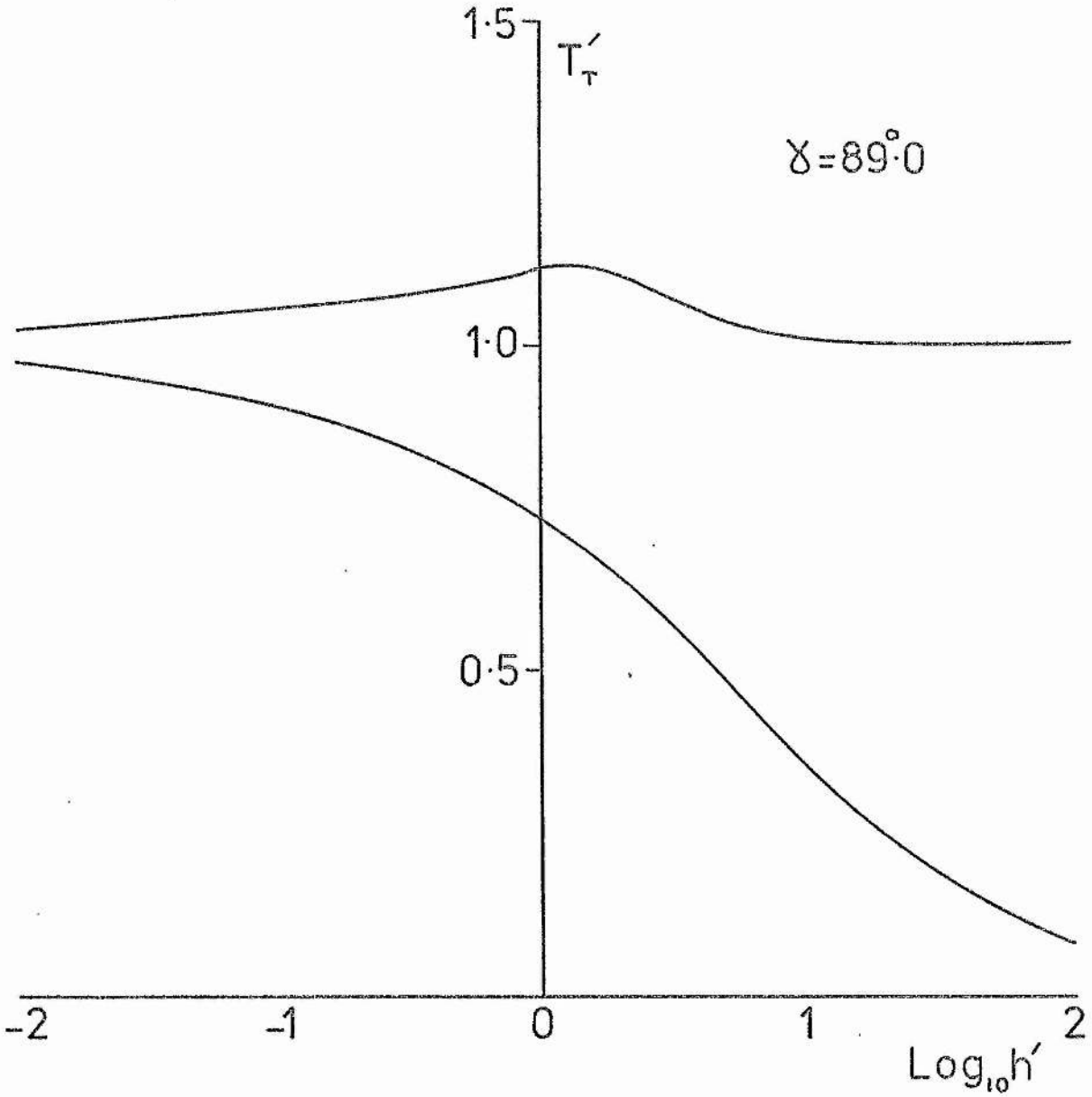

Figure (40b)

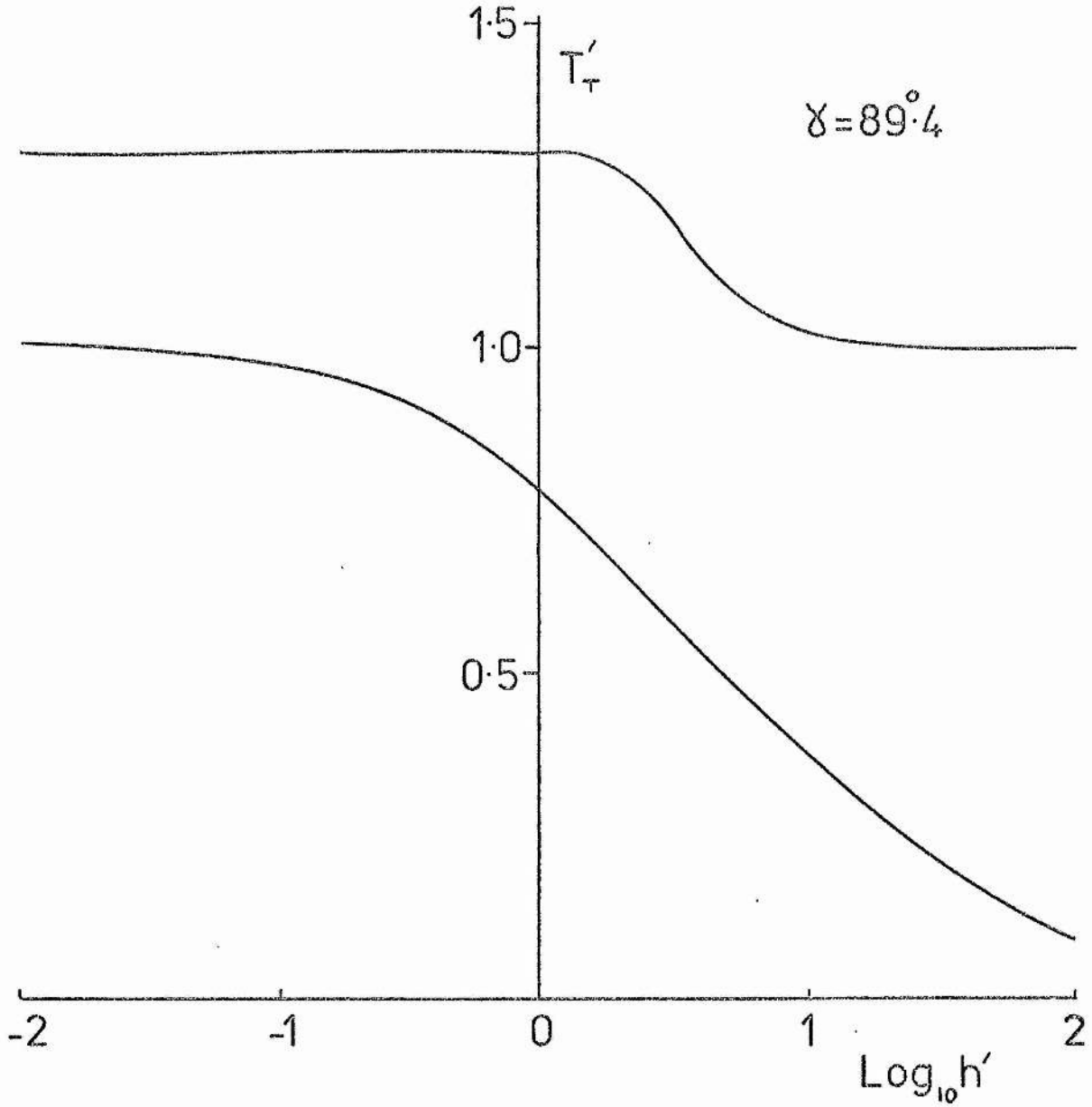

Figure (40c)

4.5.: THE NUMERICAL SOLUTION FOR THE TEMPERATURE STRUCTURE OF PLASMA IN A SHEARED MAGNETIC FIELD.

The equations which give the equilibrium values of temperature and density in the magnetic field are, from (4.10) and (4.11), (without mechanical heating, as in section 4.3)

$$\frac{d}{dz}(R\rho T) = -\rho g \quad , \tag{4.33}$$

$$-\frac{K_{11}}{B}\frac{dB}{dS}\frac{dT}{dS} + \frac{d}{dS}\left(K_{11}\frac{dT}{dS}\right) = \chi \rho^2 T^{\alpha}, \tag{4.34}$$

where $$K_{11} = K_0 T^{5/2},$$

and S measures the distance along a magnetic field line. We will not consider mechanical heating here, because we wish to show that the thermal instability found in the order of magnitude calculation of section 4.3 is supported by a full solution to equations (4.33) and (4.34).
We can write (4.33) and (4.34) in terms of x only, by calculating $z(x)$, along a field line, namely

$$z = \frac{1}{\ell}\log_e\left\{\frac{\cos kx}{\cos kx_0}\right\} \quad , \tag{4.35}$$

and by using $$\frac{dx}{dS} = \frac{B_x}{B} = -\frac{\ell}{k}\cos kx \, . \tag{4.36}$$

Therefore equations (4.33) and (4.34) become

$$\frac{d}{dx}(R\rho T) = \rho g \frac{k}{\ell}\tan kx \quad , \tag{4.37}$$

$$-K_0 T^{5/2}\left(\frac{B_x}{B}\right)^2 k \tan kx \frac{dT}{dx}$$

$$+\frac{B_x}{B}\frac{d}{dx}\left(K_0 T^{5/2}\frac{B_x}{B}\frac{dT}{dx}\right) = \chi \rho^2 T^{\alpha} \, . \tag{4.38}$$

4.5.: THE NUMERICAL SOLUTION FOR THE TEMPERATURE STRUCTURE OF PLASMA IN A SHEARED MAGNETIC FIELD (Contd.)

Equations (4.37) and (4.38) are next made dimensionless by putting

$$T = T_0 T' \;,\quad x = \frac{\pi}{k} x' \;,\quad \rho = \rho_0 \rho' \;,\quad \frac{\rho}{k} = \cos\gamma,$$

$$g = \frac{R k T_0}{\pi} g' \;,\quad B_x = B\, B_x' \;,$$ where from (4.36) $B_x' = -\cos\gamma \cos(\pi x')$

Then (4.37) and (4.38) can be re-written for computational purposes as the following three first order equations for T, $\xi \equiv dT/dx$ and ρ :

$$\frac{dT'}{dx'} = \xi' \;, \tag{4.39}$$

$$\frac{d\xi'}{dx'} = \sec^2\gamma \sec^2(\pi x')\, \bar{\gamma}\, \rho'^2\, T'^{(\alpha - 2.5)} - 2.5\frac{\xi'^2}{T'} + 2\pi \tan(\pi x')\, \xi' \;, \tag{4.40}$$

$$\frac{d\rho'}{dx'} = \frac{\rho'}{T'}\left(-\xi' + g' \sec\gamma \tan(\pi x')\right) \;, \tag{4.41}$$

where $$\bar{\gamma} = \frac{\chi \rho_0^2 T_0^{\alpha}}{K_0 T_0^{7/2}} \left(\frac{\pi}{k}\right)^2 .$$

Equations (4.39), (4.40) and (4.41) are solved numerically for $\xi'(x')$, $T'(x')$ and $\rho'(x')$ subject to the boundary conditions that at the base of a field line, at $x' = \pm x_0'$, $T' = 1$ and $\rho' = 1$ and at the top of a field line, at $x' = 0$, $\frac{dT'}{dx'} = 0$.

4.5.: THE NUMERICAL SOLUTION FOR THE TEMPERATURE STRUCTURE OF PLASMA IN A SHEARED MAGNETIC FIELD (Contd.)

From equation (4.35) we see that at $x'=0$ the field line is at its highest point, h' say, and that as x' approaches x_0' the height of the field line above the x-axis, z, approaches zero. The parameter x_0' or h' defines a single field line, where from (4.35)

$$h' = -\frac{\log_e(\cos(\pi x_0'))}{\pi \cos\gamma}$$

which is drawn in Figure (31a), page 210, for several values of γ, the shear angle.

The temperature along a field line, $T'(x')$ is plotted in Figure (41) page 243, for several different field lines, i.e. different values of x_0', and for a shear angle $\gamma = 89.9^\circ$. Also we have taken $\overline{\gamma} = 3.74 \times 10^{-4}$ and $g' = 0.4$ (which correspond to the values $\rho_0 = 1.7 \times 10^{-16}$ g cm^{-3}, $T_0 = 2 \times 10^6$ °K and $\frac{\pi}{k} = 5 \times 10^9$ cm). This shows us that, when x_0' is small, then $T' \simeq 1$ all along the field line, but that, as x_0' is increased, the temperature at the top (i.e. $x'=0$) of the field line, T_c', falls and then starts to rise again up to $T_c' \simeq 1$. In Figure (42) page 244, we have superimposed on the diagram of the magnetic field, Figure (30a), dashed lines of constant temperature T', the solution to the full equilibrium equations (4.33) and (4.34) which are shown in detail in Figure (41). This shows us the overall temperature structure in the magnetic field region and in particular that a region of low temperature develops.

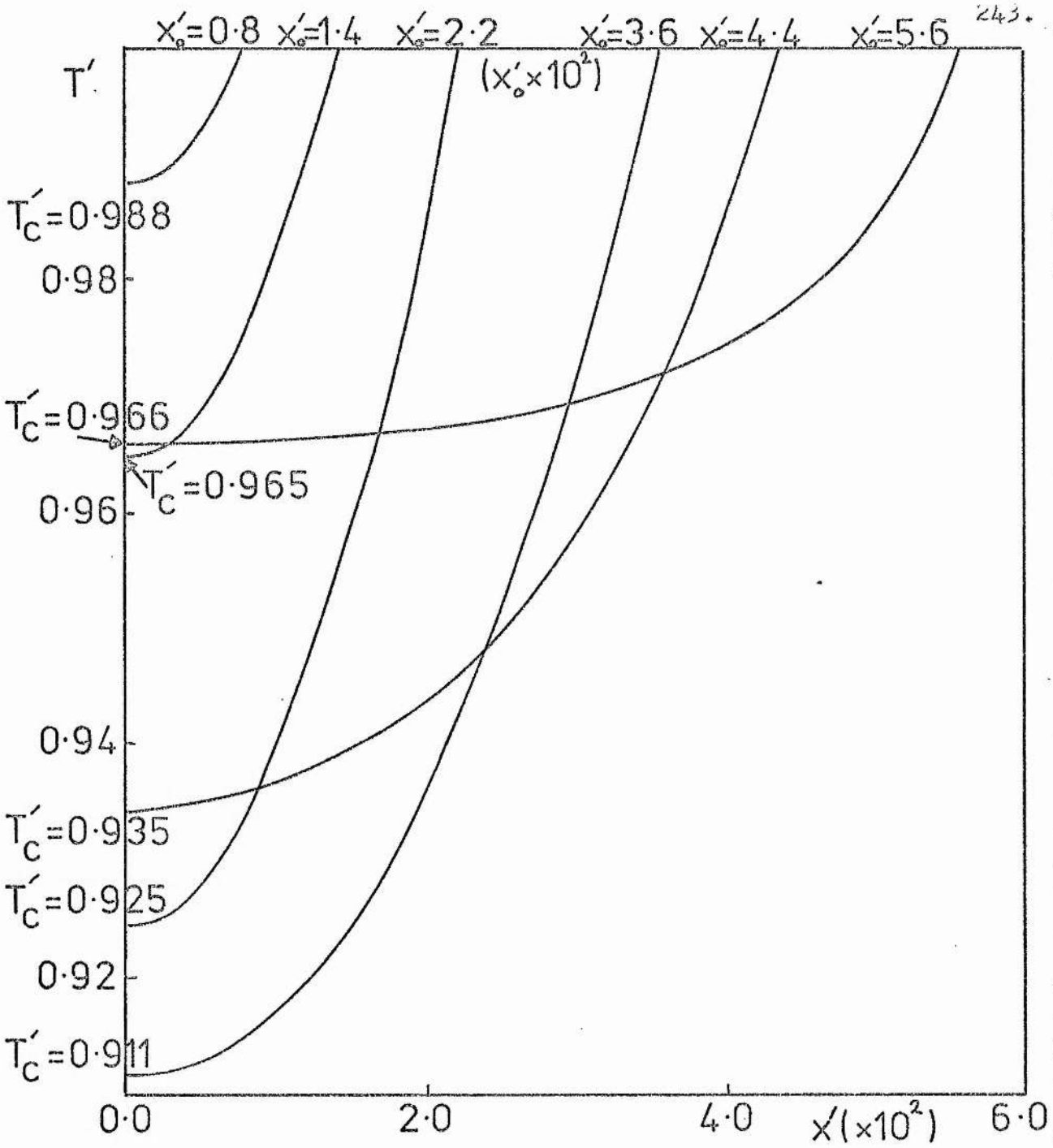

Figure (41). The numerical solution, to the full equilibrium equations (4.33) and (4.34) for the temperature T' as a function of horizontal position, x', along a field line. The solutions are shown for several different field lines which have foot points at $x'=x'_o$. This is drawn for a shear angle $\gamma=89{\cdot}9^\circ$ and with $\bar{\gamma}=3{\cdot}7\times10^{-4}$ and $g'=0{\cdot}4$ (corresponding to $\rho_o=1{\cdot}7\times10^{-16}$ g cm^{-3} $T_o=2\times10^6\,^\circ$K and $\frac{\pi}{k}=5\times10^9$cm).

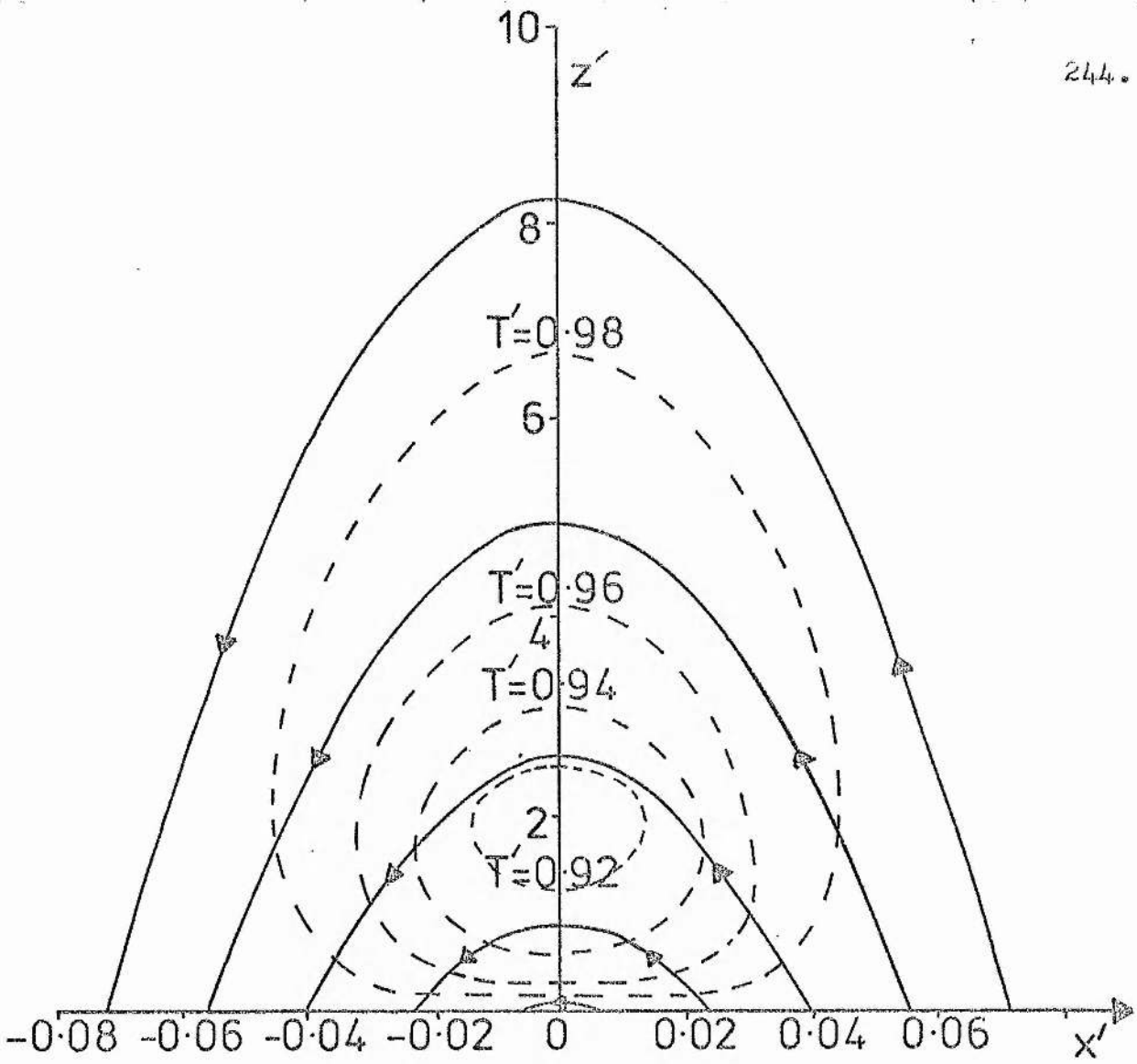

Figure (42). Solid lines indicate the magnetic field of Figure(30a). Dashed lines are contours of constant temperature T' the solution to the full equilibrium equations (4.33) and (4.34). This is drawn for a shear angle $\gamma = 89°9$ and with $\bar{\delta} = 3{\cdot}7 \times 10^{-4}$, $g' = 0{\cdot}4$ (corresponding to $\rho_0 = 1{\cdot}7 \times 10^{-16}$ g cm^{-3}, $T = 2 \times 10^{6}$°K and $\frac{\pi}{k} = 5 \times 10^{9}$ cms).

4.5.: THE NUMERICAL SOLUTION FOR THE TEMPERATURE STRUCTURE OF PLASMA IN A SHEARED MAGNETIC FIELD (Contd.)

The value of the temperature T_c', at the top of a field line shown in Figure (41), page 243, is plotted in Figure (43) page 246, as a function of X_o', the value of x' at which the field line crosses the x-axis, for several values of γ, and for $\bar{\gamma} = 3{\cdot}74 \times 10^{-4}$ and $g' = 0{\cdot}4$. As γ increases, we see that T_c' is reduced at every value of X_o'. Also when $\gamma = 89^{\circ}{\cdot}99$ the value of T_c' falls very rapidly near $X_o' = 10^{-2{\cdot}7}$ and there is no solution for X_o' greater than this value, but less than $10^{-1{\cdot}1}$, so that we expect the plasma in this region to become unstable. (It may be that there are no solutions for $\gamma = 89^{\circ}{\cdot}99$ when $X_o' > 10^{-1{\cdot}1}$ but this corresponds to heights $h' > 100$, which is too large to be important to quiescent prominence formation). Thus Figure (43) shows that when γ is increased above a certain critical value, γ_c, the plasma in the sheared magnetic field becomes unstable.

The field line which first becomes unstable has its foot points at $X_o' = x_c'$, which corresponds to the value of X_o' at the minimum of the $T_c'(x_o')$ curve which has $\gamma = \gamma_c$. The value of h' corresponding to X_c' is called h_c' and, for ordinary coronal values ($\rho_o = 1{\cdot}7 \times 10^{-16}$ g cm^{-3}, $T_o = 2 \times 10^6$ °K and $\pi/k = 5 \times 10^9$ cm so that $\bar{\gamma} = 3{\cdot}74 \times 10^{-4}$ and $g' = 0{\cdot}4$), we find $\gamma_c = 89^{\circ}{\cdot}94$ and $h_c' = 1{\cdot}6$. Lastly, we plot, in Figure (44), page 247, the critical value of the shear angle γ_c as a function of the parameter $\bar{\gamma}$, which, given by (4.24) is the ratio of the radiative loss to the thermal conduction at the base of the magnetic field region.

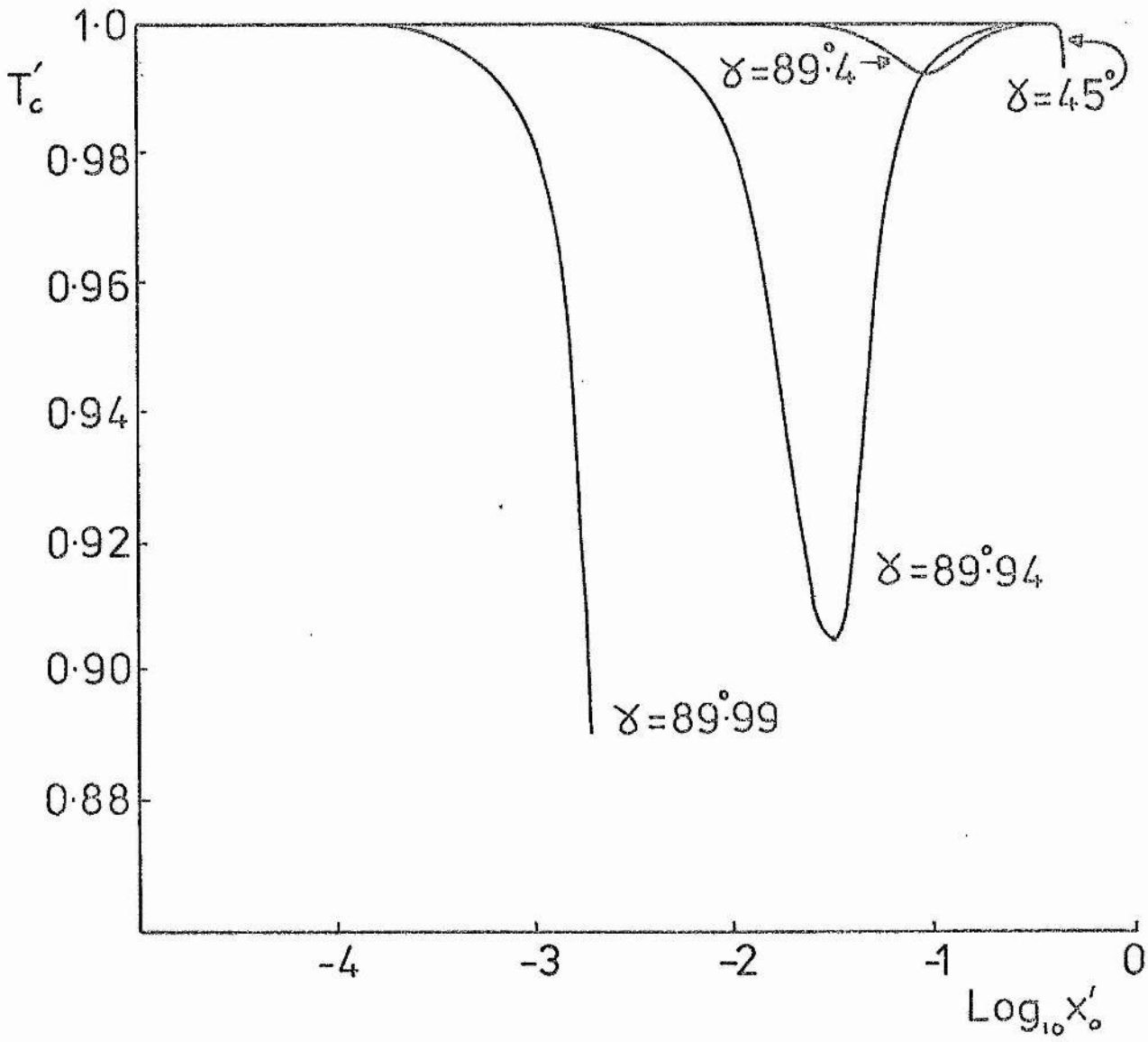

Figure (43). The temperature T_c' at the top (i.e. $X' = 0$) of a field line (from the numerical solution to the full equilibrium equations (4.33) and (4.34)), as a function of X_o', the value of X' at which the field line crosses the x-axis. This is drawn for several values of the shear angle γ and with $\bar{\gamma} = 3{\cdot}7 \times 10^{-4}$ and $g' = 0{\cdot}4$ (corresponding to $\rho_o = 1{\cdot}7 \times 10^{-16}$ g cm^{-3}, $T = 2 \times 10^6$ °K and $\frac{\Pi}{k} = 5 \times 10^9$ cm).

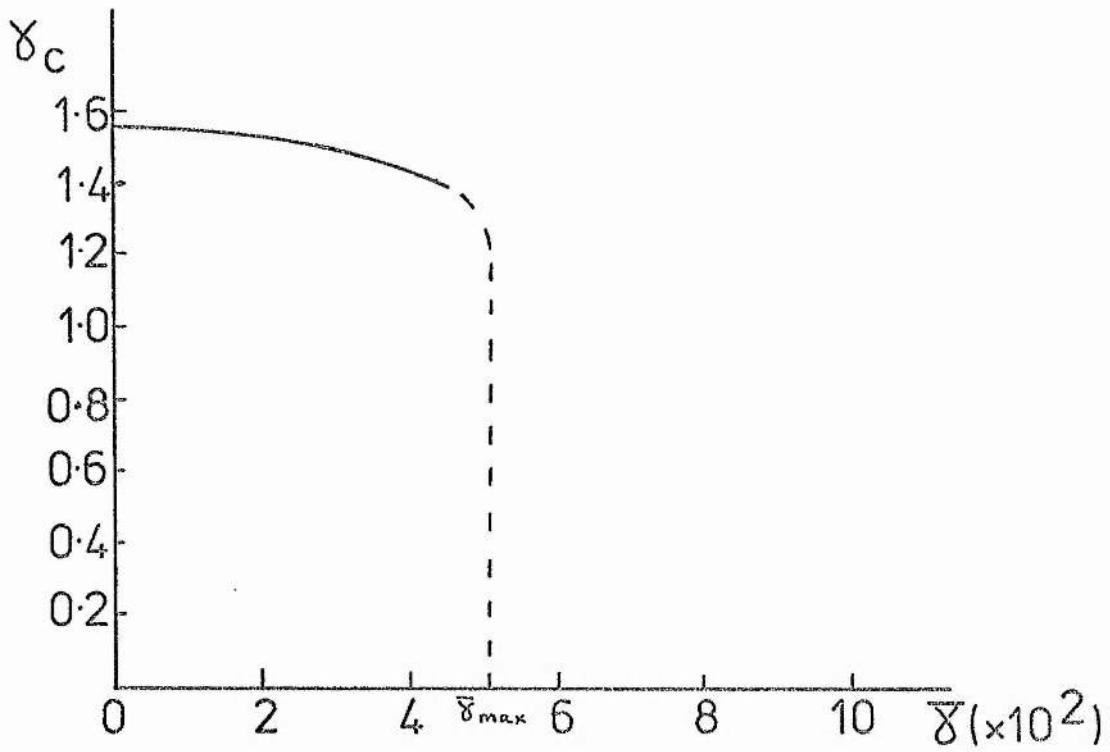

Figure (44). The critical shearing angle γ_c as a function of the parameter $\bar{\gamma}$, which, given by (4.24) is the ratio of the radiative loss to thermal conduction at the base of the magnetic field. The critical shear angle, γ_c, is such that if the shear angle γ, is greater than γ_c then there is a region of X_o' in which the field lines with footpoints at X_o' have no equilibrium, as shown in Figure (43) page 246. Part of the curve shown dashed, has not yet been calculated. The critical value of $\bar{\gamma}$ is $\bar{\gamma}_{max}$ such that, if $\bar{\gamma} > \bar{\gamma}_{max}$, there are no equilibrium solutions for all values of shear angle.

4.5. : THE NUMERICAL SOLUTION FOR THE TEMPERATURE STRUCTURE OF PLASMA IN A SHEARED MAGNETIC FIELD. (Contd.)

We have not, however, because of the lengthy time involved in calculating each point, been able to draw the complete curve, but we have been able to establish its approximate shape. We see in Figure (44), page 247, that as $\overline{\gamma}$ is increased from zero, the value of γ_c falls, as it does in the corresponding case, Figure (36), page 225, in the order of magnitude calculation, but it falls more slowly. Then we see that, when $\overline{\gamma}$ is increased further, γ_c falls more rapidly. The curve then goes through a region in which we are uncertain about its value. Finally it crosses the $\overline{\gamma}$ axis at $\overline{\gamma}_{max}$, which is defined such that if $\overline{\gamma} > \overline{\gamma}_{max}$ then the magnetic field structure is unstable for all values of shear angle. The value of $\overline{\gamma}_{max}$ is 0·05 which compares with the order of magnitude value of 0.19. The value of the maximum density, ρ_{max}, above which the magnetic field region will be unstable for all shear angles is then

$$\rho_{max} = \left(\frac{\overline{\gamma}_{max}\ 1{\cdot}9 \times 10^{-9}}{(\pi/k)^2} \right)^{1/2} \text{g cm}^{-3}.$$

If $(\pi/k) = 5 \times 10^9$ cm, the approximate height of a quiescent prominence, then $\rho_{max} = 1{\cdot}9 \times 10^{-15}$ g cm^{-3}.

4.6.: SUMMARY

In this chapter a model is presented for the formation of quiescent prominences in a sheared magnetic field. We demonstrate, by methods progressing from a rough order of magnitude calculated to a numerical solution to the full equations, that, in a magnetic arch system in thermal equilibrium between radiative loss and thermal conduction and in mechanical equilibrium under a balance between gravity and a density gradient, thermal instability can occur if the magnetic field is sheared enough. We expect that such an instability will cool matter down since, when the thermal conductivity is reduced, by increasing the length of the field lines through shearing, then the radiative loss dominates the energetics which has a cooling effect. This cooling down will then draw in matter, probably along the field lines, since condensation across the magnetic field is greatly hindered. Such a condensation may well develop into a prominence.

We firstly discussed force-free fields in general and pointed out that they can only occur if the magnetic pressure is very much greater than the gas pressure, which is true in active regions. Then we discussed the properties of a particular force-free field, first considered by Nakagawa & Tanaka (1974), which has the property that the height, h, of the top of an arch rises into the atmosphere as the footpoints are sheared uniformly. The variation the height, h, as a function of the shear angle γ is plotted.

4.6.: SUMMARY (Contd.)

In our model we have included gravity so that, for field lines reaching higher and higher into the atmosphere, the density, at the top of the field arch, will fall. This reduction in density implies that t_{cool}, the timescale for heat to be radiated out of a volume, increases. However, the length scale for thermal conduction also increases with higher field lines, so that $t_{\parallel}$, the timescale for heat to be conducted into a volume, increases. The instability criterion ($t_{\parallel}/t_{cool} > 1$) is thus satisfied only if, with increasing height, the length scale is increased more than the density is decreased. We know that $t_{\parallel}/t_{cool}$ has a maximum value at $h \simeq \Lambda_0$ (the scale height of the atmosphere) of $(t_{\parallel}/t_{cool})_{max} \simeq 0{\cdot}1\, n^2$, where the length of a field line is $L \simeq n h$. Thus, if n is increased enough through shearing, $t_{\parallel}/t_{cool}$ will be greater than unity so that the plasma becomes unstable. This instability is next investigated in more detail. We assume an order of magnitude form for the thermal balance. For the mechanical balance we assume that temperature variations are not important so that the pressure gradient gives a reduction of density with height. We take an approximate form for the dependence of the length of a field line on the shear angle and solve the equations of thermal and mechanical balance for the temperature at the top of a flux tube as a function of the height to which that flux tube reaches.

4.6.: SUMMARY (Contd.)

We show how these equilibrium solutions depend on the shear angle γ , on the parameter $\bar{\gamma}$, the ratio of radiative loss to thermal conduction at the base of the magnetic field region, and on a parameter g' , the ratio of the width of the magnetic field region to the scale height. For ordinary coronal values of $\bar{\gamma}$ and g' we find that, as γ is increased above a critical value γ_c, a range of height develops in which there is no hot equilibrium solution. This occurs first, as we show analytically, at $h = 0$, and then spreads to greater heights as γ increases. The value of γ_c for ordinary coronal conditions is approximately 87°. We suggest that, when the shear angle exceeds γ_c, the plasma becomes unstable and cools under the influence of the radiative loss. This critical angle for instability at low heights is found analytically to depend on $\bar{\gamma}$; as $\bar{\gamma}$ increases, the value of γ_c falls and, in particular, we find that if the coronal density is a factor of 10 larger than the ordinary corona so that $\rho_0 = 1{\cdot}7 \times 10^{-15}$ g cm^{-3} then $\bar{\gamma}$ is increased by a factor of 100 and γ_c is reduced to 63°. We also find that, if $\bar{\gamma}$ is increased beyond $\bar{\gamma}_{max}$, the plasma has no equilibrium solution for any shear angles. The value of $\bar{\gamma}_{max}$ is 0.19, and the corresponding value of density, ρ_{max} , is $3{\cdot}8 \times 10^{-15}$ g cm^{-3} (for $T_0 = 2 \times 10^6$ °K and the width of the magnetic field region $\frac{\pi}{k} = 5 \times 10^9$ cm). Thus if the density at the base of the magnetic arch system is greater than ρ_{max}, the plasma is unstable even when $\gamma = 0$. We then investigate the equilibrium of this system at greater heights using similar approximations.

4.6.: SUMMARY (Contd.)

The plasma has a region of h in which there is no equilibrium solution if $\gamma/g'^{2} > 0{\cdot}4$ .This ratio does not depend on the shear angle or the width of the flux region and is purely a function of ρ_0 and T_0, the density and temperature at the base of the field lines. We find that the height at which this occurs is $h \simeq 1/(0{\cdot}86\, g')$. With $\pi/k = 5 \times 10^{9}$ cm , we get $h = 10^{4}\Lambda_0$ which is too large to be important to quiescent prominences; however, if $\pi/k = 7 \times 10^{9}$ cm , say, then $h = \Lambda_0$, and this permanently unstable region could be important.

We then extended the above analysis to include continuous mechanical heating in the energy balance. In this case, no unstable regions develop as the shear angle increases and the temperature rises instead of falling, as the shear is increased. This maintainence of equilibrium is to be expected since now the radiative loss can be balanced by mechanical heating when thermal conduction is reduced by shearing.

Finally, we solved the full equilibrium mechanical and thermal balance numerically. This time we ignored mechanical heating and concentrated on the thermal instability which the order of magnitude calculation had predicted. We were able to calculate the temperature along each field line and demonstrated that a region of low temperature develops. Furthermore, if the shear angle is large enough ($\gamma > \gamma_c$), within the low temperature region there develops a region in which there are no hot equilibrium solutions, as we found in the order of magnitude case.

4.6.: SUMMARY (Contd.)

Again the dependence of the critical shear angle γ_c on the parameters $\bar{\gamma}$ and g' is found. For ordinary coronal values of $\bar{\gamma}$ and g', $\gamma_c \simeq 89.9^\circ$, but, as $\bar{\gamma}$ is increased, γ_c falls (as in the order of magnitude case).

Again there exists a value $\bar{\gamma}_{max}$, above which the magnetic arch system is unstable for all shear angles γ. This yields a maximum value for ρ_{max}, the density at the base of the magnetic field.

Each of the progressively more accurate methods show the same feature: that a region, in which no hot equilibrium solution can exist, develops if the shear angle is greater than some critical value, γ_c. The order of magnitude calculation indicates that there are two possible sites, one at low and the other at large values of height.

In the numerical solution to the full equations we concentrate on the low height range and demonstrate how the parameter $\bar{\gamma}$ greatly influences the problem. In agreement with the order of magnitude case we see that γ_c becomes progressively lower as $\bar{\gamma}$ increases.

CHAPTER 5

CONCLUSIONS AND SUGGESTIONS FOR FURTHER WORK

We have here investigated the thermal and tearing mode instabilities in the corona and upper chromosphere. The effect of these two instabilities has been examined in a neutral current sheet, one application being, as suggested by Kuperus and Tandberg-Hanssen (1967), in the formation of quiescent prominences. We have also considered the thermal balance in an arch magnetic field system, showing that such a structure can become thermally unstable if the foot points are sheared enough, a result which could be relevant to the formation of prominences in magnetic arches.

In chapter 2 we study a neutral current sheet in thermal equilibrium (between mechanical heating, radiative loss, and thermal conduction) and in mechanical equilibrium (between the Lorentz force across the sheet and a gas pressure gradient). With an approximate representation of the thermal conduction we investigate the equilibrium and stability of the sheet. As the length of the sheet increases we find that it passes through a series of stable equilibria until a certain value, L_{max} is reached, when the sheet cools down to a new stable equilibrium. For coronal conditions (temperature $T_0 = 10^6$°K and number density $n = 10^8 cm^{-3}$), values for L_{max} ($6 \times 10^9 cm$) and the cooling time ($t \simeq 10^5 sec$ when the magnetic field B ≈1 Gauss) are in fair agreement with the observed values (height $\simeq 5 \times 10^9 cm$ and formation time $\simeq 10^5 sec$) for quiescent prominences.

Chapter 5.

CONCLUSIONS AND SUGGESTIONS FOR FURTHER WORK (Contd.)

Apart from the main application of the theory, namely to current sheet models for prominences, the analysis may also be relevant to smaller sheets which form in the chromosphere, provided they are not so thin that ohmic heating and heat conduction across the magnetic field become important.

This work could be extended in several ways. Other energy terms such as the release of gravitational potential energy or the effect of the particle motions caused by spicules, could be considered in the thermal balance in the corona and upper chromosphere. One could also examine the effect of changing the mechanical heating law since the actual amount of energy transported by this means is unclear.

The theory of thermal instability in a neutral sheet could be advanced by using the technique of Cross & Van Hoven (1971), or by using some other means, to find the growth rate of the instability when the structure within the current sheet is taken into account. One could then see how the thermal instability is influenced by the other instabilities such as the tearing mode.

In chapter 3 we calculate the growth rate of the tearing mode instability in a neutral current sheet with no energy sources or sinks, using the method devised by Cross & Van Hoven (1971) to study the instability in a sheared magnetic field of constant magnitude. We find that the maximum growth rate can be significantly larger in the current sheet than that found in the sheared field by Cross & Van Hoven.

Chapter 5

CONCLUSIONS AND SUGGESTIONS FOR FURTHER WORK (Contd.)

Also we find, in our case, that when β, the ratio of gas to magnetic pressure, is reduced so that the density in the sheet increases, the growth rate decreases in value. In addition, we investigate the effect, on the tearing mode instability in a current sheet, of including a transverse component of the magnetic field. We find that the growth rate, ω, of the instability is significantly inhibited if the value of the transverse field is large enough. In particular, ω, is reduced to the diffusion rate, τ_D^{-1}, if the transverse field component B_t is approximately equal to $\frac{3}{4} B_a$, where B_a is the field strength at the edge of the current sheet. Also the dimensionless growth rate, $\omega_o \tau_D$, is reduced to $\omega_o \tau_D / n$ when B_t is increased from zero to $B_t = B_a \sqrt{n} / (3.8 S^{0.34})$, where S is the ratio of the diffusion time scale to the Alfvén time scale.

Possible extensions to the above analysis include the effects of reducing the value of β and of compressibility on this instability. It was noted that when $\beta >> 1/S$ the plasma behaves incompressibly, but, with thin enough current sheets and high enough values of magnetic field, one has $S \gtrsim \beta^{-1}$ so that compressibility would be important. Another instability which could occur in a neutral sheet is the infinite conductivity interchange instability, so it would be interesting to consider its influence, either by the numerical techniques of Cross & Van Hoven, or, since the equations are greatly simplified when there is no resistivity, by analytic means.

Chapter 5

CONCLUSIONS AND SUGGESTIONS FOR FURTHER WORK (Contd.)

In chapter 4 a model is presented for the formation of quiescent prominences in a sheared, force-free magnetic field. We demonstrate by methods progressing from a rough, order of magnitude calculation to a numerical solution to the full equations, that in such a magnetic structure thermal instability can occur if the magnetic field is sheared enough. We assume thermal equilibrium between radiative loss and thermal conduction and mechanical equilibrium along field lines with a balance between gravity and a pressure gradient. We find, for example, that if the density at the base of the field is a factor of ten larger than the normal coronal value, as it may be in coronal condensations, ($\simeq 1.7 \times 10^{-15}$ g cm^{-3}) then there is a range of heights with no equilibrium if the shear angle is greater than 63°. We expect the resulting instability to cool the plasma and draw matter along the field to create a prominence. The presence of a large enough mechanical heating is found to prevent the instability occurring.

This work could be extended by investigating the stabilizing effect of the mechanical heating in more detail using the numerical solution to the full equations. One could also extend the range of parameters examined in the numerical work and, in particular, establish in greater detail the variation of the critical angle γ_c above which instability occurs, with $\overline{\gamma}$ the ratio of radiative loss to thermal conduction at the base of the magnetic field region.

Chapter 5

CONCLUSIONS AND SUGGESTIONS FOR FURTHER WORK (Contd.)

Also the effect of varying g', the ratio of the scale length of the magnetic region to the scale height of the atmosphere would be of interest. With an order of magnitude calculation we could examine the effect on the equilibrium of having the temperature at the top of the magnetic arch, larger than the temperature at the base. Such an analysis would fit in with observations which imply that the temperature at the top of these arch structures is somewhat larger than the external coronal value.

REFERENCES

Anzer, U.: 1969, Solar Phys. 8, 37.

Axisa, F., Matres, M.J., Pick, M., and Soru-Escaut, I.
:1973, Solar Phys. 29, 163.

Babcock, H.D. and Babcock, H.W.: 1955, Astrophys, J. 121, 349.

Barston, E.M.: 1969, Phys. Fluids 12, 2162.

Beckers, J.H.: 1972, Ann. Rev. Astron and Astrophys, 10, 73.

Bernstein, I.B.: Frieman, E.K., Kruskal, M.D., and Kulsrud, R.M.:
1958, Proc. Roy. Soc. A244, 17.

Billings, D.E. and Alvarez, M.: 1975, Solar Phys. 40, 23.

Bruzek, A. and Kuperus, M.: 1972, Solar Phys. 24, 3.

Cox, D.P. and Tucker, W.H.: 1969, Astrophys. J. 157, 1157.

Cross, M.A.: 1972, Ph.D. Thesis,Univ. of California.

Cross, M.A. and Van Hoven, G.: 1971, Phys. Rev. A4, 2347.

d'Azambuja, L. and d'Azambuja, M.: 1948, Ann. Obs. Paris-Meudon.
6, 7.

de Jager, C.: 1959, Handbuch der Physik 52, 80.

Dodson, H.W.: 1948, Monthly Notices Roy. Astron. Soc. 108, 383.

Doherty, L.R. and Menzel, D.H.: 1965, Astrophys. J. 141, 251.

Dunn, R.: 1960, Ph.D. Thesis, Harvard Univ.

Ellison, M.A.: 1937, Monthly Notices Roy. Astron. Soc. 104, 22.

Field, G.B.: 1965, Astrophys. J. 142, 531.

Furth, H.P., Killeen, J., and Rosenbluth, M.N.: 1963,
Phys. Fluids 6, 459.

Gabriel, A.H.: 1976, Phil. Trans. Roy. Soc. Lon. A281, 339.

Harvey, J.W.: 1969, Ph.D. Thesis, Univ. of Colorado.

Heyvaerts, J.: 1974, Astron. and Astrophys. 37, 65.

Heyvaerts, J. and Priest, E.R.: 1976, Solar Phys. 47, 223.

Hildner, E.: 1971, Ph.D. Thesis, Univ. of Colorado.

REFERENCES

Hildner, E.: 1974, Solar Phys. 35, 123.

Hirayama, T.: 1971, Solar Phys. 17, 50.

Hunter, J.H.: 1966, Icarus 5, 321.

Hunter, J.H.: 1970, Astrophys. J. 161, 451.

Ioshpa, B.A.: 1968, Results of Res. on Intl. Geophys. Projects, Solar Activity 3, 44.

Kippenhahn, R. and Schluter, A.: 1957, Z. Astrophys. 43, 36.

Kippenheur, K.O.: 1953, in G. Kuiper (ed.), The Sun, Ch.4, p. 327, Chicago Univ. Press.

Kleczek, J.: 1958, Bull. Astron. Inst. Czech. 9, 115.

Kuperus, M.: 1965, Rech. Astron. Utrecht 17, 1.

Kuperus, M. and Tandberg-Hanssen, E.: 1967, Solar Phys. 2, 39.

Kuperus, M. and Raadu, M.A.: 1974, Astron. and Astrophys. 31, 189.

Lust, R. and Zirin, H.: 1960, Z. Astrophys. 49, 8.

Martin, S.: 1973, Solar Phys. 31, 3.

McMath, R.R. and Petit, E.: 1938, Publ. Astr. Soc. Pacific 51, 154.

Nakagawa, Y.: 1970, Solar Phys. 12, 419.

Nakagawa, Y. and Malville, J.M.: 1969, Solar Phys. 9, 102.

Nakagawa, Y. and Tanaka, K.: 1974, Astrophys J. 190, 711.

Orrall, F.Q. and Zirker, J.B.: 1961, Astrophys. J. 134, 72.

Parker, E.N.: 1953, Astrophys. J. 117, 431.

Parker, E.N.: 1963, Astrophys. J. Suppl. 8, 177.

Pneuman, G.W. and Kopp, R.A.: 1977, to be published.

Priest, E.R.: 1969, Ph.D. Thesis, Univ. of Leeds.

Raadu, M.A. and Nakagawa, Y.: 1971, Solar Phys. 20, 64.

Raadu, M.A. and Kuperus, M.: 1973, Solar Phys. 28, 77.

Raju, P.K.: 1968, Monthly Notices Roy. Astron. Soc. 139, 479.

Rombolt, B.: 1967, Acta Astron. 17, 329.

Rust, D.: 1966, Ph.D. Thesis, Univ. of Colorado.

REFERENCES

Rust, D.: 1967, Astrophys. J. 150, 313.

Rust, D.: 1972, A.F.C.R.L. Environmental Res. Paper.

Saito, K. and Tandberg-Hanssen, E.: 1973, Solar Phys. 31, 105.

Secchi, A.: 1875, Le Soleil, Gauthier-Villars, Paris, Vols. 1 and 2.

Smith, S.F.: 1968, in K.O. Kippenheuer (ed.), "Structure and Development of Solar Active Regions", I A U Symp. 35, 267.

Smith, S.F. and Ramsey, H.: 1967, Solar Phys. 2, 158.

Spitzer, L.: 1962, Physics of Fully Ionized Gases, 2nd ed., J. Wiley & Sons, London.

Tandberg-Hanssen, E.: 1974, Solar Prominences, D. Reidel Publ. Co. Dordrecht, Holland.

Tandberg-Hanssen, E. and Anzer, U.: 1970, Solar Phys. 15, 158.

Uchida, Y. and Sakurai, T.: 1977, to be published.

Van Hoven, G. and Cross, M.A.: 1971, Phys. Fluids, 14, 1141.

Vernazza, J., Avrett, E., and Loeser, R.: 1973, Astrophys J. 184, 605.

Waldmeier, M.: 1970, Solar Phys. 15, 167.

Wesley, W.H.: 1927, Mem. Roy. Astron. Soc. 64, Appendix.

Weyman, R.: 1960, Astrophys, J. 132, 380.

Zanstra, H.: 1955a, Gas Dynamics of Cosmic Clouds, ed. J.M. Burgers and H.C. van de Hulst (Amsterdam: North-Holland Publ. Co.) chap. XIII.

Zanstra, H.: 1955b, in A. Beer (ed.), Vistas in Astronomy 1, 256.

Zirin, J.B.: 1966, The Solar Atmosphere, Blaisdell Publ. Co.